



Engineered Curli-Expressing Probiotic Bacteria as a Platform for Therapeutics and Diagnostics

The Harvard community has made this article openly available. [Please share](#) how this access benefits you. Your story matters

Citation	Praveschotinunt, Pichet. 2019. Engineered Curli-Expressing Probiotic Bacteria as a Platform for Therapeutics and Diagnostics. Doctoral dissertation, Harvard University, Graduate School of Arts & Sciences.
Citable link	http://nrs.harvard.edu/urn-3:HUL.InstRepos:42029630
Terms of Use	This article was downloaded from Harvard University's DASH repository, and is made available under the terms and conditions applicable to Other Posted Material, as set forth at http://nrs.harvard.edu/urn-3:HUL.InstRepos:dash.current.terms-of-use#LAA

**Engineered Curli-Expressing Probiotic Bacteria as a Platform for
Therapeutics and Diagnostics**

A dissertation presented

by

Pichet Praveschotinunt

to

The Harvard John A. Paulson School of Engineering and Applied Sciences

in partial fulfillment of the requirements

for the degree of

Doctor of Philosophy

in the subject of

Engineering Sciences

Harvard University

Cambridge, Massachusetts

May 2019

© 2019 Pichet Praveschotinunt

All rights reserved

Engineered Curli-Expressing Probiotic Bacteria as a Platform for Therapeutics and Diagnostics

Abstract

Extracellular matrix-associated proteins play important roles in host-microbe interactions. We and others have identified curli amyloid fibers, which are major components of the extracellular matrix produced by Enterobacteriaceae during biofilm formation, to be a highly robust and versatile platform for microbial engineering. To exploit these curli amyloid fibers, we have developed a platform called “Biofilm Integrated Nanofiber Display” (BIND), in which we genetically engineered CsgA, a major subunit of curli fibers, to have novel properties either by adding functional domains or by modifying the CsgA sequence to influence the properties of curli fibers.

In this work, we demonstrate the ability of the BIND platform to influence the host-microbe interaction *in vitro*, the amelioration of colitis in murine models using engineered probiotics, the formation of self-renewal living hydrogels, and the non-invasive tracking of engineered bacteria *in vivo*.

We used BIND to rationally design a bacterial strain that could interact with mucosal epithelium models. We engineered a commensal strain of *E. coli* to produce curli fibers fused to the trefoil factor family (TFF) peptides. These engineered microbes showed improved affinity for soluble mucins, Caco-2 intestinal cell lines, and goat intestinal explants. Some curli-TFF conjugates/fusions also enhanced cell migration of simulated Caco-2 wounds, which reflected

their bioactivity comparable to their soluble TFF counterparts. Next, we engineered probiotic *E. coli* Nissle 1917 (EcN) to produce curli-TFFs *in vitro* and *in vivo* and confirmed that these engineered bacteria were non-pathogenic. Inoculation with the probiotic conferred improved protective effects against dextran sodium sulfate induced colitis in mouse models associated with barrier function enforcement and immunomodulation. We also found that engineered commensal *E. coli* expressing curli-TFFs could be fabricated into living hydrogels consisting of concentrated bacterial cultures. Such hydrogels had the ability to selectively interact with the gastrointestinal (GI) tract and to self-renew *in vitro* and *in vivo*. Finally, we demonstrated a method for tracking engineered microbes within the GI tract via non-standard amino acid incorporation into extracellular curli fibers followed by click chemistry-based labeling.

Overall, this work lays the foundation for a novel and versatile platform for creating engineered probiotics with programmable therapeutic and diagnostic functions.

Table of contents

Abstract.....	iii
Table of contents.....	v
Acknowledgements.....	ix
CHAPTER 1 INTRODUCTION.....	1
1.1 ENGINEERED LIVE BIOTHERAPEUTICS	2
1.1.1 Engineered bacteria for therapeutics and diagnostics	2
1.1.2 Clinical and preclinical applications of engineered bacteria	2
1.1.3 Engineered probiotic <i>Escherichia coli</i> Nissle 1917 for clinical applications	4
1.2 ENGINEERING OF BACTERIAL AMYLOID FIBERS	7
1.2.1 Bacterial biofilms and functional amyloids	7
1.2.2 Curli functional amyloid system	9
1.2.3 Biofilm Integrated Nanofiber Display (BIND) system.....	11
1.2.4 Curli fibers and therapeutic applications	13
1.2.5 Inflammatory bowel diseases and trefoil factor family peptides	15
1.3 NON-INVASIVE TRACKING OF ENGINEERED BACTERIA <i>IN VIVO</i>	18
1.3.1 The need for non-invasive tracking of engineered bacteria	18
1.3.2 Non-standard amino acid incorporation into the protein of interest	20
1.3.3 Copper-free click chemistry for biomedical applications.....	22
1.4 DISSERTATION OVERVIEW: TOWARD THE DEVELOPMENT OF CURLI-EXPRESSING PROBIOTIC BACTERIA AS A THERAPEUTIC AND DIAGNOSTIC PLATFORM	23
1.5 REFERENCE	26
CHAPTER 2 MODULATING BACTERIAL AND GUT MUCOSAL INTERACTIONS WITH ENGINEERED BIOFILM MATRIX PROTEINS.....	35
2.1 ABSTRACT	36
2.2 INTRODUCTION	36
2.3 RESULTS AND DISCUSSION.....	39
2.3.1 TFF-fused curli fibers are produced, secreted, and assembled by commensal <i>E. coli</i>	39
2.3.2 Engineered curli matrices bind to mucins and modify their biophysical properties	43
2.3.3 Engineered curli matrix enhances bacterial binding to mammalian cell surfaces	46
2.3.4 Curli-bound trefoil factors maintain their signaling bioactivity	47
2.4 CONCLUSIONS.....	48
2.5 MATERIALS AND METHODS	49
2.5.1 Cell Strains and Plasmids.....	49
2.5.2 Curli nanofiber expression	50
2.5.3 Quantitative Congo Red (CR) binding assays	51

2.5.4	<i>Whole-cell filtration ELISA</i>	51
2.5.5	<i>Semi-purification of curli nanofibers via filtration</i>	52
2.5.6	<i>Adhesion of engineered bacteria to epithelial cells</i>	53
2.5.7	<i>Invasion of engineered bacteria into epithelial cells</i>	53
2.5.8	<i>Mucin binding assay</i>	54
2.5.9	<i>Bacterial binding to gut mucosa ex vivo</i>	54
2.5.10	<i>Rheology of mucin-curli gels</i>	55
2.5.11	<i>Cell migration assay</i>	56
2.5.12	<i>Scanning electron microscopy</i>	56
2.6	ACKNOWLEDGMENTS	57
2.7	REFERENCES	58

CHAPTER 3 ENGINEERED *E. COLI* NISSLE 1917 FOR THE DELIVERY OF MATRIX-TETHERED THERAPEUTIC DOMAINS TO THE GUT..... 62

3.1	ABSTRACT	63
3.2	INTRODUCTION	63
3.3	RESULTS AND DISCUSSION.....	67
3.3.1	<i>Probiotic Associated Therapeutic Curli Hybrids (PATCH)</i>	67
3.3.2	<i>TFF-fused curli fibers are successfully secreted and assembled by engineered <i>E. coli</i> Nissle 1917</i>	68
3.3.3	<i>Engineered curli fibers do not confer pathogenicity to EcN in vitro</i>	71
3.3.4	<i>Engineered EcN can transiently colonize the mouse gut and express curli fibers in situ</i>	74
3.3.5	<i>Engineered EcN ameliorates disease activity in a mouse model of DSS-induced colitis</i>	79
3.3.6	<i>Anti-inflammatory effects of engineered EcN are associated with immunomodulation and barrier function enhancement</i>	84
3.4	CONCLUSIONS.....	87
3.5	MATERIALS AND METHODS	90
3.5.1	<i>Cell strains and plasmids</i>	90
3.5.2	<i>Mice</i>	92
3.5.3	<i>In vitro expression of engineered curli fiber</i>	92
3.5.4	<i>Quantitative Congo Red binding assay</i>	93
3.5.5	<i>Whole-cell filtration ELISA</i>	93
3.5.6	<i>Electron microscopy</i>	94
3.5.7	<i>Cell culture</i>	94
3.5.8	<i>Invasion assay</i>	95
3.5.9	<i>Translocation assay</i>	95
3.5.10	<i>Epithelial integrity</i>	96
3.5.11	<i>IL-8 production</i>	96
3.5.12	<i>In vivo residence time study</i>	96
3.5.13	<i>In vivo imaging of engineered microbes</i>	97
3.5.14	<i>Curli immunohistochemistry</i>	97
3.5.15	<i>Fecal filtration ELISA</i>	98

3.5.16	<i>Dextran Sodium Sulfate (DSS) model of mouse colitis and treatment protocol</i>	99
3.5.17	<i>Determination of disease activity</i>	100
3.5.18	<i>Histological studies</i>	100
3.5.19	<i>Luminex multiplex immunoassay</i>	101
3.5.20	<i>Gene expression analysis by qRT-PCR</i>	102
3.5.21	<i>Statistics</i>	103
3.5.22	<i>Additional tables</i>	104
3.6	ACKNOWLEDGEMENTS	108
3.7	REFERENCES	109

CHAPTER 4 GENETICALLY PROGRAMMABLE SELF-REGENERATING BACTERIAL HYDROGELS 115

4.1	ABSTRACT	116
4.2	INTRODUCTION	116
4.3	RESULTS AND DISCUSSION	118
4.3.1	<i>From bacterial culture to customized hydrogels</i>	118
4.3.2	<i>Genetic modulation of hydrogel material properties</i>	121
4.3.3	<i>Delivery methods and formulations of engineered hydrogels</i>	125
4.3.4	<i>Selective tissue binding of modified curli nanofibers</i>	127
4.3.5	<i>Self-regeneration of biofabricated hydrogel</i>	132
4.4	CONCLUSIONS	135
4.5	MATERIALS AND METHODS	137
4.5.1	<i>Cell strains and plasmids</i>	137
4.5.2	<i>Mice</i>	137
4.5.3	<i>Curli nanofiber expression</i>	138
4.5.4	<i>Preparation of live hydrogel</i>	138
4.5.5	<i>Preparation of cell-free hydrogel</i>	138
4.5.6	<i>In situ hydrogel growth</i>	139
4.5.7	<i>Hydrogel rheology</i>	139
4.5.8	<i>Injection and spraying</i>	140
4.5.9	<i>Nanoparticle formation</i>	140
4.5.10	<i>Cryogel and powder</i>	140
4.5.11	<i>Hydrogel adhesion to goat colon tissue</i>	140
4.5.12	<i>Hydrogel staining with fluorescent dye</i>	141
4.5.13	<i>Oral administration of live gel and GI tract ex vivo optical imaging</i>	141
4.5.14	<i>Live gel residence time</i>	142
4.5.15	<i>Hydrogel stability in simulated GI fluids</i>	142
4.5.16	<i>ELISA of CsgA-TFF2 from fecal samples</i>	142
4.5.17	<i>Probing live gel functionality in vivo</i>	143
4.5.18	<i>Self-generation of living hydrogel</i>	144
4.5.19	<i>Toxicity of hydrogel in vivo</i>	144
4.5.20	<i>MTT assay</i>	144
4.5.21	<i>Electron microscopy</i>	145
4.6	ACKNOWLEDGEMENTS	145

4.7	REFERENCES	146
CHAPTER 5	TRACKING OF ENGINEERED BACTERIA <i>IN VIVO</i> USING NON-STANDARD AMINO ACID INCORPORATION	150
5.1	ABSTRACT	151
5.2	INTRODUCTION	151
5.3	RESULTS AND DISCUSSION.....	155
5.3.1	<i>Azide-containing proteins are successfully secreted and assembled extracellularly from engineered E. coli Nissle 1917</i>	<i>155</i>
5.3.2	<i>Engineered curli fibers containing non-standard amino acids can perform click chemistry in vitro.....</i>	<i>160</i>
5.3.3	<i>Click labeling is specific to mutant curli fibers</i>	<i>162</i>
5.3.4	<i>Labeling efficiency of engineered bacteria.....</i>	<i>163</i>
5.3.5	<i>Engineered probiotic bacteria with mutant curli fibers are able to perform click chemistry in vivo in murine model</i>	<i>164</i>
5.4	CONCLUSIONS.....	168
5.5	MATERIALS AND METHODS	171
5.5.1	<i>Cell strains and plasmids.....</i>	<i>171</i>
5.5.2	<i>Mice.....</i>	<i>173</i>
5.5.3	<i>In vitro expression of curli fibers.....</i>	<i>173</i>
5.5.4	<i>Quantitative Congo Red binding assay.....</i>	<i>174</i>
5.5.5	<i>Whole-cell filtration ELISA.....</i>	<i>174</i>
5.5.6	<i>Electron microscopy</i>	<i>175</i>
5.5.7	<i>Growth curves and doubling times</i>	<i>176</i>
5.5.8	<i>In vitro labeling of click microbes</i>	<i>176</i>
5.5.9	<i>Labeling of simulated curli fiber mats</i>	<i>177</i>
5.5.10	<i>Purification and identification of proteins labeled in vitro</i>	<i>177</i>
5.5.11	<i>Flow cytometry and confocal microscopy</i>	<i>178</i>
5.5.12	<i>In vivo tracking of click microbes</i>	<i>179</i>
5.5.13	<i>Whole GI tract ex vivo fluorescence imaging</i>	<i>180</i>
5.5.14	<i>Whole cecum fluorescence and protein analysis</i>	<i>180</i>
5.6	ACKNOWLEDGMENTS	181
5.7	REFERENCES	183
CHAPTER 6	CONCLUSIONS, LIMITATIONS AND FUTURE DIRECTIONS	188
6.1	SUMMARY	189
6.2	LIMITATIONS.....	192
6.3	FUTURE DIRECTIONS.....	196
6.3.1	<i>Potential of the PATCH platform</i>	<i>196</i>
6.3.2	<i>Improvement of engineered plasmids for the PATCH platform</i>	<i>197</i>
6.3.3	<i>Non-invasive tracking of engineered bacteria with probes that are suitable for human medical imaging</i>	<i>198</i>
6.4	CONCLUDING REMARKS	199
6.5	REFERENCES	201

Acknowledgements

First of all, I would like to express my deepest gratitude to my dissertation advisor, Prof. Neel Joshi. I thank Neel for his encouragement and guidance throughout my Ph.D. journey. He is an amazing role model that I look up to as a scientist. I always appreciated Neel's kindness, practicality and flexibility. Neel granted me freedom to explore different research areas. He always made sure that my research went smoothly and guided me through difficult times. I am lucky to be a part of this wonderful research group and be under Neel's supervision.

Next, I would like to show appreciation to my dissertation committee members, Prof. Wendy Garrett and Prof. David Mooney, for their suggestions and guidance throughout my Ph.D. career. Their expertise in inflammatory bowel disease, microbiome, immunology and bioengineering has been extremely helpful toward the culmination of my work.

I would like to recognize all past and present members of the Joshi lab for bringing joy to the workplace, for creating a culturally diverse environment and for giving me valuable academic guidance. In particular, I thank Anna Duraj-Thatte for being an amazing collaborator and a great friend. She has always been helpful academically and emotionally throughout my six-year journey at Harvard. I will miss all the joy and the dramas, and her party requests. I thank Noémie-Manuelle Dorval Courchesne for collaborating with me in various projects and being a nice friend. I always appreciate Noémie's composure and organizational skills. I thank Martin Nussbaumer, Anton Kan, Giorgia Cannici and Avinash Manjula Basavanna for being nice lab mates and great friends. I will miss the party times we had together. I thank Miguel Suástegui for his help during my job search. I thank Peter Nguyen for giving me academic help and for training me when I first joined the lab.

I would like to acknowledge many graduate and undergraduate students I have met during my time in the lab. I thank Iliia Gelfat for helping me with mouse experiments and asking me interesting questions, which made me think about the projects from a new perspective. I thank Daniel Birnbaum and Richie Tay for always chatting with me about movies and food in the lab. Those conversations made my time in the lab quite enjoyable. I am also grateful to Dan for reading and editing my thesis. I thank Zsofia Magarian for her help during my job search. I thank Ilona den Hartog and Chaochen Lu for being great collaborators and friends. We had an amazing time together during the NSAA project. I am grateful to have Franziska Bahl as my master student mentee. Her friendliness and optimism sparked joy in the lab and the Wyss institute as a whole. I thank all my undergraduate mentees including Trevor Nash, Frederick Ward, Daniel Um, Mofeyifoluwa Edun, Jessica Kim, Harvard Biodesign IGEM 2014 and 2016 teams for all their research efforts. I enjoyed mentoring these amazing undergraduate researchers.

I also benefited from help and advice from many collaborators outside of the Joshi lab. I would like to acknowledge David Benson Chou for his help with histopathology. I thank Amanda Graveline, Frank Urena and Andyna Vernet for training and helping me with many mouse experiments. I acknowledge Frederic Vigneault for his help with the qRT-PCR, Shanda Lightbown for her help with the LUMINEX system, Elaine Lim for her help with the RNA-Seq, Thomas Ferrante for his help with fluorescence microscopes, Garry Cuneo for his help with the flow cytometry, Adam Graham and Carolyn Marks for their support with SEM sample preparation and imaging, Magdalena Kasendra and Rachelle Prantil-Baun for their help with organ-on-chips and the tissue homogenizer, Alexis Rovner for her continuous support in the NSAA project including recombineering troubleshooting and OTS plasmids, and Li Zuo and Prof. Jerrold Turner for their

help with a tight junction protein analysis. I also would like to thank all the other collaborators, lab managers, faculty assistants, and administrative staffs at Harvard SEAS and the Wyss Institute for all their assistance throughout my years at Harvard.

I am grateful for the use of several shared facilities affiliated with Harvard, including the Harvard Digestive Diseases Center (HDDC), the Harvard Center for Nanoscale Systems (CNS) and Harvard Medical School ICCB-Longwood Screening Facility, DF/HCC Rodent Histopathology Core, HMS Biopolymers Facility, and the Wyss Institute for Biologically Inspired Engineering. I acknowledge National Institutes of Health, the Blavatnik Biomedical Accelerator Fund and the Wyss Institute for funding my research. I gratefully acknowledge the Royal Thai Scholarship for the continuous support for my education.

I would like to show gratitude for my friends in the Wyss Institute (Vasanth, Chris, Eneko, Frank), Harvard , Boston and Cambridge (Polnop, Pantra, Wannawiruch, Min, Thiparat, Phoom, Anont, Wichinpong, Pichet, Pete, Janewit, Pornchai, Chaiyaboot, Waradon, Sarita, Apittha, Nutthakorn, Chanat, Nipawan, Supontep, Chonlada, Thitinan, Boonsom, Nicha, Napaporn, Watcharaphol, Taweewat and many more) who made my stay here very pleasant. I would like to acknowledge Anupong, in particular, for thoroughly reading and meticulously editing this dissertation. His contribution has significantly improved the quality of this dissertation and I am gratefully appreciated.

I would like to acknowledge many teachers and friends who have joined me in the educational journey, starting from Jindapong School, Satriwitthaya 2 School (Raphat, Tipwara, Piyachat), Mahidol Wittayanusorn School (Jittikarn, Natnaree, Tararat, Montira, Wanwalai, Arachaporn, Chayanon, Chayoot, Treetases, Prakrit, Pongphak, Puvée, Siwakorn, Nicha, Natcha,

Suparat, Jirayu, Sittipong, Napassawan, Kamolpan, Lapatrada, Roykrong, Paradee, Monthakan, Saralee, Poramapa, Pornhatai, Soraya, Pongsakorn), Royal Thai Scholars (Praphapan, Peerawat, Nudthawud, Pattipong), The Masters School, Duke University (Pantana, Chutima, Sukrit, Atipporn, Teeravit, Nujin, Rudeechanok, Natasha), Harvard University and many more that I have not mentioned. All of you have significantly shaped who I am today and I could not possibly make it to this point without your guidance and friendship.

I am extremely grateful for Justin Cheng, who is always caring, supportive and encouraging me throughout the Ph.D. journey. I am grateful for all the food trips and long vacations that we have had. They kept me sane during all the ups and downs. Thanks for always believing that I can do it.

Finally, I would like to express gratitude to my family who plays essential roles throughout this journey. First of all, I thank my extended family members for their emotional and financial support throughout my life. Next, I am extremely thankful to have my godmother, Mae Long, and my nannies, P'Jam, P'Duan, P'Jeed (and more) in my life. All of them provide me with love and support, and deeply care for me unconditionally as if I was one of their relatives. I could not make it to this point without them. I thank my sister, Patcha (Bow), for bringing the joy to our home and showing me that endurance and hard work are the keys to success. I would like express my deepest appreciation to my parents, Khun Pongchai and Khun Busaba, for their contributions to every aspect of my life. They have raised me to be a fighter, to fight my way through all the hardship in life with my knowledge and skills. Their encouragement and emotional support have contributed to my academic success, and have made this dissertation possible.

I would like to dedicate this dissertation to my parents, Khun Pongchai and Khun Busaba, my godmother, Mae Long, and my nannies, P'Jam, P'Duan, and P'Jeed, for their unconditional love and support.

ความพยายามอยู่ที่ไหน ความสำเร็จอยู่ที่นั่น – สุภาษิตไทย

Where there is a will, there is a way. – English Proverb

Page intentionally left blank

Chapter 1 Introduction

1.1 Engineered live biotherapeutics

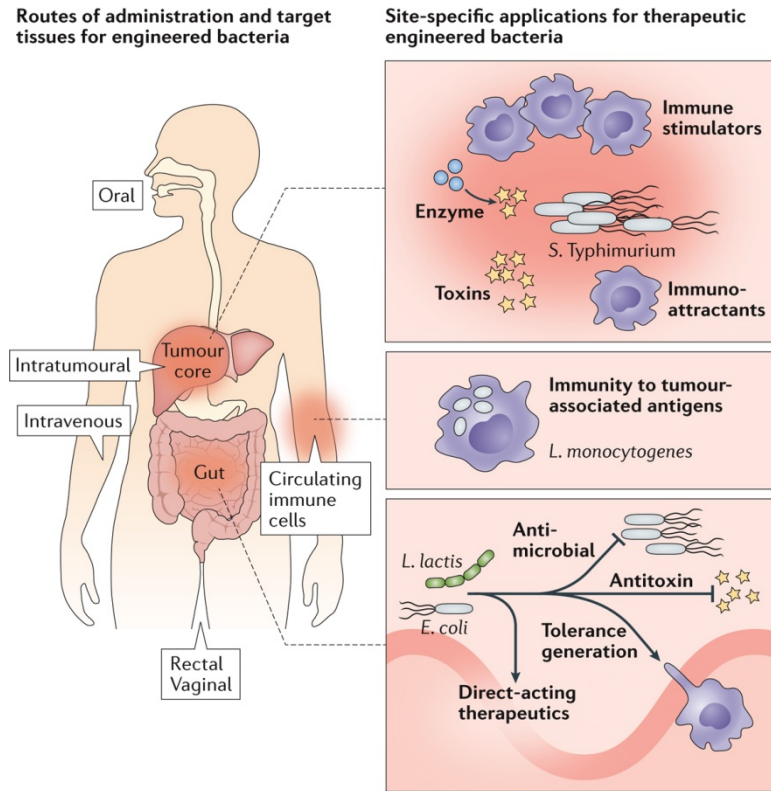
1.1.1 Engineered bacteria for therapeutics and diagnostics

The human microbiome, which refers to a complex ecosystem of bacteria, archaea, protists, yeasts, phages, and other microorganisms residing inside or on the surface of the human body, has a profound influence on human health. This community of well-tolerated microbes occupies the interfaces between the human body and the external environment, including the gut lining, the respiratory tract, the reproductive tract, the mouth, and the skin. Understanding the human microbiome could allow for the development of novel medical technologies to control and prevent many diseases¹. Some microbes can be used to deliver therapeutics to different parts of the body in a targeted and controllable manner². Recent advances in genetic engineering have led to the utilization of genetically engineered bacteria as “smart” therapeutic and diagnostic tools. Their intimate interaction with the human body, responsiveness to environmental cues, and ability to produce and secrete biomolecules of interest could allow engineered microbes to one day exceed the performance of traditional therapeutics and diagnostics³.

1.1.2 Clinical and preclinical applications of engineered bacteria

Numerous examples of preclinical and clinical uses of engineered bacteria have been recently reviewed by Ozdemir et al.² and Riglar et al.³, demonstrating the versatility and applicability of engineered bacteria as a treatment platform. Notable examples include the use of engineered bacteria as therapeutics for specific diseases such as inflammatory bowel disease (IBD)⁴⁻⁷, HIV/AIDS^{8,9}, and cancer¹⁰. Example routes of administration and target tissues for engineered bacteria, as well as their general mechanisms of action involved in the therapeutic

effects, are depicted in Figure 1.1. Attenuated *Salmonella enterica* serovar Typhimurium have been engineered in different ways to home to hypoxic areas at the core of tumors where traditional drugs are unable to reach. These bacteria slow tumor growth by stimulating the secretion of interleukin-2 (IL-2) or the expression of toll-like receptor (TLR) 5 agonists to attract immune cells^{10,11}, hypoxia-induced secretion of cytolysin to induce tumor necrosis¹², and production of cytosine deaminase to convert the prodrug 5-fluorocytosine into the active anticancer drug 5-fluorouracil inside tumors^{13,14}. Another group of engineered bacteria widely used for anticancer therapeutics are attenuated *Listeria monocytogenes* expressing tumor-associated antigens. They have been shown to be safe for delivery to the bloodstream and to stimulate dendritic cells with cancer antigens, leading to immune system activation and tumor clearance¹⁵. Another class of engineered bacteria, designed for gut administration, can be programmed for a wide variety of applications. For example, gut-focused engineered *Lactococcus lactis* have been shown to secrete therapeutic anti-inflammatory molecules including IL-10⁷, IL-27¹⁶, anti-TNF α ¹⁷, and trefoil factor family (TFF) peptides⁴. Many interesting works on engineered *E. coli* to combat gut pathogens, secrete therapeutics, and neutralize toxins are discussed in the next section.



Nature Reviews | Microbiology

Figure 1.1 Examples of mechanisms for engineered living therapeutics. (Left) Routes of administration of engineered bacteria include, but are not limited to, oral, intratumoural, intravenous, rectal, and vaginal. (Right, top) Different mechanisms by which engineered *Salmonella enterica* serovar Typhimurium can target hypoxic tissues at the tumor core, such as the release of toxins, prodrug-cleaving enzymes, immune stimulators, and immune attractants. (Right, middle) Immune cells immunized against cancer cells via engineered *Listeria monocytogenes*. (Right, bottom) Engineered *Lactococcus lactis* or *Escherichia coli* release therapeutics, induce immunotolerance to autoantigen, and protect the host against toxins and pathogens within the gut. Reprinted by permission from Springer Nature Customer Service Centre GmbH: Springer Nature, Nature Reviews Microbiology, Riglar et al³, Copyright© 2018.

1.1.3 Engineered probiotic *Escherichia coli* Nissle 1917 for clinical applications

Since its discovery in 1917, *E. coli* Nissle (EcN) has been used in humans to treat various GI-related conditions and is currently available on the dietary supplement market as Mutaflor¹⁸⁻²⁰. Due to its transient colonization in humans, genetic tractability, long-term track record of human use, and outstanding safety profile, EcN is one of the most prevalent organism chassis for engineered live therapeutics and diagnostics^{21,22}. As shown in the mechanistic illustration in Figure

1.1, there have been several recent works on engineered EcN utilizing synthetic biology to combat pathogens and toxins. For example, Duan et al. programmed EcN to produce cholera autoinducer 1 (CAI-1), a quorum sensing molecule, to prevent the virulence of *Vibrio cholera* in a mouse model²³. Hwang et al. engineered EcN to sense and kill *Pseudomonas aeruginosa* *in vitro* and in *Caenorhabditis elegans* and mouse models²⁴. Similarly, Paton et al. utilized *E. coli* R1 strain to recombinantly express a surface displayed Shiga toxin receptor mimic that could absorb and neutralize Shiga toxin effectively in a mouse model²⁵.

In addition to directly producing therapeutics, EcN can be programmed to interface with natural metabolites *in situ*. For instance, Ho et al. engineered EcN to bind specifically to heparin sulfate proteoglycans displayed on colorectal cancer cells and to secrete myrosinase. Myrosinase converts glucosinolates, which are components of cruciferous vegetables, into the anticancer molecule sulforaphane, thereby inhibiting various models of colorectal cancer *in vitro* and *in vivo*²⁶. Synlogic, a company that centers its products on engineered EcN as a therapeutic platform, recently reported two revolutionary works on utilizing engineered EcN for treatments of metabolic syndromes. The first work focused on phenylketonuria (PKU), a genetic disorder characterized by the patients' inability to metabolize phenylalanine (Phe). Synlogic designed EcN to produce Phe-metabolizing enzymes in response to anoxic conditions within the GI tract. The engineered EcN reduced the blood Phe level in a PKU mouse model and a healthy monkey model. The authors also devised ways to detect biomarkers of strain activity and to study the pharmacodynamic properties of the strain using fecal samples²⁷. The second work focused on hyperammonemia, a metabolic disorder characterized by an excess of ammonia in the blood as a result of urea cycle disorders and hepatic encephalopathy. In this case, the authors engineered EcN to convert ammonia to L-arginine

and showed the effectiveness of the strain *in vitro* and in ornithine transcarbamylase-deficient and thioacetamide-induced liver injury mouse models of hyperammonemia²⁸.

Besides the efforts on utilizing EcN as therapeutics, EcN has been designed for use in diagnostic applications. For example, Danino et al. discovered that EcN could selectively expand in metastatic liver cancer cells in mice via the hepatic portal system, and they leveraged this knowledge to devise a method for detecting liver metastasis in mice. They engineered EcN with a stable recombinant plasmid system (required no antibiotic) to express LacZ reporter that would cleave systemically delivered substrates creating small molecules detectable in the urine, thus indicating the liver metastases in the mouse model²⁹. Daeffler et al. and Riglar et al. concurrently developed systems for EcN to sense tetrathionate and thiosulfate, which are produced during gut inflammation, by expressing the tetrathionate and the thiosulfate sensing systems from *S. typhimurium*. The engineered EcN were used for the *in vivo* sensing of inflammation in a mouse model of DSS induced colitis^{30,31}. Palmer et al. modified this system further so that EcN would not only sense the tetrathionate during a *Salmonella* infection but also respond by producing microcins to inhibit the growth of *Salmonella in vitro*³². More examples of engineered EcN for biomedical applications have been reviewed in Ou et al.³³ and Pedrolli et al³⁴. As synthetic biology and genetic engineering advance, scientists can take advantage of the sense-and-respond system in live therapeutics to create better theranostic medicines that simultaneously detect and inhibit the disease, enabling more effective treatments compared to traditional medicines. In the next section, the specific tools that we have chosen for the engineering efforts in this dissertation are discussed.

1.2 Engineering of bacterial amyloid fibers

1.2.1 Bacterial biofilms and functional amyloids

Microorganisms in nature do not live as suspended single cells. Rather, they gather at air-liquid or solid-liquid interfaces to form polymicrobial structures such as films, sludges, flocs, or “biofilms” (Figure 1.2A). Microbes contribute about 10% of the biofilm dry mass, while the extracellular matrix makes up the rest. The extracellular materials, mostly produced by the organisms, are known as extracellular polymeric substances (EPS), which consist of extracellular DNA (eDNA), polysaccharides, and proteins (Figure 1.2B). The matrix protects organisms against harsh environmental conditions such as desiccation, antibiotics, host immune defense, etc³⁵. Because of these properties, biofilm components are often considered virulence factors, and researchers are actively studying the dispersion of biofilms as a means to prevent virulence³⁶⁻³⁹.

However, looking at biofilms from a different perspective, we observe many properties that make biofilms appropriate for programmable and modular extracellular nanomaterials. Such properties include the ability to withstand harsh conditions, large surface area, the ability to alter bacterial adhesion to surfaces, and, most importantly, the ability to self-renew due to the presence of embedded live bacteria⁴⁰. Researchers have attempted to engineer different components of biofilms including different polysaccharides, which made up the bulk of biofilms. Nevertheless, efforts have had limited success due to the complex metabolic engineering required to alter non-standardized polysaccharide production pathways. In contrast, protein components of the biofilms tend to be relatively easy to manipulate as one can directly alter the genes that encode for such proteins using genetic engineering⁴¹.

Proteinaceous components in the EPS include cell surface adhesins, flagella and pili, secreted extracellular proteins such as enzymes and microcins, outer membrane vesicle proteins, and functional amyloids⁴². Functional amyloids are fiber forming proteins that provide structural integrity to many biofilms. They are characterized by the “cross- β ” structure where β -sheets run parallel to the axis of the fiber and each fiber consists of multiple such β -sheets stacked together vertically⁴³. Such protein fibers are highly resistant to proteolysis, self-replicative, and self-assembling. They can be found in many organisms, ranging from bacteria to mammals. Besides providing the biofilm’s structural integrity, functional amyloids can adopt functions such as adhesion during biofilm formation, aerial structure formation, regulation of melanin synthesis, and information transfer⁴⁴. Because of their physical and biochemical robustness, genetic tractability, self-assembling property, and presence across many species, we were particularly interested in an engineering platform using functional amyloids. We believed that such engineering efforts to program the properties of functional amyloids would be impactful for many applications outlined in Figure 1.2C and in upcoming sections. We have identified a suitable starting point for our engineering effort to be the curli functional amyloid system from *E. coli*.

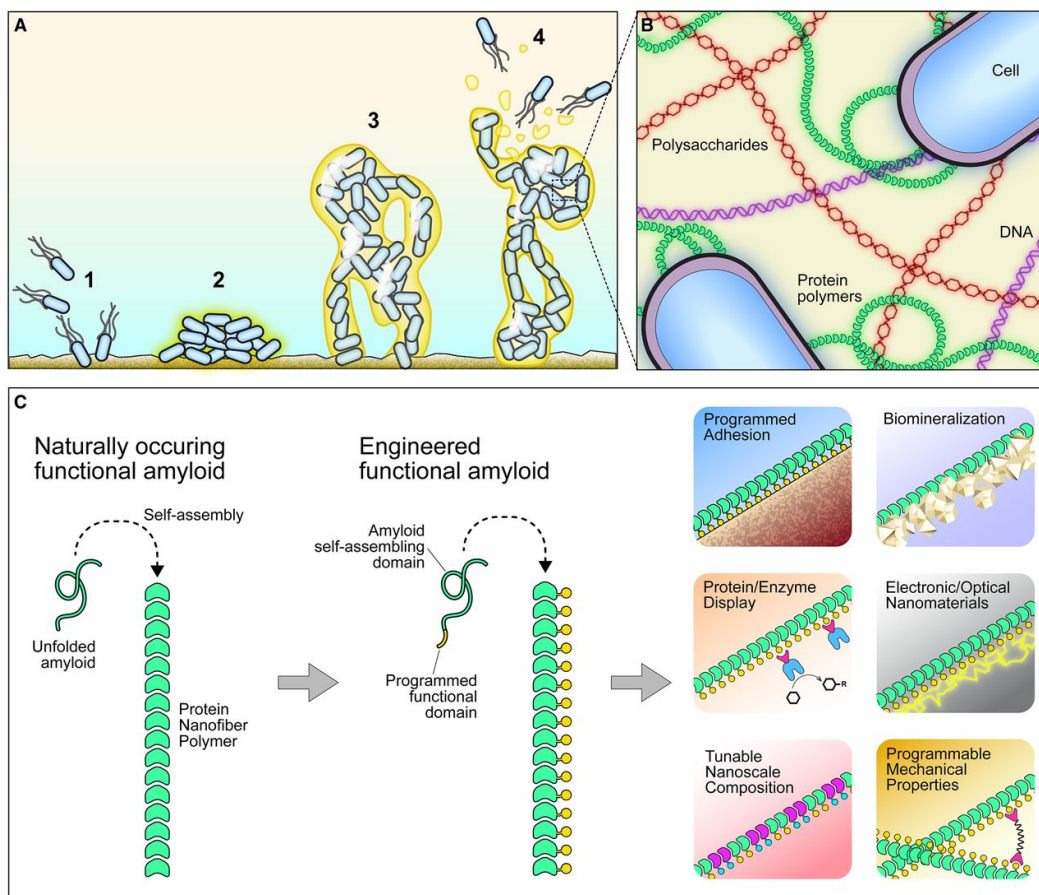


Figure 1.2 Bacterial biofilms and synthetic biology for engineered biofilm matrix. (A) Schematics of biofilm formation, (B) Major biofilm components including cells and EPS, which consists of eDNA, polysaccharides and protein polymers, (C) Comparison between naturally occurring functional amyloids and engineered functional amyloids as well as, the artificially programmed functions and applications of engineered functional amyloids. Reproduced from Nguyen et al.⁴⁵ (Open Access).

1.2.2 Curli functional amyloid system

Curli fibers are extracellular nanofibers produced by *Enterobacteriaceae* that provide structural integrity to their biofilms. The structure of curli is relatively conserved among *E. coli* and *Salmonella* species^{43,46}. Seven genes in the “curli operons”, or the bi-directional *csgBAC* and *csgDEFG* operons, collaborate during curli biogenesis. CsgD is the master regulator that activates transcription of the *csgBAC* operon. Similar to other functional amyloids, curli fibers consist of β -sheet-containing subunits: the major curlin subunit CsgA and the minor curlin subunit CsgB. CsgA

is produced in an unfolded conformation in the cytoplasm and gets secreted into the periplasm via the SecYEG pathway. In the periplasm, CsgC works as a chaperone to keep CsgA from premature folding. CsgG complexes with CsgE and CsgF to effectively secrete CsgA across the outer membrane, where CsgA starts to assume a β -sheet-rich conformation when coming in contact with CsgB. CsgB is proposed to help initiate the nucleation and polymerization of CsgA onto the cell surface (Figure 1.3) ⁴⁷⁻⁴⁹. This process results in curli nanofibers (4-7 nm in diameter, tens of microns in length) that are extremely resistant to harsh conditions such as extreme pH, boiling temperature, and exposure to organic chemicals, detergents, or proteases⁵⁰.

As mentioned previously, we and others have conceived the idea of engineering functional amyloids as a platform for programmable nanomaterial production^{40,51}. Recognizing the modularity of the CsgA monomer, we envisioned using genetic engineering to alter its sequence or to append functional domains, such that the engineered CsgA would have physical and biochemical properties that are tailored to the desired applications. This has led to the birth of the Biofilm Integrated Nanofiber Display (BIND) platform, which is discussed in the next section.

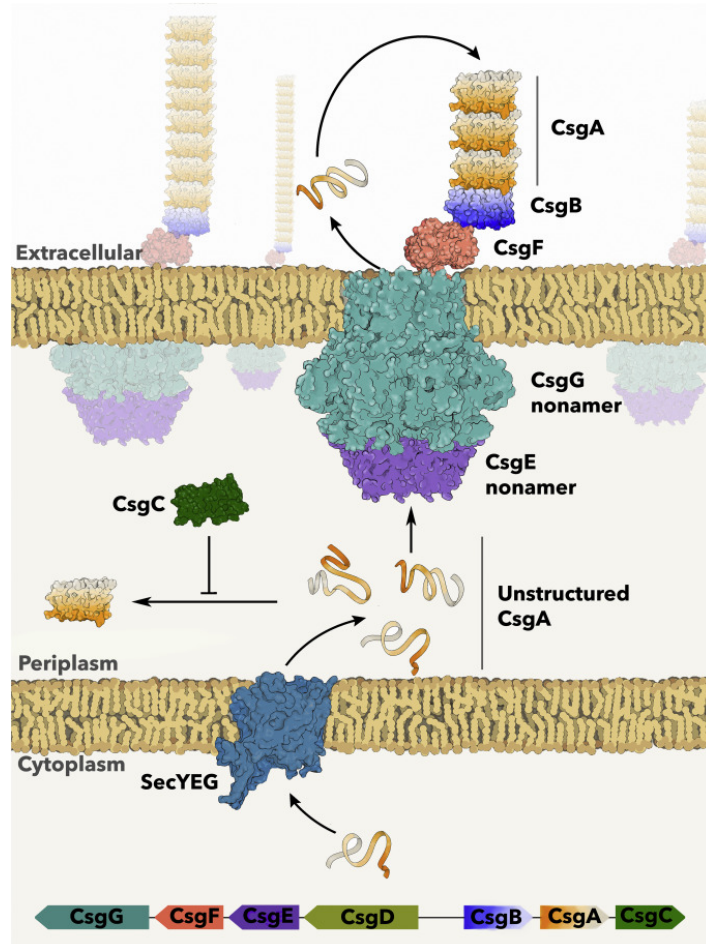


Figure 1.3 Schematic of curli biogenesis. Starting from the *csg* bi-directional operon at the bottom, unfolded CsgA is secreted through the SecYEG pathway and kept in the unfolded state by CsgC. Soluble CsgA is secreted through the CsgG pore and CsgE nonamer complex. CsgA assumes a β -sheet-rich conformation and polymerizes through CsgB-mediated nucleation. Reprinted from Deshmukh et al⁴⁹, Copyright© 2018, with permission from Elsevier.

1.2.3 Biofilm Integrated Nanofiber Display (BIND) system

Our method for engineering curli nanofibers starts with a straightforward concept: the introduction of a functional peptide domain to the C-terminus of the *csgA* sequence via genetic engineering. This creates a chimeric protein containing a CsgA monomer fused with a functional domain. The chimeric protein is then produced and secreted extracellularly with the help of the curli operon members. The CsgA fusion protein can undergo polymerization and form a curli nanofiber network, displaying the fused functional peptide that can alter the property of the fiber

network in a controllable manner⁴⁰. Some of the properties that we initially aimed to engineer into the curli fibers included adhesion to specific surfaces, nanoparticle templating, enzyme catalysis, covalent or non-covalent affinity tag display, and hydrophobicity and conductivity modulation⁴⁵. One of the benefits of this method is that, with the desired property in mind, one could search the existing literature for the peptide sequence of interest and use molecular cloning techniques to add the sequence directly to CsgA, giving rise to endless possibilities for the platform. We call this platform “Biofilm Integrated Nanofiber Display” or BIND (Figure 1.4)⁴⁰.

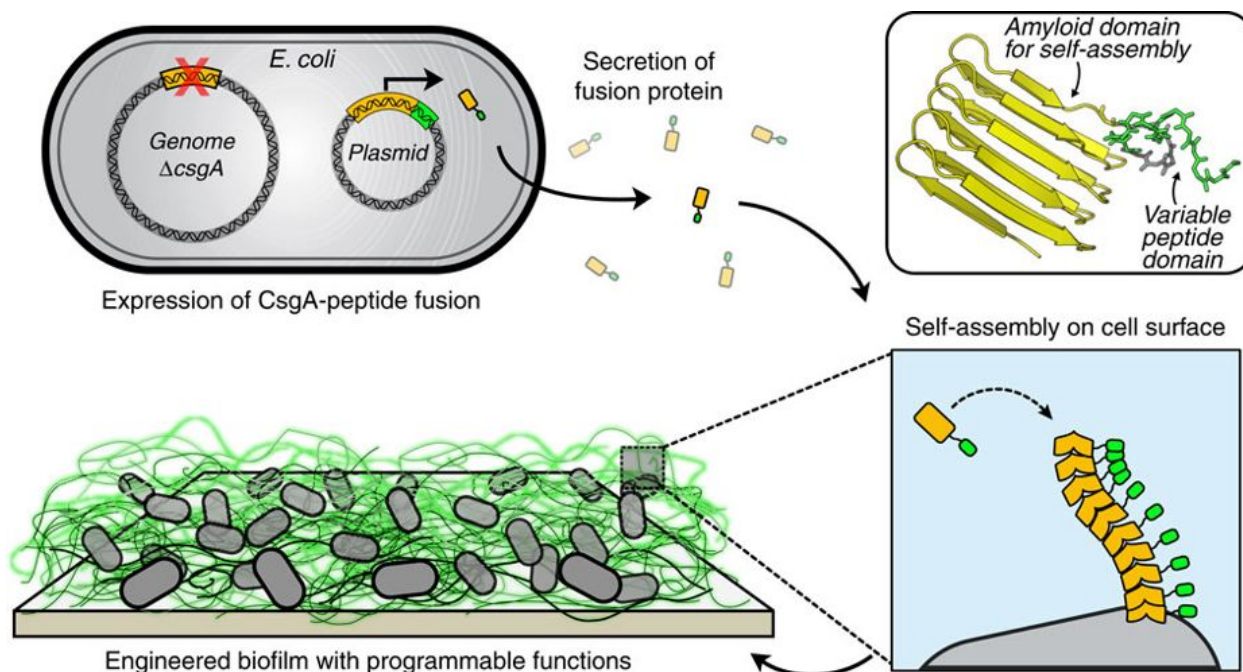


Figure 1.4 Schematic of the BIND platform. *E. coli* $\Delta csgA$ recombinantly expresses and secretes fusion proteins containing a CsgA domain (yellow) and a functional peptide domain (green). The CsgA fusion proteins self-assemble into extracellular amyloid fiber networks tethered to the cell surface. Reprinted by permission from Springer Nature Customer Service Centre GmbH: Springer Nature, Nature Communications, Nguyen et al⁴⁰, Copyright© 2014.

We have validated this concept through a series of research efforts. Nguyen et al. demonstrated the feasibility of this concept by appending twelve different peptides, with sizes ranging from 7 to 59 amino acids to CsgA. These peptides had various functions such as templating

nanoparticles, binding to metals, covalently bonding with larger peptide pairs, etc. Eleven out of the twelve of those fusions were successfully expressed, and maintained amyloidogenic properties. Moreover, the engineered curli nanofibers exhibited programmable functions based on their fused peptides⁴⁰. Catalytic surfaces could also be created by covalently immobilizing SpyCatcher-fused enzymes onto curli nanofiber networks displaying SpyTag^{52,53}. In addition, engineered curli fibers have been used to absorb precious rare earth elements or remove mercury for bioremediation of water^{54,55}. The BIND system could also be scaled up using a filtration purification to obtain highly pure engineered nanofibers, thus allowing large-scale abiotic production of nanomaterials⁵⁶.

Concurrently, other research groups also used engineered curli systems for different applications. Chen et al. programmed the fiber assembly of engineered CsgA into block copolymers with two different functions⁵⁷. Van Gerven et al. pushed the size limit of the CsgA-fused peptide to 260 amino acids without compromising protein production, secretion, and fiber formation, further expanding the choice of functional proteins that could be utilized in this system. Nevertheless, the folding and secondary structure of the fusion domains should be taken into consideration⁵⁸. This set of examples shows the versatility of the BIND system. In this thesis, we considered the utility of this platform for biomedical applications by combining it with engineered probiotics.

1.2.4 Curli fibers and therapeutic applications

To consider using curli fibers as a therapeutic platform, we must evaluate their interaction with the host's GI tract and how that influences the immune system of the host. There is a complex interplay between the host immune system and curli. Conflicts in the scientific literature have arisen between curli-associated bacterial virulence and the beneficial effects of curli. Indeed, some

works on *S. typhimurium* and *E. coli* infection showed that the infection is associated with curli expression, indicating that curli might play some role as a virulence factor for these bacteria^{59,60}. However, a counterargument is that curli might also play a protective role by priming the immune system and enhancing epithelial barrier functions⁶¹. It is known that curli fibers are recognized by the immune system, leading to a signaling cascade that impacts the interaction between host and microbes. The immune cells recognize curli via the TLR2/TLR1/CD14 heterocomplex⁶²⁻⁶⁴. Intestinal epithelial cells respond directly to curli fibers, causing the activation of the PI3K pathway. This reduces epithelial barrier permeability, leading to lower bacterial invasion to underlying tissues (Figure 1.5)⁶⁵. Curliated commensal bacteria may exert barrier protective effects through this mechanism, but additional work is required to confirm such a complex interaction⁶¹.

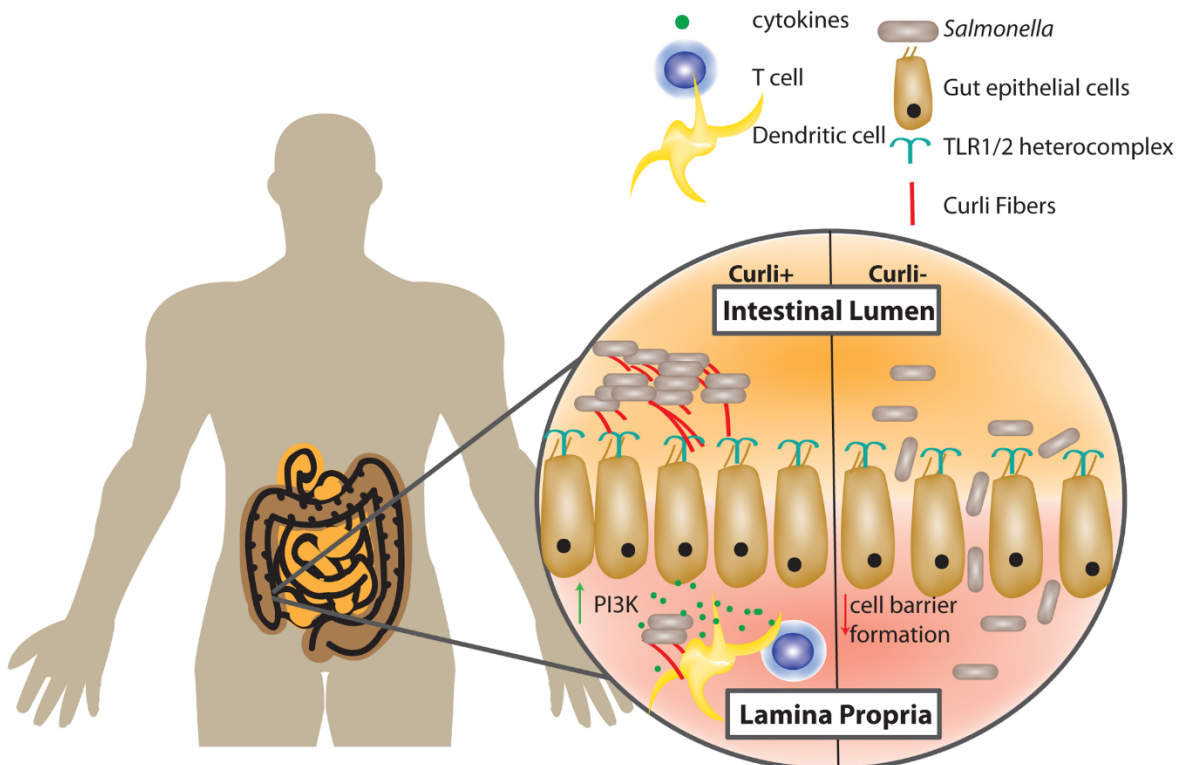


Figure 1.5 Gut epithelial cells and the immune system recognize curli fibers through TLR2/1 heterocomplex, causing PI3K signaling cascade upregulation. This leads to an increase in barrier function. Reproduced from Hufnagel et al⁶¹ (Open Access).

Besides the interaction with the immune system, TLR2 agonists and curli fibers have been shown to have some anti-inflammatory activity within the GI tract. Mutations in the TLR2 gene have been associated with more severe symptoms in a subset of IBD patients. The reduction in TLR2 signaling may result in reduced commensal-dependent intestinal barrier defense, leading to mucosal injury and increased susceptibility to colitis. In contrast, treatment with synthetic TLR2 agonists to activate the TLR2 signaling cascade has led to reduction in mucosal inflammation by augmenting tight junction-associated barrier integrity of the intestinal epithelium and possibly TLR2-induced anti-inflammatory immune responses⁶⁶⁻⁶⁸. Similarly, curli fibers which can be recognized through TLR2/1 receptors have been shown to activate the TLR2 pathway, leading to IL-10 production, and thus reduce the severity of TNBS-induced colitis in a mouse model⁶⁹. With these preliminary evidences, we have decided to test the feasibility of the BIND platform in combination with probiotic EcN as a possible therapeutic candidate for IBD.

1.2.5 Inflammatory bowel diseases and trefoil factor family peptides

Inflammatory bowel disease (IBD), including Crohn's disease and ulcerative colitis, is a set of autoimmune diseases characterized by excessive inflammation in parts of the digestive tract (Figure 1.6). The etiology of the disease is not well understood, but genetic predisposition, immune system disorders, and environmental factors all seem to contribute. IBD are chronic diseases with no cure. Treatment to maintain remission involves the use of anti-inflammatory drugs ranging from aminosalicylates to corticosteroids to biologics, depending on the severity of the disease⁷⁰. Biologic drugs are usually quite potent for patients with severe symptoms, but systemic delivery of such drugs can lead to unwanted side effects, and not all patients respond well to the drugs. The heterogeneity of the disease, which involves a complex interplay between many cytokines and

redundant pathways, also hinders the development of highly effective drugs. Many drugs such as anti-IL17A, anti-IL13, IL10, etc. have not fared well in clinical trials, and many other biologics under development are predicted to be faced with similar challenges⁷¹.

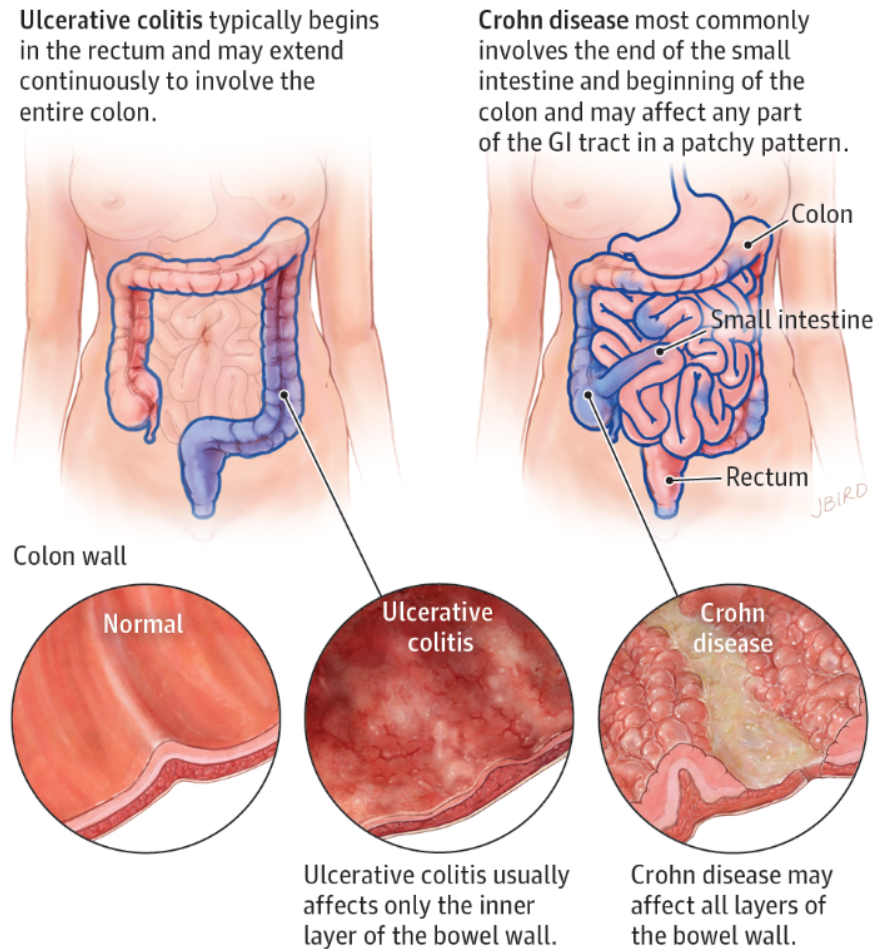


Figure 1.6 Characteristics of Crohn's disease and ulcerative colitis. Reproduced with permission from Jin et al.⁷² Copyright© 2014 American Medical Association. All rights reserved.

With the knowledge that IBD is profoundly associated with gut microbial dysbiosis, researchers have come up with ways to restore the balance to the gut microbiome, such as by using antibiotics, probiotics, microbial consortia, engineered microbes, and fecal transplant. These approaches are still under development and have not shown a clear clinical outcome yet⁷³. We are particularly interested in the local treatment of IBD symptoms using engineered probiotic bacteria.

As mentioned earlier, most existing IBD drugs are systemic anti-inflammatory agents, leaving room for the development of local microbial therapeutics inside the GI tract. Systemic anti-inflammatory drugs and local microbial therapeutics may be combined to attack the disease from both sides, potentially producing a synergistic outcome. We envisioned using the BIND platform as a tool for engineering probiotic EcN for the treatment of IBD. We think that IBD represents an appropriate first disease model for developing the BIND platform toward biomedical applications because IBD is strongly associated with microbial imbalance and because curli already has some baseline anti-inflammatory activity.

As for the functional domains that would be fused to CsgA and displayed on the curli fibers for this specific IBD application, we have chosen the trefoil factor family (TFF) peptides (Figure 1.7) based on multiple rationales. First, the lengths of TFFs are well within the limit of peptides that can be fused and secreted with CsgA. Next, the secondary structures of the TFFs make them resistant to degradation by gastrointestinal proteases and to mechanical stress⁷⁴. It is also known that TFFs have strong binding to mucosal surfaces, which could give a selective advantage to EcN expressing curli fused TFFs by promoting binding to the mucosa⁷⁴⁻⁷⁶. Lastly, but most importantly, TFFs may confer therapeutic effects against IBD via epithelial restitution and barrier function enhancement, which are underexplored mechanisms in traditional IBD treatment. Epithelial restitution refers to the process in which epithelial cells migrate over the denuded area of the gut mucosa. In this process, the cells are vulnerable to apoptosis. TFFs are known to have anti-apoptotic effects and to enhance epithelial cell migration, thereby promoting epithelial restitution of cells over the ulcerative areas. Moreover, TFF3 has been shown to help maintain the tight junction proteins and enhance intestinal barrier function. This decreases mucosal permeability,

these conditions and to facilitate the development of therapeutics that could alleviate these symptoms. Study of the microbiome can be broadly divided into two categories. The first set of techniques focuses on bioinformatics of patient specimens such as fecal samples, rectal swabs, and colonic lavage. These specimens can be analyzed via 16S rRNA gene amplicon sequencing, whole genome shotgun sequencing, metabolomics, transcriptomics, etc., to reveal microbial diversity in the subject, temporal changes in such diversity (if multiple samples are collected over time), and inferred functions of the microbial community. However, these types of bioinformatics studies are not designed to capture host-microbe interactions⁷⁹. On the other hand, another set of techniques relies on harvested tissues, such as luminal brush samples and biopsies from patients or GI tract tissues from lab animals that contain components from both the host and the microbe. These tissues can be analyzed via histological examination, fluorescence *in situ* hybridization (FISH), or immunostaining to reveal spatial distribution of the microbial contents and host-microbe interactions (Figure 1.8). These processes happen at the endpoint of animal experiments or require a tissue biopsy, hindering longitudinal time-lapse study^{79,80}. Thus, there is a need for a less invasive technique to track the spatiotemporal dynamics of microbes *in vivo*. Such a technique could be used to reveal real-time information about the interactions of microbes inside the host, which would be important for the study of microbiome-related diseases and for the development of engineered bacteria for therapeutic and diagnostic applications. Since engineered microbes multiply over time inside the host, they do not exhibit a typical pharmacokinetic profile like traditional drugs. With non-invasive, real-time tracking of engineered microbes, we can visualize their distribution and trafficking inside the body, which would be helpful for understanding their pharmacokinetic profiles and hence the dosages required for treatment.

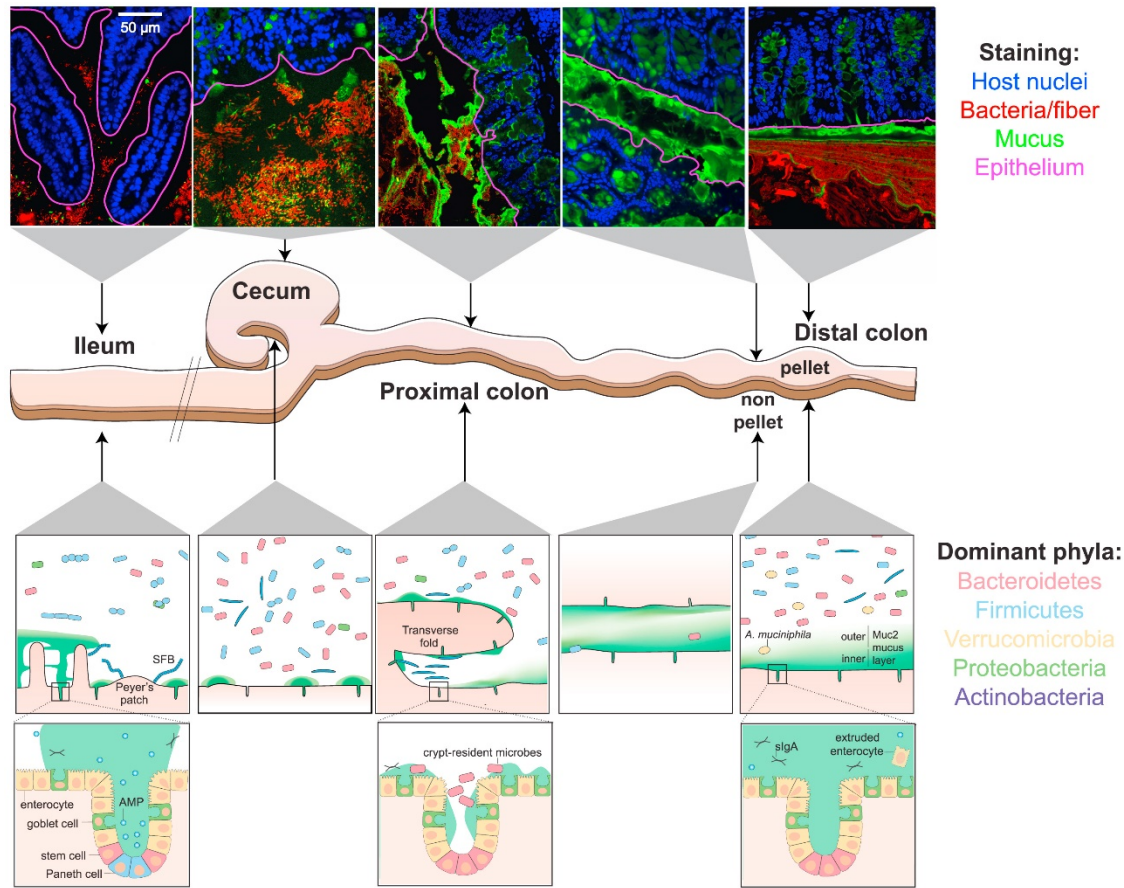


Figure 1.8 Biogeography of mouse gut microbiota. (Top) confocal micrographs of tissue sections with corresponding stain identifiers on the right panel. (Middle) the schematic of corresponding localization in the GI tract. (Bottom) the schematic of types of bacteria, mucus layers, and epithelia of each section along the GI tract. Phyla names are indicated to the right. Reprinted from Tropini et al.⁸⁰, Copyright© 2017, with permission from Elsevier.

1.3.2 Non-standard amino acid incorporation into the protein of interest

One way to perform real-time microbiota imaging would be to engineer the microbes to express fluorescent or luminescent proteins, which can be tracked in a non-invasive manner using *in vivo* imaging systems (IVIS). However, this approach would be restricted to small animals because light emitted from fluorescence or luminescence is too weak to penetrate the skin of large animals⁸¹⁻⁸³. Therefore, to perform *in vivo* tracking of engineered microbes inside humans, one

must be able to selectively label the microbes of interest in the natural gut environment with probes that enable non-invasive imaging techniques such as MRI and PET/CT scans.

Non-invasive, bioorthogonal click chemistry is a powerful tool that could be used to conjugate not only fluorescent probes but also MRI and PET/CT probes to target proteins in engineered gut microbes⁸⁴⁻⁸⁷. To allow click chemistry labeling to occur on bacterial surfaces, click chemistry components must be programmed into the bacteria. Geva-Zatorsky et al. incorporated engineered oligosaccharides containing azide groups onto the surface of *Bacteroides fragilis* and other gut bacteria and performed click chemistry labeling with fluorescence probes before administering them into mice. This method allowed *in vivo* tracking of the bacteria, revealing different microbial niches, colonization, and host-microbe interaction over a limited amount of time⁸⁸. However, because the labeling is performed outside the animal before administration, the signal would fade over time, preventing long-term monitoring of target bacteria *in vivo*.

Recent developments in synthetic biology have allowed non-standard amino acids (NSAAs) to be incorporated into engineered proteins in *E. coli*. A synthetic vector such as pEVOL, which contains an orthogonal translational system from *Methanocaldococcus jannaschii*, allows the incorporation of NSAAs into mutant proteins containing in-frame amber stop codons (UAG)^{89,90}. Over fourteen different NSAAs have been incorporated using the pEVOL system including *p*-azido-L-phenylalanine (pAzF), which contains an azide group for the click reaction⁸⁹. The pAzF amino acid could be incorporated into engineered microbes to enable bioorthogonal click chemistry labeling. Furthermore, the Church lab and the Isaacs lab have generated a recoded *E. coli* strain that does not contain any amber stop codon and release factor-1, which is the factor responsible for ribosomal release at the amber codon, thereby eliminating unwanted NSAA

incorporation into native proteins and premature termination of engineered amber codon-containing proteins^{91,92}. These works show that it is possible to program microbes such as engineered EcN to incorporate NSAAs for *in vivo* labeling with minimal off-target effects on the bacteria.

1.3.3 Copper-free click chemistry for biomedical applications

In order to perform *in vivo* labeling of azide-displaying bacteria, one can utilize copper-free click chemistry, which is selective, kinetically favorable, physiologically stable and bio-orthogonal. The traditional click reaction requires copper as a catalyst. The cytotoxicity of copper has limited the application of click chemistry *in vivo*. However, copper-free click chemistry has emerged as a less toxic alternative. The Strain Promoted Azide-Alkyne Click (SPAAC) reaction between dibenzocyclooctyne (DBCO) and azide (Figure 1.9) does not require copper for catalysis and can occur *in vivo* without interfering with native biochemical processes⁹³. Successful proof-of-concept studies demonstrated the utilization of the SPAAC reaction for *in vivo* labeling of chondrocytes, brain sialoglycans, and tumor cells⁹⁴⁻⁹⁶. Therefore, it is promising that this reaction could be adopted for *in vivo* labeling of engineered bacteria displaying azide groups. The incorporation of NSAAs into the engineered bacteria and the use of SPAAC reaction to label those microbes *in vivo* were combined to achieve a proof-of-concept study described in the next section.

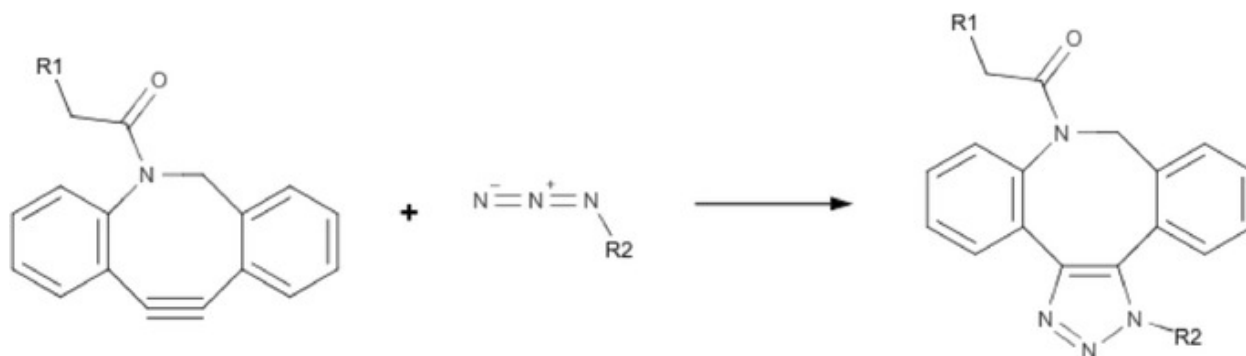


Figure 1.9 The Strain Promoted Azide-Alkyne Click (SPAAC) reaction of dibenzocyclooctyne (DBCO) and azide⁹³ (Open Access).

1.4 Dissertation overview: Toward the development of Curli-expressing probiotic bacteria as a therapeutic and diagnostic platform

This dissertation focuses on the development of engineered probiotic bacteria as a platform for therapeutics and diagnostics. The motivation of this work is to combine BIND, a microbial engineering platform for building living scaffolds with programmable functions, with probiotic bacteria to display therapeutic proteins and enable *in vivo* bacterial labeling. We began with an *in vitro* proof-of-concept work showing engineered *E. coli* expressing functional trefoil factor family (TFF) peptides on curli fibers. The work is then expanded to the incorporation of BIND into probiotic *E. coli* Nissle 1917 (EcN) capable of expressing curli fused TFFs, *in vitro* and *in vivo* testing for therapeutic efficacy, and generation of living hydrogels as an alternative delivery mode. In addition, non-invasive tracking of engineered EcN using non-standard amino acid (NSAA) incorporation and copper-free click chemistry is also studied in this work to demonstrate *in vivo* labeling of bacteria as well as the versatility of the platform.

In chapter 2, knowing that extracellular appendages play an important role in mediating host-microbe interaction, we proceeded to engineer curli fibers from a commensal strain of *E. coli* to

rationally program their interaction with the mucosal epithelium. The *E. coli* were designed to produce chimeric curli fibers fused to TFF domains. Compared to wild-type fibers, the biofilms of the engineered bacteria demonstrated preferential binding to mucins, Caco-2 intestinal epithelial cells, and goat intestine explants, and they also modulated mucin rheology. When treated with purified curli fused TFFs, Caco-2 cells behaved similarly in terms of cell migration behaviors as when they were exposed to soluble TFFs, especially with curli-TFF3 fusion, which could accelerate cell migration compared to other groups. This work demonstrated the potential usage of curli fibers and the BIND platform for the display of bioactive domains that could influence host-microbe interactions as well as exert therapeutic effects.

In chapter 3, we proposed to engineer probiotic bacteria capable of inducing epithelial healing as a novel treatment for inflammatory bowel disease (IBD). Following the work in chapter 2, we genetically engineered EcN to produce curli fused TFFs, which are known to promote intestinal barrier function and epithelial restitution. We confirmed that EcN were able to secrete engineered fibers *in vitro* and in the mouse gut. We observed a protective effect from EcN expressing curli fused TFF3 against a dextran sodium sulfate induced colitis murine model. The effect was associated with barrier function improvement and immunomodulation. This work sets a precedent for the utilization of the engineered curli platform in probiotic bacteria to produce therapeutic protein networks.

In chapter 4, we demonstrated a novel class of materials using engineered *E. coli* expressing curli fusions to create live bacteria-embedded hydrogels. Such materials were generated by concentrating curli-producing cultures and treating the concentrated cultures with surfactants. The living hydrogels were able to grow and self-renew when incubated in growth promoting

conditions. Their rheological properties could be modulated at the genetic level or at the manufacturing level. The hydrogels could be customized through genetic engineering to interact with components of the gastrointestinal tract. This hydrogel offers a new way to deliver the engineered bacteria embedded in pre-produced, therapeutic curli fibers, which can react to sites of diseases such as ulcers promptly while maintaining the ability to release the engineered bacteria over time.

In chapter 5, we switched the focus from therapeutic applications to the diagnostic application of non-invasive tracking of engineered bacteria. We programmed the bacteria to incorporate NSAAs into surface displayed curli fibers and labeled them via copper-free click chemistry. We engineered EcN to incorporate *p*-azido-L-phenylalanine (pAzF) in place of the amber stop codon by utilizing an orthogonal translation system (OTS). The amber stop codon was introduced to CsgA, a subunit of curli fibers, resulting in curli fibers displaying azide groups from pAzF, which could be labeled via the click reaction with a Cy5-dye conjugated with a dibenzocyclooctyne (DBCO) group. We demonstrated the labeling *in vitro* and in a mouse model. We found the labeling to be detectable for several days after the administration of the dye. This work sets a groundwork for the development of *in vivo* bacteria labeling techniques which could be compatible with other imaging modalities like MRI or PET/CT.

The primary conclusions of the dissertation are presented in chapter 6, together with recommendations for future research based on this dissertation.

1.5 Reference

1. Arnold, W. M. *et al.* in *Genomic Applications in Pathology* (eds George Jabboure Netto & Karen L. Kaul) 783-798 (Springer International Publishing, 2019).
2. Ozdemir, T., Fedorec, A. J. H., Danino, T. & Barnes, C. P. Synthetic Biology and Engineered Live Biotherapeutics: Toward Increasing System Complexity. *Cell Syst.* **7**, 5-16 (2018).
3. Riglar, D. T. & Silver, P. A. Engineering bacteria for diagnostic and therapeutic applications. *Nature Reviews Microbiology.* **16**, 214 (2018).
4. Vandenbroucke, K. *et al.* Active delivery of trefoil factors by genetically modified *Lactococcus lactis* prevents and heals acute colitis in mice. *Gastroenterology.* **127**, 502-513 (2004).
5. Vandenbroucke, K. *et al.* Orally administered *L. lactis* secreting an anti-TNF Nanobody demonstrate efficacy in chronic colitis. *Mucosal Immunology.* **3**, 49 (2009).
6. Braat, H. *et al.* A Phase I Trial With Transgenic Bacteria Expressing Interleukin-10 in Crohn's Disease. *Clinical Gastroenterology and Hepatology.* **4**, 754-759 (2006).
7. Steidler, L. *et al.* Treatment of Murine Colitis by *Lactococcus lactis* Secreting Interleukin-10. *Science.* **289**, 1352-1355 (2000).
8. Pusch, O. *et al.* An anti-HIV microbicide engineered in commensal bacteria: secretion of HIV-1 fusion inhibitors by lactobacilli. *AIDS.* **20**, 1917-1922 (2006).
9. Lagenaar, L. A. *et al.* Prevention of vaginal SHIV transmission in macaques by a live recombinant *Lactobacillus*. *Mucosal Immunology.* **4**, 648 (2011).
10. Zheng, J. H. *et al.* Two-step enhanced cancer immunotherapy with engineered *Salmonella typhimurium* secreting heterologous flagellin. *Science Translational Medicine.* **9**, eaak9537 (2017).
11. Saltzman, D. A. *et al.* Attenuated *Salmonella typhimurium* Containing Interleukin-2 Decreases MC-38 Hepatic Metastases: A Novel Anti-tumor Agent. *Cancer Biotherapy and Radiopharmaceuticals.* **11**, 145-153 (1996).
12. Ryan, R. M. *et al.* Bacterial delivery of a novel cytolysin to hypoxic areas of solid tumors. *Gene Therapy.* **16**, 329 (2009).
13. Cunningham, C. & Nemunaitis, J. A phase I trial of genetically modified *Salmonella typhimurium* expressing cytosine deaminase (TAPET-CD, VNP20029) administered by intratumoral injection in combination with 5-fluorocytosine for patients with advanced or

- metastatic cancer. Protocol no: CL-017. Version: April 9, 2001. *Human gene therapy*. **12**, 1594-1596 (2001).
14. Nemunaitis, J. *et al.* Pilot trial of genetically modified, attenuated Salmonella expressing the E. coli cytosine deaminase gene in refractory cancer patients. *Cancer gene therapy*. **10**, 737-744 (2003).
 15. Pamer, E. G. Immune responses to *Listeria monocytogenes*. *Nature Reviews Immunology*. **4**, 812 (2004).
 16. Hanson, M. L. *et al.* Oral Delivery of IL-27 Recombinant Bacteria Attenuates Immune Colitis in Mice. *Gastroenterology*. **146**, 210-221.e213 (2014).
 17. Vandembroucke, K. *et al.* Orally administered *L. lactis* secreting an anti-TNF Nanobody demonstrate efficacy in chronic colitis. *Mucosal Immunol*. **3**, 49-56 (2010).
 18. Sonnenborn, U. & Schulze, J. The non-pathogenic *Escherichia coli* strain Nissle 1917 – features of a versatile probiotic. *Microbial Ecology in Health and Disease*. **21**, 122-158 (2009).
 19. Schultz, M. Clinical use of E. coli Nissle 1917 in inflammatory bowel disease. *Inflamm Bowel Dis*. **14**, 1012-1018 (2008).
 20. Wassenaar, T. M. Insights from 100 Years of Research with Probiotic E. Coli. *Eur J Microbiol Immunol (Bp)*. **6**, 147-161 (2016).
 21. Joeres-Nguyen-Xuan, H. T., Boehm, K. S., Joeres, K. L., Schulze, K. J. & Kruis, K. W. Survival of the probiotic *Escherichia coli* Nissle 1917 (EcN) in the gastrointestinal tract given in combination with oral mesalazine to healthy volunteers. *Inflammatory Bowel Diseases*. **16**, 256-262 (2010).
 22. Kurtz, C. *et al.* Translational Development of Microbiome-Based Therapeutics: Kinetics of E. coli Nissle and Engineered Strains in Humans and Nonhuman Primates. *Clinical and Translational Science*. **11**, 200-207 (2018).
 23. Duan, F. & March, J. C. Engineered bacterial communication prevents &em>Vibrio cholerae virulence in an infant mouse model. *Proceedings of the National Academy of Sciences*. **107**, 11260 (2010).
 24. Hwang, I. Y. *et al.* Engineered probiotic *Escherichia coli* can eliminate and prevent *Pseudomonas aeruginosa* gut infection in animal models. *Nature Communications*. **8**, 15028 (2017).
 25. Paton, A. W., Morona, R. & Paton, J. C. A new biological agent for treatment of Shiga toxin-producing *Escherichia coli* infections and dysentery in humans. *Nature Medicine*. **6**, 265 (2000).

26. Ho, C. L. *et al.* Engineered commensal microbes for diet-mediated colorectal-cancer chemoprevention. *Nature Biomedical Engineering*. **2**, 27-37 (2018).
27. Isabella, V. M. *et al.* Development of a synthetic live bacterial therapeutic for the human metabolic disease phenylketonuria. *Nat Biotechnol*. **36**, 857-864 (2018).
28. Kurtz, C. B. *et al.* An engineered E. coli Nissle improves hyperammonemia and survival in mice and shows dose-dependent exposure in healthy humans. *Science Translational Medicine*. **11**, eaau7975 (2019).
29. Danino, T. *et al.* Programmable probiotics for detection of cancer in urine. *Science Translational Medicine*. **7**, 289ra284 (2015).
30. Riglar, D. T. *et al.* Engineered bacteria can function in the mammalian gut long-term as live diagnostics of inflammation. *Nature Biotechnology*. **35**, 653 (2017).
31. Daeffler, K. N. M. *et al.* Engineering bacterial thiosulfate and tetrathionate sensors for detecting gut inflammation. *Molecular Systems Biology*. **13**, 923 (2017).
32. Palmer, J. D. *et al.* Engineered Probiotic for the Inhibition of Salmonella via Tetrathionate-Induced Production of Microcin H47. *ACS Infectious Diseases*. **4**, 39-45 (2018).
33. Ou, B. *et al.* Genetic engineering of probiotic Escherichia coli Nissle 1917 for clinical application. *Appl Microbiol Biotechnol*. **100**, 8693-8699 (2016).
34. Pedrolli, D. B. *et al.* Engineering Microbial Living Therapeutics: The Synthetic Biology Toolbox. *Trends in Biotechnology*. **37**, 100-115 (2019).
35. Flemming, H.-C. & Wingender, J. The biofilm matrix. *Nature Reviews Microbiology*. **8**, 623 (2010).
36. Phillips, P. L. & Schultz, G. S. Molecular Mechanisms of Biofilm Infection: Biofilm Virulence Factors. *Advances in wound care*. **1**, 109-114 (2012).
37. Antunes, L. C. M. & Ferreira, R. B. R. Biofilms and bacterial virulence. *Reviews in Medical Microbiology*. **22** (2011).
38. Kong, C. *et al.* Suppression of Staphylococcus aureus biofilm formation and virulence by a benzimidazole derivative, UM-C162. *Scientific Reports*. **8**, 2758 (2018).
39. Rijavec, M., Müller-Premru, M., Zakotnik, B. & Žgur-Bertok, D. Virulence factors and biofilm production among Escherichia coli strains causing bacteraemia of urinary tract origin. *Journal of Medical Microbiology*. **57**, 1329-1334 (2008).
40. Nguyen, P. Q., Botyanszki, Z., Tay, P. K. & Joshi, N. S. Programmable biofilm-based materials from engineered curli nanofibres. *Nat Commun*. **5**, 4945 (2014).

41. Nguyen, P. Q., Courchesne, N. D., Duraj-Thatte, A., Praveschotinunt, P. & Joshi, N. S. Engineered Living Materials: Prospects and Challenges for Using Biological Systems to Direct the Assembly of Smart Materials. *Adv Mater.* (2018).
42. Fong, J. N. C. & Yildiz, F. H. Biofilm Matrix Proteins. *Microbiology spectrum.* **3**, 10.1128/microbiolspec.MB-0004-2014 (2015).
43. Erskine, E., MacPhee, C. E. & Stanley-Wall, N. R. Functional Amyloid and Other Protein Fibers in the Biofilm Matrix. *Journal of Molecular Biology.* **430**, 3642-3656 (2018).
44. Maury, C. P. J. The emerging concept of functional amyloid. *Journal of Internal Medicine.* **265**, 329-334 (2009).
45. Nguyen, P. Q. Synthetic biology engineering of biofilms as nanomaterials factories. *Biochemical Society Transactions.* **45**, 585 (2017).
46. Chapman, M. R. *et al.* Role of Escherichia coli curli operons in directing amyloid fiber formation. *Science.* **295**, 851-855 (2002).
47. Barnhart, M. M. & Chapman, M. R. Curli biogenesis and function. *Annu Rev Microbiol.* **60**, 131-147 (2006).
48. Blanco, L. P., Evans, M. L., Smith, D. R., Badtke, M. P. & Chapman, M. R. Diversity, biogenesis and function of microbial amyloids. *Trends Microbiol.* **20**, 66-73 (2012).
49. Deshmukh, M., Evans, M. L. & Chapman, M. R. Amyloid by Design: Intrinsic Regulation of Microbial Amyloid Assembly. *Journal of Molecular Biology.* (2018).
50. Collinson, S. K., Emödy, L., Müller, K. H., Trust, T. J. & Kay, W. W. Purification and characterization of thin, aggregative fimbriae from Salmonella enteritidis. *Journal of bacteriology.* **173**, 4773-4781 (1991).
51. Chen, A. Y. *et al.* Synthesis and patterning of tunable multiscale materials with engineered cells. *Nature Materials.* **13**, 515 (2014).
52. Botyanszki, Z., Tay, P. K. R., Nguyen, P. Q., Nussbaumer, M. G. & Joshi, N. S. Engineered catalytic biofilms: Site-specific enzyme immobilization onto E. coli curli nanofibers. *Biotechnology and Bioengineering.* **112**, 2016-2024 (2015).
53. Nussbaumer, M. G. *et al.* Bootstrapped Biocatalysis: Biofilm-Derived Materials as Reversibly Functionalizable Multienzyme Surfaces. *ChemCatChem.* **9**, 4328-4333 (2017).
54. Tay, P. K. R., Nguyen, P. Q. & Joshi, N. S. A Synthetic Circuit for Mercury Bioremediation Using Self-Assembling Functional Amyloids. *ACS Synthetic Biology.* **6**, 1841-1850 (2017).

55. Tay, P. K. R., Manjula-Basavanna, A. & Joshi, N. S. Repurposing bacterial extracellular matrix for selective and differential abstraction of rare earth elements. *Green Chemistry*. **20**, 3512-3520 (2018).
56. Noémie-Manuelle Dorval Courchesne, A. D.-T., Pei Kun R. Tay, Peter Q. Nguyen, and Neel S. Joshi. Scalable Production of Genetically Engineered Nanofibrous Macroscopic Materials via Filtration. *ACS Biomater. Sci. Eng.* **3**, 733–741 (2017).
57. Chen, A. Y. *et al.* Synthesis and patterning of tunable multiscale materials with engineered cells. *Nat Mater.* **13**, 515-523 (2014).
58. Van Gerven, N. *et al.* Secretion and functional display of fusion proteins through the curli biogenesis pathway. *Molecular Microbiology*. **91**, 1022-1035 (2014).
59. Bian, Z., Brauner, A., Li, Y. H. & Normark, S. Expression of and cytokine activation by Escherichia coli curli fibers in human sepsis. *Journal Of Infectious Diseases*. **181**, 602-612 (2000).
60. Humphries, A., DeRidder, S. & Bäumlér, A. J. Salmonella enterica Serotype Typhimurium Fimbrial Proteins Serve as Antigens during Infection of Mice. *Infection and Immunity*. **73**, 5329 (2005).
61. Hufnagel, D. A., Tükel, Ç. & Chapman, M. R. Disease to Dirt: The Biology of Microbial Amyloids. *PLoS Pathogens*. **9**, e1003740 (2013).
62. Rapsinski, G. J. *et al.* Toll-like receptor 2 and NLRP3 cooperate to recognize a functional bacterial amyloid, curli. *Infect Immun*. **83**, 693-701 (2015).
63. Rapsinski, G. J., Newman, T. N., Oppong, G. O., van Putten, J. P. & Tükel, C. CD14 protein acts as an adaptor molecule for the immune recognition of Salmonella curli fibers. *J Biol Chem*. **288**, 14178-14188 (2013).
64. Tükel, C. *et al.* Toll-like receptors 1 and 2 cooperatively mediate immune responses to curli, a common amyloid from enterobacterial biofilms. *Cell Microbiol*. **12**, 1495-1505 (2010).
65. Oppong, G. O. *et al.* Epithelial cells augment barrier function via activation of the Toll-like receptor 2/phosphatidylinositol 3-kinase pathway upon recognition of Salmonella enterica serovar Typhimurium curli fibrils in the gut. *Infect Immun*. **81**, 478-486 (2013).
66. Cario, E. Barrier-protective function of intestinal epithelial Toll-like receptor 2. *Mucosal Immunol*. **1 Suppl 1**, S62-66 (2008).
67. Cario, E., Gerken, G. & Podolsky, D. K. Toll-like receptor 2 controls mucosal inflammation by regulating epithelial barrier function. *Gastroenterology*. **132**, 1359-1374 (2007).

68. Cario, E., Gerken, G. & Podolsky, D. K. Toll-like receptor 2 enhances ZO-1-associated intestinal epithelial barrier integrity via protein kinase C. *Gastroenterology*. **127**, 224-238 (2004).
69. Oppong, G. O. *et al.* Biofilm-associated bacterial amyloids dampen inflammation in the gut: oral treatment with curli fibres reduces the severity of hapten-induced colitis in mice. *npj Biofilms and Microbiomes*. **1**, 15019 (2015).
70. Fakhoury, M., Negrulj, R., Mooranian, A. & Al-Salami, H. Inflammatory bowel disease: clinical aspects and treatments. *Journal of Inflammation Research*. **7**, 113-120 (2014).
71. Billsborough, J., Targan, S. R. & Snapper, S. B. Therapeutic Targets in Inflammatory Bowel Disease: Current and Future. *The American Journal Of Gastroenterology Supplements*. **3**, 27 (2016).
72. Jin, J. Inflammatory Bowel Disease JAMA Patient Page. *JAMA*. **311**, 2034-2034 (2014).
73. McIlroy, J., Ianiro, G., Mukhopadhyaya, I., Hansen, R. & Hold, G. L. Review article: the gut microbiome in inflammatory bowel disease—avenues for microbial management. *Alimentary Pharmacology & Therapeutics*. **47**, 26-42 (2018).
74. Thim, L. Trefoil peptides: from structure to function. *Cellular and Molecular Life Sciences CMLS*. **53**, 888-903 (1997).
75. Thim, L., Madsen, F. & Poulsen, S. S. Effect of trefoil factors on the viscoelastic properties of mucus gels. *Eur J Clin Invest*. **32**, 519-527 (2002).
76. Aamann, L., Vestergaard, E. M. & Gronbaek, H. Trefoil factors in inflammatory bowel disease. *World J Gastroenterol*. **20**, 3223-3230 (2014).
77. Shreiner, A. B., Kao, J. Y. & Young, V. B. The gut microbiome in health and in disease. *Current opinion in gastroenterology*. **31**, 69-75 (2015).
78. Bull, M. J. & Plummer, N. T. Part 1: The Human Gut Microbiome in Health and Disease. *Integrative medicine (Encinitas, Calif.)*. **13**, 17-22 (2014).
79. Claesson, M. J., Clooney, A. G. & O'Toole, P. W. A clinician's guide to microbiome analysis. *Nature Reviews Gastroenterology & Hepatology*. **14**, 585 (2017).
80. Tropini, C., Earle, K. A., Huang, K. C. & Sonnenburg, J. L. The Gut Microbiome: Connecting Spatial Organization to Function. *Cell Host & Microbe*. **21**, 433-442 (2017).
81. Cronin, M. *et al.* High Resolution In Vivo Bioluminescent Imaging for the Study of Bacterial Tumour Targeting. *PLOS ONE*. **7**, e30940 (2012).

82. Karimi, S. *et al.* In Vivo and In Vitro Detection of Luminescent and Fluorescent Lactobacillus reuteri and Application of Red Fluorescent mCherry for Assessing Plasmid Persistence. *PLOS ONE*. **11**, e0151969 (2016).
83. Rhee, K.-J. *et al.* Determination of spatial and temporal colonization of enteropathogenic E. coli and enterohemorrhagic E. coli in mice using bioluminescent in vivo imaging. *Gut Microbes*. **2**, 34-41 (2011).
84. Knight, J. C. & Cornelissen, B. Bioorthogonal chemistry: implications for pretargeted nuclear (PET/SPECT) imaging and therapy. *American journal of nuclear medicine and molecular imaging*. **4**, 96-113 (2014).
85. Srivastava, A. K. *et al.* Advances in using MRI probes and sensors for in vivo cell tracking as applied to regenerative medicine. *Disease models & mechanisms*. **8**, 323-336 (2015).
86. Jia, L., Li, X., Cheng, D. & Zhang, L. Fluorine-18 click radiosynthesis and microPET/CT evaluation of a small peptide-a potential PET probe for carbonic anhydrase IX. *Bioorganic & Medicinal Chemistry*. **27**, 785-789 (2019).
87. Hapuarachchige, S. & Artemov, D. Click Chemistry in the Development of Contrast Agents for Magnetic Resonance Imaging. *Topics in magnetic resonance imaging : TMRI*. **25**, 205-213 (2016).
88. Geva-Zatorsky, N. *et al.* In vivo imaging and tracking of host-microbiota interactions via metabolic labeling of gut anaerobic bacteria. *Nat Med*. **21**, 1091-1100 (2015).
89. Young, T. S., Ahmad, I., Yin, J. A. & Schultz, P. G. An Enhanced System for Unnatural Amino Acid Mutagenesis in E. coli. *Journal of Molecular Biology*. **395**, 361-374 (2010).
90. Venditti, V., Fawzi, N. L. & Clore, G. M. An efficient protocol for incorporation of an unnatural amino acid in perdeuterated recombinant proteins using glucose-based media. *Journal of biomolecular NMR*. **52**, 191-195 (2012).
91. Lajoie, M. J. *et al.* Genomically Recoded Organisms Expand Biological Functions. *Science*. **342**, 357 (2013).
92. Rovner, A. J. *et al.* Recoded organisms engineered to depend on synthetic amino acids. *Nature*. **518**, 89-93 (2015).
93. Eeftens, J. M., van der Torre, J., Burnham, D. R. & Dekker, C. Copper-free click chemistry for attachment of biomolecules in magnetic tweezers. *BMC biophysics*. **8**, 9-9 (2015).
94. Yoon, H. I. *et al.* Bioorthogonal Copper Free Click Chemistry for Labeling and Tracking of Chondrocytes In Vivo. *Bioconjugate Chemistry*. **27**, 927-936 (2016).

95. Xie, R. *et al.* In vivo metabolic labeling of sialoglycans in the mouse brain by using a liposome-assisted bioorthogonal reporter strategy. *Proceedings of the National Academy of Sciences of the United States of America*. **113**, 5173-5178 (2016).
96. Koo, H. *et al.* Bioorthogonal Copper-Free Click Chemistry In Vivo for Tumor-Targeted Delivery of Nanoparticles. *Angewandte Chemie International Edition*. **51**, 11836-11840 (2012).

Page intentionally left blank

Chapter 2 Modulating bacterial and gut mucosal interactions with engineered biofilm matrix proteins

2.1 Abstract

Extracellular appendages play a significant role in mediating communication between bacteria and their host. Curli fibers are a class of bacterial fimbria that is highly amenable to engineering. We demonstrate the use of engineered curli fibers to rationally program interactions between bacteria and components of the mucosal epithelium. Commensal *E. coli* strains were engineered to produce recombinant curli fibers fused to the trefoil family of human cytokines. Biofilms formed from these strains bound more mucins than those producing wild-type curli fibers, and modulated mucin rheology as well. When treated with bacteria producing the curli-trefoil fusions mammalian cells behaved identically in terms of their migration behavior as when they were treated with the corresponding soluble trefoil factors. Overall, this demonstrates the potential utility of curli fibers as a scaffold for the display of bioactive domains and an untapped approach to rationally modulating host-microbe interactions using bacterial matrix proteins.

2.2 Introduction

The mucosal surfaces of the gastrointestinal (GI) tract serve several important protective functions, including lubricating the epithelium, decreasing the shear forces experienced by its constituent cells, and trapping debris and bacteria¹. They do this, in part, through the formation of a microporous gel-like mucus layer composed of proteoglycans (i.e. mucins) that are secreted by the epithelial cells. As the outermost layer of the GI tract, mucus plays a critical role in mediating the interaction between bacteria and the host, especially in the colon, where the highest concentrations of microbes are found. It does this by providing a physical barrier to separate bacteria from the epithelial cells, but also by regulating bacterial growth rate and preventing

bacterial aggregation². Defects in the mucus layer that are the result of dysregulation of mucin production or excessive degradation of mucins can have dire physiological consequences, including compromising intestinal barrier function and chronic inflammation that is caused or exacerbated by bacterial penetration into the epithelium³.

Naturally occurring pathogens and commensals employ several strategies to persist within the mucus layer, for example by feeding off the mucin glycans⁴. Another commonly found strategy is the surface display of adhesins and extracellular appendages with specific mucin binding capabilities⁵. Indeed, in some cases, deletions of individual genes encoding such adhesive proteins can abolish the colonization ability of a commensal microbe, or the pathogenicity of an invasive species, highlighting their importance for organismal fitness in the gut environment⁵. The display of engineered chimeric adhesins on the surface of non-pathogenic *E. coli* has even been demonstrated to enhance their localization to tumors when injected intravenously⁶. Furthermore, some adhesins can influence host biology directly through immunomodulation, and binding to innate immune receptors on the host cell surface^{7,8}.

As a result of the proliferation of basic science aimed at understanding host-microbe interactions, there has been a corresponding swell of interest in engineering microbes for diagnostic and therapeutic purposes. Many of these efforts attempt to exploit features of commensal and probiotic microbes such that they can serve as genetically programmable sensors and drug delivery devices^{9,10}. This is usually accomplished through the engineered secretion of soluble molecular factors that can directly influence host biological processes^{11,12}. Although this overall approach continues to show promise as a therapeutic strategy, there are also challenges,

one of which is achieving a sufficiently high local concentration of therapeutic molecule at the site of disease.

We propose an alternative strategy to the secretion of soluble therapeutic factors, in the form of reprogramming biofilm matrix proteins. Here, we report our efforts to repurpose curli fibers of *E. coli*, the best studied and most frequently used organism for engineered probiotic efforts, to act as a display system for bioactive domains^{12,13}. The result of this effort is an engineered bacterium that produces a self-assembled matrix *in situ* with programmable function (Figure 2.1). We show that we can program such a matrix to display specific protein domains that function simultaneously to enhance adhesion to mucins and epithelial cell surfaces, and modify cell behavior.

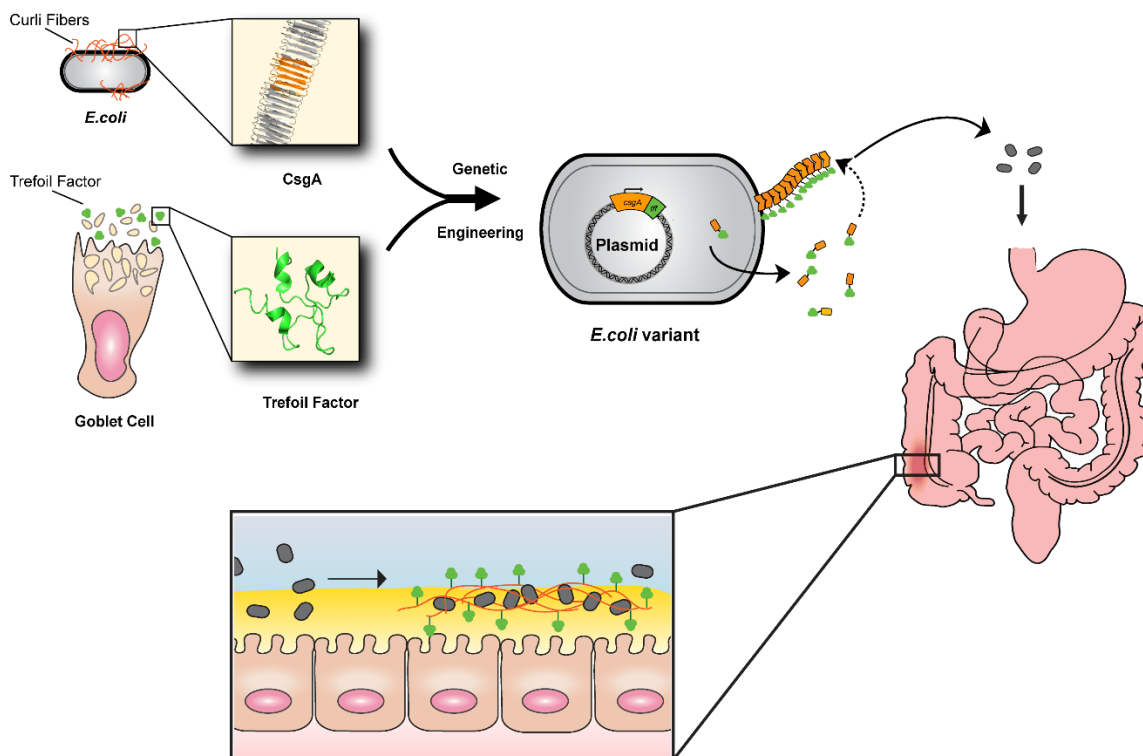


Figure 2.1 Repurposing commensal *E. coli* curli fiber proteins through TFF display, A. Schematic overview of reprogrammed *E. coli* curli nanofibers. CsgA, the main proteinaceous component of *E. coli*

biofilm matrix, assembles into extracellular amyloid fibers after secretion in the monomeric form (top, inset shows one CsgA monomer highlighted in orange). Trefoil factors, like TFF3 (PDB ID: 1PE3, green), are cytokines secreted by mucus producing cells. *E. coli* was engineered to display the trefoil factors as genetic fusions to the C-terminus of CsgA. CsgA-TFF chimeras are self-assembled into nanofibers extracellularly (B), where they can modulate interactions with mucosal epithelium tissues (C).

2.3 Results and Discussion

2.3.1 TFF-fused curli fibers are produced, secreted, and assembled by commensal *E. coli*

Curli is a functional amyloid that is produced by *E. coli* and other *Enterobacteriaceae* during biofilm formation¹⁴. We have previously shown that the main structural component of curli fibers, CsgA, can be fused to a range of heterologous domains without abolishing its ability to be secreted and assembled extracellularly¹⁵. In order to enhance the interaction of curli nanofibers with the gut mucosa, we genetically fused CsgA to the trefoil factors (TFF1, TFF2, and TFF3), a family of human cytokines that are secreted by mucus-producing cells and goblet cells into the gut lumen and contribute to the maintenance of homeostasis (Figure 2.2). The entire TFF sequences were fused to the C-terminus of CsgA via a flexible linker domain in a manner that is very similar to previously published CsgA fusion proteins¹⁶. All three TFFs exhibit specific mucin binding activities^{14,17,18}, enabling them to increase the viscosity of co-secreted mucins, possibly enhancing barrier function locally^{19,20}. In addition to their biophysical effects, they also help maintain barrier function by promoting epithelial restitution and reinforcing tight junctions, among other mechanisms^{21,22}. This has led to their investigation as therapeutics in the treatment of IBD, although delivery remains a challenge²³. Furthermore, they range in size from 59-106 amino acids, making them compatible with the constraints of the curli secretion system.

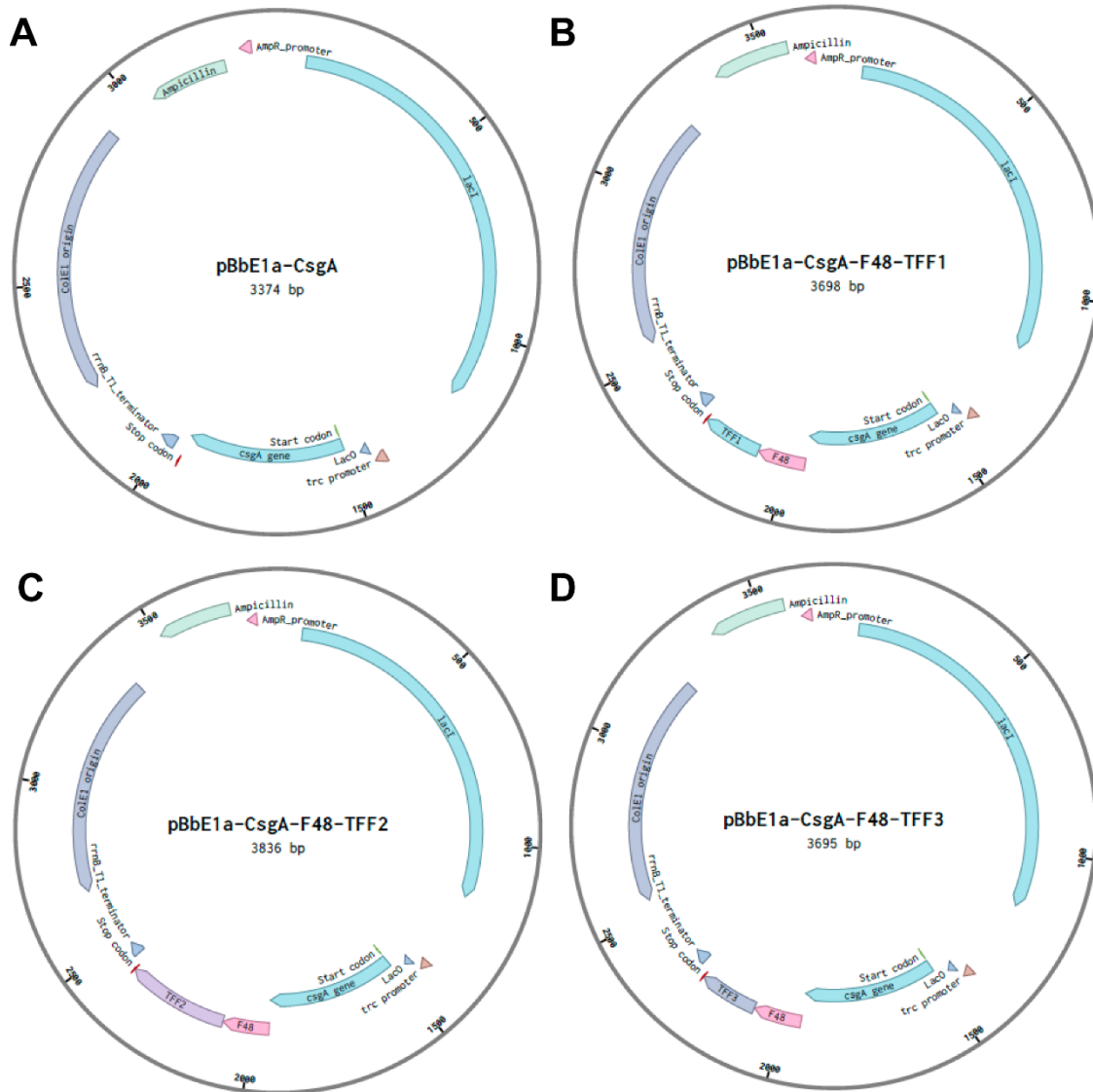


Figure 2.2 Plasmid construction, (A) Plasmid map of pBbE1a vector containing wild type CsgA, (B) Plasmid map of pBbE1a vector containing CsgA fused with flexible linker (48 aa) and trefoil factor-1 at C-terminus, (C) Plasmid map of pBbE1a vector containing CsgA fused with flexible linker (48 aa) and trefoil factor-2 at C-terminus, (D) Plasmid map of pBbE1a vector containing CsgA fused with flexible linker (48 aa) and trefoil factor-3 at C-terminus

We envisioned that the amyloidogenic fusion proteins would self assemble into a nanofibrous matrix with mucoadhesive and epithelial wound healing properties (Figure 2.1). Accordingly, we prepared plasmids encoding CsgA-TFF fusions under the control of an isopropyl β -D-1-thiogalactopyranoside (IPTG) inducible promoter. These were transformed into a

commensal *E. coli* strain (PHL628- Δ *csgA*) suited to curli overproduction^{24,25}. A Congo Red (CR) dye binding assay, commonly used to test for the presence of amyloids, suggested that all three fusions could be successfully produced and assembled with comparable efficiency to the wild-type CsgA protein (Figure 2.3A, Figure 2.4). We also performed a whole-cell filtration ELISA using antibodies against CsgA, which confirmed that the fusion proteins were successfully secreted and assembled extracellularly (Figure 2.3B). We did observe a decrease in signal for the TFF2 and TFF3 constructs, which could reflect a legitimate difference in production, but could also reflect an altered affinity of these constructs for the anti-CsgA antibody, or accessibility of the TFF epitopes due to extensive fiber aggregation. Similar ELISA assays using antibodies against the individual trefoil factors confirmed the presence of the appropriate TFF for each variant (Figure 2.3C). Scanning electron microscopy (SEM) analysis confirmed that all three fusion proteins assembled into nanofibrous structures typical of curli fibers, although CsgA-TFF2 and CsgA-TFF3 fibers did appear to aggregate more than those of wt-CsgA and CsgA-TFF1 (Figure 2.3D).

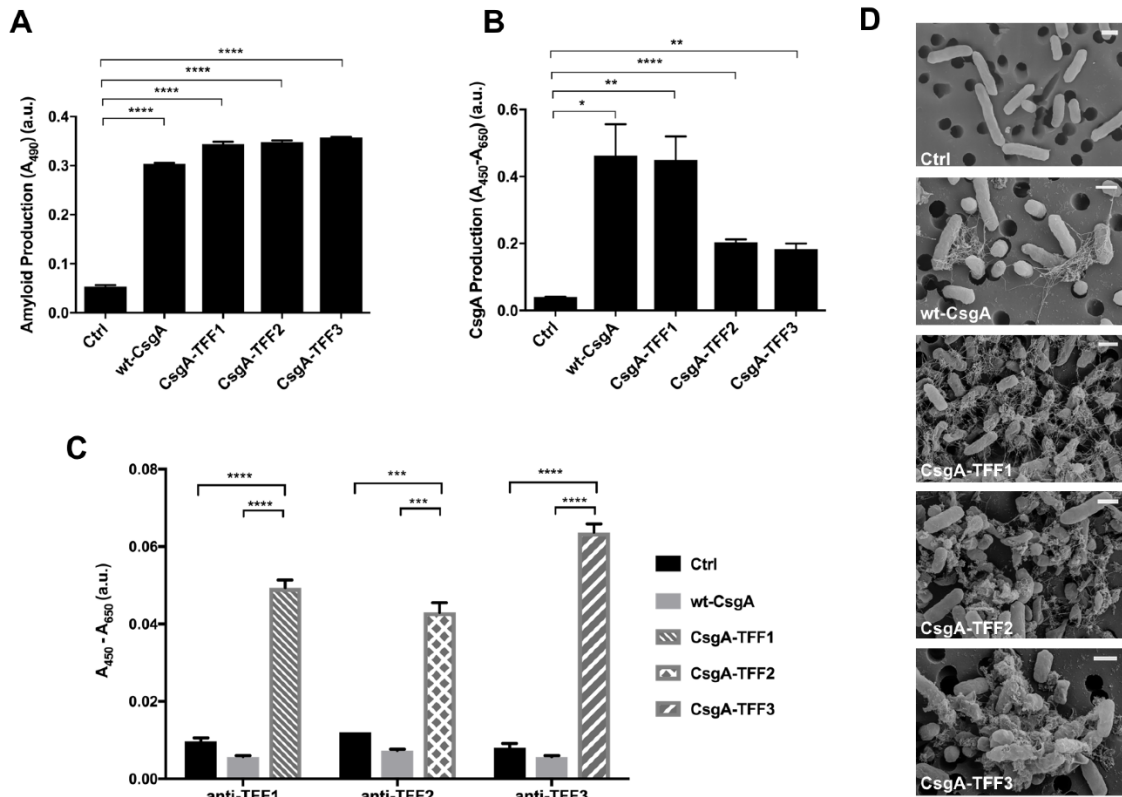


Figure 2.3 CsgA-trefoil factor fusions retain secretion and self-assembly functionality, Congo Red staining assays (A), and whole-cell filtration ELISA assays with anti-CsgA antibody detection (B) confirm the formation of recombinant curli amyloids. Ctrl indicates cells containing a plasmid with no CsgA encoding gene. (C) Whole cell filtration ELISA was also used to detect each of the displayed trefoil factors, with the corresponding anti-TFF antibodies. (D) SEM images of *E. coli* PHL628- Δ csgA strain transformed with plasmids encoding for no curli (Ctrl), wt-CsgA, and curli with displayed trefoil factors (CsgA-TFF1, CsgA-TFF2, CsgA-TFF3). All scale bars are 1 μ m. Ordinary one way ANOVA with Dunnett's multiple comparison test n=3, *P<0.05, **P<0.01, ***P<0.001, ****P<0.0001

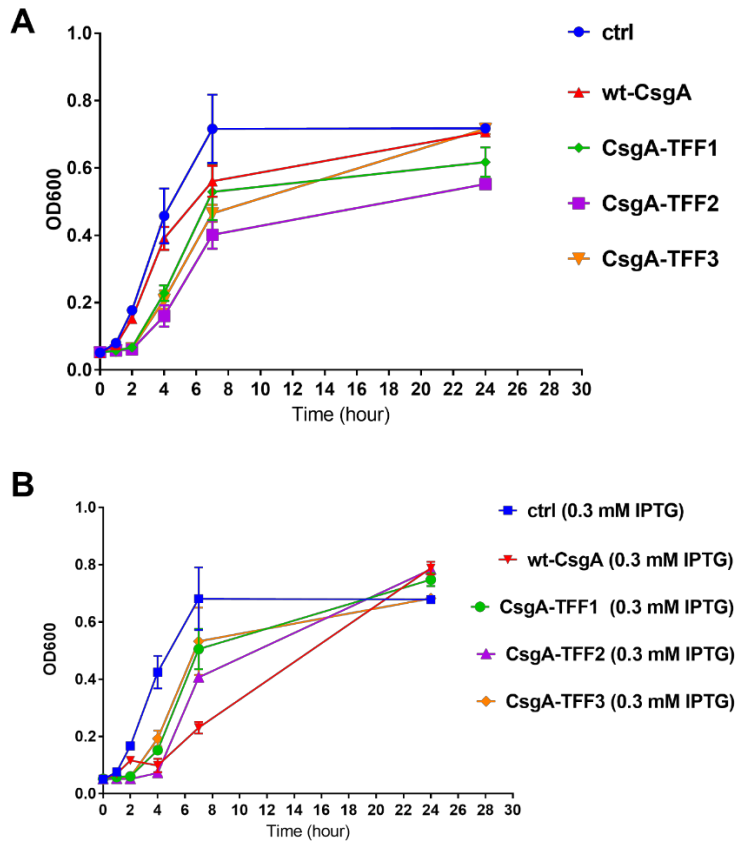


Figure 2.4 Growth curves of engineered bacteria (A) the growth curve indicating OD600 of PHL628 $\Delta csgA$ variants over time in Luria Broth at 37°C 225 rpm shaking incubator, (B) the growth curve indicating OD600 of PHL628 $\Delta csgA$ variants over time in Luria Broth with 0.3 mM Isopropyl β -D-1-thiogalactopyranoside (IPTG) at 37°C 225 rpm shaking incubator

2.3.2 Engineered curli matrices bind to mucins and modify their biophysical properties

Given that commensal forms of *E. coli* reside mostly in the outer colonic mucus layer²⁶, we sought to evaluate the effects of TFF display on the interaction of the engineered *E. coli* with mucins. Soluble endogenous trefoil factors have a characteristic triple-loop structure that is held together by intramolecular disulfide bonds. The TFFs are known to bind to mucin proteins through a combination of nonspecific hydrophobic interactions and disulfide exchange with the cysteine rich von Willebrand factor (VWF) domains common to all mucins¹⁷. To determine the mucin binding activity of curli-displayed TFFs, we first assessed the binding of type II porcine gastric

mucins (a common model system for gastrointestinal mucins) to filtered biofilms. As expected, all of the CsgA-TFF fusions enhanced binding of the biofilms to mucins significantly, with CsgA-TFF3 binding to more than 4 times the amount of mucin as wt-CsgA (Figure 2.5A). In order to evaluate the binding activity of the engineered *E. coli* strains with mucins in a more physiologically relevant model, we developed an ex vivo assay with a section of goat intestine (i.e. the “sausage” assay, Figure 2.5B). After incubating the engineered strains in fresh tubular sections of colon and gently washing to remove unbound bacteria, we found that all three TFF fusions led to higher CR staining intensity on the mucosal surface compared to bacteria producing wt-CsgA or no CsgA. We also stained the intestine samples with thioflavin T (ThT), which, along with CR, is commonly used as a stain for amyloid deposits in histopathology of animal tissues. Upon binding to amyloids, ThT fluorescence intensity increases significantly. Although there was a large amount of background signal from the tissue itself, making direct comparison of the CR and ThT staining difficult, samples treated with curli-producing bacteria showed significantly more staining compared to the tissue alone. Furthermore, samples treated with bacteria producing curli-fused TFFs bound more ThT than those treated with bacteria producing wild-type CsgA.

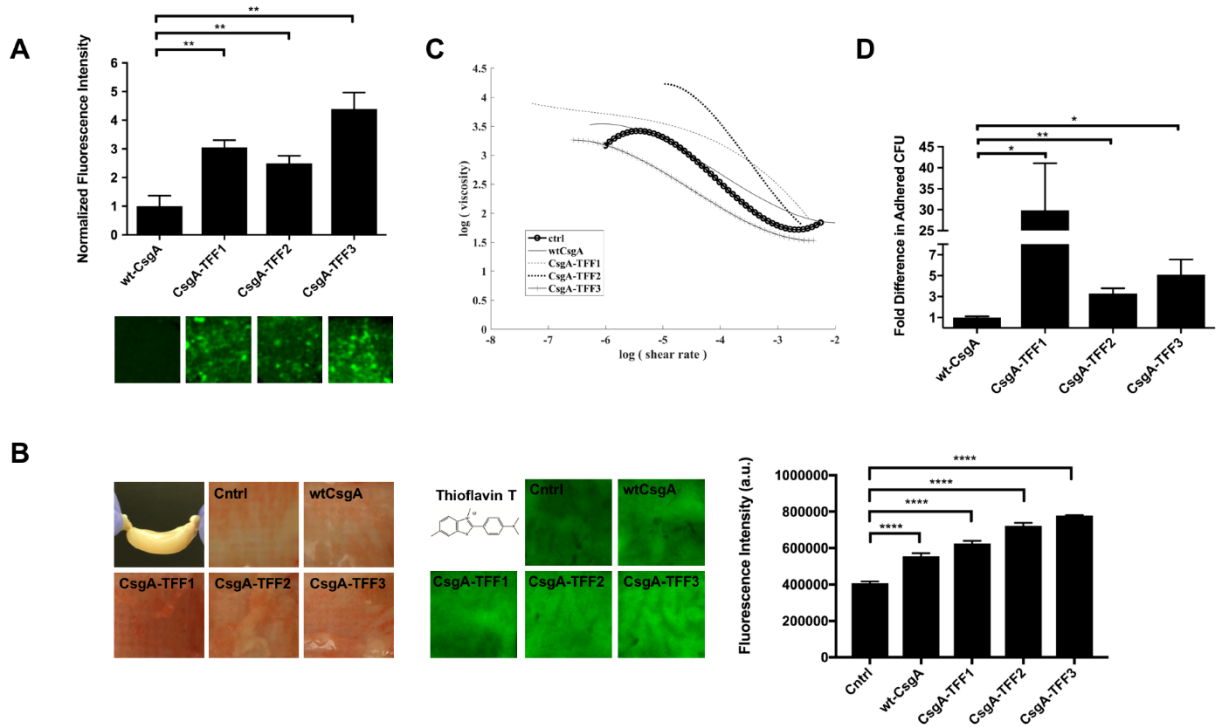


Figure 2.5 Engineered curli matrix enhances *E. coli* adhesion to gut mucosa. (A) anti-Muc-2 detection of mucins after incubation on top of filtered biofilms producing curli-TFF fusions, (B) Congo Red and Thioflavin T staining of goat colon after incubation with engineered curliated *E. coli* variants. (C) Viscosity vs. shear rate analysis for mucins combined with curliated bacterial cultures. Ctrl indicates cells containing a plasmid with no CsgA encoding gene. (D) Bacterial adhesion to Caco-2 cell monolayers. Ordinary one way ANOVA with Dunnett's multiple comparison test n=10, *P<0.05, **P<0.01, ***P<0.001, ****P<0.0001

In addition to binding to mucins, soluble TFFs have been shown to modulate the viscoelastic properties of mucin^{20,27}. For example, TFF2 increases the viscosity of porcine gastric mucins. In the same study TFF1 and TFF3 did not increase the viscosity of the mucins, but instead formed small complexes with the mucins that could be easily visualized with optical microscopy. We sought to demonstrate similar principles of biophysical modification for the curli-displayed TFFs. Accordingly, bacteria expressing CsgA-TFF fusions were combined with type II mucins from porcine stomach and the mixture subjected to rheological analysis. While bacteria expressing wt-CsgA appeared to have only a minor effect on mucin viscosity as a function of shear rate, CsgA-

TFF1 and CsgA-TFF2 fusions exhibited ~3-fold and ~10-fold increases in viscosity at a shear rate of 10^{-5} s^{-1} , respectively (Figure 2.5C).

2.3.3 Engineered curli matrix enhances bacterial binding to mammalian cell surfaces

In addition to their mucin binding activity, bacterial adhesins also play a role in signaling through direct contact with epithelial cells²⁸. Therefore, we wanted to determine how TFF display affects the interaction of engineered *E. coli* with the epithelial cell surface. There are some known binding interactions between TFFs and various epithelial cell lines^{29,30}, and specific binding interactions between TFF2 and CXCR4 have also been reported³¹. We performed an adhesion assay by co-incubating engineered PHL628- Δ csgA with Caco-2 cell monolayers for 2 hours, followed by washing to remove non-adherent bacteria. The number of remaining bacterial cells was determined by CFU counting on antibiotic selective plates after lysis of the mammalian cells. All three displayed TFFs significantly enhanced bacterial binding to the cell surface compared to wild-type curli fibers, with TFF1 display increasing bacterial adhesion by almost 30-fold (Figure 2.5D). In order to confirm that bacterial cell invasion did not lead to an over-estimation of adhesion, we also performed an invasion assay with Caco-2 cell monolayers. Two hours after inoculation of the Caco-2 cells with induced bacterial cultures, extracellular bacteria were killed with a non-cell permeable antibiotic (gentamicin). After lysis of the mammalian cells, we did not observe any CFU of the engineered bacteria on selective agar plates, confirming that curli fiber expression increased cell adhesion without inducing an invasive phenotype.

2.3.4 Curli-bound trefoil factors maintain their signaling bioactivity

Previous studies have shown that TFFs play important roles in regulating biological responses to GI inflammation and injury. The mechanisms by which they regulate this response are numerous and not completely understood, but all three TFFs are upregulated in response to injury and promote cell migration to restore barrier function to denuded mucosal lesions³². In order to determine if the curli-bound TFFs maintained their signaling bioactivity, we performed an *in vitro* cell migration assay. This type of assay is difficult to perform in the presence of bacteria because prolonged co-culture is not possible under standard conditions. Therefore, we used semi-purified curli fibers prepared through a filtration protocol recently developed in our lab¹⁶. Following induction of a defect in a confluent Caco-2 monolayer by scratching with a pipet tip, the cells were co-incubated with semi-purified curli fibers overnight. Defect closure induced by engineered curli fibers was compared to that induced by the corresponding soluble TFFs. Surprisingly, we found that, of the soluble TFFs, only TFF3 enhanced defect closure, while soluble TFF2 actually decreased the defect closure rate and TFF1 did not have a significant effect (Figure 2.6C). TFF3 maintained its ability to promote cell migration when bound to curli fibers (Figure 2.6A, B). TFF1 and TFF2 did not show a difference in defect closure compared to untreated controls, but showed a slight decrease compared to curli fibers composed of wt-CsgA.

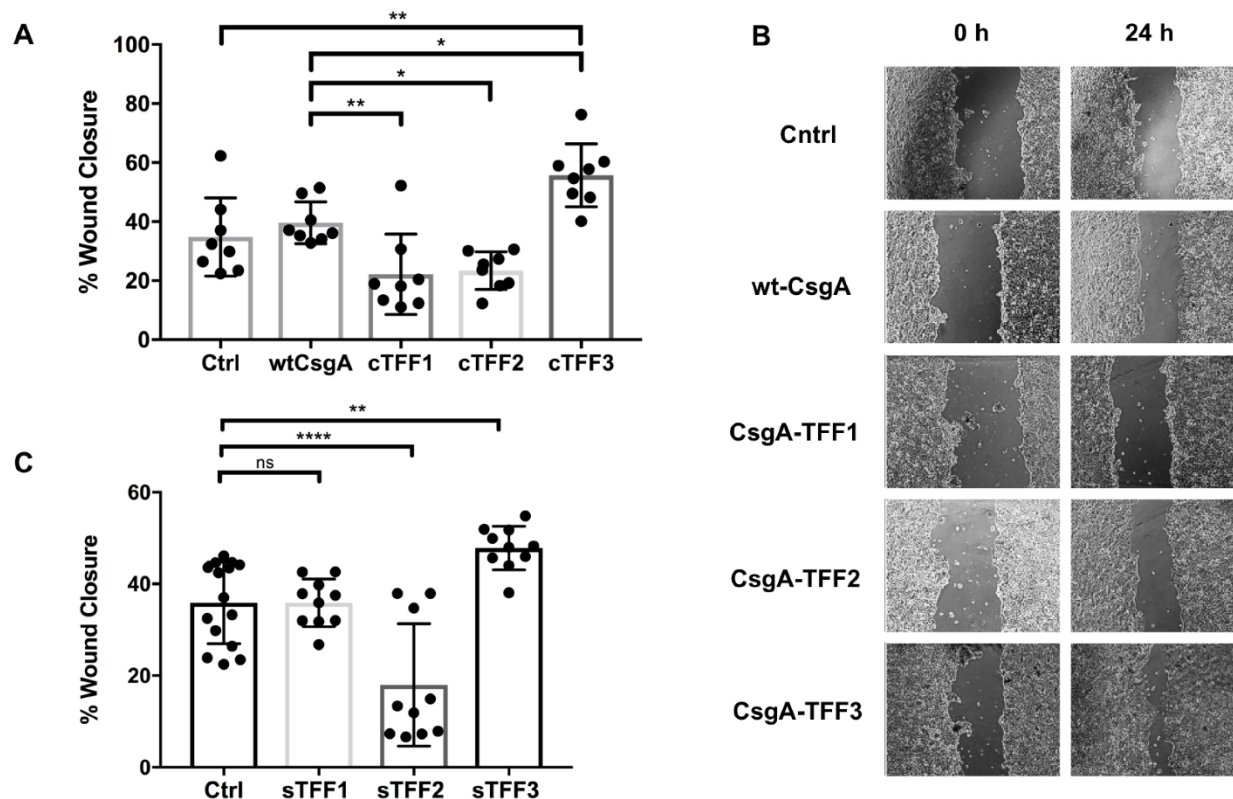


Figure 2.6 Bioactivity of displayed trefoil factors on the curli matrix, (A) Percent cell monolayer defect closure for Caco-2 cell monolayers during incubation with various soluble semi-purified curli variants. Bars represent mean % defect closure after 24 hours. Ctrl indicates scratched Caco-2 monolayers with no treatment. (B) Representative images of defects and their progressive closure after 24 hours in the presence of various curli fiber variants. (C) Corresponding cell migration assay with soluble trefoil factors. Ordinary one way Anova $n=10$, $**P<0.01$, $***P<0.001$ Ordinary one way ANOVA with Dunnett's multiple comparison test $n=10$, $*P<0.05$, $**P<0.01$, $***P<0.001$, $****P<0.0001$

2.4 Conclusions

Overall, this work demonstrates the first example of engineered curli fibers undergoing programmed interaction with a biological and tissue surfaces through the display of bioactive domains. Overall, it represents the early stages of a new approach to reprogramming host-microbe interactions. The ability to fuse large (>50 amino acid) polypeptide domains, including whole proteins on CsgA without abolishing secretion and self-assembly capabilities has been shown³³ However, this work demonstrates that even domains like TFF2, which contains seven internal

disulfide bonds, can be successfully displayed using this approach. The two primary functions of TFFs that make them potentially useful for treating inflammation in the GI tract²³ – binding to mucins to enhance their protective properties, and promoting epithelial wound healing – are preserved *in vitro* even while the TFFs are bound to curli fibers. The platform we report here offers the opportunity to present TFFs and other bioactive domains as a multivalent array in a cohesive material format. Indeed, the versatility of the curli biosynthetic machinery suggests that this approach could be easily adapted for the display of other therapeutic domains. Curli-based materials could even be programmed with multiple bioactive functions simultaneously, as we have shown previously^{15,34}. Current efforts in our group are focused on implementing this overall approach in commensal strains suitable for oral delivery with the long-term goal of creating an engineered therapeutic probiotic capable of creating a responsive, resident biomaterial inside the GI tract with therapeutic properties. This material, which can be pre-programmed to exhibit specific features, could then be administered orally to treat a range of diseases.

2.5 Materials and Methods

2.5.1 Cell Strains and Plasmids

Genes encoding for the CsgA-TFF1-3 fusion proteins were synthesized (Integrated DNA Technologies) and cloned by overlap extension into pBbE1a vectors by using Gibson Assembly³⁵. All experiments involving engineered curli expression were performed in a *csgA* deletion strain (MG1655, *malA:kan^r ompR234 ΔcsgA*, a.k.a. PHL628- Δ *csgA*) that was kindly provided by the Hay Laboratory (Cornell University).

Table 2-1 Amino acid sequence of wild-type CsgA and CsgA variants in this study (Orange = CsgA, Black = Linker, Green = TFFs)

CsgA Variants	Amino acid sequence
Wild-type CsgA	MKLLKVAIAAIVFSGSALAGVVPQYGGGGNHGGGGNNSGPNSELNIY QYGGGNSALALQTDARNSDLTITQHGGGNGADVGGQSDSSIDLTRG FGNSATLDQWNGKNSEMTVKQFGGGNGAAVDQTASNSSVNVTVGFG NNATAHQY
CsgA-F48-TFF1	MKLLKVAIAAIVFSGSALAGVVPQYGGGGNHGGGGNNSGPNSELNIY QYGGGNSALALQTDARNSDLTITQHGGGNGADVGGQSDSSIDLTRG FGNSATLDQWNGKNSEMTVKQFGGGNGAAVDQTASNSSVNVTVGFG NNATAHQYGGGSGGGSGGGSGGGSGGGSGGGSGGGSGGGSGGGSGGG SGGGSGGGSEAQTETCTVAPRERQNCGFPVTPSQCANKGCCFDDTVRG VPWCFYPNTIDVPPEEECEF
CsgA-F48-TFF2	MKLLKVAIAAIVFSGSALAGVVPQYGGGGNHGGGGNNSGPNSELNIY QYGGGNSALALQTDARNSDLTITQHGGGNGADVGGQSDSSIDLTRG FGNSATLDQWNGKNSEMTVKQFGGGNGAAVDQTASNSSVNVTVGFG NNATAHQYGGGSGGGSGGGSGGGSGGGSGGGSGGGSGGGSGGGSGGG SGGGSGGGSEKPSQCQCSRLSPHNRTNCGFPGITSDQCFDNGCCFDSSVT GVPWCFHPLPKQESDQCVMEVSDRRNCGYPGISPEECASRKCCFSNFIFE VPWCFPPKSVEDCHY
CsgA-F48-TFF3	MKLLKVAIAAIVFSGSALAGVVPQYGGGGNHGGGGNNSGPNSELNIY QYGGGNSALALQTDARNSDLTITQHGGGNGADVGGQSDSSIDLTRG FGNSATLDQWNGKNSEMTVKQFGGGNGAAVDQTASNSSVNVTVGFG NNATAHQYGGGSGGGSGGGSGGGSGGGSGGGSGGGSGGGSGGGSGGG SGGGSGGGSEEVVGLSANQCAVPAKDRVDCGYPHVTPKECNNRGCFFD SRIPGVPWCFKPLQEAECTF

2.5.2 Curli nanofiber expression

To express curli nanofibers, PHL628- Δ *csgA* was transformed with pBbE1a plasmids encoding for wt-CsgA, CsgA-TFF1, CsgA-TFF2, or CsgA-TFF3, or a control plasmid without any CsgA encoding gene. Transformed cells were streaked onto fresh Luria Broth (LB) agar plates supplemented with 100 μ g/mL carbenicillin and were grown overnight at 37 °C. A single colony was picked, inoculated in LB medium containing 100 μ g/mL carbenicillin and incubated overnight at 37 °C. The overnight culture was diluted 1:100 in fresh LB medium with 100 μ g/mL carbenicillin grown and the protein expression was carried out overnight at 37 °C.

2.5.3 Quantitative Congo Red (CR) binding assays

Congo Red (CR) binding assays were adapted from previously described protocols (Marcus A. et al, 2012). Briefly, 1 mL of bacterial culture, 20 hours after induction, was pelleted by centrifugation at 8000 rpm for 10 minutes. The pellet was gently resuspended in 1 mL of 15 µg/mL Congo Red (Sigma-Aldrich) solution in PBS and incubated at room temperature for 10 minutes. Subsequently, the mixture was centrifuged at 14000 rpm for 10 minutes. 150 µL of the supernatant was then transferred to a transparent 96-well plate (FALCON). The untreated Congo Red solution in PBS was used as a negative control. The absorbance of the supernatant at 490 nm was determined using a plate reader (BioTek Synergy H1 Multi-Mode Plate Reader), and the amount of bound Congo Red was quantified by subtraction.

2.5.4 Whole-cell filtration ELISA

A whole-cell ELISA assay was adapted from a previously published protocol³⁶ and used to quantitatively detect both the presence of extracellular assembled CsgA, and the presence of trefoil factors 1-3. PHL628- Δ *csgA* transformants were inoculated in 5 mL of LB liquid media supplemented with 100 µg/mL of carbenicillin, grown to mid-log phase and either induced with 0.3 mM of IPTG or grown without added IPTG based on optimal curli expression. Subsequently, cells were incubated at 37°C for 20 hours before analysis. The cultures were chilled on ice and diluted to an OD₆₀₀ of 0.3 using TBS buffer (0.05M Tris, pH 7.4). 25 µL of the diluted samples were added to a Multiscreen-GV 96-well filter plate (0.22 µm pore size; EMD Millipore) and filtered through. The wells were washed three times with wash buffer (TBS, 0.1% Tween-20) and incubated with 200 µL of blocking solution (1% bovine serum albumin and 0.01% H₂O₂ in wash buffer) for 1.5 hours at 37 °C. The wells were washed three times with wash buffer, incubated with

50 μ L of either anti-CsgA antibody³⁷ (1:10,000 dilution in wash buffer), anti-TFF1 antibody (Sigma-Aldrich) (1:500 dilution), anti-TFF2 antibody (Sigma-Aldrich) (1:500 dilution), or anti-TFF3 antibody (Sigma-Aldrich) (1:450 dilution) for 1.5 hours at 25 °C and washed three times with wash buffer. The samples were incubated with a goat anti-rabbit HRP conjugated antibody (Thermo Fisher Scientific) (1:5,000 dilution) for 1 hour at 25°C, washed three times with wash buffer and reacted with 100 μ L of Ultra-TMB (3,3',5,5'-tetramethylbenzidine) ELISA substrate (Thermo Fisher Scientific) at 25 °C for 20 minutes. The reaction was stopped by the addition of 50 μ L of 2 M H₂SO₄. 100 μ L of this reaction was transferred to a clear 96-well plate. Plate Reader (BioTek) was used to analyze the sample by measuring the absorbance at 450 nm and a reference wavelength at 650 nm.

2.5.5 Semi-purification of curli nanofibers via filtration

The purification of curli nanofibers was adapted from a previously described method¹⁶. Culture expressing either the curli-TFF fusions or wild-type curli fibers was concentrated onto a 47 mm polycarbonate filter membrane with 10 μ m pores (EMD Millipore) using vacuum filtration. The membrane-deposited fibers were rinsed 3 times with 25 mL of sterile DI water. Next, the filtered fibers were incubated with 5 mL of 5% (m/v) sodium dodecyl sulfate (SDS) in water for 5 min, followed by vacuum filtration of the liquid and 3 rinses with 25 mL of DI water. Semi-purified curli nanofibers were removed from the filter membrane by gently scraping the filter with a flat spatula. Purified curli nanofibers were lyophilized and stored at 4 °C.

2.5.6 Adhesion of engineered bacteria to epithelial cells

10^5 Caco-2 cells at passage 5-15 were plated in a 24-well plate (Falcon) in 500 μ L of DMEM with Glutamax with 15% FBS and 1% Penicillin-Streptomycin (Gibco) and incubated at 37 °C in a 5% CO₂ incubator for 48 hours to reach confluency. Induced bacterial cultures were centrifuged, washed with PBS, and resuspended to an OD₆₀₀ value of 0.5 in DMEM with 1 g/L glucose and 1% FBS (Gibco). The Caco-2 monolayers were washed twice with 500 μ L PBS to remove the antibiotic. 500 μ L of the bacterial samples were added to the Caco-2 monolayers and incubated for 2 hours before removal by aspiration. The Caco-2 cells were washed twice with 500 μ L PBS to remove unbound bacteria. In order to count the remaining viable bacteria, cells were removed from the underlying plates by exposure to 250 μ L of 0.05% Trypsin-EDTA (Gibco) followed by incubation at 37 °C for 10 minutes. 750 μ L of LB media were added to the well and the cells were rigorously resuspended. The samples were serially diluted and plated on antibiotic selective plates (carbenicillin, 100 μ g/mL) to enumerate colony forming units (CFU) of adhered bacteria.

2.5.7 Invasion of engineered bacteria into epithelial cells

The Caco-2 cell plates were prepared as described for the adhesion assay. Induced bacterial cultures were centrifuged, washed with PBS, and resuspended to an OD₆₀₀ value of 0.5 in DMEM with 1 g/L glucose and 1% FBS (Gibco). The Caco-2 monolayers were washed twice with 500 μ L PBS to remove the antibiotic. 500 μ L of the bacterial samples were added to the Caco-2 monolayers and incubated for 2 hours before removal by aspiration. The Caco-2 cells were washed twice with 500 μ L PBS. 500 μ L of DMEM with 1 g/L glucose and 1% FBS supplemented with 100 μ g/mL gentamicin (Sigma) was added to each well and incubated for 1 hour to kill extracellular bacteria. In order to count the invaded bacteria, Caco-2 cells were lysed by incubating

with 1 mL of 1% Triton-X (Sigma) 37 °C for 10 minutes. The sample in each well was mixed by multiple pipetting, serially diluted and plated on antibiotic selective plates (carbenicillin, 100 µg/mL) to enumerate colony forming units (CFU) of invaded bacteria.

2.5.8 Mucin binding assay

To test the adhesion of engineered curli nanofibers to mucin, bacterial cultures expressing curli fibers were transferred onto a 47 mm polycarbonate filter membranes with 10 µm pores, via vacuum filtration. The filtered biomass of engineered nanofibers was subjected to 10 mg/mL of mucin type II from porcine stomach (Sigma-Aldrich) and the mixture was co-incubated for 1.5 hours at room temperature. Mucin binding experiments were performed on wild-type curli fibers and bare untreated filter membranes to assess the degree of nonspecific binding. Next, the liquid was filtered through, and the membrane was rinsed with 3 times with 5 mL of DI water to remove non-specifically bound mucins. Finally, the membranes with engineered curli fibers and bound mucin were blocked with 5% milk in TBST overnight at 4 °C before being incubated with 5 µg/mL FITC-conjugated anti-MUC2 (MyBioSource) for 2 hours. After further washes with blocking solution, fluorescence was detected using a FluorChem M system (Protein Simple).

2.5.9 Bacterial binding to gut mucosa *ex vivo*

Fresh goat colon (female, 7 months old) was obtained from local butcher (Boston, MA). After removal of fecal matter, 9 cm of colon length was excised. The colon was not washed further in order to maintain the integrity of the mucus layer. The distal end of the colon was tied off ~2 cm from the end to seal one end of the colon. 5 mL of bacteria expressing the engineered curli fibers (OD₆₀₀ ~1 in PBS) was then added to the opening in the proximal side of colonic tube, and

the proximal tube end was also tied off, leaving the fluid-filled colon with a “sausage-like” appearance. The filled “sausage” was placed gently in a 50 mL sample tube filled with PBS and subjected to light shaking for 1 hour at room temperature. Next, the “sausage” was removed from the sample tube, each end of the colon was opened, and 5 mL of PBS was flowed through the open “sausage” tube to remove unbound bacteria. The opened colon tube was then cut open longitudinally, flattened into a sheet, and placed with the mucosal side facing up in a container filled with 15 $\mu\text{g}/\text{mL}$ Congo Red. After 15 minutes of incubation the tissue was rinsed thoroughly with PBS to remove unbound dye.

2.5.10 Rheology of mucin-curli gels

50 mL of bacterial culture expressing curli fibers was pelleted and washed with a 50 mL of PBS. The bacterial pellet was then resuspended in 10 mL of 10 mg/mL mucin type II from porcine stomach (Sigma-Aldrich) and kept lightly shaking at room temperature for 1 hour. Next, the bacteria/mucin mixture was pelleted and the pellet was used directly for rheological measurements, performed on a TA Instruments AR-G2 rheometer with plate-plate geometry. 8 mm plates were used for strain sweeps and frequency sweeps with a gap width of 500 μm and a moisture trap. Strain sweep measurements were carried out from a strain amplitude of 0.1% to 25% at 25.0 $^{\circ}\text{C}$ (± 0.1 $^{\circ}\text{C}$) and a frequency of 1.0 Hz to determine small deformation linearity. Frequency sweep experiments were then performed from 0.1 - 100 Hz at 25.0 $^{\circ}\text{C}$ with a controlled strain amplitude of 1.0 %, which was within the linear response range for all samples. All measurements were performed in triplicate.

2.5.11 Cell migration assay

The human colonic carcinoma cell line Caco-2 BBE1 (ATCC) was maintained between 60-80% confluency in DMEM supplemented with 15% FBS and 1% penicillin/streptomycin (Gibco) at 37 °C in a 5% CO₂ incubator and passaged several times before performing experiments. Next, 2 x10⁵ cells were seeded in each well of a 6-well plate to achieve 100% confluency. Then, the medium was replaced by DMEM medium with 1% FBS and 1% penicillin/streptomycin and incubated overnight at 37 °C. After confluency was reached, a scratch (i.e. “defect”) was made in the cell monolayer with a pipette tip. After defect formation, cells were allowed to incubate for 24 hours in DMEM medium and 1% FBS along with 200 nM of semi-purified curli fibers (CsgA-TFF1, CsgA-TFF2, CsgA-TFF3, wt-CsgA) or the corresponding soluble trefoil factors (Sigma-Aldrich), respectively. Defect size after 0 and 24 hours was measured using ImageJ (NIH). Each experiment was performed in triplicate.

2.5.12 Scanning electron microscopy

200 µL of curliated bacterial cultures were vacuum filtered onto Nuclepore filters (0.22 µm pore size; GE Healthcare Bio-Sciences), rinsed, and fixed with 2% formaldehyde and 2% glutaraldehyde solution overnight at 4 °C. Then, samples were washed with Millipore water for 15 minutes, dehydrated with gradient steps of ethanol (25%, 50%, 75%, 100%, 100%) – 15 minutes for each step – and dried with Critical Point Dryer (Autosamdri®-931, Tousimis®). Finally, the samples were sputter coated with 80:20 Pt:Pd and analyzed on a Zeiss Supra55VP FE-SEM.

2.6 Acknowledgments

This work was done in collaboration with Dr. Anna Duraj-Thatte, Trevor R. Nash, and Frederick R. Ward. This work made use of the Harvard Center for Nanoscale Systems and was supported by National Science Foundation (DMR, 1410751), National Institutes of Health (1R01DK110770-01A1) and the Wyss Institute for Biologically Inspired Engineering. Adapted from Anna M. Duraj-Thatte, Pichet Praveschotinunt, Trevor R. Nash, Frederick R. Ward & Neel S. Joshi “Modulating bacterial and gut mucosal interactions with engineered biofilm matrix proteins” *Scientific Reports* 8, (2018), Open Access.

2.7 References

1. Johansson, M. E. & Hansson, G. C. Immunological aspects of intestinal mucus and mucins. *Nat Rev Immunol.* 16, 639-649 (2016).
2. Caldara, M. et al. Mucin biopolymers prevent bacterial aggregation by retaining cells in the free-swimming state. *Curr Biol.* 22, 2325-2330 (2012).
3. Johansson, M. E. et al. Bacteria penetrate the normally impenetrable inner colon mucus layer in both murine colitis models and patients with ulcerative colitis. *Gut.* 63, 281-291 (2014).
4. Marcobal, A., Southwick, A. M., Earle, K. A. & Sonnenburg, J. L. A refined palate: bacterial consumption of host glycans in the gut. *Glycobiology.* 23, 1038-1046 (2013).
5. Juge, N. Microbial adhesins to gastrointestinal mucus. *Trends Microbiol.* 20, 30-39 (2012).
6. Pinero-Lambea, C., Ruano-Gallego, D. & Fernandez, L. A. Engineered bacteria as therapeutic agents. *Curr Opin Biotechnol.* 35, 94-102 (2015).
7. Turroni, F. et al. Role of sortase-dependent pili of *Bifidobacterium bifidum* PRL2010 in modulating bacterium-host interactions. *Proc Natl Acad Sci U S A.* 110, 11151-11156 (2013).
8. Tukul, C. et al. Toll-like receptors 1 and 2 cooperatively mediate immune responses to curli, a common amyloid from enterobacterial biofilms. *Cell Microbiol.* 12, 1495-1505 (2010).
9. Claesen, J. & Fischbach, M. A. Synthetic microbes as drug delivery systems. *ACS Synth Biol.* 4, 358-364 (2015).
10. Maxmen, A. Living therapeutics: Scientists genetically modify bacteria to deliver drugs. *Nat Med.* 23, 5-7 (2017).
11. Duan, F. F., Liu, J. H. & March, J. C. Engineered commensal bacteria reprogram intestinal cells into glucose-responsive insulin-secreting cells for the treatment of diabetes. *Diabetes.* 64, 1794-1803 (2015).
12. Braat, H. et al. A phase I trial with transgenic bacteria expressing interleukin-10 in Crohn's disease. *Clin Gastroenterol Hepatol.* 4, 754-759 (2006).
13. Ou, B. et al. Genetic engineering of probiotic *Escherichia coli* Nissle 1917 for clinical application. *Appl Microbiol Biotechnol.* 100, 8693-8699 (2016).
14. Barnhart, M. M. & Chapman, M. R. Curli biogenesis and function. *Annu Rev Microbiol.* 60, 131-147 (2006).

15. Nguyen, P. Q., Botyanszki, Z., Tay, P. K. & Joshi, N. S. Programmable biofilm-based materials from engineered curli nanofibres. *Nat Commun.* 5, 4945 (2014).
16. Noémie-Manuelle Dorval Courchesne, A. D.-T., Pei Kun R. Tay, Peter Q. Nguyen, and Neel S. Joshi. Scalable Production of Genetically Engineered Nanofibrous Macroscopic Materials via Filtration. *ACS Biomater. Sci. Eng.* 3, 733–741 (2017).
17. Tomasetto, C. et al. pS2/TFF1 interacts directly with the VWFC cysteine-rich domains of mucins. *Gastroenterology.* 118, 70-80 (2000).
18. Newton, J. L., Allen, A., Westley, B. R. & May, F. E. The human trefoil peptide, TFF1, is present in different molecular forms that are intimately associated with mucus in normal stomach. *Gut.* 46, 312-320 (2000).
19. Kindon, H., Pothoulakis, C., Thim, L., Lynch-Devaney, K. & Podolsky, D. K. Trefoil peptide protection of intestinal epithelial barrier function: cooperative interaction with mucin glycoprotein. *Gastroenterology.* 109, 516-523 (1995).
20. Thim, L., Madsen, F. & Poulsen, S. S. Effect of trefoil factors on the viscoelastic properties of mucus gels. *Eur J Clin Invest.* 32, 519-527 (2002).
21. Hoffmann, W. Trefoil factors TFF (trefoil factor family) peptide-triggered signals promoting mucosal restitution. *Cell Mol Life Sci.* 62, 2932-2938 (2005).
22. Meyer zum Buschenfelde, D., Tauber, R. & Huber, O. TFF3-peptide increases transepithelial resistance in epithelial cells by modulating claudin-1 and -2 expression. *Peptides.* 27, 3383-3390 (2006).
23. Aamann, L., Vestergaard, E. M. & Gronbaek, H. Trefoil factors in inflammatory bowel disease. *World J Gastroenterol.* 20, 3223-3230 (2014).
24. Conway, T. & Cohen, P. S. Commensal and Pathogenic *Escherichia coli* Metabolism in the Gut. *Microbiol Spectr.* 3 (2015).
25. Vidal, O. et al. Isolation of an *Escherichia coli* K-12 mutant strain able to form biofilms on inert surfaces: involvement of a new *ompR* allele that increases curli expression. *J Bacteriol.* 180, 2442-2449 (1998).
26. Li, H. et al. The outer mucus layer hosts a distinct intestinal microbial niche. *Nat Commun.* 6, 8292 (2015).
27. Kjellek, S., Nexø, E., Thim, L. & Poulsen, S. S. Systemically administered trefoil factors are secreted into the gastric lumen and increase the viscosity of gastric contents. *Br J Pharmacol.* 149, 92-99 (2006).
28. Kline, K. A., Falker, S., Dahlberg, S., Normark, S. & Henriques-Normark, B. Bacterial adhesins in host-microbe interactions. *Cell Host Microbe.* 5, 580-592 (2009).

29. Oertel, M. et al. Trefoil factor family-peptides promote migration of human bronchial epithelial cells: synergistic effect with epidermal growth factor. *Am J Respir Cell Mol Biol.* 25, 418-424 (2001).
30. Yu, G. et al. Cell migration-promoting and apoptosis-inhibiting activities of Bm-TFF2 require distinct structure basis. *Biochem Biophys Res Commun.* 400, 724-728 (2010).
31. Hoffmann, W. Trefoil factor family (TFF) peptides and chemokine receptors: a promising relationship. *J Med Chem.* 52, 6505-6510 (2009).
32. Taupin, D. & Podolsky, D. K. Trefoil factors: initiators of mucosal healing. *Nat Rev Mol Cell Biol.* 4, 721-732 (2003).
33. Van Gerven, N. et al. Secretion and functional display of fusion proteins through the curli biogenesis pathway. *Molecular Microbiology.* 91, 1022-1035 (2014).
34. Botyanszki, Z., Tay, P. K., Nguyen, P. Q., Nussbaumer, M. G. & Joshi, N. S. Engineered catalytic biofilms: Site-specific enzyme immobilization onto *E. coli* curli nanofibers. *Biotechnol Bioeng.* 112, 2016-2024 (2015).
35. Gibson, D. G. et al. Enzymatic assembly of DNA molecules up to several hundred kilobases. *Nat Methods.* 6, 343-345 (2009).
36. Itoh, S. et al. New rapid enzyme-linked immunosorbent assay to detect antibodies against bacterial surface antigens using filtration plates. *Biol Pharm Bull.* 25, 986-990 (2002).
37. Chapman, M. R. et al. Role of *Escherichia coli* curli operons in directing amyloid fiber formation. *Science.* 295, 851-855 (2002).

Page intentionally left blank

**Chapter 3 Engineered *E. coli* Nissle 1917 for the
delivery of matrix-tethered therapeutic domains to
the gut**

3.1 Abstract

There is an unmet need for new treatment methods for inflammatory bowel disease (IBD) that can reliably maintain remission without leading to detrimental side effects. Beneficial bacteria have been utilized as an alternative treatment for IBD albeit with low efficacy. We genetically engineered *Escherichia coli* Nissle 1917 (EcN) to create an anti-inflammatory fibrous matrix *in situ*. This matrix consists of EcN-produced curli nanofibers displaying trefoil factors (TFFs), known to promote intestinal barrier function and epithelial restitution. We confirmed that engineered EcN was able to secrete the curli-fused TFFs *in vitro* and *in vivo*, and was non-pathogenic. We observed an enhanced protective effect of engineered EcN against dextran sodium sulfate induced colitis in mice, associated with barrier function reinforcement and immunomodulation. This work sets the foundation for the development of a novel therapeutic platform in which the *in situ* production of a therapeutic protein matrix from beneficial bacteria can be exploited.

3.2 Introduction

Inflammatory Bowel Disease (IBD) describes a group of autoimmune diseases that cause chronic inflammation of the small and large intestine. This group of diseases affects about 3 million adults in the U.S.¹. A complete picture of IBD etiology remains a subject of intense research and debate, and the development of the disease has been linked to multiple factors, including dysregulated immune responses, genetic predisposition, and an altered balance of microbiota (i.e. dysbiosis)². However, the complex interplay between these factors has greatly hindered the development of effective therapies. Conventional IBD treatment relies on pharmacological

interventions that scale with the severity of the disease, starting with aminosalicylates and antibiotics, and proceeding to corticosteroids and immunosuppressants, with the goal of dampening inflammation by influencing host biology or by decreasing the chance of bacterial infection of mucosal wounds. The consequences of disease flare-ups can be severe and mount over time, leading to 23-45% of ulcerative colitis patients and 75% of Crohn's disease patients requiring surgical removal of portions of their gastrointestinal (GI) tract at some point in their lives³. Therefore, the ability to induce deep remission and sustain it indefinitely is the long-term goal of IBD treatments.

Some early successes with therapies that target tumor necrosis factor (TNF) initially indicated a promising future for biologics in the treatment of severe cases of IBD. However, progress in the development of new therapeutics has been slow, with several notable clinical failures arising from drug candidates with strong results in small animal models⁴. A common theme in these failures is that the efficacy for a given treatment varies according to patient sub-population or environmental factors (e.g. diet, social behaviors). Given the heterogeneity in disease etiology, it is likely that multi-pronged and perhaps patient-specific management strategies will be necessary to achieve effective clinical outcomes⁵.

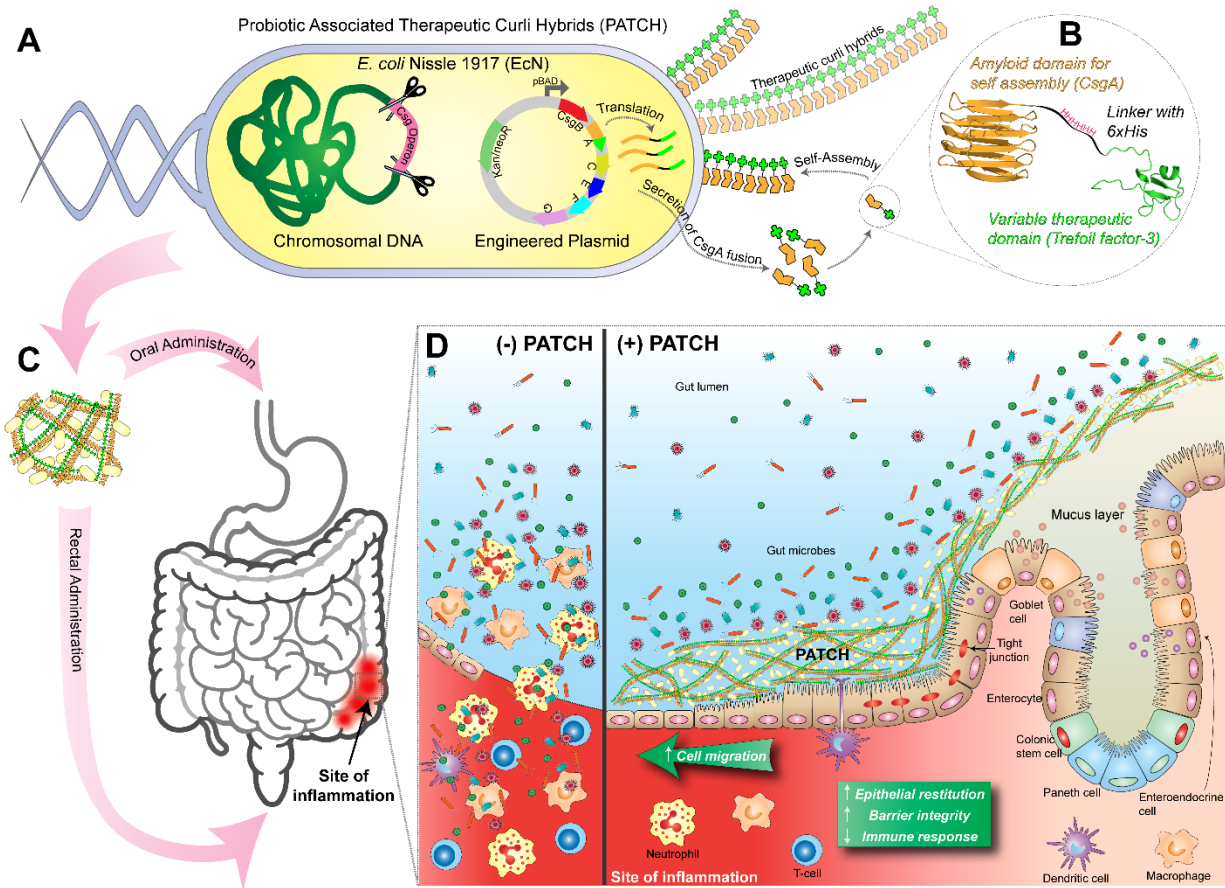


Figure 3.1 Probiotic Associated Therapeutic Curli Hybrids (PATCH). (A) Schematic overview of engineered curli production. Genetically engineered *E. coli* Nissle 1917 (EcN) with *csg* (curli) operon deletion (PBP8 strain) containing plasmids encoding a synthetic curli operon capable of producing chimeric CsgA proteins (yellow chevrons with appended bright green domains), which are secreted and self-assembled extracellularly into therapeutic curli hybrid fibers. (B) CsgA (yellow), the main proteinaceous component of *E. coli* biofilm matrix, was genetically fused to a therapeutic domain – in this case, TFF3 (PDB ID: 19ET, bright green), which is a cytokine secreted by mucus producing cells. The flexible linker (black) includes a 6xHis tag for detection purposes. (C) Engineered bacteria are produced in bulk before delivery to the subject via oral or rectal routes. A site of colonic inflammation is highlighted in red. (D) Interaction of PATCH and the colonic mucosa. Inflammatory lesions in IBD result in loss of colonic crypt structure, damage to epithelial tissue and compromised barrier integrity (left panel, (-) PATCH). The resulting invasion of luminal contents and recruitment of immune cells to the site exacerbates the local inflammation. The application of PATCH (right panel, (+) PATCH) reinforces barrier function, promotes epithelial restitution, and dampens inflammatory signaling to ameliorate IBD activity.

An emerging area of IBD research deals with gut microbes. Although it remains unclear whether dysbiosis can incite disease, it is clear that global reductions in gut microbiome diversity are correlated with IBD severity⁶. Furthermore, it is also clear that many microbiota can exacerbate

IBD-associated inflammation via compromised epithelial barrier function⁷. These factors have led to the exploration of living bacteria as therapeutic entities that can be delivered orally (i.e. “bugs as drugs”). Several naturally occurring commensal and beneficial strains have been explored as therapeutics, with limited success mostly stemming from their low potency and inability to persist in the GI tract^{8,9}. Genetically engineered microbes have also been explored, mostly as a means to secrete biologic drugs (e.g. IL-10, anti-TNF) locally in the colon¹⁰⁻¹². Many such efforts have also shown high efficacy in animal models but have yet to yield clinical successes, in part because of difficulties in achieving and maintaining sufficiently high concentrations of the therapeutic molecule at the site of disease. Indeed, concerns have been raised about the compatibility of this strategy with immunomodulatory biologics, since the mucosal epithelial barrier hinders their trafficking to their target cells in the lamina propria^{13,14}. Nevertheless, the promise of effective treatments that can be produced cheaply, delivered orally, and minimize systemic side effects has continued to fuel interest in microbes as therapeutics.

Here we present an alternative approach to engineered microbial therapies for IBD treatment. Instead of secreting soluble therapeutic proteins, we programmed bacteria to assemble a multivalent material decorated with anti-inflammatory domains in the gut. The displayed domains are designed to target the material to the mucosal layer of the epithelium and promote host processes that reinforce epithelial barrier function (Figure 3.1). The bacterially-produced scaffold for the living material is based on curli fibers, a common proteinaceous component of bacterial extracellular matrices. Hence, we refer to our approach as Probiotic Associated Therapeutic Curli Hybrids (PATCH). We demonstrate that PATCH is capable of ameliorating inflammation caused by dextran sodium sulfate (DSS) induced colitis in a mouse model.

3.3 Results and Discussion

3.3.1 Probiotic Associated Therapeutic Curli Hybrids (PATCH)

We used *E. coli* Nissle 1917 (EcN) as our cellular chassis for PATCH. EcN is well-studied, has a long track record of safety in humans, and is a popular starting point for engineered therapeutic microbe efforts because of its compatibility with canonical genetic engineering techniques for bacteria¹⁵. In addition to its use as an over-the-counter supplement for general GI disorders, EcN has also been evaluated in comparison to mesalazine for maintaining remission in ulcerative colitis in randomized control trials¹⁶. While EcN lead to some favorable outcomes, overall efficacy was low and relapse rates were high, impeding its use as a first-line treatment for IBD^{16,17}. Like other Enterbacteriaceae, EcN resides mostly in the colon, where it colocalizes with areas affected by many types of IBD¹⁸. Moreover, facultative anaerobes like EcN are known to thrive in the highly oxidative environment of the inflamed GI tract¹⁹, making EcN an ideal starting point for our engineering efforts.

We chose the trefoil factor (TFF) family of human cytokines as our bioactive domain for display on curli fibers. TFFs are small, 7-12 kDa proteins secreted by mucus producing cells in the GI tract and other mucosal surfaces, primarily to promote epithelial restitution²⁰. TFFs also reportedly have tumor suppressing, apoptosis blocking, and barrier function augmenting bioactivity, though the precise mechanisms for these effects are still not well understood^{20,21}. TFFs have been explored for IBD treatment, but oral delivery did not yield therapeutic outcomes, as they were found to adhere too strongly to the mucus layer of the small intestine¹¹. We sought to

overcome this by tethering them to the curli fiber matrix after local production in the ileum, cecum, and colon.

3.3.2 TFF-fused curli fibers are successfully secreted and assembled by engineered *E. coli* Nissle 1917

In order to implement the PATCH system, we created plasmid-based genetic constructs encoding for the self-assembling monomer unit of curli fibers (CsgA) fused to each of the three TFFs (TFF1-3). The TFFs were appended to the C-terminus of CsgA via a flexible glycine-serine linker containing an internal 6xHIS tag in a manner that we have previously shown to not interfere with extracellular secretion and self-assembly²². The library of plasmids was designed such that each gene encoding a CsgA-TFF fusion was co-transcribed with the other genes necessary for effective curli secretion and assembly (*csgB*, *csgC*, *csgE*, *csgF*, *csgG*). Together, these formed a “synthetic curli operon” that was placed under the control of an inducible promoter (P_{BAD}) in a pBbB8k plasmid backbone bearing a kanamycin selection marker (Figure 3.1). The inclusion of the other genes of the curli operon was necessary to increase secretion efficiency, because the curli genes in the EcN chromosome are downregulated at physiological temperature and osmolarity²³. Nevertheless, we also employed an EcN mutant in which all of the chromosomal curli genes were deleted (EcN $\Delta csgBACDEFG::Cm^R$, a.k.a PBP8) in order to preclude the possibility of curli fiber expression from native genes confounding our experimental results²⁴.

In order to confirm that curli fibers decorated with TFFs could be produced by EcN, as they can in laboratory strains of *E. coli*²², we transformed EcN with the panel of synthetic curli plasmid constructs, in addition to a vector encoding GFP in place of the curli genes as a negative control. The transformed cells were cultured at 37°C in high osmolarity media to mimic physiological

conditions and induced with L-(+)-arabinose. A quantitative Congo Red binding (CR) assay, normally used for curli fiber detection^{22,25}, indicated that wild-type CsgA and all three CsgA-TFF fusions could be expressed and assembled into curli fibers under physiological conditions, while EcN with the GFP-expressing control vector showed no CR binding (Figure 3.2A).. Extracellular assembly was further confirmed using whole-cell ELISA assays probing for the 6xHIS tag (Figure 3.2B). Scanning electron microscopy of the samples confirmed that recombinant wild-type CsgA and all the CsgA-TFF fusions assembled into nanofibrous structures resembling native curli fiber in appearance (Figure 3.2C-G). Curli production experiments performed with PBP8 led to similar trends. In some cases, basal expression of the *csgA* genes was observed without induction (Figure 3.3A, B). We have also confirmed the presence of the displayed TFF3 using similar whole cell ELISA assay (Figure 3.2H).

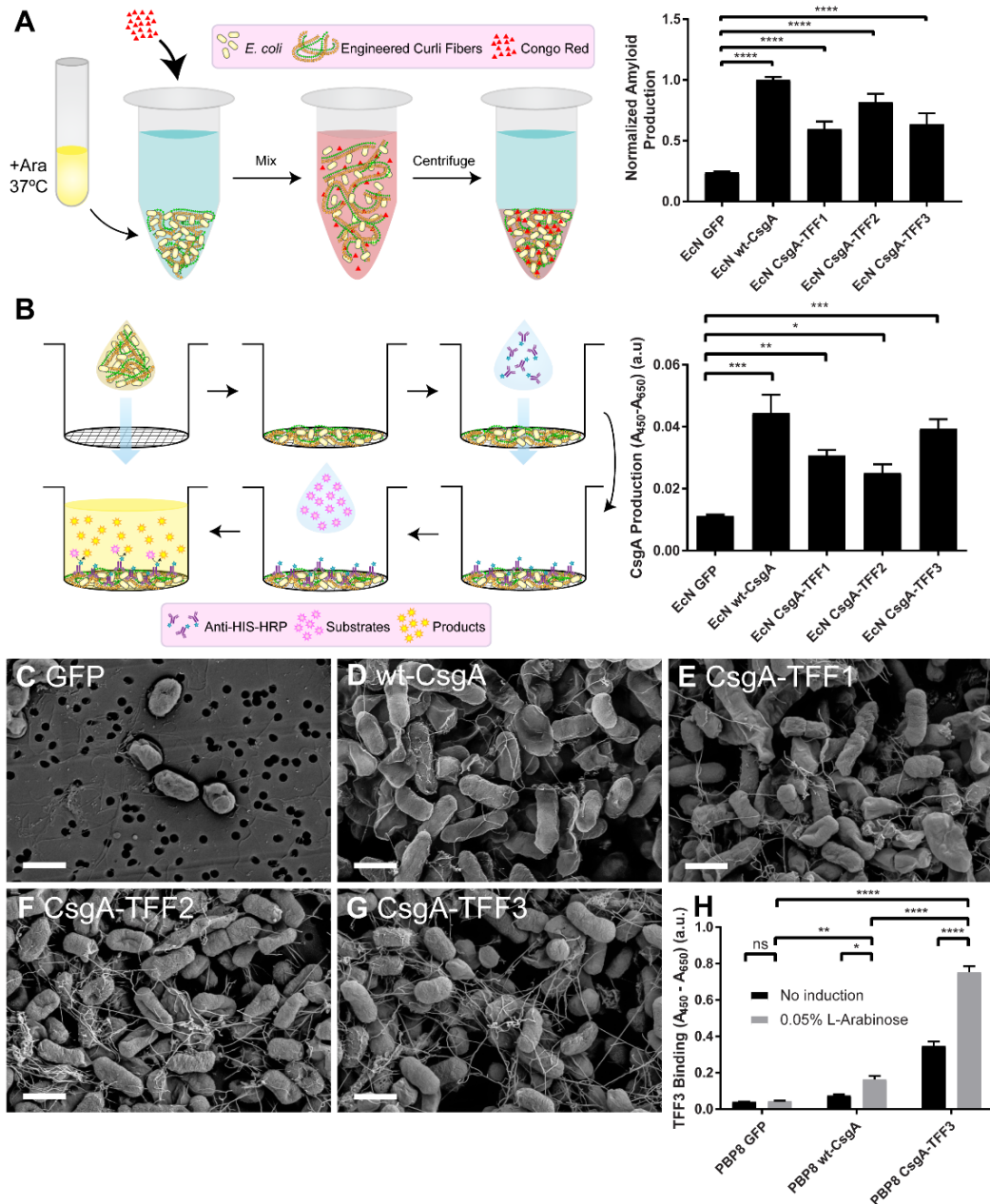


Figure 3.2 Production of curli fiber variants from engineered EcN. (A) Schematic of quantitative Congo Red (CR) binding assay (left). Normalized amyloid production of each EcN variant, as measured by CR binding assay (right), after induction with arabinose (Ara) at 37°C in LB media. (B) Schematic of whole-cell filtration ELISA for the monitoring of modified curli production from bacterial culture (left). Relative CsgA production between EcN variants, derived from anti-6xHis antibody-based detection. (C-G) Scanning electron micrographs of EcN transformed with plasmids encoding various proteins: (C) GFP (D) wt-CsgA (E) CsgA-TFF1 (F) CsgA-TFF2 (G) CsgA-TFF3 (scale bar = 1 μ m). (H) Relative TFF3 production (using anti-TFF3 antibody) of induced and non-induced PBP8 library. Data are represented as mean \pm SEM. See materials and methods for statistics.

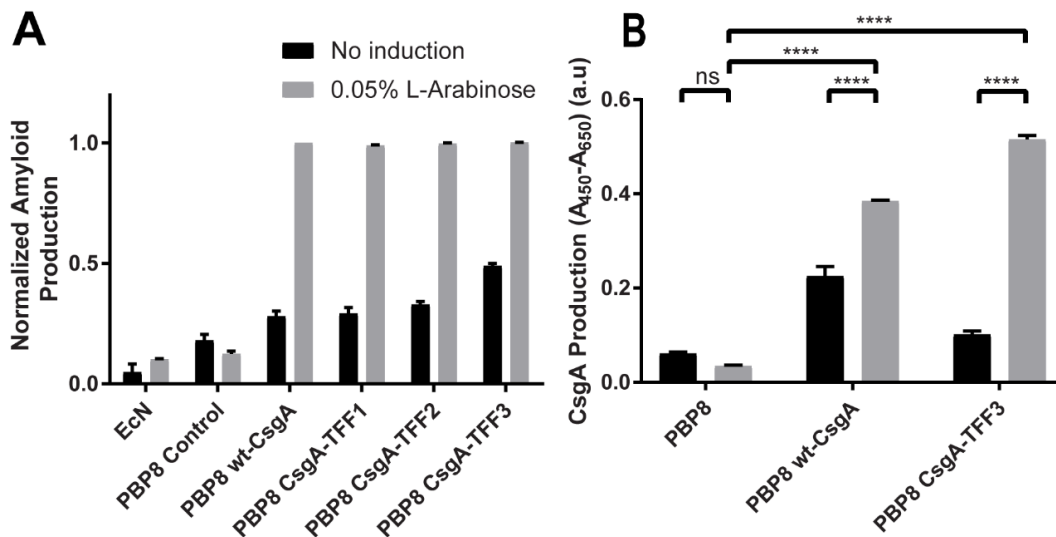


Figure 3.3 (A) Normalized amyloid production of induced and non-induced PBP8 library. (B) Relative CsgA production of induced and non-induced PBP8 library. Data are represented as mean \pm SEM. See materials and methods for statistics.

3.3.3 Engineered curli fibers do not confer pathogenicity to EcN *in vitro*

We had previously demonstrated that the CsgA-TFF3 fusion, when produced by a laboratory strain of *E. coli*, could bind to mucins and promote mammalian cell migration in an *in vitro* model with a human colorectal adenocarcinoma cell line (Caco-2)²². Before proceeding to *in vivo* studies, we wanted to confirm that modified curli fiber overproduction did not induce a pathogenic phenotype in PBP8. Therefore, we performed invasion and barrier function assays on Caco-2 cells grown to confluency in transwells. None of the EcN derived strains (i.e. PBP8 – curli genes deleted, PBP8 wt-CsgA – expressing the wild-type CsgA sequence, PBP8 CsgA-TFF3 – expressing the CsgA-TFF3 fusion) exhibited increased invasiveness into polarized Caco-2 monolayers when compared to unmodified EcN (Figure 3). Invasion for Caco-2 monolayers was low across all groups in comparison to a positive control, *Salmonella typhimurium* (SL 1344) (A). Similarly, in a translocation assay in which bacteria were collected from the basolateral chamber of the transwell²⁶, we observed essentially no translocation of any of the EcN derived strains (B).

We also monitored barrier function in the transwells as a function of bacterial strain. Trans-epithelial electrical resistance (TEER) measurements showed lower TEER values for all of the EcN derived strains compared to *S. typhimurium* – 40-50% vs. 70%, respectively (Figure 3.5). We also tested barrier function *in vitro* via the translocation of fluorescently labeled dextrans by adding them to the apical chamber of the transwell after 24 hours of incubation with the bacteria^{26,27}. We observed almost no translocation for any of the EcN derived strains, while the positive control (*S. typhimurium*) led to significant translocation of the polymer to the basolateral chamber (C). While Caco-2 cells are a crude mimic of the mucosal epithelium, they are known to respond to exposure to pathogenic bacteria in predictable ways that include the activation of pro-inflammatory signaling cascades and release of cytokines such as IL-8^{26,28-31}. We monitored the response of polarized Caco-2 cells to apical bacterial exposure for 24 hours and found that EcN and the PBP8 variants showed no significant differences in IL-8 production, while *S. typhimurium* showed a 4-fold increase compared to cells with no bacterial exposure (D). Overall, the transwell assays indicated that neither PBP8, nor the expression of wt-CsgA or CsgA-TFF3 led to any phenotypes that compromised epithelial integrity compared to unmodified EcN.

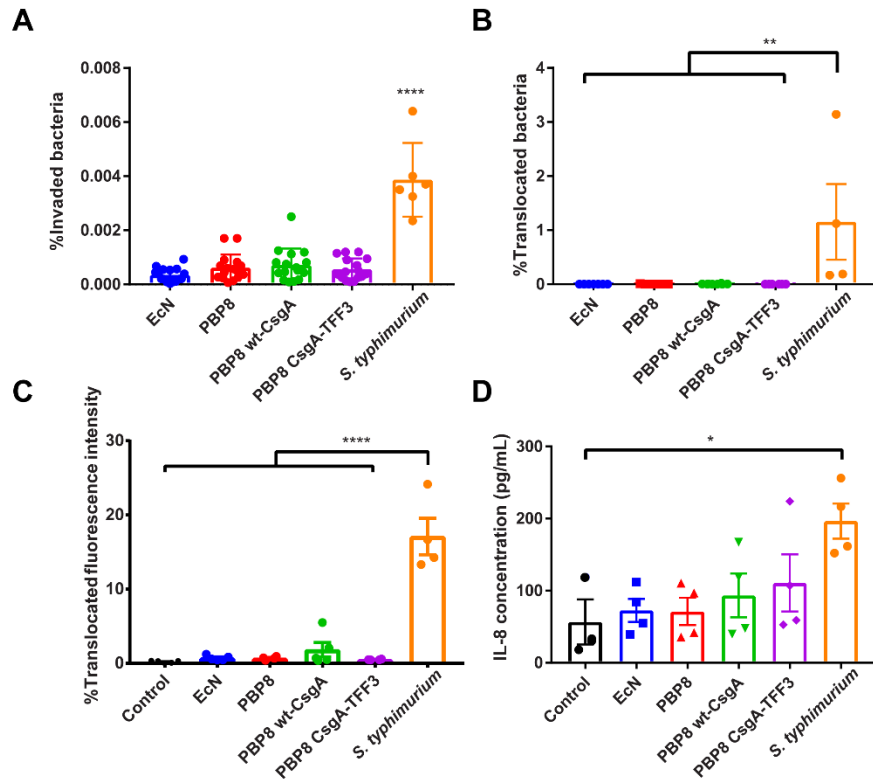


Figure 3.4 Effects of curli fiber expression on EcN pathogenicity. (A) Percent of bacteria that invaded a monolayer of Caco-2 after 2 hours of co-incubation with EcN, PBP8 variants, and *S. typhimurium*. (B) Bacterial translocation to the basolateral compartment of polarized Caco-2 cells exposed to bacterial library for 5 hours. (C) Epithelial permeability of polarized Caco-2 24 hours post-infection, quantified via FITC-dextran (MW 3,000-5000) translocation. (D) IL-8 secretion from the basolateral compartment of polarized Caco-2 cells 24 hours post-infection. Data are represented as mean ± SEM. See materials and methods for statistics.

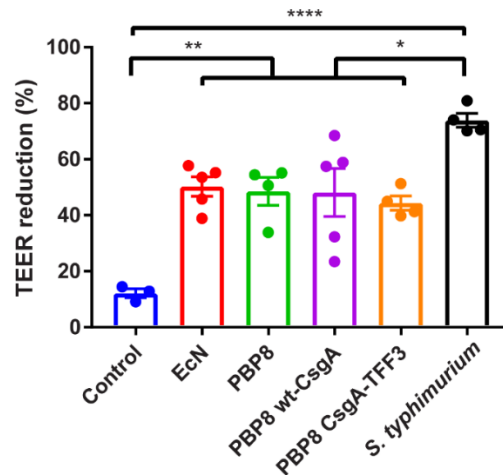


Figure 3.5 Changes in the trans-epithelial electrical resistance (TEER) of polarized Caco-2 cells at 24 hours after infection, and the percentage of reduction was calculated. Data are represented as mean \pm SEM. See materials and methods for statistics.

3.3.4 Engineered EcN can transiently colonize the mouse gut and express curli fibers *in situ*

Our initial *in vivo* experiments focused on demonstrating the viability and persistence of engineered EcN strains in the mouse GI tract after oral administration. For these experiments, we employed an EcN strain with a genomically integrated luminescence operon (*luxABCDE*) to facilitate *in vivo* tracking^{32,33}. After transformation of this EcN strain with the panel of plasmids encoding the synthetic curli operons, the strains were administered to healthy mice (C57BL/6NCrl) via oral gavage, concurrent with drinking water containing kanamycin and L-(+)-arabinose in order to maintain the plasmids and induce curli expression. A single dose of 10^8 colony forming units (CFU) led to persistent colonization (>32 days) of the mouse GI tracts for all but one of the curli producing strains (EcN wt-CsgA, EcN CsgA-TFF2, and EcN CsgA-TFF3), as measured by CFU counted from fecal samples. Notably, EcN wt-CsgA maintained a CFU count of 10^8 - 10^9 CFU/g over the course of the experiment, similar to that of EcN transformed with a pBbB8k plasmid encoding for green fluorescent protein (GFP) as a control (Figure 3.6A). This suggested that wild-type curli fiber overproduction *in vivo* did not compromise the fitness of the engineered

EcN any more than recombinant production of any heterologous intracellular protein. In comparison, EcN CsgA-TFF2 and EcN CsgA-TFF3 concentrations fell over the course of the experiment to $\sim 10^6$ - 10^7 CFU, suggesting that production of the CsgA-TFF fusions was stressful enough to compromise the colonization ability of EcN in the stringent environment of the mouse gut. We speculate that this may be due to the large size of the TFF fusion domains³⁴, in addition to their propensity to form internal disulfide bonds that could hinder extracellular export. Indeed, the difference in growth rates between wt-CsgA and CsgA-TFF producing strains is reflected in the *in vitro* growth rates (Figure 3.7). We further confirmed the presence of the engineered EcN strains in living animals by visualization of the bacterial luminescence on days 2, 6, and 10 after oral administration using an *in vivo* imaging system (IVIS). As expected, the luminescence of the EcN could be observed in the abdomen of all mice that had received bacteria (Figure 3.6B and Figure 3.8).

In addition to the engineered bacteria themselves, we sought to confirm that the engineered curli fibers were being produced *in situ*. We therefore performed ELISA using an anti-6xHis antibody on homogenized fecal samples obtained 5 days after oral administration. We found that, as expected, only mice that had received curli producing strains (EcN wt-CsgA and EcN CsgA-TFFs) showed signal above background levels (Figure 3.6C). In comparison, EcN producing GFP only showed only background signal. Finally, we used immunohistochemistry at the experimental endpoint to visualize the engineered curli fibers directly in tissue sections of the proximal and distal colon (Figure 3.9). The curli fibers were probed with a fluorescently labeled anti-6xHis antibody (*magenta*), while anti-MUC2 (*red*), anti-E-cadherin (*green*), and Hoechst (*blue*) stains were used to visualize the mucins and colonic epithelial cells. We found that due to the fixing and

staining protocol, which were designed to preserve the integrity of the intestinal mucins, the Hoechst and E-cadherin antibodies stained not only the colonic cells, but also DNA and cytoskeletal elements found in the feces and other contents of the gut lumen present in the tissue sections. Nevertheless, the distinct pattern and arrangement of colonic cells in the sections could be used to identify the epithelial border and differentiate them from luminal content. The anti-6xHis staining revealed that wt-CsgA could be observed throughout the gut lumen and near the most superficial layers of mucus, while the PBS control showed minimal background staining. Interestingly, the CsgA-TFF3 signal co-localized with the MUC2 signal, suggesting that the mucin binding activity of the TFFs promoted mucus integration of the engineered curli fibers.

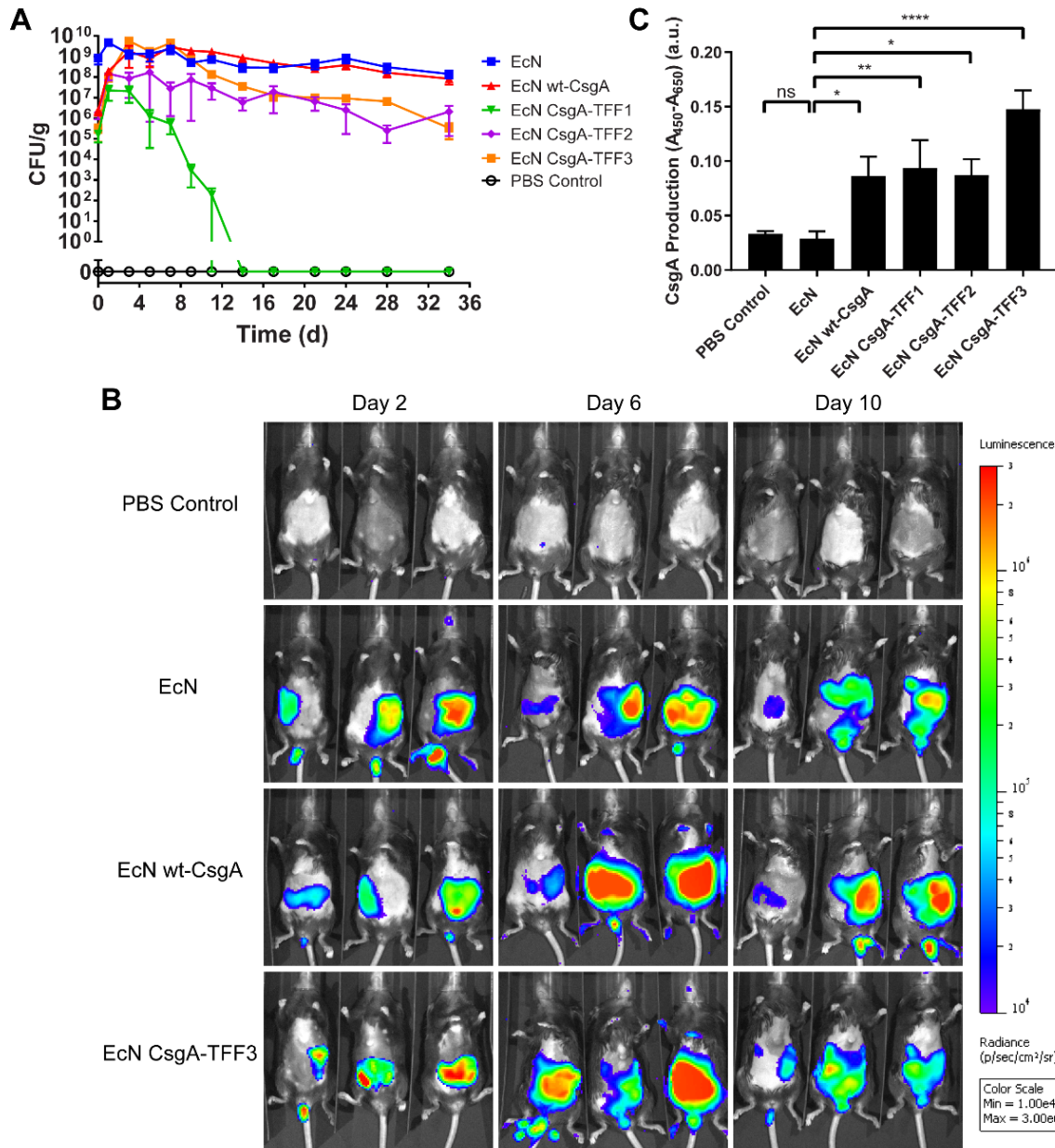


Figure 3.6 Residence time of engineered EcN in the mouse gut and *in vivo* curli expression. (A) *In vivo* residence time for EcN variants, as measured by CFU counting from fecal samples. (B) IVIS images of mice that received either PBS or luminescent EcN variants at various time points post-inoculation. (C) Relative CsgA production from fecal sample analysis from mice administered 5 days post-inoculation, as measured by ELISA. Data are represented as mean \pm SEM. See materials and methods for statistics.

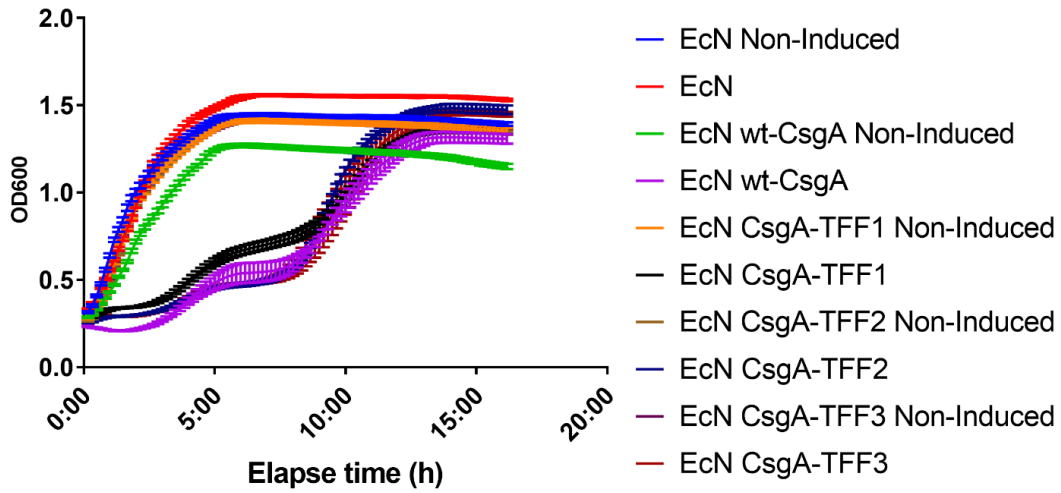


Figure 3.7 *In vitro* growth curve of EcN Prop-luc library (N=6). Data are represented as mean \pm SEM. See materials and methods for statistics.

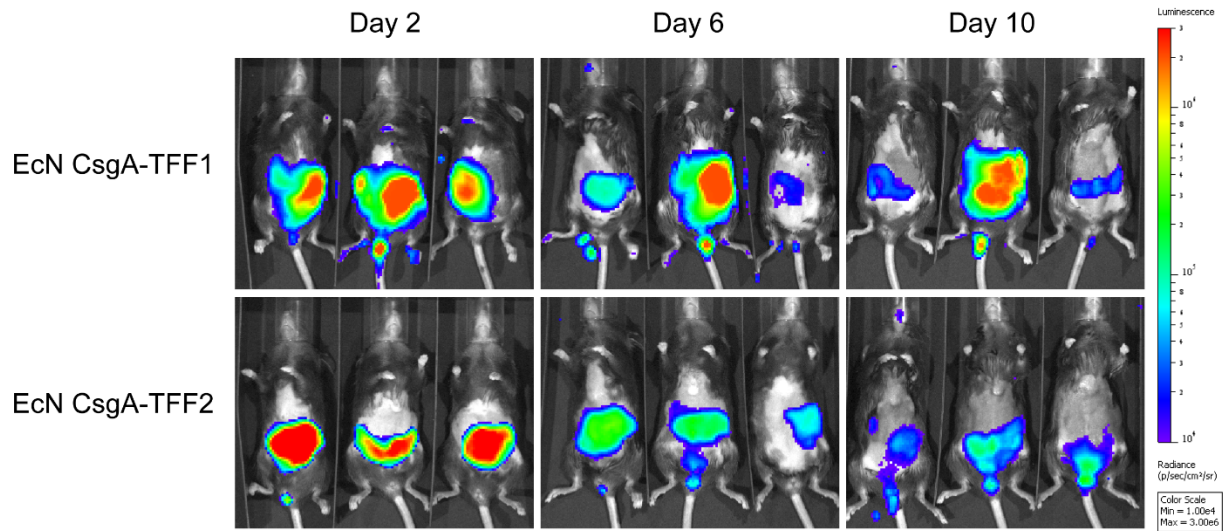


Figure 3.8 IVIS images of mice received EcN Prop-luc CsgA-TFF1 or EcN CsgA-TFF2. Images were taken at day 2, 6 and 10 post-inoculated.

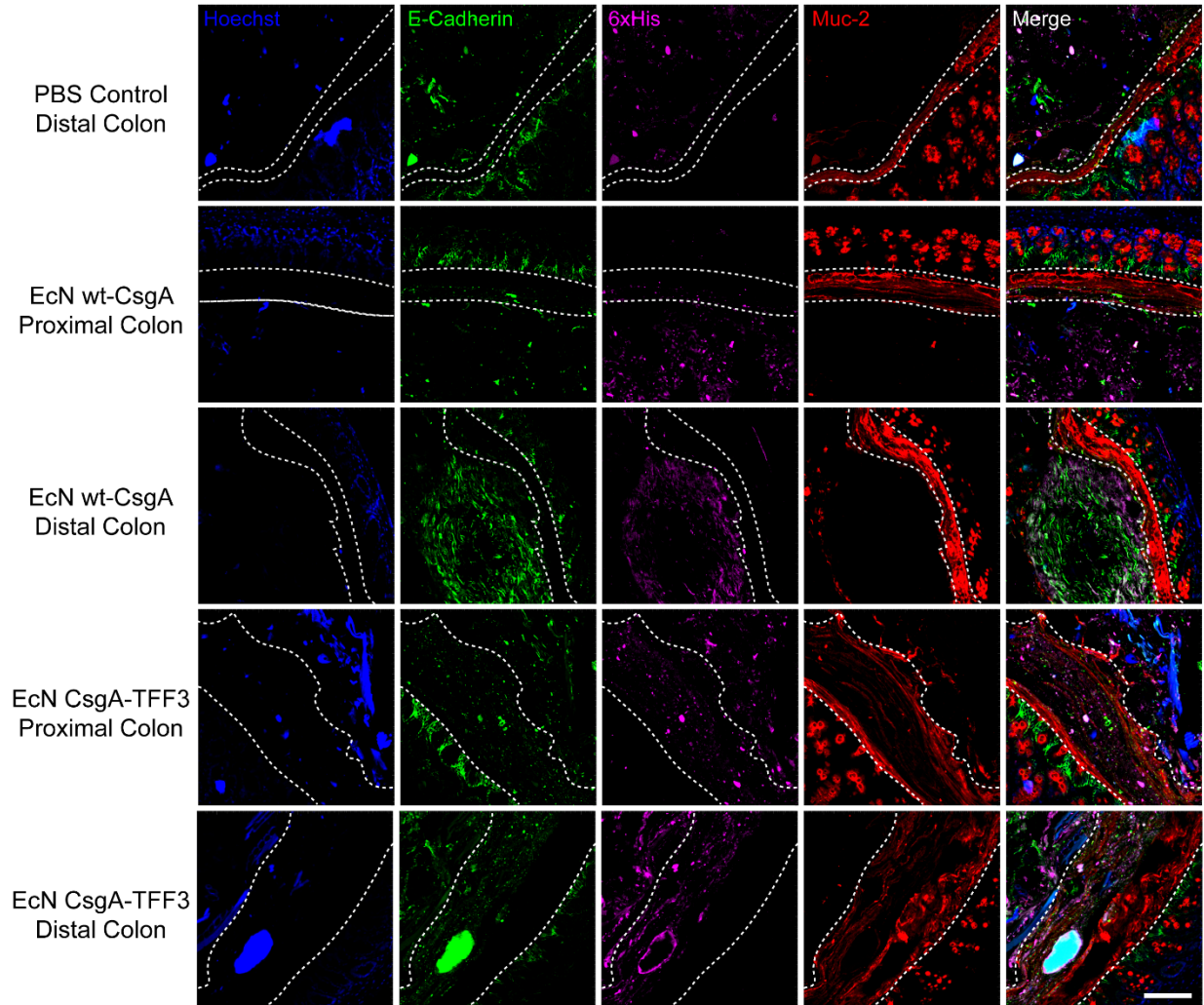


Figure 3.9 Immunohistological visualization of engineered curli fibers in tissue sections from proximal and distal colons of mice receiving different bacteria. Sectioning protocol was designed to preserve mucus and luminal content. Sections were stained with Hoescht (blue) and fluorescently labeled antibodies: anti-E-cadherin (green), anti-6xHis (magenta), anti-Muc2 (red). Last column shows an overlay of all stains. The white dotted lines represent the boundary of the epithelium and mucus layers (scale bar = 100 μ m).

3.3.5 Engineered EcN ameliorates disease activity in a mouse model of DSS-induced colitis

Based on the ability of the engineered EcN strains to colonize the mouse GI tract and the previously demonstrated wound healing and mucin binding activity of CsgA-TFF3 curli fibers *in vitro*²², we sought to investigate their efficacy in a dextran sodium sulfate (DSS) model of murine colonic injury and inflammation^{35,36}. DSS is a chemical colitogen that can be administered orally

to induce epithelial damage and compromised barrier function in the mouse colon. Unmodified EcN and TFF secretion from *Lactococcus* spp. have each individually shown some efficacy against the DSS model, so we reasoned that their combination with the PATCH system would have similarly beneficial effects¹¹.

We examined the protective effects of engineered CsgA-TFF3 produced by PBP8 using female C57BL/6NCrl mice that had been administered 3% DSS over five days to induce colonic inflammation. Pilot experiments with oral administration of PBP8 strains were not very effective in decreasing disease symptoms. However, histological analysis and further literature consultation revealed that DSS induced colitis was most severe in the distal colon, whereas the engineered bacteria resided mostly in the cecum and proximal colon (Figure 3.10)^{24,37,38}. In order to circumvent this peculiarity of the murine DSS model and investigate the efficacy of our approach, we pivoted to rectal administration of the bacteria so that they could easily co-localize with the affected tissues. Notably, we do not envision that this issue would affect the efficacy of engineered bacteria in other models or in humans, as both oral and rectal deliveries are viable routes of drug administration depending on the patient's disease localization.

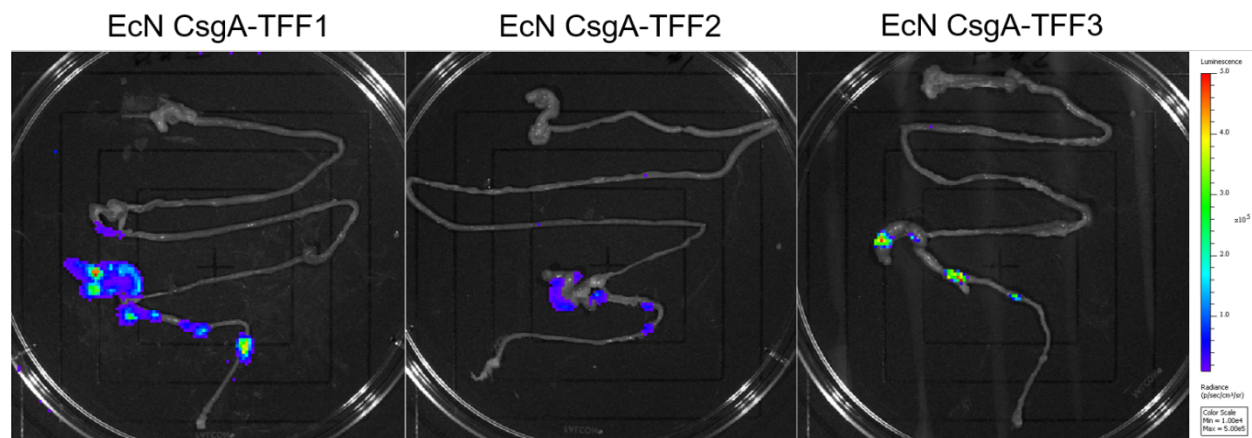


Figure 3.10 *Ex vivo* IVIS images of mouse guts received EcN Prop-luc CsgA-TFF1, EcN CsgA-TFF2, and EcN CsgA-TFF3 showing localization of the engineered EcN. Images were taken at day 2 post-inoculated.

As outlined in Figure 3.11A, the mice received daily administrations of PBP8 rectally for three days prior to DSS intake, during five days of DSS intake, and during a five day recovery period. DSS treatment in mice that had not received any bacteria (PBS DSS⁺) led to intestinal inflammation that could be observed by weight loss and increases in disease activity index (DAI, a composite measure of weight loss, diarrhea index and rectal bleeding, Table 3-2) compared to mice in a healthy control group without DSS treatment (PBS DSS⁻). Mice that received bacteria expressing CsgA-TFF3 (PBP8 CsgA-TFF3 DSS⁺) had significantly ameliorated weight loss and reduced DAI over the course of the experiment and almost returned to the same state as the healthy control group 5 days after DSS removal (Figure 3.11B,C). Mice that received engineered bacteria that were either producing cytosolic GFP as a control (PBP8 DSS⁺) or producing wild-type CsgA (PBP8 wt-CsgA DSS⁺) showed results similar to the disease group without any bacterial administration. The mice were sacrificed at day 10 for investigation of their colons to examine the effects of PBP8 CsgA-TFF3 on the induced colitis. DSS inflammation is associated with colon length reduction³⁹. We found that colon length did not differ significantly between the PBP8 CsgA-TFF3 group and the healthy control group, suggesting that *in situ* CsgA-TFF3 production

attenuated colonic inflammation caused by DSS. In comparison, the colitic control, PBP8, and PBP8 wt-CsgA groups all had shorter colons (Figure 3.11D).

We also assessed the effects of bacterial administration on gut inflammation using histology. Common histological characteristics of DSS induced colitis include immune cell infiltration involving multiple tissue layers as well as loss of colonic crypts and epithelial damage^{40,41}. We employed a histological scoring system based on previously published accounts (Table 3-3)⁴⁰⁻⁴². All of the groups that received DSS treatment had significantly higher histopathology scores than the healthy control group, indicating more inflammatory effects (Figure 3.11E). The histology score for the PBP8 CsgA-TFF3 group was the lowest of all the groups that received DSS, though the difference was not quite significant according to our scoring and statistics criteria. Images of the histology sections from the colitic control group showed complete loss of crypt structure, goblet cell depletion, immune cell infiltration into the lumen, and edema of the tissues around the colon, all of which reflect the severe inflammatory effects of DSS treatment (Figure 3.11F). In contrast, tissue sections from mice treated with bacteria showed some qualitative improvements, with better preservation of crypt structure. The PBP8 CsgA-TFF3 group also showed lower inflammatory cell infiltration, less edema, and more intact epithelium. One explanation for the histological similarity among the DSS treated groups could be that the tissue sections were obtained 5 days after DSS treatment had stopped. Therefore, natural healing processes could have obscured any quantitative differences in histopathology between the groups that received DSS and bacteria.

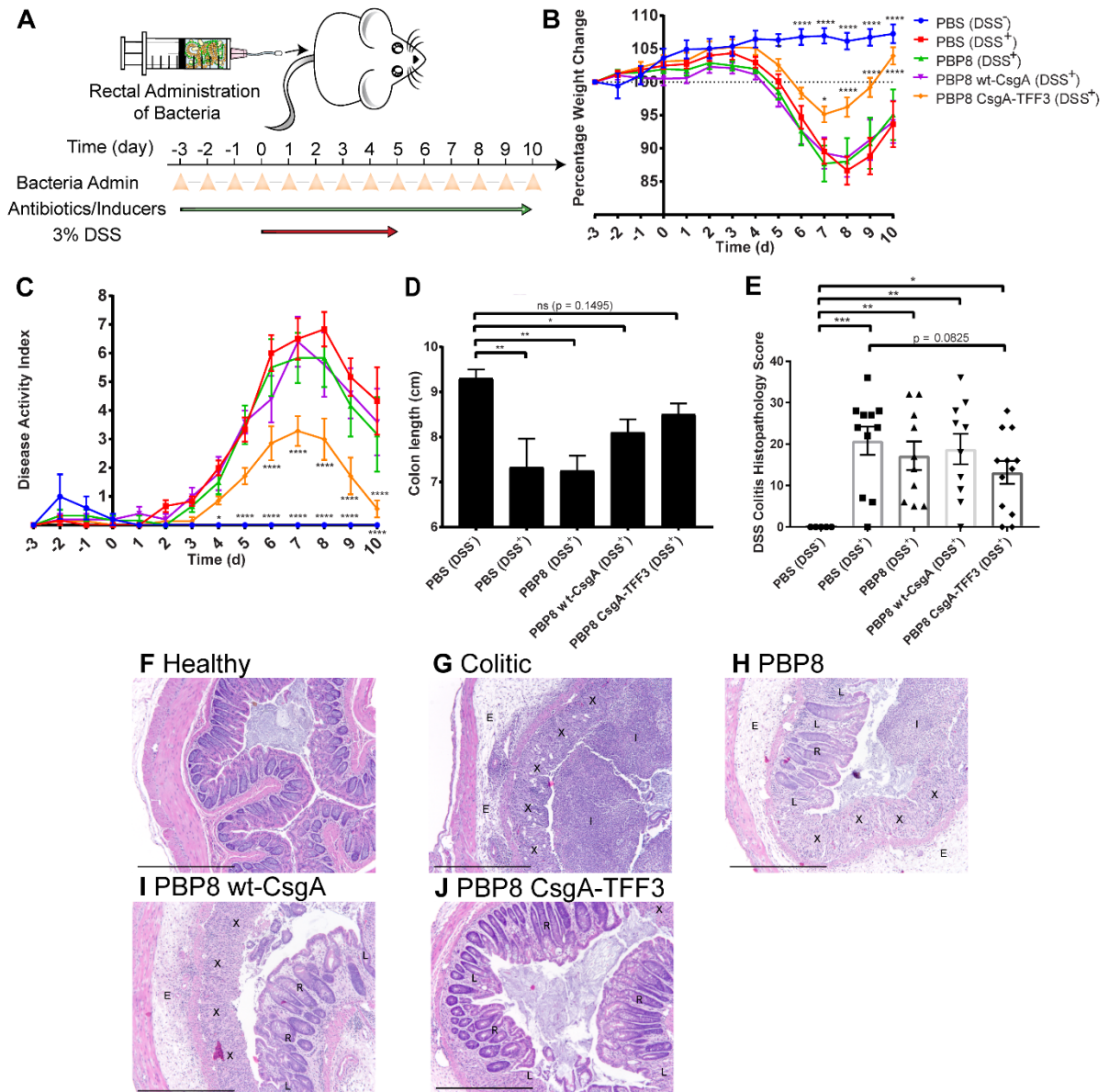


Figure 3.11 Therapeutic efficacy of engineered EcN against mouse model of DSS-induced colitis. (A) Schematic of administration schedule. PBP8 variants (10^8 CFU) were administered rectally daily. Antibiotics and inducers were administered continuously via drinking water. Weight change (B, $N = 9$) and disease activity index (C, $N = 5-7$) over time, averaged across two independent experiments. Activity index criteria are described in Table 1. (D) Colon length at endpoint from two independent experiments ($N = 5-7$). (E) Combined DSS colitis histopathology score reflecting severity of inflammation (see Table 3-3 for details), at endpoint from two independent experiments ($N = 5-10$). (F-J) Representative histology of distal colon sections stained with haematoxylin and eosin from each experimental group: (F) PBS (DSS-) – healthy control, (G) PBS (DSS+) – colitic, (H) PBP8 (DSS+), (I) PBP8 wt-CsgA (DSS+), (J) PBP8 CsgA-TFF3 (DSS+). Image markers indicate complete loss of crypt and goblet cell depletion (X), immune cell

infiltration (I), tissue edema (E), partial loss of the crypts (L), and recovery of crypts (R) (scale bar = 500 μ m). Data are represented as mean \pm SEM. See materials and methods for statistics.

3.3.6 Anti-inflammatory effects of engineered EcN are associated with immunomodulation and barrier function enhancement

In order to start probing the mechanism of the apparent protective effects of the PATCH system with CsgA-TFF3, we analyzed gene expression and protein production profiles from colonic tissue homogenates across the experimental groups. The DSS colitis model leads to several such changes, including downregulation of genes associated with epithelial barrier function and upregulation of genes associated with inflammatory signaling^{43,44}. With respect to tight junction protein-1 (TJP-1), a.k.a. zona occludens-1 (ZO-1), the PBP8 CsgA-TFF3 group showed significantly higher mRNA levels than the colitic control group (Figure 3.12A). This is in line with the known functions of TFFs in mammalian hosts even though other markers of barrier function associated with TFF bioactivity (occludin, claudin-2, and intestinal TFF3, Figure 3.13A-C) did not show changes according to qRT-PCR analysis. Notably, the PBP8 wt-CsgA group also exhibited high *tjp-1* mRNA levels. This should be explained by known interactions between wt-CsgA and toll-like receptor 2 (TLR2), which can indirectly lead to moderate increases in *tjp-1* expression^{45,46}. Although the effects of TFF3 fusion to CsgA on its interaction with host receptors is not clear from this work, it is possible that both domains could contribute to modulating local gene expression.

Matrix metalloproteinase-9 (MMP-9), whose function is to breakdown extracellular matrix proteins in inflammatory environments, is upregulated during IBD and is an essential mediator of tissue injury during DSS colitis. Blockade of MMP-9 has also been explored as a clinical treatment for IBD⁴⁷. In our experiments, the colitic control and PBP8 control groups showed elevated *mmp9* mRNA levels compared to the healthy control group, while the PBP8 CsgA-TFF3 group showed

significantly lower *mmp9* expression (Figure 3.12B). Prostaglandin-endoperoxidase synthase 2 (PTGS-2), a.k.a. cyclooxygenase-2 (COX-2), showed similar results to MMP-9, with the PBP8 CsgA-TFF3 group significantly lower than the colitic group, and comparable with the healthy control group (Figure 3.12C). PTGS-2 is an enzyme whose production is induced in the colon during active IBD⁴⁸. Its inhibition has also been investigated as an anti-inflammatory treatment, and has ameliorated colitis in a murine DSS model⁴⁹. Similar to the case of MMP-9, the PBP8 wt-CsgA group also showed reduced *ptgs2* expression, which likely reflects the known interactions of unmodified curli fibers with the gut epithelium observed in this work and elsewhere⁵⁰.

Finally, we used a parallelized ELISA assay (Luminex), to probe cytokine levels from tissue homogenates obtained from mice at the experimental endpoint. We found that IL-6, IL-17A, and TNF- α concentrations decreased in colonic tissues for the PBP8 CsgA-TFF3 group compared to the colitic group (Figure 3.12D-E, Figure 3.13H). IL-1 β concentrations were also lower, but not statistically significant (Figure 3.13E). Cytokines such as TGF- β , IL-10 and IFN- γ were not significantly affected by any of the bacterial treatments (Figure 3.13D, F-G). The affected cytokines (IL-6, IL-17A, TNF- α and IL-1 β) directly relate to differentiation and secretion of T helper 17 (Th17) cells, which is a lineage of CD4⁺ cells that mediates innate and adaptive immunity against various pathogens at mucosal sites⁵¹.

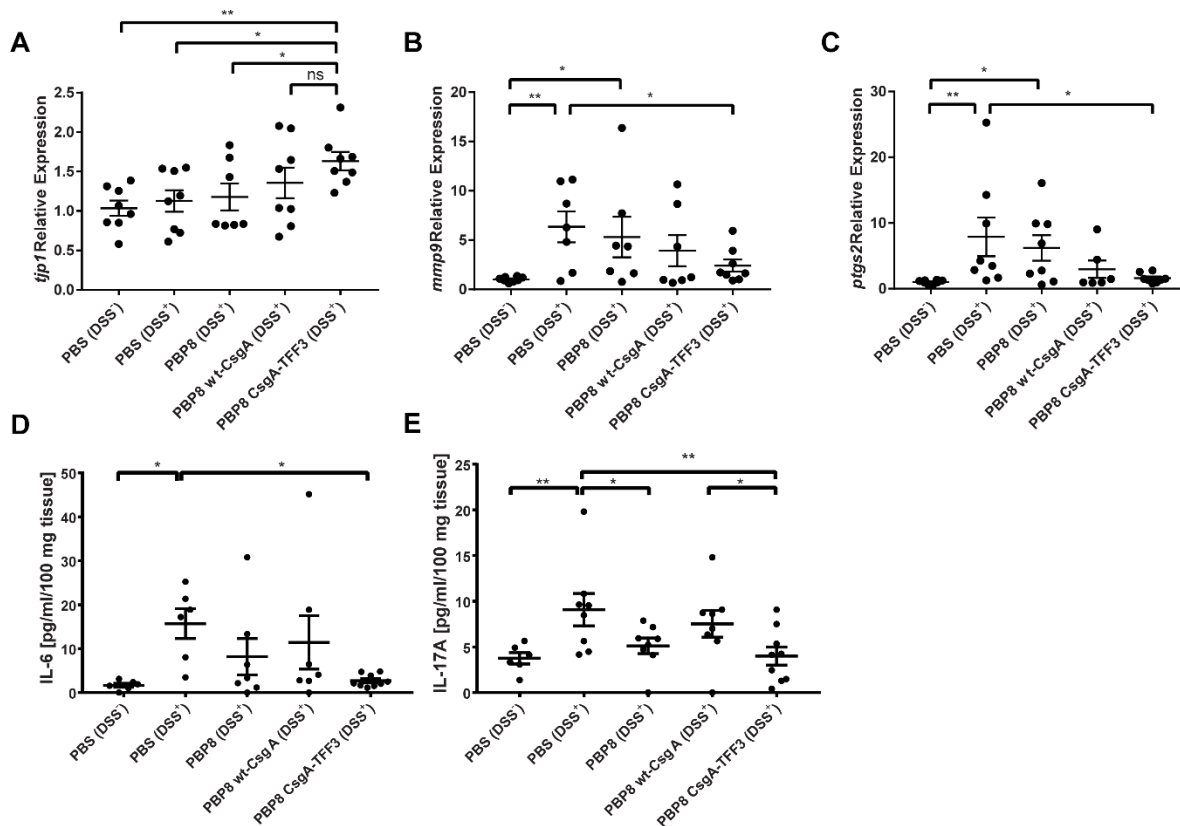


Figure 3.12 Effects of engineered EcN treatment on colonic gene and cytokine expression in DSS-induced colitic mice (A-C) *tjp1*, *mmp9* and *ptgs2* expression measured by qRT-PCR from homogenized distal colon sections. Data are presented as fold change compared to the healthy control group from two independent experiments (N = 7-9). (D-E) IL-6 and IL-17A protein level determined by multiplex ELISA. Data are presented as protein concentration per 100 mg of tissue from two independent experiments (N = 6-9). Data are represented as mean ± SEM. See materials and methods for statistics.

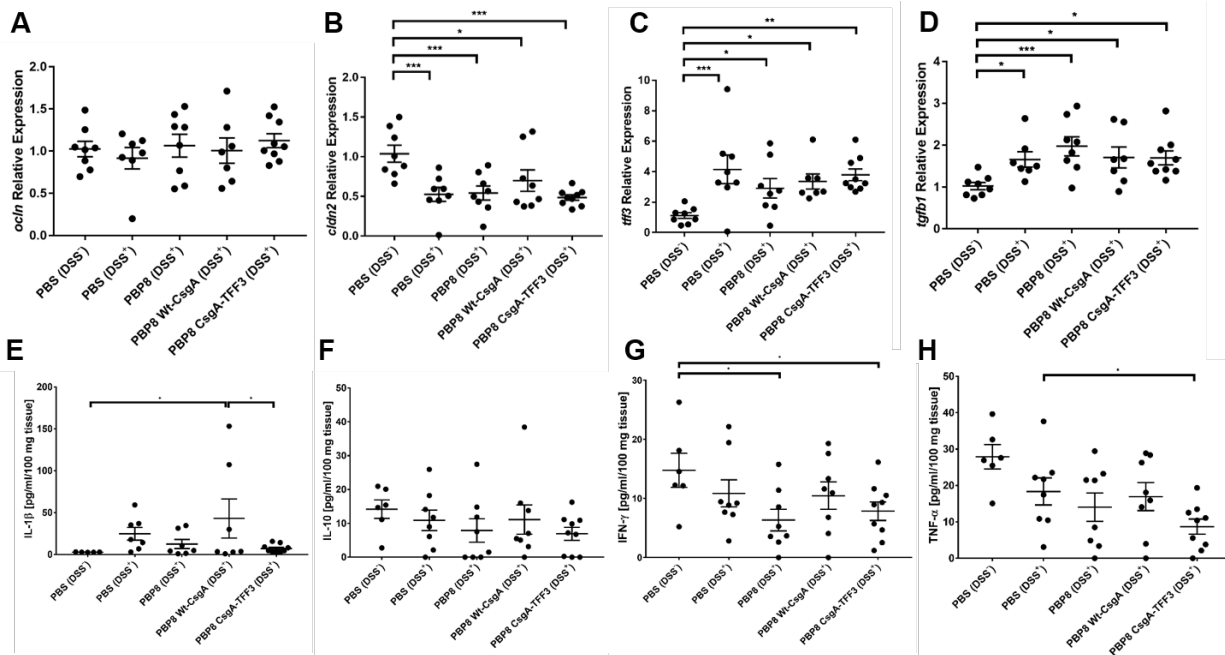


Figure 3.13 Effects of engineered EcN treatment on colonic gene and cytokine expression in DSS-induced colitic mice (A-D) *ocln*, *cldn2*, *tff3* and *tgfb1* expression measured by qRT-PCR from homogenized distal colon of mice. Data are presented as fold change compared to the healthy control group from two independent experiments (N=7-9). (E-H) IL-1 β , IL10, IFN- γ , TNF- α protein level determined by multiplex ELISA from homogenized distal colon of mice. Data are presented as protein concentration per 100 mg of tissue from two independent experiments (N=6-9). Data are represented as mean \pm SEM. See materials and methods for statistics.

3.4 Conclusions

We have developed an engineered beneficial bacterium that produces a self-assembled matrix *in situ* within the GI tract with programmable functions. Our engineering strategy (PATCH) enabled the production of a modified curli fiber matrix with fused TFFs under physiological conditions in a manner that does not appear to alter EcN's inherent lack of pathogenicity. Administration of the engineered bacterium before, during, and after the induction of colitis in mice led to amelioration of inflammation and a reduction in Th17 responses in the colon. The protective effect of PATCH with CsgA-TFF3 also correlated with enhanced mucosal barrier function and a reduction in the expression of inflammatory cytokines and enzymes in colonic

tissues. Although more detailed studies will be required to rigorously confirm the mechanism of these effects, results from the genetic and biochemical analyses we performed were in line with previous accounts of trefoil factor bioactivity, which includes immunomodulation, the promotion of epithelial restitution, and upregulation of tight junction proteins (Figure 3.1)^{20,21}.

Ongoing work in the lab is focused on improving the PATCH system in order to make it more suitable for clinical deployment. In the experiments described here, antibiotics and small molecule inducers were fed to the mice in order to maintain the plasmid's stability in the modified EcN strains and induce curli production, respectively. The antibiotics alter the gut microbiome significantly⁵². To address this issue, second generation PATCH systems should be engineered with stable plasmid systems that do not require antibiotics that have been reported on extensively elsewhere^{33,53,54}. Otherwise, the PATCH system could potentially be integrated into the genome of the bacteria, though the low copy number of the genes might result in lower amount of therapeutics. Regarding the inducers, we can replace the arabinose inducible promoter with environmentally sensitive promoters that respond to temperature or inflammatory markers to avoid the use of external inducers and further improve the system. Although we demonstrated that oral administration was a viable approach to establishing a detectable and stable population of engineered EcN strains in the murine lower intestine, we ultimately opted for rectal administration to colocalize the bacteria near diseased areas and demonstrate efficacy. However, human IBD pathology can be spread across the colon and parts of the small intestine. Furthermore, *E. coli* is similarly localized in humans, and is known to proliferate at sites of inflammation⁵⁵. Therefore, either oral or rectal delivery may be relevant for other models of IBD or in humans. We also recognize that the curli fibers themselves are not a “blank slate” material in that CsgA already has

numerous known interactions with host cells and tissues that could confound the effects of the displayed domains. In fact, wild-type curli fibers were shown to have some anti-inflammatory and barrier protective properties, which could confound our ability to observe the effects of the appended trefoil factors^{26,46,50,56}. While this may or may not impede further development of PATCH with curli fibers as a scaffold, we know that the biosynthetic machinery dedicated to curli secretion can tolerate a wide range of heterologous proteins⁵⁷. We are therefore in the process of exploring other combinations of scaffolding proteins and bioactive domains that can be secreted through the curli (a.k.a. “Type VIII”) pathway to circumvent these confounding effects and probe different therapeutic modalities.

It is worth noting that when comparing our results with current literatures on the use of traditional, oral anti-inflammatory drugs such as 5-aminosalicylic acid (5-ASA) for DSS colitis murine model treatment⁵⁸⁻⁶⁰, we found that our PATCH technology seemed to improve the weight, DAI, and colon length of the mice to a better extent than 5-ASA. Future studies include side-by-side comparison and combination of PATCH and 5-ASA would be interesting to pursue as one of the multi-pronged approach toward IBD treatment.

Effective treatments for IBD with fewer undesirable side effects are a pressing medical need. Our platform has several features that make it potentially useful for clinical applications, including compatibility with oral administration, local biologic delivery that could mitigate systemic side effects, and high local concentrations of therapeutic entities in the gut lumen due to their anchoring to a self-assembled matrix. While further work is required to determine if this strategy can overcome the limited potency of other engineered microbial endeavors in human trials, it may work well as a combination therapy with other interventions for long-term disease management.

Furthermore, the modularity of the PATCH system may make it useful for the display of domains with other therapeutic targets, including GI cancers, enzyme deficiencies, and pathogen sequestration.

3.5 Materials and Methods

3.5.1 Cell strains and plasmids

E. coli Nissle 1917 Prop-Luc strain (EcN *LuxABCDE*, erythromycin resistance) was kindly provided as a gift from Sangeeta Bhatia's lab (Massachusetts Institute of Technology). *E. coli* PBP8 strain was derived from *E. coli* Nissle 1917 by genomic deletion of the curli operon²⁴. *S. typhimurium* (strain SL1344) was provided by Pam Silver's lab (Harvard University).

The design and construction of the synthetic curli operon encoding plasmids are described in detail elsewhere²⁴. Briefly, a pBbB8k plasmid backbone contains the genes *csgBA*CEFG* as a single cistron, controlled by the *araBAD* promoter, where A* indicates either wild-type or chimeric CsgA. Gene fragments encoding 6xHis tag modified TFF1-3 domains were cloned into these vectors to create pBbB8k-CsgA-TFF1, pBbB8k-CsgA-TFF2, and pBbB8k-CsgA-TFF3 (see Table 3-5 and Table 3-6 for CsgA fusion sequences and Figure 3.14 for pBbB8k-wt-CsgA plasmid map). The list of bacteria strains and plasmids can be found in Table 3-1. The list of reagents with distributors can be found in Table 3-7.

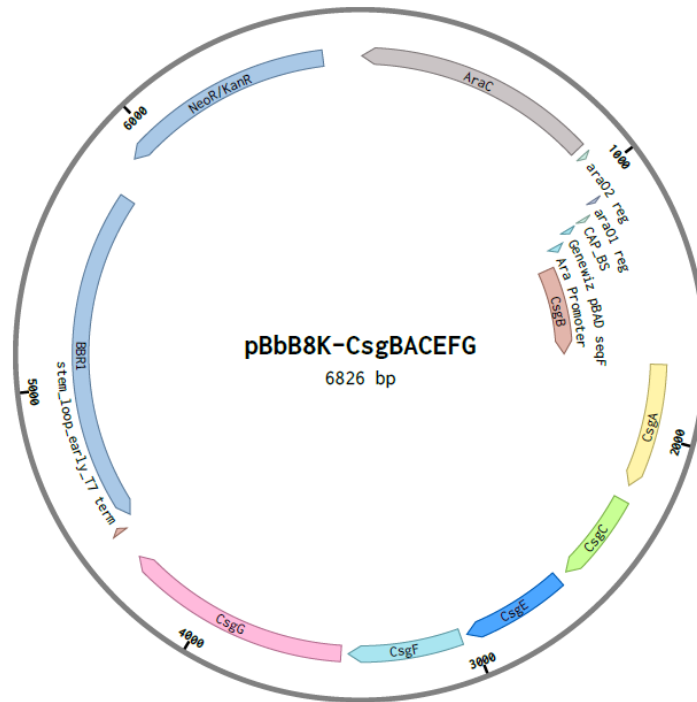


Figure 3.14 pBbB8k-wt-CsgA plasmid map.

Table 3-1 Bacterial strains and plasmids

Designation	Genotype	Reference
Bacterial strains		
E. coli Nissle 1917 (EcN)	Human commensal E. coli isolate	16
Prop-luc	EcN luxABCDE erm(Erythromycin Resistance)	61
PBP8	EcN Δcsg operon::CAT (Choloramphenicol Resistance)	24
Plasmids		
pBbB8k-GFP	GFP expressing, arabinose inducible plasmid, kanamycin resistance	Addgene#35363
pBbB8k-wt-CsgA	wt-CsgA expressing, arabinose inducible plasmid, kanamycin resistance	24

pBbB8k-CsgA-TFF1	CsgA-TFF1 expressing, arabinose inducible plasmid, kanamycin resistance	This study
pBbB8k-CsgA-TFF2	CsgA-TFF2 expressing, arabinose inducible plasmid, kanamycin resistance	This study
pBbB8k-CsgA-TFF3	CsgA-TFF3 expressing, arabinose inducible plasmid, kanamycin resistance	This study

3.5.2 Mice

Female 8- to 9-week-old C57BL/6NCr1 mice were obtained from Charles River Laboratories. Mice were accommodated in SPF conditions while sterile food (normal mouse chow, LabDiets 5K67, or non-fluorescent food, LabDiets 5V5R) and water were provided *ad libitum*. Sterile vinyl isolators equipped with food, water and bedding were used to house the mice within the Harvard Medical School animal facility. Mice had at least one week of acclimatization to the facility environment before any experiment. All experiments were conducted in accordance with US National Institutes of Health guidelines and approved by the Harvard Medical Area Standing Committee on Animals.

3.5.3 *In vitro* expression of engineered curli fiber

EcN Prop-Luc or PBP8 cells were transformed with the corresponding pBbB8k plasmids by electroporation to create variants of curli producing cells and plated onto LB agar plates containing 50 µg/mL kanamycin (Teknova) and incubated overnight at 37°C. Individual colonies were inoculated in 5 mL of LB media containing 50 µg/mL kanamycin, and grown overnight in 37°C shaking incubator. Overnight starter cultures were diluted 100-fold in new LB media containing 50 µg/mL kanamycin at desired volumes and incubated while shaking at 37°C until the refreshed

cultures reached a log phase at an optical density (OD) at 600 nm of 0.5 to 0.8. Then, protein expression was induced by adding L-(+)-arabinose to a final concentration of 0.05% (w/v). The induced cultures were grown in 37°C shaking incubator overnight to allow protein expression.

3.5.4 Quantitative Congo Red binding assay

Based on established protocols^{22,24,62}, one mL of bacterial culture was pelleted and resuspended in a 0.025 mM a solution of Congo Red (CR) in phosphate buffered saline (PBS) for 10 minutes. After pelleting the cells again, the absorbance of the supernatant at 490 nm was measured using a microplate reader. Normalized curli fiber production was calculated by subtracting the measured absorbance value from that measured for 0.025 mM Congo Red in PBS and normalized by the OD₆₀₀ of the original bacterial culture.

3.5.5 Whole-cell filtration ELISA

Following an established protocol^{22,24,62}, the bacterial cultures were diluted to OD₆₀₀ of 0.3 with tris-buffered saline (TBS). The specimens (200 µL) were transferred to a Multiscreen-GV 96-well filter plate, filtered, and washed with TBST buffer (TBS, 0.1% Tween-20). After blocking with with 1% bovine serum albumin (BSA) and 0.01% H₂O₂ in TBST for 1.5 hours at 37°C, and subsequent washing steps, 50 µL of anti-6xHis antibody-horseradish peroxidase (HRP) conjugate (1:200 dilution) was added to each well and incubated for 2 hours at 25°C. For the TFF3 antibody binding assay, samples were incubated with 50 µL of anti-TFF3 primary antibody (1:450 dilution) for 2 hours at 25°C and washed three times with TBST buffer, followed by incubation of 100 µL goat anti-mouse-HRP conjugated secondary antibody (1:5000 dilution) for 1 hour at 25°C and three subsequent washes. After the wash steps, Ultra-TMB (3,3',5,5'-tetramethylbenzidine)

ELISA substrate (100 μ L) was added to each well and incubated for 10 minutes at 25°C. To stop the reaction, 50 μ L of 2 M sulfuric acid was added to each well. 100 μ L of the final reaction was transferred to 96 well plate and measured the absorbance at 450 and 650 nm. The relative amount of displayed peptide was measured by subtracting absorbance at 450 nm with absorbance 650 nm.

3.5.6 Electron microscopy

200 μ L of the testing cultures were filtered onto Nucleopore Track-Etched membranes (0.22 μ m pore size) under vacuum and placed in fixative solution (2 % glutaraldehyde and 2 % paraformaldehyde in 0.1 M sodium cacodylate buffer) for 2 hours at room temperature. After fixation, the membranes were gently rinsed with water and subjected to an ethanol gradient (25, 50, 75, 100 and 100 % (v/v)) with a 15 minute incubation for each concentration. The samples were then transferred to a critical point dryer). The dried membranes were placed on SEM sample holders with carbon adhesives and sputter coated with 80:20 Pt/Pd (5 nm-thick). A Zeiss Ultra 55 Field Emission SEM was used to image the samples.

3.5.7 Cell culture

Caco-2 cells (ATCC) were maintained and passaged in Dulbecco's Modified Eagle Medium (DMEM) supplied with 4.5 g/L glucose and glutamax, 15% fetal bovine serum (FBS) and 1% Penicillin-Streptomycin (Gibco) in a humidified incubator at 37°C, 5% CO₂. For the translocation assay, epithelial integrity and IL-8 production experiments, Caco-2 cells were grown to confluence on 3.0 μ m semipermeable tissue culture inserts (24 wells, Transwell, Corning). After 14-21 days, the cell monolayers achieved a polarized, differentiated state and the transepithelial electrical resistance (TEER) reached 1000-1200 Ω cm².

3.5.8 Invasion assay

The assay was adapted from previously published protocol²². In brief, Caco-2 cells at passage 5-15 were plated in 24-well plates at a density of 10^5 cells per well in 500 μ L of regular cell culture media and grown to 90% confluency. The bacterial cultures were pelleted, washed with PBS and diluted to an OD₆₀₀ of 0.5 in DMEM with 1 g/L glucose and 1% FBS. The Caco-2 cells were rinsed twice with PBS to remove the antibiotic before addition of the bacteria (500 μ L). Bacteria were incubated for 2 hours with the Caco-2 cells and removed by aspiration. The Caco-2 cells were then washed twice with 500 μ L PBS before receiving 500 μ L of DMEM, 1 g/L glucose, 1% FBS and 100 μ g/mL gentamicin. After 1 hour of incubation, the media were aspirated and replaced with 1 mL of 1% Triton-X. The cells were incubated with Triton-X at 37°C for 10 minutes and repeatedly pipetted to homogenize. Each well was serially diluted and plated on kanamycin plates to count the colony forming units (CFU) of bacteria that had invaded the Caco-2 cells.

3.5.9 Translocation assay

This assay was adapted from a published protocol²⁶. EcN variants and *S. Typhimurium* SL 1344 (Silver lab, Harvard Medical School) were grown and induced, if applicable, in LB media with appropriate antibiotics, pelleted, washed with PBS and diluted to OD₆₀₀ of 0.01 in DMEM with 1% glucose and 1% FBS. One day before the experiment, the culture media of polarized Caco-2 (See additional materials and methods) were switched to their corresponding non-antibiotic counterparts with 1% glucose and 1% FBS. 600 μ L of diluted cultures were used to infect polarized Caco-2 apically. After 5 hours of incubation, 100 μ L of media were collected from apical and basolateral sides of the transwell, serially diluted and plated on antibiotic selective plates to enumerate percentage of translocated bacteria.

3.5.10 Epithelial integrity

The experiment was adapted from a published protocol²⁶. The epithelial integrity of polarized Caco-2 was determined by TEER values, and a fluorescein isothiocyanate-labeled dextran (FITC-dextran) translocation experiment. Prior to the infection, the TEER value of each polarized Caco-2 well was determined using Millicell ERS-2 Voltohmmeter. The cells were infected in the same manner as the translocation assay protocol. At 24 hours post infection, the TEER value was measured again to calculate the reduction of TEER. At the same time, 5 μ L of 10 mg/mL FITC-dextran (average molecular weight 3-5 kDa) was added apically to each transwell. Two hours after the addition, 100 μ L of media from the apical and basolateral sides were collected and transferred to a black, clear bottom, 96-well plate and the fluorescence intensity was measured using a plate reader at 485 nm excitation and 520 nm emission wavelength.

3.5.11 IL-8 production

Polarized Caco-2 cells were infected in the same manner as the translocation assay. At 24 hours post infection, 100 μ L of media from the basolateral side was collected and assayed to determine the IL-8 concentration using ELISA kit.

3.5.12 *In vivo* residence time study

This protocol was approved by the Harvard Medical Area Standing Committee on Animals (HMA IACUC) (Ref. No. 05185). Female 8- to 9-week-old C57BL/6NCrl mice were randomly assigned into six groups that each received a different variant of EcN Prop-luc bacteria: GFP, wt-CsgA, CsgA-TFF1, CsgA-TFF2, CsgA-TFF3 and PBS control. Mice were subjected to 18 hours of fasting prior to the experiment, to remove the food in the upper GI tract, but received L-(+)-

arabinose (10 g/L) and kanamycin (1g/L) via drinking water. At the beginning of the experiment (day 0), the bacterial samples were prepared by culturing them to log phase and concentrating them to OD₆₀₀ of 10 in 20% sucrose in PBS. Mice were given either 100 µL of PBS or bacterial suspensions based on their specified groups through oral gavage. Afterward, mice were returned to normal chow with L-(+)-arabinose and kanamycin drinking water. At day 0 (5 hours after the administration), 1, 3, 5, 7, 9, 11, 14, 17, 21, 24, 28, and 34, fecal samples from each mouse were collected, weighed, serially diluted and plated on antibiotic selective plates (erythromycin and kanamycin) to enumerate resident CFU over time.

3.5.13 *In vivo* imaging of engineered microbes

Mice were given an alfalfa-free chow for at least 5 days prior to the experiment to minimize autofluorescence. Mice were given the engineered EcN in the same manner as the residence time protocol in terms of special water and fasting regime. At day 2, 6, 10, mice were shaved at the abdominal area to help expose the GI tract to the IVIS machine. Mice were then imaged under anesthesia using IVIS Lumina II using luminescence filter, with field of view (FOV) = D (12.5 cm), fstop = 1 and large binning. Living Image software version 4.3.1/4.4 was used for image analysis.

3.5.14 Curli immunohistochemistry

Four groups of mice: PBS control, Prop-luc GFP, Prop-luc wt-CsgA, and Prop-luc CsgA-TFF3, were treated in a similar manner in the residence time study. Three days after the oral administration of bacteria, mice were sacrificed to collect the colonic tissues, which were divided into three 1 cm sections: proximal, medial and distal colons. The tissues were cassetted and fixed

in Carnoy's solution (100% ethanol, chloroform and glacial acetic acid in a 6:3:1 ratio), to preserve the mucus layer, for 3 hours at room temperature and transferred to PBS. The fixed tissues were embedded in paraffin and sectioned onto the slides prior to immunohistochemistry steps.

The triple immunofluorescence antigen labeling of the paraffin-embedded murine colon samples was performed with anti-6xHis-tag, Mucin-2 and E-cadherin antibodies. The paraffin sections were deparaffinized and rehydrated, followed by antigen retrieval using sodium citrate buffer (pH 6). The sections were then incubated with 1 mg/mL sodium borohydride (ICN chemicals) for 5 minutes at room temperature. After three washes with TBS, the sections were incubated with Mouse On Mouse (M.O.M.) blocking kit (Vector Labs BMK-2202) for an hour at room temperature. After three washes with TBS the sections were incubated with 5% normal donkey serum (Jackson ImmunoResearch Lab Inc, West Grove PA) for an hour at room temperature. Slides were then incubated with mouse anti-LPS (1:200, abcam ab35654), rabbit anti-Mucin-2 (Santa Cruz sc-15334) and goat anti-E-cadherin (1:200, R&D Systems AF648) overnight at 4°C. The slides were washed three times and incubated with Alexa Fluor 647 conjugated Donkey anti-mouse secondary antibody (1:300, Invitrogen), Cy3 conjugated Donkey anti-rabbit secondary antibody (1:300, Jackson ImmunoResearch Lab) and Alexa Fluor 488 conjugated Donkey anti-goat secondary antibody (1:300, Invitrogen). Samples were counterstained with DAPI and then washed three times with TBS, and the slides were mounted with Prolong Gold anti-fade mounting media (Invitrogen).

3.5.15 Fecal filtration ELISA

Homogenized fecal samples from day 5 of the residence time experiment were transferred onto the Multiscreen-GV 96-well filter plate (0.22 µm pore size). The volumes were normalized

so that about 1.25 mg of fecal samples were on each membrane. Then, the filter plate underwent similar processes: blocking, incubating with anti-6xHis-HRP antibody, and interacting with the TMB substrate, as the whole cell ELISA protocol described above.

3.5.16 Dextran Sodium Sulfate (DSS) model of mouse colitis and treatment protocol

Mice were randomly assigned to five groups: non-colitic (PBS DSS⁻), colitic (PBS DSS⁺), PBP8 with GFP control vector-treated (PBP8 DSS⁺), PBP8 with wild-type CsgA vector-treated (PBP8 wt-CsgA DSS⁺), and PBP8 with CsgA-TFF3 vector-treated (PBP8 CsgA-TFF3 DSS⁺) with n = 4-5 in each group for each set of experiments. During the course of one experiment (14 days), mice were fed with normal mouse chow *ad libitum* while animal body weight and water intake were evaluated daily. At the beginning of the experiment (day -3), mice in all groups started receiving 10 g/L L-(+)-arabinose and 1 g/L kanamycin in drinking water. Meanwhile, the PBP8 bacteria cultures were grown, induced overnight, centrifuged and resuspended to an OD₆₀₀ of 10 in 20% sucrose in PBS. Then, mice received 100 µL PBS (in PBS DSS⁻ and PBS DSS⁺ groups), PBP8, PBP8 wt-CsgA and PBP8 CsgA-TFF3 by rectal administration once daily throughout the experimental period. Three days after the start of bacterial administration (day 0), colitis was induced by the addition of DSS (MW 40,000, Alfa Aesar) to a final concentration of 3% in the drinking water that also contained L-(+)-arabinose and kanamycin. Mice in all groups except the non-colitic (PBS DSS⁻) group received DSS treatment for five days. After DSS removal (day 6), all mice were given the L-(+)-arabinose and kanamycin water until day 10 when they were sacrificed.

The colon of each mouse was removed and its length measured. The feces were gently scraped off. The distal colon of each mouse was divided into three sections (about 1 cm each). The

most proximal section was placed in RNAlater solution, frozen with liquid nitrogen and stored at -80°C until RNA extraction. The middle section was weighed, frozen with liquid nitrogen and stored at -80°C for protein quantification. The most distal section was fixed in 4% paraformaldehyde in PBS buffer overnight at 4°C for histological analysis.

3.5.17 Determination of disease activity

In addition to the body weight, each animal was monitored daily for the presence of blood in the fecal samples and the stool consistency. The parameter and its corresponding scoring that constituted the disease activity index (DAI), shown in Table 3-2, was adapted from a previously published protocol^{44,63}.

Table 3-2 Disease activity index (DAI) parameters and their associated scoring schemes

Score	Weight loss (%)	Stool consistency	Blood in stool
0	None	Normal	Normal
1	1-5	Slightly loose stool	Small presence of blood
2	5-10	Loose stool	Significant presence of blood
3	10-15	Diarrhea	Gross blood
4	>15		
DAI was calculated by addition of scores from all three parameters			

3.5.18 Histological studies

The fixed colonic samples were embedded in paraffin, sectioned (5 µm) and stained with hematoxylin and eosin. The sections were scored blindly by a pathologist for histological evidence of intestinal damage by DSS with a scoring system described previously⁴⁰⁻⁴². In brief, the sections were evaluated for the amount and depth of inflammation using a 0 to 3 score range and the extent of crypt damage using a 0 to 4 score range. Each feature got multiplied by the percentage of the

area involved as indicated in Table 3-3 and added to the total summation. The maximum possible score is 40.

Table 3-3 Histological grading scheme for DSS colitis

Parameter graded	Score	Description
Severity of inflammation	0	None
	1	Slight
	2	Moderate
	3	Severe
Depth of injury	0	None
	1	Mucosa
	2	Mucosa and submucosa
	3	Transmural
Crypt damage	0	None
	1	Basal one-third damaged
	2	Basal two-third damaged
	3	Only surface epithelium intact
	4	Entire crypt and epithelium lost
Percent involvement	x1	0-25%
	x2	26-50%
	x3	51-75%
	x4	76-100%

3.5.19 Luminex multiplex immunoassay

500 μ L of 1X mammalian cell lysis buffer and 5 mm-stainless steel beads were added to frozen tissue samples in 2 mL microcentrifuge tubes. The samples were then homogenized using TissueLyser LT at 50 Hz for 10 minutes at 4°C. Following homogenization, the samples were centrifuged at 10,000 g for 10 minutes at 4°C and the supernatants were transferred to new sample tubes. The samples were tested for six cytokines: IFN- γ , IL-1 β , IL-6, IL-10, IL-17A, and TNF- α , using a Bio-Plex Pro Mouse Cytokine Th17 Panel A 6-Plex kit in accordance with the

manufacturer's protocol. The final 96-well plate was processed using the BioPlex 3D system and the concentration of each cytokine was determined using Bio-Plex Manager software.

3.5.20 Gene expression analysis by qRT-PCR

RNA later-stabilized tissues were subjected to total RNA extraction using the TissueLyser LT and RNeasy plus mini kit in accordance with the manufacturer's protocol. RNA samples were eluted with 100 μ L RNase free water provided from the kit. Following the elution, the concentration of RNA was determined by spectroscopy using the Nanodrop 2000c. 10 ng of RNA was analyzed using specific primers for each gene of interest (Table 3-4) and a KAPA SYBR FAST One-Step qRT-PCR kit with CFX96 real time PCR detection system in accordance with the manufacturer's protocol. The Pfaffl method was used to normalize the expression result⁶⁴. In brief, the $E^{-\Delta\Delta C_t}$ value, where E was the primer efficiency of each primer pair and $-\Delta\Delta C_t$ was difference in the average C_t value of the control groups and the sample, was used to transform the C_t values of each sample into the expression values. Then, the expression values of the housekeeping gene, glyceraldehyde-3-phosphate dehydrogenase (GAPDH), were used to normalize the expression values of each gene in this study.

Table 3-4 qRT-PCR primer set

Organism	Target genes	Protein	Sequence	Reference	Tm	Accession number
Mus musculus	gapdh	Gapdh	5'- CTTTGTCAAGCTCATT TCCTGG-3'	This study	61.1	NM_008084
			5'- TCTTGCTCAGTGCCT TGC-3'		57.6	
Mus musculus	ocln	Occludin	5'- ACTATGCGGAAAGAG TTGACAG-3'	This study	58.5	NM_008756

			5'- GTCATCCACACTCAA GGTCAG-3'		58.1	
Mus musculus	tgfb1	TGF- β 1	5'- CCTGAGTGGCTGTCTT TTGA-3'	This study	59	NM_011577
			5'- CGTGGAGTTTGTTATC TTTGCTG-3'		61	
Mus musculus	mmp9	MMP-9	5'- GATCCCCAGAGCGTC ATTC-3'	This study	60.6	NM_013599
			5'- CCACCTTGTTACCTC ATTTTG-3'		61.7	
Mus musculus	ptgs2	COX2	5'- CTCACGAAGGAACTC AGCAC-3'	This study	58.6	NM_011198
			5'- GGATTGGAACAGCAA GGATTTG-3'		62.9	
Mus musculus	tff3	TFF3	5'- CTGGGATAGCTGCAG ATTACG-3'	This study	59.9	NM_011575
			5'- AGGGCACATTTGGGA TACTG-3'		59.8	
Mus musculus	tjp1	ZO-1	5'- AGCGAATGTCTAAAC CTGGG-3'	This study	59.2	NM_009386
			5'- TCCAACCTGAGCATA ACAGG-3'		58.8	
Mus musculus	cldn2	Claudin-2	5'- CCAAACGACAAGCAA ACAGG-3'	This study	61.6	NM_016675
			5'- CAGCATGGCAATGGA TGTG-3'		62.1	

3.5.21 Statistics

The investigators were not blinded to the experimental conditions during experiments and outcome assessment, except for the pathohistology analysis. Data are presented as the arithmetic means plus or minus SEM. The data were analyzed using GraphPad Prism 7. The statistical

significance of the bar and scatter bar plots were determined using one-way ANOVA followed by Dunnett's (Figure 2), Tukey's (Figure 3) or Fischer LSD multiple comparison (Figure 4, 6D, E, Figure 7). The time course experiments, such as percentage weight change and DAI, were analyzed using two-way ANOVA following by Dunnett's multiple comparison. An associated probability (*p* value) of less than 0.05 was considered significant and given one star, whereas the *p* < 0.01 was given two stars, *p* < 0.001 was given three stars, *p* < 0.0001 was given four stars, and *p* > 0.05 was given "ns" accordingly.

3.5.22 Additional tables

Table 3-5 CsgA fusion DNA sequences

Plasmid name	CsgA Fusion DNA Sequences
pBbB8k-wt-CsgA	ATGAAACTTTTAAAAGTAGCAGCAATTGCAGCAATCGTATTCTCCGGTAGC GCTCTGGCAGGTGTTGTTTCCTCAGTACGGCGGCGGCGGTAACCACGGTGGT GGCGGTAATAATAGCGGCCCAAATTCTGAGCTGAACATTTACCAGTACGGT GGCGGTA ACTCTGCACTTGCTCTGCAA ACTGATGCCCGTAACTCTGACTTG ACTATTACCCAGCATGGCGGGCGGTAATGGTGCAGATGTTGGTCAGGGCTCA GATGACAGCTCAATCGATCTGACCCAACGTGGCTTCGGTAACAGCGCTACT CTTGATCAGTGGAACGGCAAAAATTCTGAAATGACGGTTAAACAGTTCGG TGGTGGCAACGGTGCTGCAGTTGACCAGACTGCATCTAACTCCTCCGTCAA CGTGA CT CAGGTTGGCTTTGGTAACAACGCGACCGCTCATCAGTACGGCTC TGGTGGCTCTGGTGGCTCTGGCGGCAGCGGGCATCACCACCACCATCATTA A

<p>pBbB8k-CsgA-TFF1</p>	<p>ATGAAACTTTTAAAAGTAGCAGCAATTGCAGCAATCGTATTCTCCGGTAGC GCTCTGGCAGGTGTTGTTTCTCAGTACGGCGGCGGCGGTAACCACGGTGGT GGCGGTAATAATAGCGGCCCAAATTCTGAGCTGAACATTTACCAGTACGGT GGCGGTAACCTCTGCACTTGCTCTGCAAACCTGATGCCCGTAACTCTGACTTG ACTATTACCCAGCATGGCGGCGGTAATGGTGCAGATGTTGGTCAGGGCTCA GATGACAGCTCAATCGATCTGACCCAACGTGGCTTCGGTAACAGCGCTACT CTTGATCAGTGGAACGGCAAAAATTCTGAAATGACGGTTAAACAGTTCGG TGGTGGCAACGGTGCTGCAGTTGACCAGACTGCATCTAACTCCTCCGTCAA CGTGACTIONCAGGTTGGCTTTGGTAACAACGCGACCGCTCATCAGTACGGTGG AGGTTCCGGGGGGCGGTTCTGGCGGCGGAAGTGGGGGTGGCTCGGGTGGGG GATCAGGTGGAGGCAGCGGAGGTGGATCGGGGGGAGGGAGTGGTGGCGG TTCGGGTGGTGGGTGAGGGGGAGGGTCTGGGGCGGGGGTAGTCATCATCATC ATCACCATGGGGGAGGTTCCGGGCGGAGGATCGGGGGGAGGCAGCGAAGC ACAAACAGAGACCTGCACCGTTGCACCACGCGAACGTCAAAAATTGCGGGT TTCAGGGGTGACGCCATCTCAGTGCGCCAATAAGGGGTGCTGCTTCGACG ACACTGTTCCGGGCGTTCCTTGGTGTCTTATCCGAACACTATCGATGTACC TCCTGAAGAAGAATGCGAATTTTAA</p>
<p>pBbB8k-CsgA-TFF2</p>	<p>ATGAAACTTTTAAAAGTAGCAGCAATTGCAGCAATCGTATTCTCCGGTAGC GCTCTGGCAGGTGTTGTTTCTCAGTACGGCGGCGGCGGTAACCACGGTGGT GGCGGTAATAATAGCGGCCCAAATTCTGAGCTGAACATTTACCAGTACGGT GGCGGTAACCTCTGCACTTGCTCTGCAAACCTGATGCCCGTAACTCTGACTTG ACTATTACCCAGCATGGCGGCGGTAATGGTGCAGATGTTGGTCAGGGCTCA GATGACAGCTCAATCGATCTGACCCAACGTGGCTTCGGTAACAGCGCTACT CTTGATCAGTGGAACGGCAAAAATTCTGAAATGACGGTTAAACAGTTCGG TGGTGGCAACGGTGCTGCAGTTGACCAGACTGCATCTAACTCCTCCGTCAA CGTGACTIONCAGGTTGGCTTTGGTAACAACGCGACCGCTCATCAGTACGGTGG AGGGAGCGGAGGGGGTAGTGGAGGAGGCTCTGGGGGGGGCAGTGGTGGC GGCTCCGGTGGTGGGTCTGGAGGTGGAAGTGGGGGAGGGTCTGGGCGGCGG CTCGGGTGGGGGATCTGGTGGTGGGAGTGGGGGGGGTAGTCATCATCACC ACCATCATGGGGGAGGGAGCGGTGGCGGCTCTGGAGGGGGGTCCGAAAA GCCATCCCGTGCCAGTGTCTCGTTTGTGCGCCCAACAATCGCACTAATTGT GGGTTTCCCGGCATCACGTCAGACCAATGCTTTGACAACGGATGCTGCTTC GACTCGTCCGTTACGGGAGTCCCCTGGTGTTCACCCGCTGCCTAAGCAA GAGTCTGACCAATGCGTTATGGAGGTAAGCGATCGCCGTAATTGTGGTTAT CCGGGTATCAGTCTGAAGAATGCGCATCCCGCAAATGCTGCTTTAGCAAC TTCATTTTCGAAGTACCCTGGTGTTCCTCCCTAAGTCAGTAGAGGATTGTC ACTATTAA</p>
<p>pBbB8k-CsgA-TFF3</p>	<p>ATGAAACTTTTAAAAGTAGCAGCAATTGCAGCAATCGTATTCTCCGGTAGC GCTCTGGCAGGTGTTGTTTCTCAGTACGGCGGCGGCGGTAACCACGGTGGT GGCGGTAATAATAGCGGCCCAAATTCTGAGCTGAACATTTACCAGTACGGT GGCGGTAACCTCTGCACTTGCTCTGCAAACCTGATGCCCGTAACTCTGACTTG ACTATTACCCAGCATGGCGGCGGTAATGGTGCAGATGTTGGTCAGGGCTCA GATGACAGCTCAATCGATCTGACCCAACGTGGCTTCGGTAACAGCGCTACT CTTGATCAGTGGAACGGCAAAAATTCTGAAATGACGGTTAAACAGTTCGG TGGTGGCAACGGTGCTGCAGTTGACCAGACTGCATCTAACTCCTCCGTCAA CGTGACTIONCAGGTTGGCTTTGGTAACAACGCGACCGCTCATCAGTACGGTGG</p>

TGGTAGTGGTGGCGGCAGTGGTGGCGGTAGCGGCGGTGGCTCCGGTGGCG GTTCTGGCGGCGGTTCTGGTGGTGGTTCTGGCGGTGGCTCAGGTGGGGGTT CCGGCGGCGGTAGCGGCGGTGGATCTGGCGGCGGCTCTCATCATCATC ATCATGGTGGTGGTTCTGGCGGTGGCTCCGGTGGTGGCTCTGAAGAATATG TGGGCCTGAGCGGAACCAGTGC GCGGTGCCGGCGAAAGATCGCGTGGAT TGCGGCTATCCGCATGTGACCCCGAAAGAATGCAACAACCGCGGCTGCTG CTTTGATAGCCGCATTCCGGGCGTGCCGTGGTGTCTTAAACCGCTGCAGGA AGCGGAATGCACCTTTAA

Table 3-6 CsgA fusion amino acid sequences

Plasmid name	CsgA Fusion Amino Acid Sequences
pBbB8k-wt-CsgA	MKLLKVAIAAIVFSGSALAGVVPQYGGGGNHGGGGNNSGPNSELNI YQYGGGNSALALQTDARNSDLTITQHGGGNGADVGQGSDDSSIDLQ RFGNSATLDQWNGKNSEMTVKQFGGGNGAAVDQTASNSSVNVVTQ VGFGNATAHQYGS GSGSGSGSGGSHHHHHH*
pBbB8k-CsgA-TFF1	MKLLKVAIAAIVFSGSALAGVVPQYGGGGNHGGGGNNSGPNSELNI YQYGGGNSALALQTDARNSDLTITQHGGGNGADVGQGSDDSSIDLQ RFGNSATLDQWNGKNSEMTVKQFGGGNGAAVDQTASNSSVNVVTQ VGFGNATAHQYGGGSGGGSGGGSGGGSGGGSGGGSGGGSGGGSGGGSGG GSGGGSGGGSGGGSHHHHHHGGGSGGGSGGGSEAQTETCTVAPRER QNCGFPGVTPSQCANKGCCFDDTVRGPVWCFYPNTIDVPPEEECEF*
pBbB8k-CsgA-TFF2	MKLLKVAIAAIVFSGSALAGVVPQYGGGGNHGGGGNNSGPNSELNI YQYGGGNSALALQTDARNSDLTITQHGGGNGADVGQGSDDSSIDLQ RFGNSATLDQWNGKNSEMTVKQFGGGNGAAVDQTASNSSVNVVTQ VGFGNATAHQYGGGSGGGSGGGSGGGSGGGSGGGSGGGSGGGSGGGSGG GSGGGSGGGSGGGSHHHHHHGGGSGGGSGGGSEKPSPCQCSRLSPHN RTNCGFPGITSDQCFDNGCCFDSSVTGVPWCFHPLPKQESDQCVMEVS DRRNCGYPGISPEECASRKCCFSNFIFVWCFPPKSVEDCHY*
pBbB8k-CsgA-TFF3	MKLLKVAIAAIVFSGSALAGVVPQYGGGGNHGGGGNNSGPNSELNI YQYGGGNSALALQTDARNSDLTITQHGGGNGADVGQGSDDSSIDLQ RFGNSATLDQWNGKNSEMTVKQFGGGNGAAVDQTASNSSVNVVTQ VGFGNATAHQYGGGSGGGSGGGSGGGSGGGSGGGSGGGSGGGSGGGSGG GSGGGSGGGSGGGSHHHHHHGGGSGGGSGGGSEEVVGLSANQCAVP AKDRVDCGYPHVTPKECNNRGCFFDSRIPGVPWCFKPLQEAECTF*

Table 3-7 Supplementary Reagent List

Reagents and instruments (in order of appearance)	Distributors
Congo red	Sigma
50X Phosphate buffered saline (PBS)	Teknova
96 well clear bottom plate	Corning
Biotek H1 Microplate Reader	Biotek
20X Tris-buffered saline (TBS)	Sigma

20X Tris-buffered saline with 0.1% tween-20 (TBST)	Sigma
Bovine serum albumin (BSA)	Sigma
Hydrogen Peroxide	Sigma
Anti-6xHis antibody-horseradish peroxidase (HRP) (MA1-80218)	Thermo Fisher Scientific
Anti-TFF3 primary antibody (WH0007033M1)	Sigma
Goat anti-mouse-HRP conjugated secondary antibody (31430)	Thermo Fisher Scientific
Ultra-TMB (3,3',5,5'-tetramethylbenzidine) ELISA substrate	Thermo Fisher Scientific
6M Sulfuric acid	Alfa Aesar
Nucleopore Track-Etched membranes (0.22 µm pore size)	GE Healthcare Biosciences
4% Glutaldehyde in 0.1 M Sodium cacodylate buffer	Electron Microscopy Sciences
16% Paraformaldehyde	Electron Microscopy Sciences
0.4 M Sodium cacodylate buffer	Electron Microscopy Sciences
Autosamdri-931 critical point dryer	Tousimis
Carbon adhesives	Electron Microscopy Sciences
24-well plate, tissue culture treated	Falcon
DMEM with 1 g/L glucose	Gibco
Fetal bovine serum (FBS)	Gibco
Gentamicin	Sigma
Triton-X	Sigma
Millicell ERS-2 Voltohmmeter	Millipore
FITC-dextran	Sigma
96-well plate, tissue culture treated	Falcon
Human IL-8/CXCL8 Duo Set ELISA, R&D Systems	R&D System
L-(+)-arabinose	Sigma
Kanamycin	RPI
IVIS Lumina II	PerkinElmer
Multiscreen-GV 96-well filter plate	Millipore
RNAlater solution	Sigma
5X mammalian cell lysis buffer	Abcam
5 mm-stainless steel beads	Qiagen
TissueLyser LT	Qiagen
Bio-Plex Pro Mouse Cytokine Th17 Panel A 6-Plex kit	Bio-Rad
BioPlex 3D system	Bio-Rad
RNeasy plus mini kit	Qiagen

Nanodrop 2000c	Thermo Fisher Scientific
KAPA SYBR FAST One-Step qRT-PCR kit	Kapa Biosystems
CFX96 real time PCR detection system	Bio-Rad

3.6 Acknowledgements

This work was done in collaboration with Dr. Anna M. Duraj-Thatte, Ilia Gelfat, Franziska Bahl, and Dr. David B. Chou. This work made use of the Harvard Digestive Diseases Center (HDDC), the Harvard Center for Nanoscale Systems (CNS) and Harvard Medical School ICCB-Longwood Screening Facility, and the Wyss Institute for Biologically Inspired Engineering. We would like to thank Trevor R. Nash, Frederick R. Ward, Amanda Graveline, Andyna Vernet, Frank Urena, Jessica J. Kim, Daniel Um, Mofeyifoluwa Edun, Frederic Vigneault, Elaine Lim, Thomas Ferrante, Garry Cuneo, Li Zuo, Magdalena Kasendra, and Rachelle Prantil-Baun for their help. P.P. thankfully acknowledges the royal Thai government scholarship. D.B.C. gratefully acknowledges the National Institutes of Health grant (2T32CA009216-36). This work was supported by National Institutes of Health (1R01DK110770-01A1), the Blavatnik Biomedical Accelerator fund, and the Wyss Institute for Biologically Inspired Engineering.

3.7 References

1. Dahlhamer, J., P. Zammitti, E., W. Ward, B., Wheaton, A. & B. Croft, J. *Prevalence of Inflammatory Bowel Disease Among Adults Aged ≥ 18 Years — United States, 2015*. Vol. 65 (2016).
2. Fakhoury, M., Negrulj, R., Mooranian, A. & Al-Salami, H. Inflammatory bowel disease: clinical aspects and treatments. *Journal of Inflammation Research*. 7, 113-120 (2014).
3. van Loo, E. S., Dijkstra, G., Ploeg, R. J. & Nieuwenhuijs, V. B. Prevention of postoperative recurrence of Crohn's disease. *Journal of Crohn's and Colitis*. 6, 637-646 (2012).
4. Bilsborough, J., Targan, S. R. & Snapper, S. B. Therapeutic Targets in Inflammatory Bowel Disease: Current and Future. *The American Journal Of Gastroenterology Supplements*. 3, 27 (2016).
5. Wilhelm, S. M. & Love, B. L. Management of patients with inflammatory bowel disease: current and future treatments. *Clinical Pharmacist*. (2017).
6. Nagao-Kitamoto, H. *et al.* Functional Characterization of Inflammatory Bowel Disease–Associated Gut Dysbiosis in Gnotobiotic Mice. *Cellular and Molecular Gastroenterology and Hepatology*. 2, 468-481 (2016).
7. Martini, E., Krug, S. M., Siegmund, B., Neurath, M. F. & Becker, C. Mend Your Fences: The Epithelial Barrier and its Relationship With Mucosal Immunity in Inflammatory Bowel Disease. *Cellular and Molecular Gastroenterology and Hepatology*. 4, 33-46 (2017).
8. Pandey, K. R., Naik, S. R. & Vakil, B. V. Probiotics, prebiotics and synbiotics- a review. *Journal of Food Science and Technology*. 52, 7577-7587 (2015).
9. Sanders, M. E. *et al.* An update on the use and investigation of probiotics in health and disease. *Gut*. 62, 787 (2013).
10. Steidler, L. *et al.* Treatment of Murine Colitis by *Lactococcus lactis* Secreting Interleukin-10. *Science*. 289, 1352-1355 (2000).
11. Vandenbroucke, K. *et al.* Active delivery of trefoil factors by genetically modified *Lactococcus lactis* prevents and heals acute colitis in mice. *Gastroenterology*. 127, 502-513 (2004).
12. Vandenbroucke, K. *et al.* Orally administered *L. lactis* secreting an anti-TNF Nanobody demonstrate efficacy in chronic colitis. *Mucosal Immunol*. 3, 49-56 (2010).

13. Pawar, V. K. *et al.* Targeting of gastrointestinal tract for amended delivery of protein/peptide therapeutics: Strategies and industrial perspectives. *Journal of Controlled Release*. **196**, 168-183 (2014).
14. Smart, A. L., Gaisford, S. & Basit, A. W. Oral peptide and protein delivery: intestinal obstacles and commercial prospects. *Expert Opinion on Drug Delivery*. **11**, 1323-1335 (2014).
15. Ou, B. *et al.* Genetic engineering of probiotic *Escherichia coli* Nissle 1917 for clinical application. *Applied Microbiology and Biotechnology*. **100**, 8693-8699 (2016).
16. Sonnenborn, U. & Schulze, J. The non-pathogenic *Escherichia coli* strain Nissle 1917 – features of a versatile probiotic. *Microbial Ecology in Health and Disease*. **21**, 122-158 (2009).
17. Scaldaferrri, F. *et al.* Role and mechanisms of action of *Escherichia coli* Nissle 1917 in the maintenance of remission in ulcerative colitis patients: An update. *World Journal of Gastroenterology*. **22**, 5505-5511 (2016).
18. Mowat, A. M. & Agace, W. W. Regional specialization within the intestinal immune system. *Nature Reviews Immunology*. **14**, 667 (2014).
19. Lavelle, A., Lennon, G., Winter, D. C. & O'Connell, P. R. Colonic biogeography in health and ulcerative colitis. *Gut Microbes*. **7**, 435-442 (2016).
20. Taupin, D. & Podolsky, D. K. Trefoil factors: initiators of mucosal healing. *Nature Reviews Molecular Cell Biology*. **4**, 721 (2003).
21. Aamann, L., Vestergaard, E. M. & Grønbaek, H. Trefoil factors in inflammatory bowel disease. *World Journal of Gastroenterology : WJG*. **20**, 3223-3230 (2014).
22. Duraj-Thatte, A. M., Praveschotinunt, P., Nash, T. R., Ward, F. R. & Joshi, N. S. Modulating bacterial and gut mucosal interactions with engineered biofilm matrix proteins. *Scientific Reports*. **8**, 3475 (2018).
23. Monteiro, C. *et al.* Characterization of cellulose production in *Escherichia coli* Nissle 1917 and its biological consequences. *Environ Microbiol*. **11**, 1105-1116 (2009).
24. Praveschotinunt, P. *et al.* Tracking of Engineered Bacteria In Vivo Using Nonstandard Amino Acid Incorporation. *ACS Synthetic Biology*. **7**, 1640-1650 (2018).
25. Dorval Courchesne, N.-M., Duraj-Thatte, A., Tay, P. K. R., Nguyen, P. Q. & Joshi, N. S. Scalable Production of Genetically Engineered Nanofibrous Macroscopic Materials via Filtration. *ACS Biomaterials Science & Engineering*. **3**, 733-741 (2017).

26. Oppong, G. O. *et al.* Epithelial cells augment barrier function via activation of the Toll-like receptor 2/phosphatidylinositol 3-kinase pathway upon recognition of Salmonella enterica serovar Typhimurium curli fibrils in the gut. *Infect Immun.* **81**, 478-486 (2013).
27. Kominsky, D. J. *et al.* IFN- γ -Mediated Induction of an Apical IL-10 Receptor on Polarized Intestinal Epithelia. *The Journal of Immunology.* **192**, 1267 (2014).
28. Chowers, Y. *et al.* Somatostatin Through Its Specific Receptor Inhibits Spontaneous and TNF- α - and Bacteria-Induced IL-8 and IL-1 β Secretion from Intestinal Epithelial Cells. *The Journal of Immunology.* **165**, 2955 (2000).
29. Parlesak, A., Haller, D., Brinz, S., Baeuerlein, A. & Bode, C. Modulation of Cytokine Release by Differentiated CACO-2 Cells in a Compartmentalized Coculture Model with Mononuclear Leucocytes and Nonpathogenic Bacteria. *Scandinavian Journal of Immunology.* **60**, 477-485 (2004).
30. Gewirtz, A. T. *et al.* Salmonella typhimurium translocates flagellin across intestinal epithelia, inducing a proinflammatory response. *The Journal of Clinical Investigation.* **107**, 99-109 (2001).
31. Bruno, V. M. *et al.* Salmonella Typhimurium Type III Secretion Effectors Stimulate Innate Immune Responses in Cultured Epithelial Cells. *PLOS Pathogens.* **5**, e1000538 (2009).
32. Riedel, C. U. *et al.* Construction of p16Slux, a novel vector for improved bioluminescent labeling of gram-negative bacteria. *Appl Environ Microbiol.* **73**, 7092-7095 (2007).
33. Danino, T. *et al.* Programmable probiotics for detection of cancer in urine. Vol. 7 (2015).
34. Rosano, G. L. & Ceccarelli, E. A. Recombinant protein expression in Escherichia coli: advances and challenges. *Frontiers in Microbiology.* **5**, 172 (2014).
35. Eichele, D. D. & Kharbanda, K. K. Dextran sodium sulfate colitis murine model: An indispensable tool for advancing our understanding of inflammatory bowel diseases pathogenesis. *World Journal of Gastroenterology.* **23**, 6016-6029 (2017).
36. Chassaing, B., Aitken, J. D., Malleshappa, M. & Vijay-Kumar, M. Dextran sulfate sodium (DSS)-induced colitis in mice. *Curr Protoc Immunol.* **104**, Unit 15 25 (2014).
37. Kitajima, S., Takuma, S. & Morimoto, M. Histological Analysis of Murine Colitis Induced by Dextran Sulfate Sodium of Different Molecular Weights. *Experimental Animals.* **49**, 9-15 (2000).
38. Melgar, S., Karlsson, A. & Michaelsson, E. Acute colitis induced by dextran sulfate sodium progresses to chronicity in C57BL/6 but not in BALB/c mice: correlation between symptoms and inflammation. *Am J Physiol Gastrointest Liver Physiol.* **288**, G1328-1338 (2005).

39. Bento, A. F. *et al.* β -Caryophyllene Inhibits Dextran Sulfate Sodium-Induced Colitis in Mice through CB2 Receptor Activation and PPAR γ Pathway. *The American Journal of Pathology*. **178**, 1153-1166 (2011).
40. Krieglstein, C. F. *et al.* Role of Blood- and Tissue-Associated Inducible Nitric-Oxide Synthase in Colonic Inflammation. *The American Journal of Pathology*. **170**, 490-496 (2007).
41. Kabashima, K. *et al.* The prostaglandin receptor EP4 suppresses colitis, mucosal damage and CD4 cell activation in the gut. *The Journal of Clinical Investigation*. **109**, 883-893 (2002).
42. Dieleman, L. A. *et al.* Chronic experimental colitis induced by dextran sulphate sodium (DSS) is characterized by Th1 and Th2 cytokines. *Clinical and Experimental Immunology*. **114**, 385-391 (1998).
43. Xu, X.-R., Liu, C.-Q., Feng, B.-S. & Liu, Z.-J. Dysregulation of mucosal immune response in pathogenesis of inflammatory bowel disease. *World Journal of Gastroenterology : WJG*. **20**, 3255-3264 (2014).
44. Fabrega, M. J. *et al.* Intestinal Anti-inflammatory Effects of Outer Membrane Vesicles from Escherichia coli Nissle 1917 in DSS-Experimental Colitis in Mice. *Front Microbiol*. **8**, 1274 (2017).
45. Cario, E., Gerken, G. & Podolsky, D. K. Toll-like receptor 2 enhances ZO-1-associated intestinal epithelial barrier integrity via protein kinase C. *Gastroenterology*. **127**, 224-238 (2004).
46. Cario, E. Barrier-protective function of intestinal epithelial Toll-like receptor 2. *Mucosal Immunol*. **1 Suppl 1**, S62-66 (2008).
47. Garg, P. *et al.* Matrix metalloproteinase-9-mediated tissue injury overrides the protective effect of matrix metalloproteinase-2 during colitis. *American Journal of Physiology - Gastrointestinal and Liver Physiology*. **296**, G175-G184 (2009).
48. Wang, D. & DuBois, R. N. The Role of COX-2 in Intestinal Inflammation and Colorectal Cancer. *Oncogene*. **29**, 781-788 (2010).
49. Martín, A. R., Villegas, I. & Alarcón de la Lastra, C. The COX-2 inhibitor, rofecoxib, ameliorates dextran sulphate sodium induced colitis in mice. *Inflammation Research*. **54**, 145-151 (2005).
50. Oppong, G. O. *et al.* Biofilm-associated bacterial amyloids dampen inflammation in the gut: oral treatment with curli fibres reduces the severity of hapten-induced colitis in mice. *npj Biofilms and Microbiomes*. **1**, 15019 (2015).

51. Guglani, L. & Khader, S. A. Th17 cytokines in mucosal immunity and inflammation. *Current opinion in HIV and AIDS*. **5**, 120-127 (2010).
52. Hernández-Chirlaque, C. *et al.* Germ-free and Antibiotic-treated Mice are Highly Susceptible to Epithelial Injury in DSS Colitis. *Journal of Crohn's and Colitis*. **10**, 1324-1335 (2016).
53. Vidal, L., Pinsach, J., Striedner, G., Caminal, G. & Ferrer, P. Development of an antibiotic-free plasmid selection system based on glycine auxotrophy for recombinant protein overproduction in *Escherichia coli*. *Journal of Biotechnology*. **134**, 127-136 (2008).
54. Hwang, I. Y. *et al.* Engineered probiotic *Escherichia coli* can eliminate and prevent *Pseudomonas aeruginosa* gut infection in animal models. *Nat Commun*. **8**, 15028 (2017).
55. Hsieh, C.-Y. *et al.* Strengthening of the intestinal epithelial tight junction by *Bifidobacterium bifidum*. *Physiological Reports*. **3**, e12327 (2015).
56. Tukel, C. *et al.* Toll-like receptors 1 and 2 cooperatively mediate immune responses to curli, a common amyloid from enterobacterial biofilms. *Cell Microbiol*. **12**, 1495-1505 (2010).
57. Sivanathan, V. & Hochschild, A. A bacterial export system for generating extracellular amyloid aggregates. *Nature Protocols*. **8**, 1381 (2013).
58. Punchard, N. A., Greenfield, S. M. & Thompson, R. P. Mechanism of action of 5-aminosalicylic acid. *Mediators of inflammation*. **1**, 151-165 (1992).
59. Li, Y.-h. *et al.* Addition of Berberine to 5-Aminosalicylic Acid for Treatment of Dextran Sulfate Sodium-Induced Chronic Colitis in C57BL/6 Mice. *PLOS ONE*. **10**, e0144101 (2015).
60. Jin, B.-R. *et al.* Rosmarinic acid suppresses colonic inflammation in dextran sulphate sodium (DSS)-induced mice via dual inhibition of NF- κ B and STAT3 activation. *Scientific reports*. **7**, 46252-46252 (2017).
61. Danino, T. *et al.* Programmable probiotics for detection of cancer in urine. *Science Translational Medicine*. **7**, 289ra284 (2015).
62. Nguyen, P. Q., Botyanszki, Z., Tay, P. K. & Joshi, N. S. Programmable biofilm-based materials from engineered curli nanofibres. *Nat Commun*. **5**, 4945 (2014).
63. Grabig, A. *et al.* *Escherichia coli* Strain Nissle 1917 Ameliorates Experimental Colitis via Toll-Like Receptor 2- and Toll-Like Receptor 4-Dependent Pathways. *Infection and Immunity*. **74**, 4075-4082 (2006).
64. Pfaffl, M. W. A new mathematical model for relative quantification in real-time RT-PCR. *Nucleic Acids Research*. **29**, e45-e45 (2001).

Page intentionally left blank

**Chapter 4 Genetically programmable self-
regenerating bacterial hydrogels**

4.1 Abstract

A notable challenge for the design of Engineered Living Materials (ELMs) is programming a cellular system to assimilate resources from its surroundings and convert them into macroscopic materials with specific functions. Here we demonstrate an ELM that uses *E. coli* as its cellular chassis and engineered curli nanofibers as its extracellular matrix component. Cell-laden hydrogels were created by concentrating curli-producing cultures. The rheological properties of the living hydrogels were modulated by genetically encoded factors and processing steps. The hydrogels have the ability to grow and self-renew when placed under conditions that facilitate cell growth. Genetic programming enables the gels to be customized to interact with different tissues of the gastrointestinal tract selectively. This work lays a foundation for the application of ELMs with therapeutic functions and extended residence times in the gut.

4.2 Introduction

The epithelial tissues of the gastrointestinal (GI) tract are coated in a layer of mucus, which plays several critical protective roles for the underlying cells. By constantly flowing and being regenerated, it facilitates nutrient transport and removes waste^{1,2}. It also mediates interactions between microbes and the host, in ways that both promote homeostasis with commensals and inhibit invasion by pathogens^{3,4}. Defects in the mucus layer are associated with a wide range of GI diseases, including chronic inflammatory bowel diseases (IBD)⁵, cancer⁶, and infection³. However, physical and materials-based approaches to treating mucus defects have been underexplored due to the fast clearance rate of materials in the gut.

Recapitulating the dynamic properties of the GI mucosa in a synthetic system presents a unique challenge in materials design, as many of its functions depend critically on its constant self-regeneration. Many mucoadhesive polymers have been developed with the goal of increasing the delivery efficiency of encapsulated drugs^{7,8}. These polymers rely on a combination of entanglement, electrostatic attraction, hydrogen bonding, and disulfide bond formation in order to promote interaction with native mucins⁹. Some of these materials designs have been successful in slightly extending residence times within the gut after oral delivery¹⁰⁻¹². However, their residence times in the GI tract are still fundamentally limited by the turnover rate of mucins³, which can be as fast as one hour in the murine gut². An alternative strategy to creating more dynamic mucin mimetic materials would be to embed living cells that can replenish the material as it is excreted.

Engineered living materials (ELMs) are an emerging field of research that seeks to harness the biosynthetic potential of cells to create functional materials autonomously, without the need for top-down processing^{13,14}. While the field draws upon a range of disciplines, like genetic engineering, materials design, and biointerface science, a critical aspect of ELM research involves controlling the cellular processes responsible for extracellular matrix production. For example, engineered bacterial biofilm matrix proteins have been used to genetically program functions like adhesion and bioactivity^{15,16}. The long-term goal of this field is to utilize the cell as a living foundry for the production and maintenance of a material with biologically inspired functionalities, like self-regeneration and programmed biological interactions.

Here we report a straightforward procedure to fabricate living hydrogel materials. These hydrogels are composed of *E. coli* embedded in a self-generated matrix of engineered curli fibers. They are made simply and rapidly by concentrating bacterial cultures through filtration. We

demonstrate the customizability of the curli matrix by displaying mucoadhesive protein domains that can alter the trafficking of orally administered hydrogel through the mouse GI tract. The material can regenerate itself rapidly and be programmed for mucosal tissue adhesion (Figure 4.1).

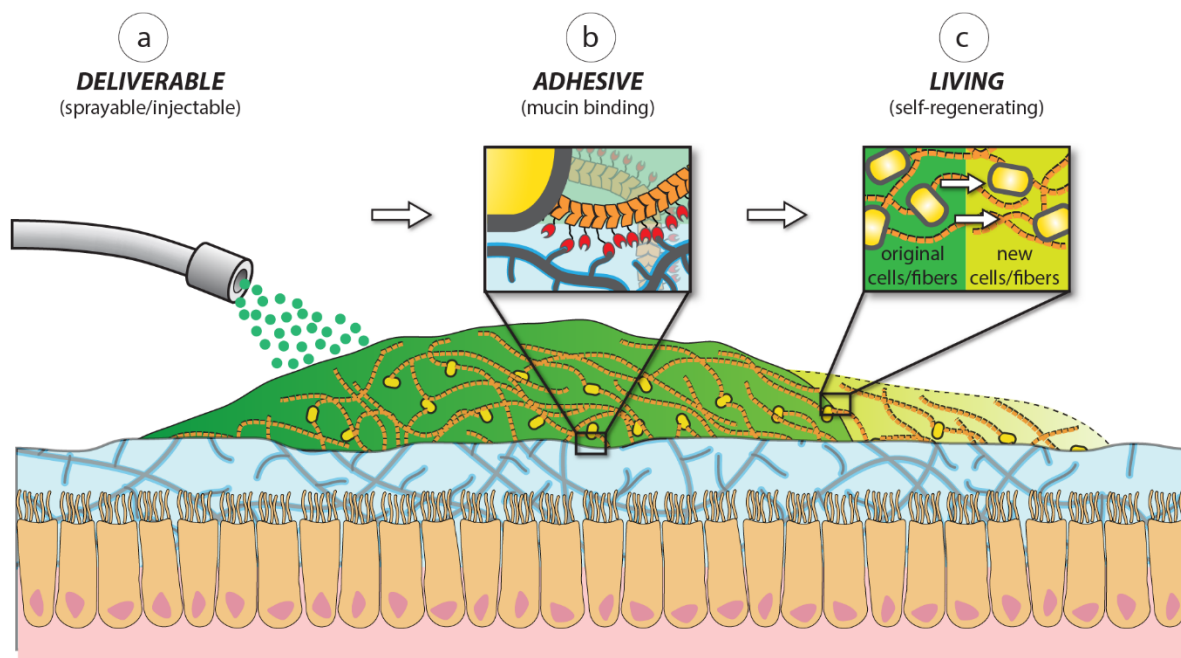


Figure 4.1 Delivery, adhesion and self-regeneration of live mucoadhesive hydrogel in the human gut. Programmable biofabricated hydrogels are deliverable (a), adhesive (b) and living (c); (a) The shear-thinning behavior of the hydrogel allows for its delivery by injection or spraying (dark green), (b) The hydrogel is biofabricated by genetically engineered bacteria programmed to produce a hydrogel with mucoadhesive properties. Mucoadhesive domains (red) displayed on curli fibers (orange) allow for adherence of the hydrogel to mucin proteins (grey) that are part of the mucosal epithelium surface. (c) The biomanufactured hydrogel contains embedded living bacteria that are able to proliferate and fabricate more mucoadhesive hydrogel material (light green). This scheme demonstrates a novel concept of a living customized biomaterial that is capable of self-regenerating.

4.3 Results and Discussion

4.3.1 From bacterial culture to customized hydrogels

Biofilm matrix proteins have recently become a popular scaffold in the fabrication of engineered biomaterials. We and others have demonstrated that curli fibers – functional amyloids secreted by *E. coli* during biofilm formation – are a versatile system for the exploration of

ELMs^{15,17}. We previously reported that the main structural component of curli nanofibers, the CsgA protein, can be fused to several functional peptides and proteins without disturbing its ability to be secreted and to self-assemble into extracellular nanofibers. This overall strategy enables the production of highly programmable biofilms with distinct nano- and microscale structures. Although these engineered biofilms are easy to grow, their exploration in contexts beyond two-dimensional colony formats and nanoscale materials characterization has so far been limited¹⁸.

While adapting a previously reported protocol for recombinant amyloid purification¹⁹, we found that some engineered amyloid curli fibers readily formed hydrogels when concentrated from bacterial culture by vacuum filtration. The protocol uses a filter membrane with 10 mm diameter pores, which facilitated the removal of bacterial cells through several washes with nucleases, denaturants (guanidinium chloride, GdmCl), and detergents (sodium dodecylsulfate, SDS). After a systematic investigation of the effects from each of the wash steps, it became clear that washes with SDS, while originally included in the protocol to remove non-specifically bound proteins, were in fact acting as gelation agents. This is a phenomenon that has been previously reported for other proteinaceous polymers, where SDS associates with the hydrophobic portions of the protein and facilitates the formation of a hydrated network²⁰. Filtered biomass from curli producing cultures formed a pasty mat that adhered strongly to the woven mesh of the membrane. Finally, treatment with SDS led to the formation of a hydrogel on the filter membrane surface after 5 minutes of incubation (Figure 4.2).

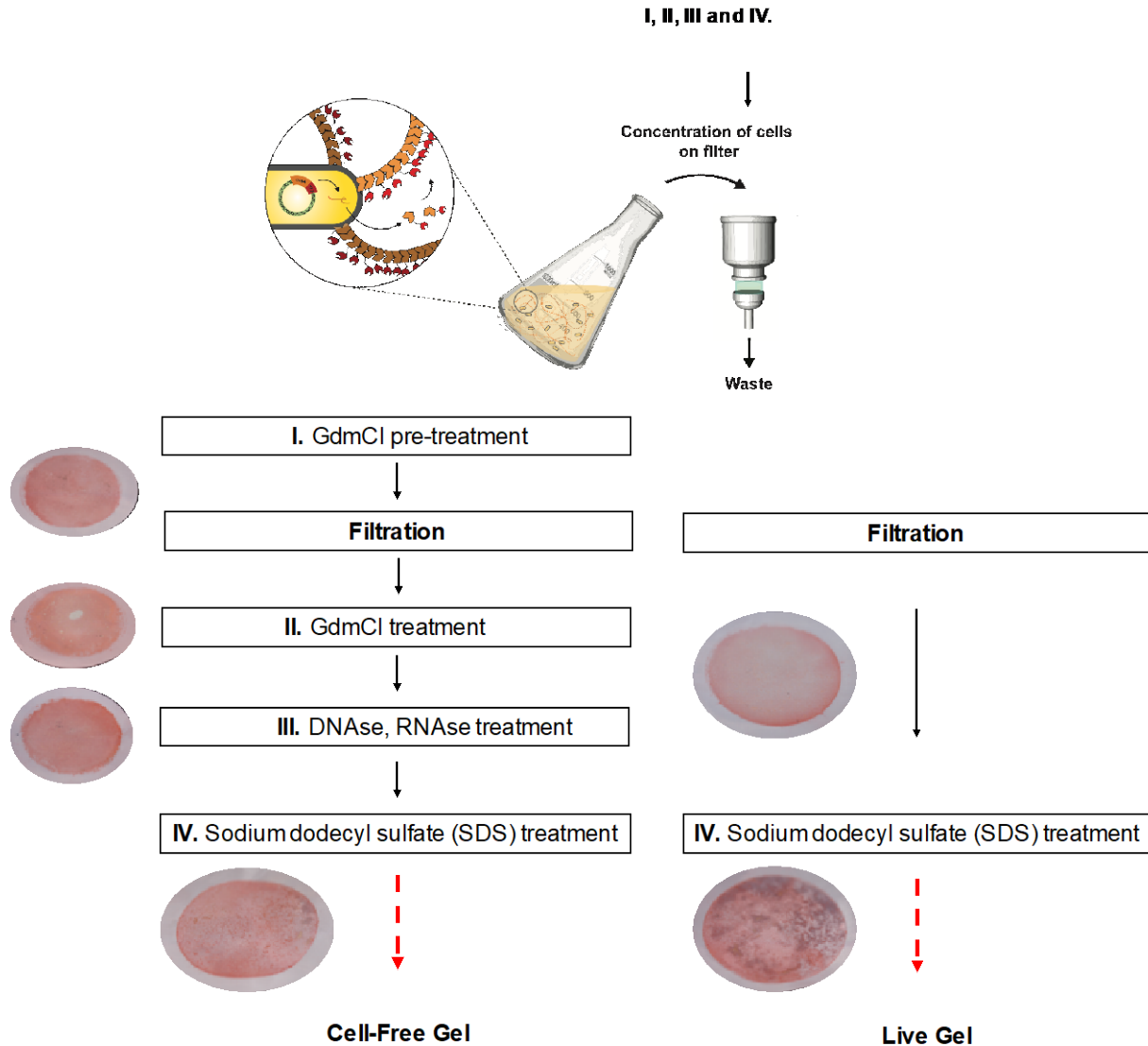


Figure 4.2 Live Gel and Cell-Free Gel fabrication. Steps of gel fabrication protocol. I-IV, where I and II cause lysis of bacteria, III removes DNA and RNA, IV induces gelation). Pictures of filter membrane stained with Congo Red appear beside each step for cTFF2 hydrogel isolation.

The protocol could be adjusted to either maintain the viability of the bacterial cells that were entrapped in the curli fiber network (i.e. a “Live Gel”), or to remove the cells (i.e. a “Cell-Free Gel”) (Figure 4.3a). In order to create Live Gels, the filtered biomass from curli-producing cultures was treated with a 5% SDS solution for 5 minutes, then washed extensively with buffer. The amount of hydrogel that could be isolated from 1 L of bacterial culture was typically 1-2 mL, which consisted of 95-97% water by mass (Table 4-1). The short incubation time in the presence

of SDS and the known tolerance of many *Enterobacteriaceae* to anionic surfactants²¹ resulted in the hydrogels containing $14 \pm 1.4 \times 10^5$ CFU per 50 μ L of gel volume. In order to produce Cell-Free Gels, curli-producing cultures were treated with 0.8 M GdmCl before filtration. We found that this step mitigated clogging of the filter pores and enabled higher gel quantities to be obtained from a single filtration step. After filtration, the curli biomass was treated with 8 M GdmCl and DNase/RNase in order to lyse cells and remove bacterial nucleic acids, which are known to bind strongly to curli fibers²². It has been previously demonstrated that 8 M GdmCl will not disassemble curli fibers¹⁹. Finally, treatment with 5% SDS yielded a hydrogel with dry weight 100-150 mg. SEM analysis of the hydrogels after critical point drying indicated a more compact network morphology for the Cell-Free Gel compared to the Live Gel (Figure 4.3a).

4.3.2 Genetic modulation of hydrogel material properties

A significant advantage of curli over many other secreted biopolymer systems is its ability to serve as a scaffold for the display of heterologous protein domains. In order to investigate the effects of domain identity on the material properties of the hydrogels, we cloned plasmid constructs encoding for CsgA fusions to three separate human-derived mucin binding proteins called the trefoil factors. The resulting curli-trefoil factor fusion proteins were named cTFF1, cTFF2, and cTFF3. After transformation of plasmids encoding each of the CsgA fusions into an *E. coli* strain (PQN4)¹⁹ harboring a genomic knockout of all its curli genes, we were able to isolate hydrogels showing qualitative variation in their appearance and microstructure. In particular, mesh size (as assessed by SEM after critical point drying) varied across the three CsgA-TFF fusions (Figure 4.3b). This could be explained by a higher propensity for aggregation or inter-fiber interactions facilitated by the various TFF domains. The structures of all three trefoil factors are notable

because of their intramolecular disulfide bonding²³, which we hypothesized could contribute to fiber crosslinking in the hydrogels through disulfide exchange reactions. In order to probe the role of disulfides and TFF tertiary structure on gel mechanical properties, we created a hydrogel composed of a fourth CsgA fusion containing the entire TFF2 sequence with all the cysteines mutated to alanine (cTFF2-NC). SEM analysis qualitatively revealed a more open network structure for this mutant (Figure 4.3b)

Table 4-1 Summary of hydrogel production

	Reagent		Gel Weight (mg)	Dry Mass (mg)	Water %	
	1	no SDS 5 min	N/A	N/A	N/A	
	2	5% SDS 1 min		97.8	2.6	97.3
	3	5% SDS 5 min		69.9	4.2	94.0
	4	5% SDS 15 min		129.8	3.1	97.6
Ionic Surfactant	5	5% SDS 1 h		117.2	5.5	95.3
	6	0.1% SDS 5 min		9.0	0.7	92.5
	7	1% SDS 5 min		96.1	2	97.9
	8	10% SDS 5 min		89.0	2.7	97.0
	9	sarcosyl		77.7	2.1	97.3
Non-ionic Surfactant	10	triton x-100	N/A	N/A	N/A	N/A
	11	tween-20	N/A	N/A	N/A	N/A
	12	0M/0M GdmCl		56.3	1.9	96.4
	13	0M/ 8M GdmCl		139	3.9	97.2
	14	0.8M/0M GdmCl		142.0	4.7	96.7
Denaturing Agents	15	0.8M/2M GdmCl		138.2	8.8	93.6
	16	0.8M/4M GdmCl		69.7	4.9	92.8
	17	0.8M/8M GdmCl		69.9	4.2	94.0
	18	0.8M/8M urea		113	6.8	93.9
Non-denaturing Agent	19	0.5%/5% DMSO		108.1	6.2	94.2
	20	0.5%/5% SDS		26.9	0.9	96.6
DNA removal	21	No DNase		114.9	3.2	97.2
	22*	DNase		69.9	4.2	94.0

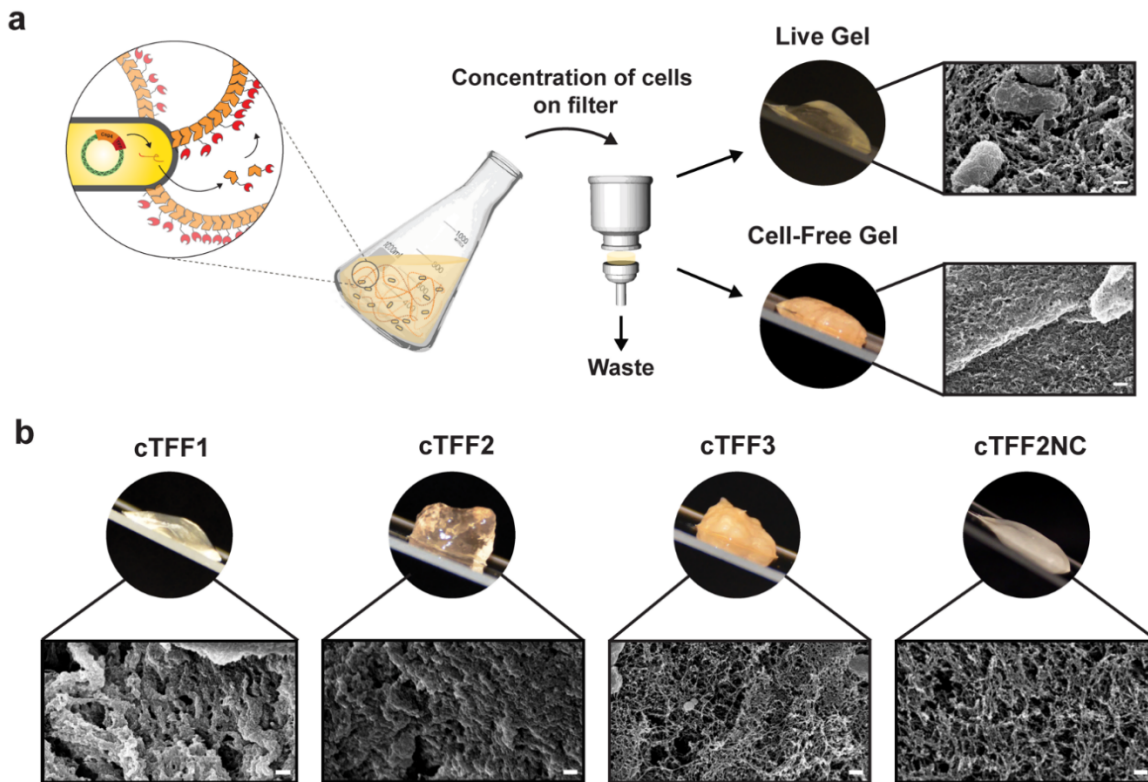


Figure 4.3 Biofabrication of curli-based hydrogels by engineered bacteria. (a) Genetically engineered curli fibers were expressed by bacteria in a liquid culture medium and concentrated by vacuum filtration. Treatment with SDS led to rapid gelation. On-filter treatments were altered to either maintain the viability of embedded bacteria (*Live Gel*), or to remove bacteria (*Cell-Free Gel*). (b) Cell-Free Gels derived from various CsgA-trefoil factor fusions, with corresponding SEM images. cTFF2-NC represents the entire CsgA-TFF2 sequence with all cysteines mutated to alanine. (scale bars 200 nm).

Rheological analysis of the hydrogel variants revealed the effects of cell removal, chemical treatment, CsgA structure, and bacterial DNA on the hydrogel properties. Comparison of the hydrogel variants of cTFF2 showed that the Cell-Free Gel had a storage modulus at 8 rad/s of 1840 Pa, ~30-fold higher than that of the corresponding Live Gel (Figure 4.4a). This agrees with the increased fiber aggregation observed by SEM. We investigated the role of disulfide exchange and tertiary structure on rheological properties by comparing cTFF2 to cTFF2-NC. Removal of cysteines from the curli fiber structure decreased the storage modulus of the Cell-Free Gels 9-fold, suggesting that disulfide exchange plays a role in inter-fiber interactions (Figure 4.4b). Significant differences in storage modulus were also observed between Cell-Free gels with different curli

protein compositions, with cTFF2 exhibiting a storage modulus of ~1.8 kPa, about 5-fold higher than either the cTFF1 or cTFF3 (Figure 4.4c). Curli fibers are also known to bind strongly to DNA, which we reasoned could affect inter-fiber interactions and aggregation propensity, especially after bacterial cell lysis. Therefore, we analyzed all three TFF gels after GdmCl treatment, but without nuclease treatment. Indeed, the presence of DNA decreased the storage modulus values for cTFF1 and cTFF2 ~50% (Figure 4.4d).

4.3.3 Delivery methods and formulations of engineered hydrogels

We next examined the robustness of the biofabricated mucoadhesive hydrogels under a range of conditions that would be useful for delivery in a biomedical context. The cTFF2 Live Gel could be easily extruded through a 21-gauge needle, demonstrating its shear-thinning properties. It also could be sprayed through a catheter tube to coat tissues with larger surface areas, suggesting its potential delivery via endoscopy directly to gastrointestinal surfaces (Figure 4.5). A straightforward sonication procedure enabled the formulation of the gel into a suspension of particles with an average hydrodynamic diameter 100 nm, which could be used to deliver the gel in a soluble form. Finally, we observed that the hydrogel state could easily be reconstituted after lyophilization by adding aqueous buffer, even after the lyophilized structure had been reduced to a powder. Overall, the hydrogel was remarkably robust and easy to work with, suggesting compatibility with several formulations with potential relevance to various biomedical applications.

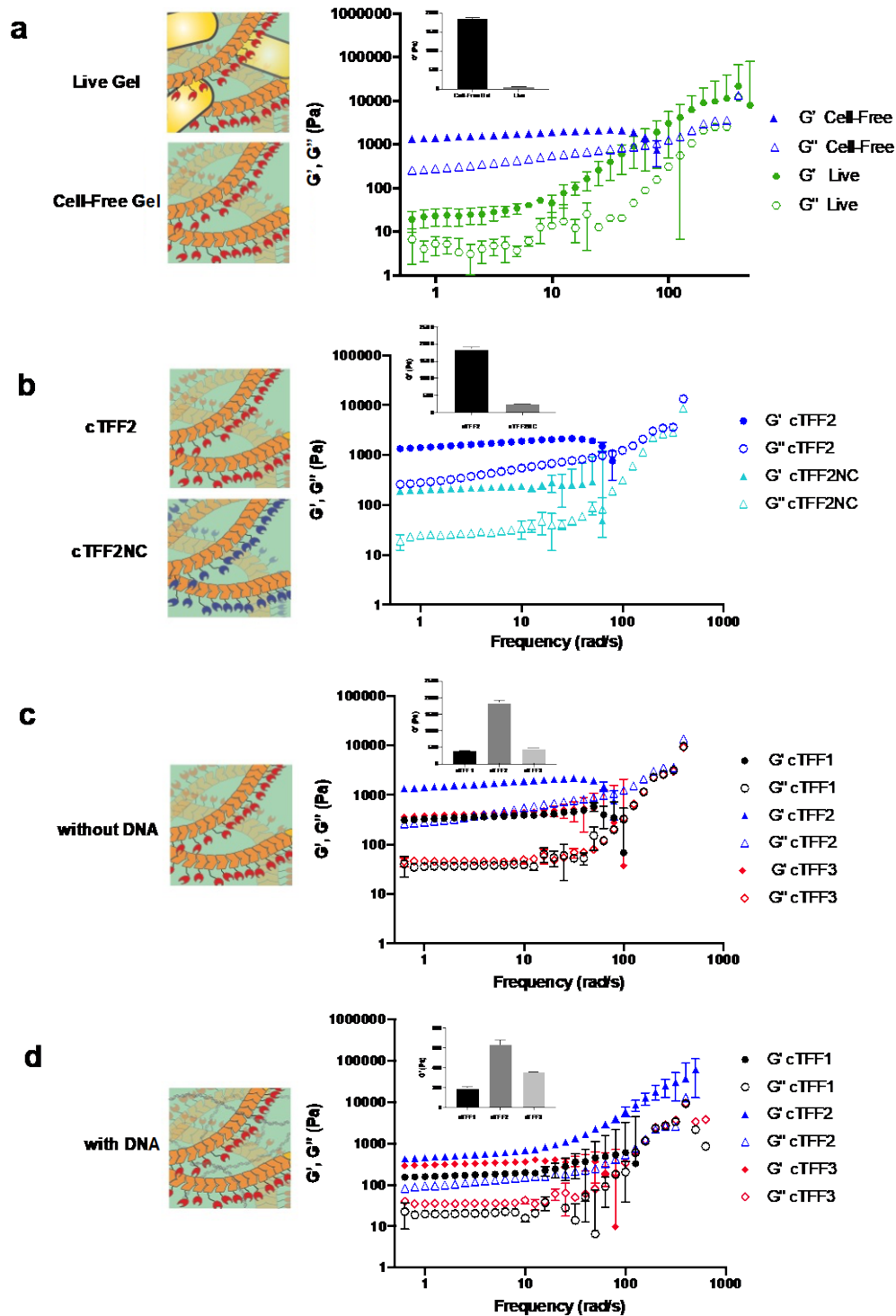


Figure 4.4 Tuning the mechanics of the biofabricated hydrogels. Frequency sweeps from oscillatory shear rheology of various curli-based hydrogels at constant strain amplitude of 1.0%. Storage modulus (G') measured at 1 rad/s shown in inset. (a) Comparison of cTFF2 Live Gel and Cell-Free Gel, without DNase/RNase treatment. (b) Comparison of cTFF2 and cTFF2-NC Cell-Free Gels, with DNase/RNase treatment. Comparison of cTFF1, cTFF2, and cTFF3 Cell-Free Gels before (c) and after (d) DNase/RNase treatment. Data points and bars indicate mean \pm SD ($n=3$).

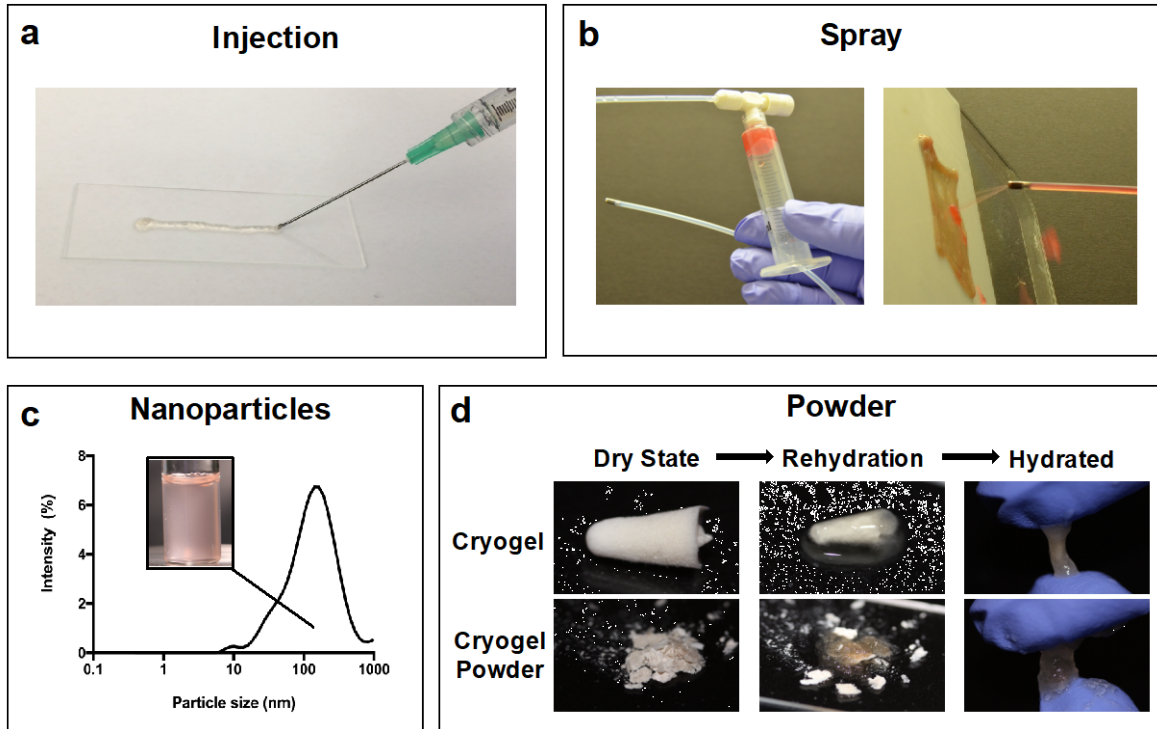


Figure 4.5 Delivery/handling methods for biofabricated Live Hydrogels. (a) Extrusion of cTFF2 Live Gel through 22-gauge needle. (b) Spraying of cTFF2 Live Gel through catheter tube. Gel is dyed with Congo Red to facilitate visualization. (c) Size distribution of cTFF2 Live Gel particles generated by sonication. (d) cTFF2 Live Gels after lyophilization and rehydration from intact (cryogel, *top*) and pulverized (cryogel powder, *bottom*) lyophilized powders.

4.3.4 Selective tissue binding of modified curli nanofibers

In order to highlight the customizability of the biofabricated hydrogels, we investigated the influence of the displayed domain identity on tissue adhesion. In one set of *ex vivo* experiments, various hydrogels were placed between two pieces of goat colon tissue affixed to a mechanical tester. With the mucosal faces of the tissue facing inward, the cTFF2 Live Gel led to an adhesion strength between tissue samples that was significantly higher than that of water – 0.81 and 0.26 N/cm², respectively (Figure 4.6a-c, Figure 4.7). This combination of parameters (i.e. cTFF2, mucosal surfaces) led to adhesion strengths that were also four-fold higher than those measured for the same hydrogel on the serosal side of the tissue (i.e. outer surface of the colon). In order to further demonstrate this tissue surface-specific adhesion, we biofabricated a hydrogel with

engineered curli fibers displaying the Extra Domain B from fibronectin, EDB-Fn3^{24,25}, which we expected to bind more strongly to the serosal side of the tissue given its affinity for other mammalian extracellular matrix proteins and cell surface receptors.²⁴ Indeed, the adhesion force of the EDB-Fn3 hydrogel on the serosal side of the tissue (0.92 N/cm²) was significantly higher than on the mucosal side of the tissue. This reversal of the adhesion trend demonstrates that the hydrogel can be genetically programmed to bind to specific tissue surfaces.

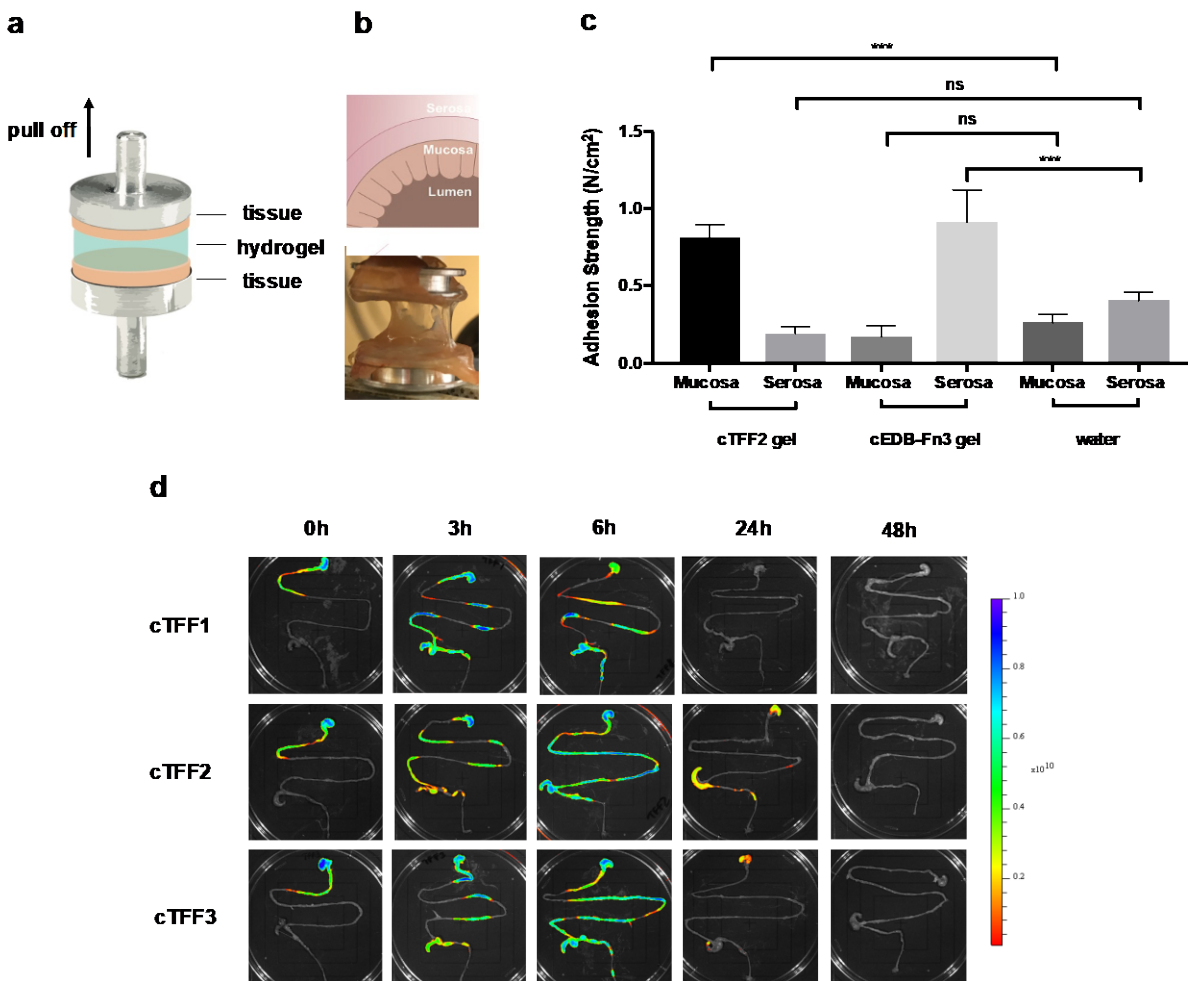


Figure 4.6 Adhesion of engineered Live Gels to tissues of the gastrointestinal tract. (a) Schematic of experimental setup. Samples of flattened goat colon were adhered to both sides of the mechanical tester and the hydrogels were placed between them. Adhesion strength was measured as the force with a constant strain of 8 mm/min (b) Schematic of a portion of colon cross-section (*top*). Image of experimental setup (*bottom*). (c) Adhesion strength for cTFF2 and cEDB-Fn3 Live Gels compared to water as a control. Experiments were performed either with both mucosal surfaces, or both serosal surfaces facing inward.

Bars indicate mean \pm s.e.m.; n=3, ***P<0.0001. (d) Visualization of pre-labeled Live Gels trafficking through the mouse intestine. IVIS images of harvested GI tracts from mice at various time points after oral administration of Cy7-labeled Live Gels (cTFF1, cTFF2, cTFF3). Color map (right) represent fluorescence intensity at $\lambda_{ex}/\lambda_{em}$, 710/ 810-875 nm. No pre-labeled gel was detectable for any of the gel types at 48 hours.

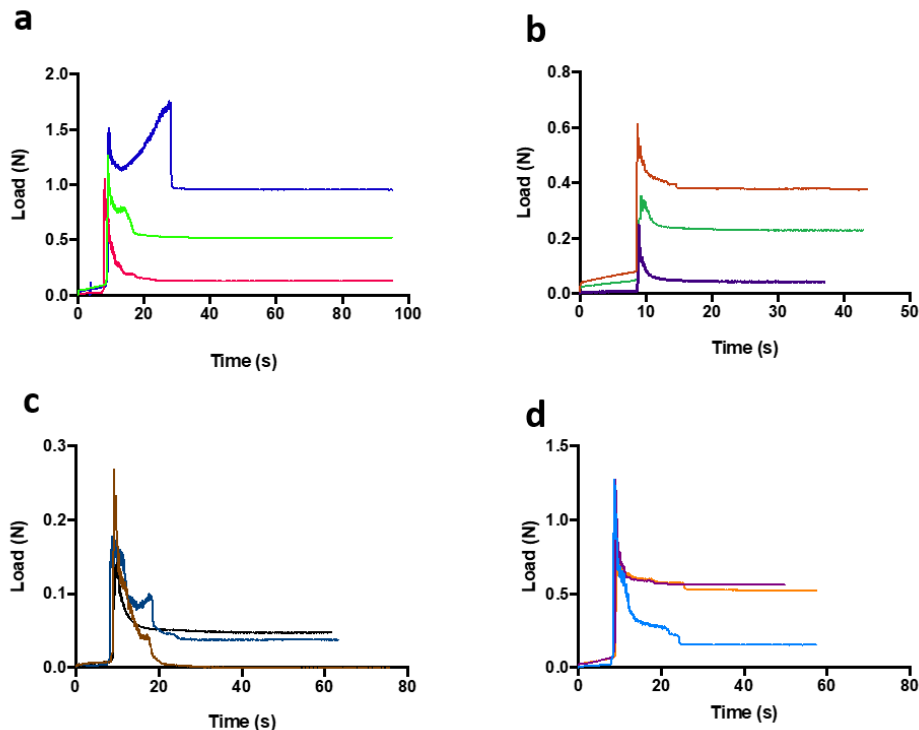


Figure 4.7 Adhesion of *ex vivo* colon tissues to Live Gels of various compositions. The plots are representative force vs. displacement curves at a constant strain rate of 8 mm/min. Curves of different colors represent different individual experiments with unique tissue samples for the following conditions: cTFF2 on mucosal side of tissue (a) cTFF2 on serosal side of tissue (b) cEBD-Fn3 on mucosal side of tissue (c) cEBD-Fn3 on mucosal side of tissue (d). Adhesion strength was reported as the maximum applied force before tissue detachment subtracted from constant force measured tissue detachment.

We also investigated the muco-adhesive properties of the cTFF1, cTFF2, and cTFF3 hydrogels *in vivo* using a mouse model. Live Gels that were chemically labeled with a fluorescent dye were administered to healthy C57BL/6 mice via oral gavage and their GI trafficking was monitored by harvesting tissues at various endpoints – 3, 6, 24 and 48 hours post-administration (Figure 4.6d). For the first 6 hours all three hydrogels were present all along the length of GI tract. However, after 24 hours, only cTFF2 and cTFF3 were detectable in the cecum, which is typically where *E. coli* can be found in the greatest concentrations in the mouse gut²⁶. cTFF2 was also

detectable in the proximal and medial colon at 24 hours. Fluorescent signal was observed in the stomach past 24 hours for some samples, but this is due to dietary autofluorescence. Although all three cTFF fusions have previously been shown to bind mucins, both *in vitro* and *ex vivo*¹⁶, these data show that specific variants can influence *in vivo* trafficking through the GI tract and extend residence times as well. Although the pre-labeled curli fiber hydrogel is cleared out after 24 hours, the embedded bacteria persist within the GI tract, allowing for the continuous production of more (unlabeled) engineered fibers (Figure 4.8b,c).

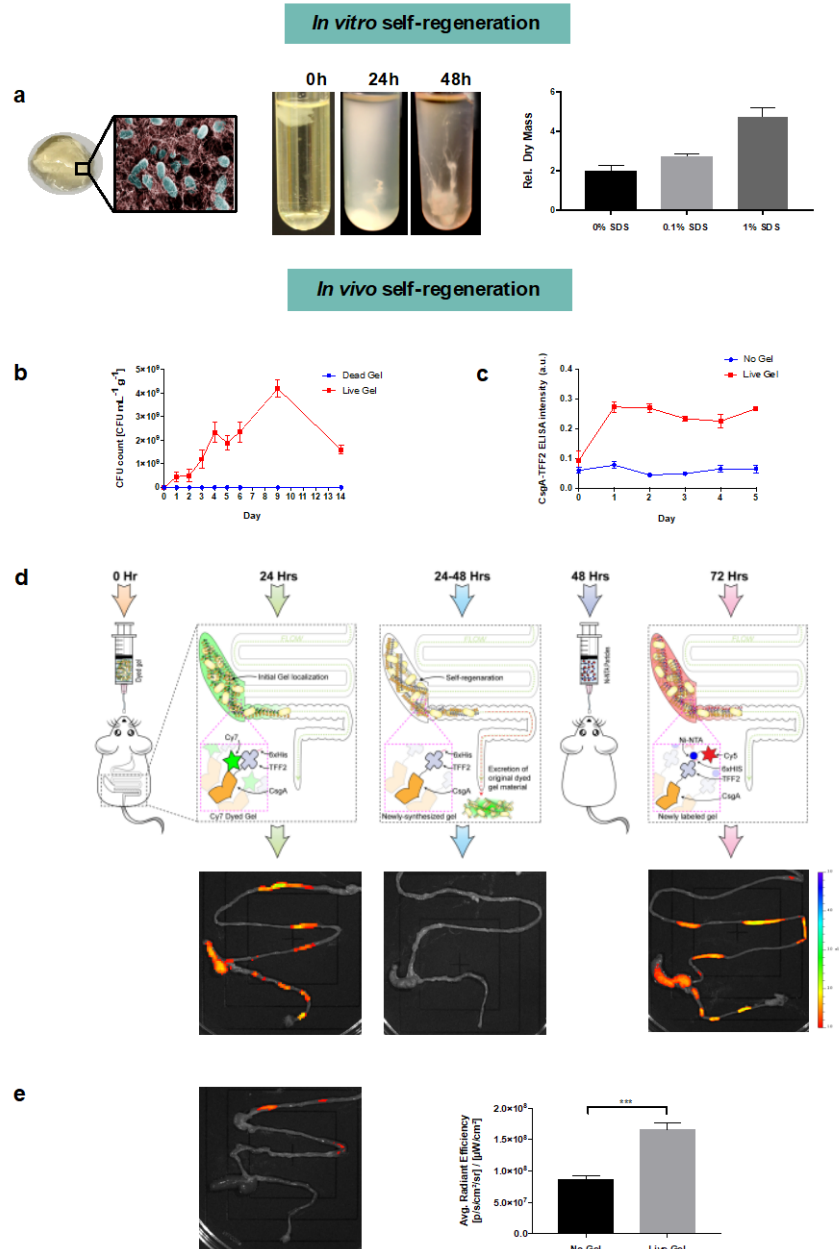


Figure 4.8 Live Gel growth. (a) *In vitro* self-regeneration of live hydrogel. cTFF2 Live Gel harvested by filtration (*top*) was placed back into bacterial growth medium (*middle*). The dry mass of Live Gels was measured after 24 hours in growth medium in the presence of various concentrations of SDS (*bottom*). Data is normalized to the average dry mass of Live Gels before the growth phase. (b-d) *In vivo* self-regeneration of live hydrogel. Tracking of engineered curli-producing PQN4 bacteria (b) and CsgA-TFF2 curli fibers (c) in mouse ($n = 3$) fecal samples over time after oral administration of Live Gel at Day 0. “Dead Gel” represents samples of Live Gel wherein bacteria had been killed. Relative curli fiber concentrations were measured by ELISA. Data points indicate mean \pm s.e.m. (d) The functionality of the self-regenerated Live Gel was confirmed *in vivo* by tracking a Cy5-Ni-NTA dye conjugate that was administered orally 48 hours after Live Gel administration. Cy5 fluorescence was measured in GI tracts ($n = 4$) harvested 72 hours after dye administration. Images (*below*) show representative IVIS data for harvested GI tracts. e) IVIS image of harvested GI tract of mouse after oral administration of Cy5-Ni-NTA dye conjugate to test nonspecific

binding. Bar graph (*bottom*) depicts mean integrated fluorescence values from the cecum and colon ($n = 4$, *** $P < 0.0004$ t-test).

In order to test the stability of these protein-based hydrogels under conditions relevant for GI transit, we monitored the cTFF2 Live Gel under a range of pH and proteolytic conditions in simulated gastric and intestinal fluids (Figure 4.9). When incubated in simulated GI fluids, cTFF2 maintains its swollen state at pH values closer to neutral and collapses reversibly in response to low pH values. Exposure to pepsin does not significantly degrade the Live Gel after 24h of incubation, which is in agreement with previous accounts of curli amyloid resistance to proteolytic degradation²⁷. Although the gel appears to be stable to proteolysis, it is possible that the displayed domains could be cleaved.

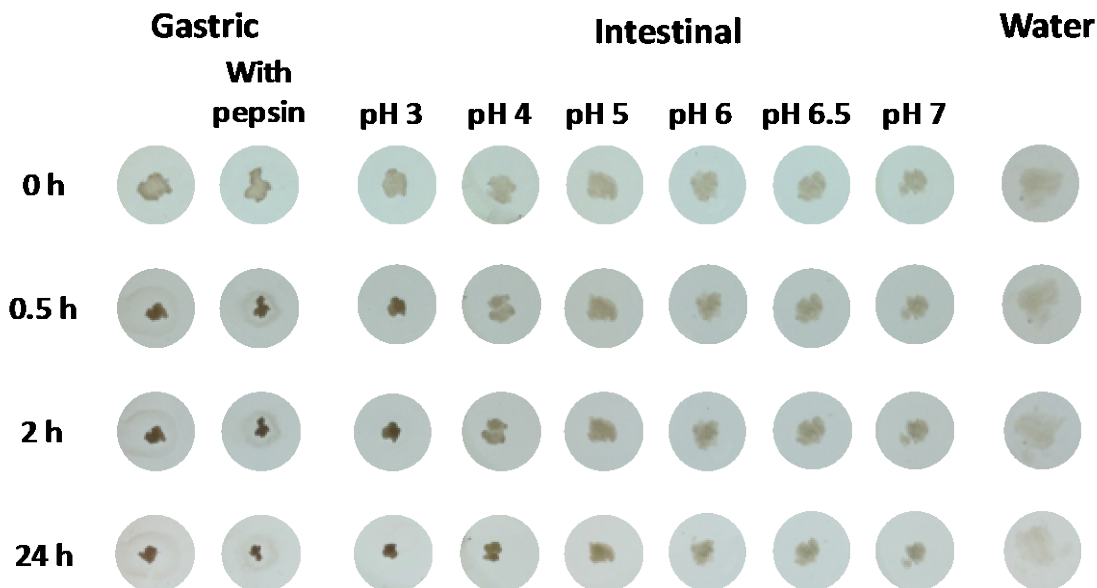


Figure 4.9 Stability of cTFF2 Live Gels in simulated gastric and intestinal fluids. Images of gels after incubation for 24 hours in simulated gastric fluids with and without pepsin, and in simulated intestinal fluids at various pH values.

4.3.5 Self-regeneration of biofabricated hydrogel

In order to test the regenerative capacity of the remaining cells embedded in the curli matrix, we prepared cTFF2 Live Gels and placed them back into growth medium under a range of SDS

concentrations, which we reasoned would promote curli nanofiber gelation. After 24 hours, the solid hydrogel mass was removed from the culture broth, washed, lyophilized, and weighed. The Live Gels placed in LB medium alone doubled in mass over 24 hours, confirming the viability and proliferative capacity of the embedded cells. In the presence of SDS, the measured dry mass of the Live Gels after the growth period increased further, with a five-fold increase observed for 1% SDS (Figure 4.8a). Although the original rationale for adding SDS was to promote gelation, the large increase in gel dry weight must arise from either a difference in cell proliferation or matrix production. Since *E. coli* is not known to grow faster in the presence of SDS, we reasoned that the latter explanation was more relevant. Indeed, even though our system places the curli genes under the control of a synthetic promoter, biofilm matrix production is known to be upregulated under stressful conditions^{28,29}. It is likely that the SDS-induced cell stress affects global regulators of biofilm formation that promote curli production indirectly.

We further investigated the self-regenerative capacity of the Live Gels *in vivo* after oral administration to C57BL/6 mice. After gavage of a cTFF2 Live Gel containing 4.2×10^5 CFU, engineered PQN4 could be isolated from fecal pellets on selective agar plates. Over the course of one week, PQN4 concentration increased from 5×10^8 CFU on day 1 and 2 to 2.5×10^9 CFU on day 6, confirming the ability of the PQN4 cells to proliferate inside the murine GI tract (Figure 4.8b). In order to confirm that the living PQN4 bacteria are able to self-regenerate the curli fiber matrix by producing more curli fibers in the murine GI tract, we tracked the presence of the CsgA-TFF2 proteins in fecal pellets for several days after gavage of the Live Gel. ELISA analysis of homogenized fecal pellets using an anti-HIS6 antibody demonstrated that CsgA-TFF2 could be detected for at least 5 days after Live Gel administration (Figure 4.8c). From the difference

between the data presented in Figure 4.6d, which shows that pre-labeled Live Gel is cleared from the GI tract after 24 hours, and the data shown in Figure 4.8c, which confirms the presence of curli fibers after 5 days, it is clear that the cells embedded in the original Live Gel are capable of residing in the GI tract for extended periods and continuously regenerating the curli fiber network *in situ*. To further confirm the presence and functionality of the self-regenerated engineered curli fiber matrix in the GI tract, we orally administered a fluorescent dye conjugated to Ni-NTA and observed its concentration in harvested GI tracts after 72 hours. The cTFF2 protein constructs that compose the Live Gel were designed with 6x-His tags at their C-terminus that we rationalized would bind and retain the dye. Indeed, mice that had been previously colonized with the Live Gel retained the dye in their cecum and proximal and medial colon while control mice that had not been administered gel showed background levels of fluorescence after 72 hours (Figure 4.8d). Since the original curli fibers of the Live Gel should have been excreted completely by the time the dye was administered, this further confirms the functionality of the Live Gel after extended residence times *in vivo*.

Additionally, the mice were healthy over the course of the experiments and no weight loss was observed. GI tracts harvested 10 days after Live Gel administration showed no evidence of shortening due to inflammation and histological analysis showed no evidence of epithelial ulceration or abnormal immune responses in the colon (Figure 4.10). *In vitro* cell viability assays for Caco-2 cells co-incubated with Live and Cell-Free Gels also confirmed their lack of cytotoxicity (Figure 4.11).

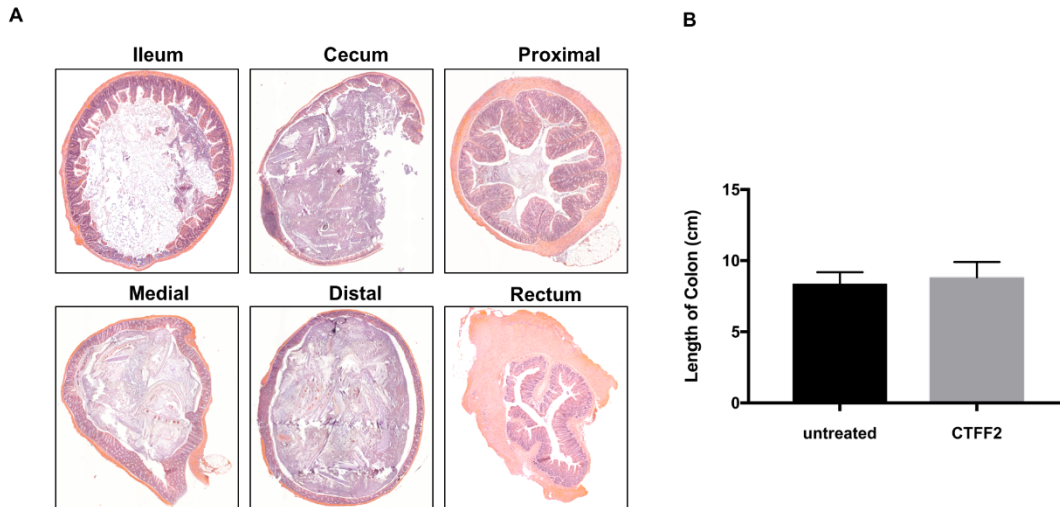


Figure 4.10 Toxicity of cTFF2 Live Gel in mice. (A) Representative histopathology of GI tract cross-sections stained with H&E harvested 10 days after oral gavage. Images show no signs of epithelial damage or immune response. (B) Comparison of colon length for untreated mice and mice treated with cTFF2 Live Gel 10 days after oral gavage.

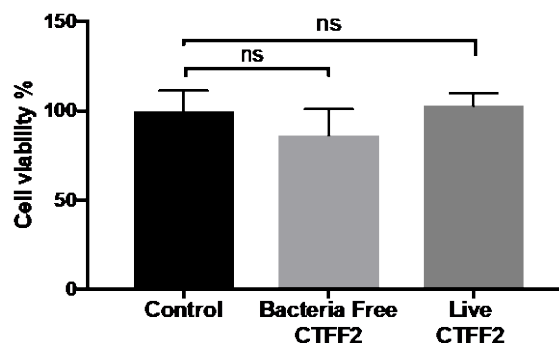


Figure 4.11 Cytotoxicity of cTFF2 Live and Cell-Free Gels *in vitro*. Viability of Caco-2 cells in the presence of the hydrogels was measured using the MTT assay; control indicates Caco-2 cells without and hydrogel.

4.4 Conclusions

We have created an ELM with *E. coli* as the cellular chassis and curli nanofibers as an extracellular matrix component. By adapting a straightforward filtration protocol, viable bacteria and expressed curli fibers were concentrated from broth culture to produce hydrogels. A key element in the hydrogel fabrication involved exposure of filtered biomass to a surfactant like SDS, which likely helps to disperse the fibers so that they can form a hydrated network instead of

precipitating. These hydrogels exhibited a range of rheological properties based on the identity of the displayed protein domain on the curli fibers and the denaturant/enzyme washes they were subjected to. The living materials were able to grow more than four-fold in mass over 24 hours when placed back into conditions that facilitate cell growth. In terms of production rate (i.e. grams of biomass per liter per day), this is comparable to bacterial cellulose production from *Gluconacetobacter xylinus*³⁰, the gold standard for microbially derived materials. The effects of SDS exposure during the hydrogel growth step on gene expression may need to be explored further given the known changes to genetic regulation for *E. coli* under such conditions. Nevertheless, oral administration of the gel to mice leads to extended residence times for the bacteria in the gut. The ability to customize the gels facilitates their selective adhesion to tissues of the GI tract and alters their trafficking after oral administration. Unlike most previous examples of curli-based materials, this work focuses on the creation of macroscopic materials, whose bulk mechanical and adhesion properties can be assessed and even tuned based on genetic programming. The material's self-renewing capabilities set it apart from other efforts to combine living cells with non-autogenic polymers to create composites. The ability of the living hydrogels to withstand a wide range of harsh conditions that may be encountered in during GI transit, combined with their ease of handling and self-renewability suggests their utility for therapeutic applications in the gut, especially those that may benefit from a cohesive material with extended residence times.

4.5 Materials and Methods

4.5.1 Cell strains and plasmids

Trefoil factor domains (TFF1, TFF2, TFF3) were fused to the C-terminus of CsgA with an intervening 36 amino acid flexible linker. Genes encoding the three fusion proteins (cTFF1, cTFF2, cTFF3) were synthesized (Integrated DNA Technologies) and cloned by overlap extension into pET21d vectors. The plasmids also contained genes encoding for other proteins necessary for curli biosynthesis, including *csgC*, *csgE*, *csgF*, and *csgG*. All five genes (*csgACEFG*) were expressed as a single transcript under the control of the T7 promoter (Table S1). All experiments used cell strain PQN4, an *E. coli* strain derived from LSR10 (MC4100, $\Delta csgA$, λ (DE3), Cam^R)¹⁹.

4.5.2 Mice

Female 6- to 8-week-old C57BL/6 mice were purchased from Charles River Laboratories. Mice were housed in SPF conditions with sterile food and water ad libitum. The animal foods included normal food (LabDiets 5K67) and non-fluorescent food (LabDiets 5V5R). Mice were maintained in sterile vinyl isolators equipped with food, water and bedding in the Harvard Medical School animal facility. Before any experiment, the mice had at least one week to acclimatize to the facility environment. All experiments were conducted in accordance with US National Institutes of Health guidelines and approved by the Harvard Medical Area Standing Committee on Animals.

4.5.3 Curli nanofiber expression

To express curli nanofibers, PQN4 cells were transformed with pET21d plasmids encoding CsgA-trefoil factor fusions (cTFF1, cTFF2, cTFF3). Transformed cells were streaked onto fresh Luria Broth (LB) agar plates supplemented with 100 µg/mL carbenicillin and 0.5% (m/v) glucose and were grown at 37°C. A single colony was picked, inoculated in LB medium containing 100 µg/mL carbenicillin and 2% (m/v) glucose and incubated overnight at 37 °C. The overnight culture was diluted 1:100 in fresh LB medium with 100 µg/mL carbenicillin and the protein expression was carried out at 37°C for 24-48 hours.

4.5.4 Preparation of live hydrogel

Bacterial cultures were induced for 48 hours before being subjected to filtration through a 47 mm (dia.) polycarbonate membrane with 10 µm pores (EMD Millipore) using vacuum filtration.¹⁹ The concentrated biomass was rinsed 3 times on the filter membrane with 25 mL of sterile DI water. Next, the filtered biomass was incubated with 5 mL of 5% (m/v) sodium dodecyl sulfate (SDS) in water for 5 minutes, followed by vacuum filtration of the liquid and 3 rinses with 25 mL of DI water. Hydrogel that was formed on the filter membrane was collected by gently scraping with a spatula, and was stored wet at 4°C or lyophilized for further studies. Cell density was determined by streaking the hydrogel on LB-agar plates for CFU counting.

4.5.5 Preparation of cell-free hydrogel

Bacterial cultures were induced for 48 hours before being treated with guanidinium chloride (GdmCl) to a final concentration of 0.8 M at 4°C for 1 hour. Treated cultures were concentrated by filtration, as described for the Live Hydrogel. To remove live bacteria, the filtered biomass was

treated with 5 mL of 8 M GdmCl for 5 minutes, followed by vacuum filtration of the liquid and 3 rinses with 25 mL of sterile DI water. The remaining biomass was treated with 5 mL of an aqueous solution (2 μ M MgCl₂) of nuclease (Benzonase, Sigma-Aldrich, 1.5 U/mL) for 10 minutes to remove DNA/RNA bound to curli fibers. Finally, the semi-purified bacteria-free biomass was incubated with 5 mL of 5% (m/v) SDS in water for 5 minutes followed by vacuum filtration of the liquid and 3 rinses with 25 mL of DI water. The bacteria-free hydrogel was collected from the filter membranes and stored wet at 4°C or lyophilized for the further studies.

4.5.6 *In situ* hydrogel growth

In order to investigate the growth of new material from living cells embedded within the hydrogel, 50 mg of cTFF2 Live Hydrogel was added to 2 mL of LB containing 100 μ g/mL carbenicillin, with or without SDS (0.1, 1%) and incubated at 37°C for 24, 48 and 72 hours. At each endpoint, the cultured hydrogels with medium were filtered through a nylon filter (70 μ m pore size, Falcon, Corning) and thoroughly washed with water to remove any remaining bacteria and loosely bound curli fibers. The filtered hydrogels were collected from the membrane and lyophilized in order to determine their dry weights.

4.5.7 Hydrogel rheology

Small strain amplitude oscillatory rheology measurements were performed on a TA Instruments AR-G2 rheometer with plate-plate geometry. 8 mm plates were used for strain sweeps and frequency sweeps with a gap width of 500 μ m and moisture trap. Strain sweep measurements were carried out from a strain amplitude of 0.1% to 25% at 25.0°C (+/- 0.1°C) and a frequency of 1.0 Hz to determine small deformation linearity. Frequency sweeps were then performed from 0.1

Hz to 100 Hz at 25.0°C with a controlled strain amplitude of 1.0%, which was within the linear response range for all samples.

4.5.8 Injection and spraying

Hydrogels were loaded into a 5 mL syringe attached to either a needle (22-gauge) or an endoscopic spray catheter Glo-Tip® Spray Catheter (2.33 mm diameter, Cook Medical, USA).

4.5.9 Nanoparticle formation

50 mg of cTFF2 Cell-Free Gel was transferred into 1.5 mL tube with 0.5 mL of DI water and placed in a sonicating bath for 1 hour. The size distribution of the gel particles was measured using a particle sizer (Malvern Zen 3600 Zetasizer).

4.5.10 Cryogel and powder

Hydrogels obtained via filtration were lyophilized to create cryogels and then pulverized into powder. Cryogels and powdered material were rehydrated in DI water to reform hydrogels.

4.5.11 Hydrogel adhesion to goat colon tissue

To test adhesion of cTFF2 Live Gel to the gut mucosa, the freshly made hydrogel was placed on the mucosal or the serosal site of the goat colon. The fresh goat colon was cut open longitudinally along the main axis. The sliced colon samples were fixed on standard SEM pin stub mount (Ø12.7 mm x 8 mm pin height, Electron Microscopy Sciences) by instant glue (Loctite 495, Henkel). The 50 µl of cTFF2 was applied onto the tissue sample and cover with the second layer of tissue fixed to SEM pin stub. These layered tissue-hydrogel-tissue sandwiches were kept at

room temperature for 30 minutes to achieve integration of the hydrogel with the gut mucosa. Finally, SEM pin stubs with hydrogel and tissue samples were loaded on the bottom stage of the mechanical tester (ADMET) and pulled off with a constant strain of 8 mm/min. The applied force was monitored and the maximum force before full detachment of the patch was measured as the adhesion force. All the experiments were performed in triplicate.

4.5.12 Hydrogel staining with fluorescent dye

1 mL of Live Gel was immersed in 4 mL phosphate saline buffer (PBS), and stained with 2.5 mg of Sulfo-Cyanine7 (Cy7) NHS ester (Lumiprobe Corporation) dissolved in PBS. After 3 hours of incubation at room temperature, the hydrogel was thoroughly rinsed with water on a 70 μm pore nylon filter (Falcon, Corning) by immersion of the filter in a DI water bath overnight. The water was changed multiple times to allow for complete removal of unbound dye.

4.5.13 Oral administration of live gel and GI tract *ex vivo* optical imaging

Before the administration of Cy7-labeled hydrogel, mice were fed with alfalfa-free food for at least 5 days to minimize background autofluorescence. After washes as described in the protocol described above, labeled cTFF1-3 hydrogels (150 μL) were administered by oral gavage to C57BL/6 mice. At $t = 0, 3, 6, 24$ and 48 hours after gavage, a mouse in each condition was euthanized to harvest the whole GI tract for *ex vivo* imaging. The whole GI tract was placed on the lid of 150 x 25 mm polystyrene tissue culture plates (Falcon) before imaging with the IVIS Lumina II (PerkinElmer). The IVIS instrument was equipped with 10 narrow-band excitation filters (30 nm bandwidth) and 4 broadband emission filters (60- and 75-nm bandwidth). At each time point, the whole GI tracts were imaged with IVIS Lumina II using excitation filter at 710 nm, and 675

nm for background subtraction, and emission filter at 810-875 nm, with field of view (FOV) = D (12.5 cm), fstop = 2 and medium binning. Imaging analysis was done with Living Image software version 4.3.1/4.4

4.5.14 Live gel residence time

After 18 hours of starvation with ampicillin (2 g/L) containing water, mice were fed with 150 μ L of cTFF2 Live Gels or PBS for control and returned to normal food. Fecal samples were collected once per day from day 0 to day 5. Fecal samples were weighed, homogenized using TissueLyser LT system (Qiagen), serially diluted and plated on antibiotic selective plates (carbenicillin) to enumerate resident CFU over time.

4.5.15 Hydrogel stability in simulated GI fluids

Simulated gastric (with and without pepsin) and intestinal fluids were obtained (Sigma-Aldrich). Aliquots of intestinal fluids were prepared and their pH was adjusted from 3 to 7 using HCl to mimic different sections of the GI tract. 50 mg of cTFF2 Live Gel was placed in 1 mL of each fluid and observed over the course of 24 hours. Pictures were taken using white light rear illumination.

4.5.16 ELISA of CsgA-TFF2 from fecal samples

After 18 hours of starvation with ampicillin (2 g/L) containing water, mice were gavaged with 150 μ L of cTFF2 Live Gels or PBS as a control. Fecal samples were collected daily for five days and homogenized. Supernatants from the sample homogenates were transferred onto Multiscreen-GV 96-well filter plates (0.22 μ m pore size; Millipore). The volumes were normalized

so that 1 mg of fecal samples were on each membrane. After three washes with buffer (TBS, 0.1% Tween-20 (Sigma)), 150 μ L of blocking solution (1% bovine serum albumin (BSA) (Sigma) and 0.01% hydrogen peroxide (Sigma) in wash buffer) were added to each well and incubated at 37°C for 1.5 hours and the blocking was repeated three times. 50 μ L of anti-HIS antibody-horseradish peroxidase (HRP) conjugate (1:250 dilution) (Thermo Fisher Scientific, MA1-80218) was added to each well and incubated for 1.5 hours at 25°C. 100 μ L of Ultra-TMB (3,3',5,5'-tetramethylbenzidine) ELISA substrate (Thermo Fisher Scientific) was added to each well and incubated for 5 minutes. 50 μ L of 2 M sulfuric acid (Alfa Aesar) was added to each well to stop the reaction. 100 μ L of the reaction was transferred to 96-well flat bottom plate and absorbance values were measured at 450 and 650 nm. Relative CsgA-TFF2 concentration was reported as the difference between absorbance at 450 nm and absorbance at 650 nm.

4.5.17 Probing live gel functionality *in vivo*

Following a protocol for oral administration of cTFF2 Live Gel similar to that described for the labeled hydrogel above, mice were first gavaged with unlabeled cTFF2 Live Gels (150 μ L). 48 hours after gavage, the mice were gavaged with 100 μ L of 100 μ M Cy5 Bis Nickel-nitrilotriacetic acid (Ni-NTA) complex solution (AAT Bioquest). Mice were euthanized 24 hours after gavaging the dye and whole GI tracts were harvested for *ex vivo* imaging using an IVIS Lumina II instrument. We used an excitation filter at 675 nm and at 640 nm for background subtraction, and emission filter at 695-770 nm, with field of view (FOV) = D (12.5 cm), fstop = 2 and medium binning. Imaging analysis was done with Living Image software version 4.3.1/4.4.

4.5.18 Self-generation of living hydrogel

30 mg of biofabricated live hydrogel was added to 3 mL of fresh Luria Broth (LB) supplemented with 100 µg/mL carbenicillin with presence of 0, 0.1% and 1% (m/v) SDS and incubated at 37°C for 48 hours. Hydrogel growth was monitored after 24 and 48 hours of incubation. At each time point, the hydrogel was removed from the culture medium; transferred to a Falcon cell strainer; and washed several times to remove debris, remaining medium and fibers that were not part of hydrogel. The washed hydrogel was transferred into an Eppendorf tube and lyophilized to obtain a dry weight.

4.5.19 Toxicity of hydrogel *in vivo*

The cTFF2 Live Gel was administrated by oral gavage to C57BL/6 mice (n=5). Mouse health was monitored for 10 days after hydrogel administration. On day 10, mice were euthanized and their GI tracts were harvested. Colon length was measured and the whole GI tract was segmented and sent for histology.

4.5.20 MTT assay

The cytotoxicity of the Live and Cell-Free cTFF2 hydrogels was tested *in vitro* by exposing them to the human colonic carcinoma cell line Caco-2 BBE1 (ATCC). Caco-2 cells that were maintained between 60 and 80% confluency in DMEM supplemented with 10% FBS and 1% penicillin/streptomycin at 37°C in a 5% CO₂ incubator were trypsinized to create a cell suspension. 4x10⁴ cells were seeded into wells that contained 100 µl of hydrogel. After 24 hours incubation at 37°C with 5% CO₂, 0.5 mg/mL of MTT (3-[4,5-dimethylthiazol-2-yl]-2,5-diphenyl tetrazolium bromide) was added to each well and incubated for 2 hours. After the incubation period, culture

medium was removed and the developed formazan crystals were dissolved by adding 100 μ l of MTT solubilization solution (Sigma-Aldrich) and incubated for 4 hours. Finally, the absorbance in each well was recorded at 570 nm. Background readings were obtained at 690 nm. Control wells contained either cells only or no cells and MTT only.

4.5.21 Electron microscopy

Scanning electron microscopy (SEM) samples were prepared by fixing hydrogels with 2% (m/v) glutaraldehyde and 2% (m/v) paraformaldehyde for 2 hours at room temperature. The gels were gently washed with water, and the solvent was gradually exchanged to ethanol with an increasing ethanol 15-minute incubation step gradient (25, 50, 75 and 100% (v/v) ethanol). The gels were dried in a critical point dryer, placed onto SEM sample holders using silver adhesive (Electron Microscopy Sciences), and sputtered until they were coated in a 5 nm layer of Pt/Pd. Imaging was performed using a Zeiss Ultra 55 Field Emission SEM.

4.6 Acknowledgements

This work was done in collaboration with Dr. Anna Duraj-Thatte, Dr. Noémie-Manuelle Dorval Courchesne, Jarod Rutledge, Dr. Yuhan Lee, and Prof. Jeffrey M. Karp. This work made use of shared facilities at the Harvard Center for Nanoscale Systems and at the Wyss Institute for Biologically Inspired Engineering at Harvard University and was supported by National Science Foundation (DMR, 1410751), National Institutes of Health (1R01DK110770-01A1) and the Wyss Institute for Biologically Inspired Engineering. The authors thank Giorgia Cannici for her assistance in preparation and editing of supplementary video.

4.7 References

1. Johansson, M. E. & Hansson, G. C. Immunological aspects of intestinal mucus and mucins. *Nat Rev Immunol.* **16**, 639-649 (2016).
2. Johansson, M. E. Fast renewal of the distal colonic mucus layers by the surface goblet cells as measured by in vivo labeling of mucin glycoproteins. *PLoS One.* **7**, e41009 (2012).
3. Caldara, M. *et al.* Mucin biopolymers prevent bacterial aggregation by retaining cells in the free-swimming state. *Curr Biol.* **22**, 2325-2330 (2012).
4. Lieleg, O. & Ribbeck, K. Biological hydrogels as selective diffusion barriers. *Trends Cell Biol.* **21**, 543-551 (2011).
5. Antoni, L., Nuding, S., Wehkamp, J. & Stange, E. F. Intestinal barrier in inflammatory bowel disease. *World J Gastroenterol.* **20**, 1165-1179 (2014).
6. Bernstein, H. *et al.* Patchy field defects of apoptosis resistance and dedifferentiation in flat mucosa of colon resections from colon cancer patients. *Ann Surg Oncol.* **9**, 505-517 (2002).
7. Lam, P. L. & Gambari, R. Advanced progress of microencapsulation technologies: in vivo and in vitro models for studying oral and transdermal drug deliveries. *J Control Release.* **178**, 25-45 (2014).
8. Boddupalli, B. M., Mohammed, Z. N., Nath, R. A. & Banji, D. Mucoadhesive drug delivery system: An overview. *J Adv Pharm Technol Res.* **1**, 381-387 (2010).
9. Schattling, P., Taipaleenmaki, E., Zhang, Y. & Stadler, B. A Polymer Chemistry Point of View on Mucoadhesion and Mucopenetration. *Macromol Biosci.* **17** (2017).
10. Banerjee, A., Lee, J. & Mitragotri, S. Intestinal mucoadhesive devices for oral delivery of insulin. *Bioeng Transl Med.* **1**, 338-346 (2016).
11. Bagan, J. *et al.* Mucoadhesive polymers for oral transmucosal drug delivery: a review. *Curr Pharm Des.* **18**, 5497-5514 (2012).
12. Brooks, A. E. The Potential of Silk and Silk-Like Proteins as Natural Mucoadhesive Biopolymers for Controlled Drug Delivery. *Front Chem.* **3**, 65 (2015).
13. Nguyen, P. Q., Courchesne, N. D., Duraj-Thatte, A., Praveschotinunt, P. & Joshi, N. S. Engineered Living Materials: Prospects and Challenges for Using Biological Systems to Direct the Assembly of Smart Materials. *Adv Mater.* (2018).
14. Chen, A. Y., Zhong, C. & Lu, T. K. Engineering living functional materials. *ACS Synth Biol.* **4**, 8-11 (2015).

15. Nguyen, P. Q., Botyanszki, Z., Tay, P. K. & Joshi, N. S. Programmable biofilm-based materials from engineered curli nanofibres. *Nat Commun.* **5**, 4945 (2014).
16. Duraj-Thatte, A. M., Praveschotinunt, P., Nash, T. R., Ward, F. R. & Joshi, N. S. Modulating bacterial and gut mucosal interactions with engineered biofilm matrix proteins. *Sci Rep.* **8**, 3475 (2018).
17. Chen, A. Y. *et al.* Synthesis and patterning of tunable multiscale materials with engineered cells. *Nat Mater.* **13**, 515-523 (2014).
18. Cao, Y. *et al.* Programmable assembly of pressure sensors using pattern-forming bacteria. *Nat Biotechnol.* **35**, 1087-1093 (2017).
19. Noémie-Manuelle Dorval Courchesne, A. D.-T., Pei Kun R. Tay, Peter Q. Nguyen, and Neel S. Joshi. Scalable Production of Genetically Engineered Nanofibrous Macroscopic Materials via Filtration. *ACS Biomater. Sci. Eng.* **3**, 733–741 (2017).
20. Wu, X. *et al.* Sodium dodecyl sulfate-induced rapid gelation of silk fibroin. *Acta Biomater.* **8**, 2185-2192 (2012).
21. Rajagopal, S., Sudarsan, N. & Nickerson, K. W. Sodium dodecyl sulfate hypersensitivity of clpP and clpB mutants of Escherichia coli. *Appl Environ Microbiol.* **68**, 4117-4121 (2002).
22. Gallo, P. M. *et al.* Amyloid-DNA Composites of Bacterial Biofilms Stimulate Autoimmunity. *Immunity.* **42**, 1171-1184 (2015).
23. Thim, L. & May, F. E. Structure of mammalian trefoil factors and functional insights. *Cell Mol Life Sci.* **62**, 2956-2973 (2005).
24. Schiefner, A., Gebauer, M. & Skerra, A. Extra-domain B in oncofetal fibronectin structurally promotes fibrillar head-to-tail dimerization of extracellular matrix protein. *J Biol Chem.* **287**, 17578-17588 (2012).
25. Ventura, E. *et al.* Alternative splicing of the angiogenesis associated extra-domain B of fibronectin regulates the accessibility of the B-C loop of the type III repeat 8. *PLoS One.* **5**, e9145 (2010).
26. Chapman, M. R. *et al.* Role of Escherichia coli curli operons in directing amyloid fiber formation. *Science.* **295**, 851-855 (2002).
27. Blanco, L. P., Evans, M. L., Smith, D. R., Badtke, M. P. & Chapman, M. R. Diversity, biogenesis and function of microbial amyloids. *Trends Microbiol.* **20**, 66-73 (2012).
28. Coenye, T. Response of sessile cells to stress: from changes in gene expression to phenotypic adaptation. *FEMS Immunol Med Microbiol.* **59**, 239-252 (2010).

29. Prigent-Combaret, C., Vidal, O., Dorel, C. & Lejeune, P. Abiotic surface sensing and biofilm-dependent regulation of gene expression in *Escherichia coli*. *J Bacteriol.* **181**, 5993-6002 (1999).
30. Jozala, A. F. *et al.* Bacterial cellulose production by *Gluconacetobacter xylinus* by employing alternative culture media. *Appl Microbiol Biotechnol.* **99**, 1181-1190 (2015).

Page intentionally left blank

Chapter 5 Tracking of Engineered Bacteria *In Vivo*

Using Non-Standard Amino Acid Incorporation

5.1 Abstract

The rapidly growing field of microbiome research presents a need for better methods of monitoring gut microbes *in vivo* with high spatial and temporal resolution. We report a method of tracking microbes *in vivo* within the gastrointestinal tract by programming them to incorporate non-standard amino acids (NSAA) and labeling them via click chemistry. Using established machinery constituting an orthogonal translation system (OTS), we engineered *Escherichia coli* to incorporate p-azido-L-phenylalanine (pAzF) in place of the UAG (amber) stop codon. We also introduced a mutant gene encoding for a cell surface protein (CsgA) that was altered to contain an in-frame UAG codon. After pAzF incorporation and extracellular display, the engineered strains could be covalently labeled via copper-free click reaction with a Cy5 dye conjugated to the dibenzocyclooctyl (DBCO) group. We confirmed the functionality of the labeling strategy *in vivo* using a murine model. Labeling of the engineered strain could be observed using oral administration of the dye to mice several days after colonization of the gastrointestinal tract. This work sets the foundation for the development of *in vivo* tracking microbial strategies that may be compatible with non-invasive imaging modalities and are capable of longitudinal spatiotemporal monitoring of specific microbial populations.

5.2 Introduction

Studies of interactions between resident microbes and their hosts are revealing a variety of previously unknown mechanisms by which microbes influence human physiology. The human gastrointestinal (GI) tract, which contains both the highest diversity and number of microbes in the human body, is a dynamic environment whose microbial composition can be affected by many

factors, including: diet, age, and immune profile^{1,2}. Such changes have been linked to a wide range of disease states, including inflammatory bowel disease, obesity, resistance to pathogens, diabetes, and neurodegenerative disease¹⁻³. These correlations have led to a need for reliable methods to monitor host-microbe interactions. A great deal has been learned about the compositional changes of the gut microbiome from DNA and RNA sequencing of fecal and tissue samples⁴⁻⁸. This approach can be non-invasive, and yields significant information about many bacterial species simultaneously, but does not give precise information about the spatiotemporal localization or density of specific microbes in the host. Other techniques, like fluorescence *in situ* hybridization (FISH) and immunofluorescence staining of microbes from harvested tissues, offer more spatial information^{9,10}. However, these methods are inherently invasive and require tissue biopsies in larger animals, or can be performed at the endpoints of small animal studies, which hinders longitudinal studies and real-time tracking. Therefore, less invasive tools to track the spatiotemporal dynamics of gut microbes *in vivo* would be useful for microbiome study.

The need for such tools is further underscored by recent efforts to use living microbes as orally deliverable therapeutics and diagnostics¹¹⁻¹⁶. Unlike traditional drugs, whose pharmacokinetics and pharmacodynamics (PK/PD) can be tracked experimentally with medical imaging techniques, or predicted based on well-established models, microbial PK/PD is comparatively harder to characterize. Indeed, microbes exhibit a range of context-dependent active processes, including self-replication, chemotaxis, and biochemical communication with other cells in their environment, that make it difficult to determine their bio-distribution in a time-resolved manner. Thus, if living microbes are to be treated as sophisticated versions of drugs or drug

delivery vehicles, we must develop better tools to track their trafficking and interactions with their surroundings using medically-relevant imaging techniques.

There are some techniques to track labeled microbes *in vivo*. One common method involves genetically engineering microbes to express luciferase or fluorescent proteins so that they can be imaged using *in vivo* imaging techniques¹⁷⁻¹⁹. However, the poor tissue permeability of optical wavelengths limits the use of such techniques to small animals. Additionally, since most of the GI tract is anaerobic, low oxygen availability can inhibit the proper function of certain fluorophores and chromophores and limit the signal that is produced²⁰. Furthermore, the spatial resolution of optical imaging on small animals reveals little about the location of the microbes in the gut or in other organs. Another recent example used click chemistry to fluorescently label anaerobic bacteria displaying azido sugars on their surface²¹⁻²³. This enabled pre-labeled bacteria to be tracked during their transit through the GI tract. However, the technique required metabolic incorporation of azido sugars in the bacteria prior to ingestion, so progeny cells were no longer labeled, precluding the longitudinal tracking of the microbes beyond 24 hours.

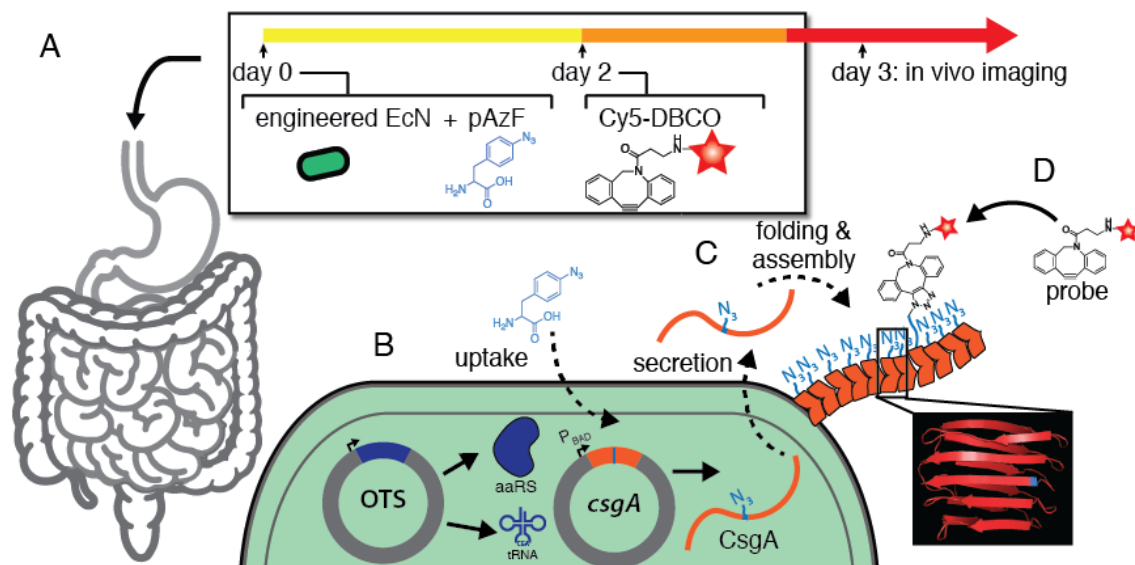


Figure 5.1 Tracking of engineered bacteria in vivo using non-standard amino acid incorporation, (A) Bacteria, pAzF, and imaging probe (Cy5-DBCO) are delivered orally in sequence as shown. (B) The bacteria have been engineered to express an orthogonal translation system (OTS) and a gene containing an in-frame UAG codon (*csgA*, orange). (C) Bacteria residing in the gastrointestinal tract incorporate pAzF and display it on their surface through the secretion and assembly of extracellular curli fibers (orange chevrons) at any point during their residency. (D) The displayed azide functional group can be targeted by an imaging probe in order to label the engineered bacterial population.

An ideal *in vivo* tracking system for microbes in humans and other large animals should satisfy two primary criteria. First, the spatial localization of the microbes should be ascertainable with some precision using medically-relevant and widely available imaging modalities. Second, it should be feasible to track the microbes longitudinally over the course of several days to months. This line of reasoning led us to a design wherein a biorthogonal click reaction is used to target an imaging probe to microbes that can stably display an appropriate click-able functional group. The imaging probe could then be delivered orally at any time point after microbial ingestion. The versatility of the click reaction would also make this approach adaptable to multiple imaging modalities, depending on the need. Here we report a proof of concept study that satisfies the criteria stated above. The click-able functional group was introduced by virtue of an orthogonal translation system (OTS) that enables the probiotic *Escherichia coli* Nissle 1917 (EcN) to incorporate the

NSAA *p*-azido-L-phenylalanine (pAzF) at UAG (amber) stop codons²⁴. The strain also harbors a gene expressing an extracellularly displayed protein, *csgA*, containing an in-frame UAG codon mutation. Together, these modifications enable the bacteria to incorporate and display the bioorthogonal chemical handle during residence in the GI tract that can be targeted by a click-able imaging probe of choice (Figure 5.1).

5.3 Results and Discussion

5.3.1 Azide-containing proteins are successfully secreted and assembled extracellularly from engineered *E. coli* Nissle 1917

In order for the incorporated pAzF to be accessible to imaging probes, we reasoned that it had to be displayed extracellularly. We incorporated the requisite in-frame UAG codon into the *csgA* gene, which encodes for curli fibers. Curli are a biofilm matrix component native to *E. coli* that are produced through the secretion and self-assembly of the CsgA protein into cell-anchored amyloid fibers^{25,26}. We created two plasmid constructs – pBbB8k-wt and pBbB8k-mut that contained either the wild-type (wt) or mutant *csgA* (mut *csgA*), respectively, in the same cistron as the other curli genes necessary for secretion and assembly, all under the control of an inducible promoter (P_{BAD}). The mut *csgA* was generated in such a way that the UCA codon that normally encodes for serine at position 89 in the CsgA amino acid sequence was mutated to an amber stop codon (UAG) (Figure 5.2), which can be recognized by the OTS to incorporate the pAzF in this location during translation. S89 was chosen for the location of the mutation because the native serine residue is predicted to be surface-accessible in the assembled amyloid state, based on multiple structural models of the parallel β -sheet structure of CsgA²⁷⁻²⁹. Hence, we reasoned that

the location of the mutation would interfere neither with CsgA's structure nor its assembly into amyloid fibers. A separate plasmid construct (pEVOL-pAzF) harbored the OTS, encoding for a tRNA and an aminoacyl tRNA synthetase that worked together to incorporate pAzF specifically and orthogonally at UAG codons. All *in vitro* experiments were performed with an EcN-derived strain called PBP8, harboring chromosomal deletions of all the curli genes (EcN:: Δ csgBACDEFG). The genotype of PBP8 was confirmed by sequencing (Figure 5.3) and its phenotype was confirmed by decreased staining with the amyloid-specific dye, Congo Red^{30,31}, compared to the parent EcN strain under conditions known to produce curli fibers (Figure 5.4)^{32,33}.

wtCsgA	1	MKLLKVAAIAAIVFSGSALAGVVPQYGGGGNHGGGGNNSGPNSELNIYQYGGGNSALALQ
mutCsgA	1	MKLLKVAAIAAIVFSGSALAGVVPQYGGGGNHGGGGNNSGPNSELNIYQYGGGNSALALQ
wtCsgA	61	TDARNSDLTITQHGGNGADVGGSDSSIDLTLQRFNGSATLDQWNGKNSEMTVKQFGG
mutCsgA	61	TDARNSDLTITQHGGNGADVGGSDDS-IDLTLQRFNGSATLDQWNGKNSEMTVKQFGG
wtCsgA	121	GNGAAVDQTASNSSVNVTVQVFGNNAHAHQYSGGGSGGSGGSGHHHHHH
mutCsgA	120	GNGAAVDQTASNSSVNVTVQVFGNNAHAHQYSGGGSGGSGGSGHHHHHH

Figure 5.2 Protein sequences of wild type CsgA and mutant CsgA, which contains an amber stop codon (UAG) for the incorporation of non-standard amino acid.

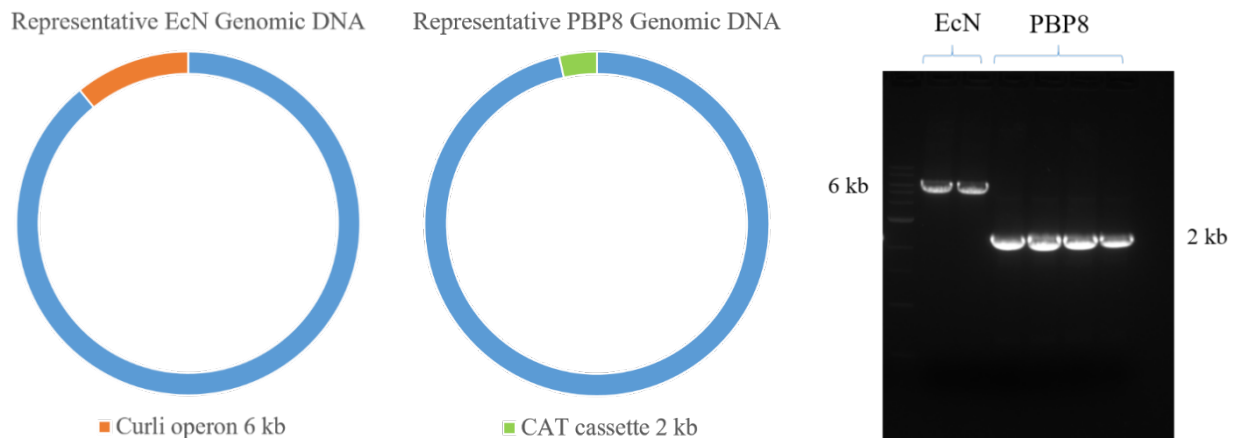


Figure 5.3 Curli operon deletion of *E. coli* Nissle 1917 (left panel) representative genomic DNA of EcN with curli operon labeled in orange (middle panel) representative genomic DNA of PBP8 with chloramphenicol acetyl transferase (CAT) cassette labeled in green replacing curli operon (right panel)

DNA gel shift assay verifying the change of curli operon into CAT cassette by PCR amplification of the sequence adjacent to the curli operon in EcN and PBP8 genomic DNA

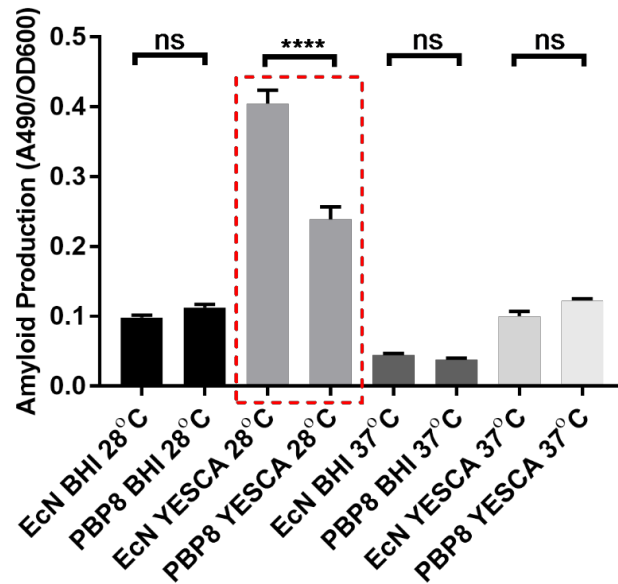


Figure 5.4 Confirmation of curli production deficiency in PBP8 cells. EcN and PBP8 cells were grown using brain heart infusion (BHI) media (high osmolarity) and YESCA media (low osmolarity) at 28°C (low temperature) and 37°C. It is known that EcN produces curli fibers when grown in low osmolarity media at low temperature. Hence, we observe the high production at YESCA 28°C. However, with the PBP8 strain, the curli operon is deleted. Therefore, we observe significant reduction in the amyloid production under this condition.

PBP8 co-transformed with pEVOL-pAzF and either pBbB8k-wt or pBbB8k-mut successfully produced amyloid fibers in the presence of inducer and pAzF, as confirmed by a quantitative Congo Red (CR) binding assay. In contrast, when any of the necessary components – OTS, *csgA* mut gene, or inducer – were omitted, less CR binding was observed (Figure 5.5A). The identity of the extracellular amyloid was confirmed with a whole-cell filtration ELISA that measured the C-terminal His-6 tag on both wt and mutant CsgA (Figure 5.5B). Electron microscopy of induced cultures further confirmed the ability of the co-transformed PBP8 to produce amyloid fibers with the same morphological features as wild-type curli fibers (Figure 5.5C). Notably, induced mutants in the absence of pAzF produced a truncated version of CsgA, which could also assemble into amyloid fibers (Figure 5.6). However, overproduction of this

truncated CsgA could lead to slower growth of the engineered cells, which did not happen when the cells were induced in the presence of pAzF (Figure 5.7).

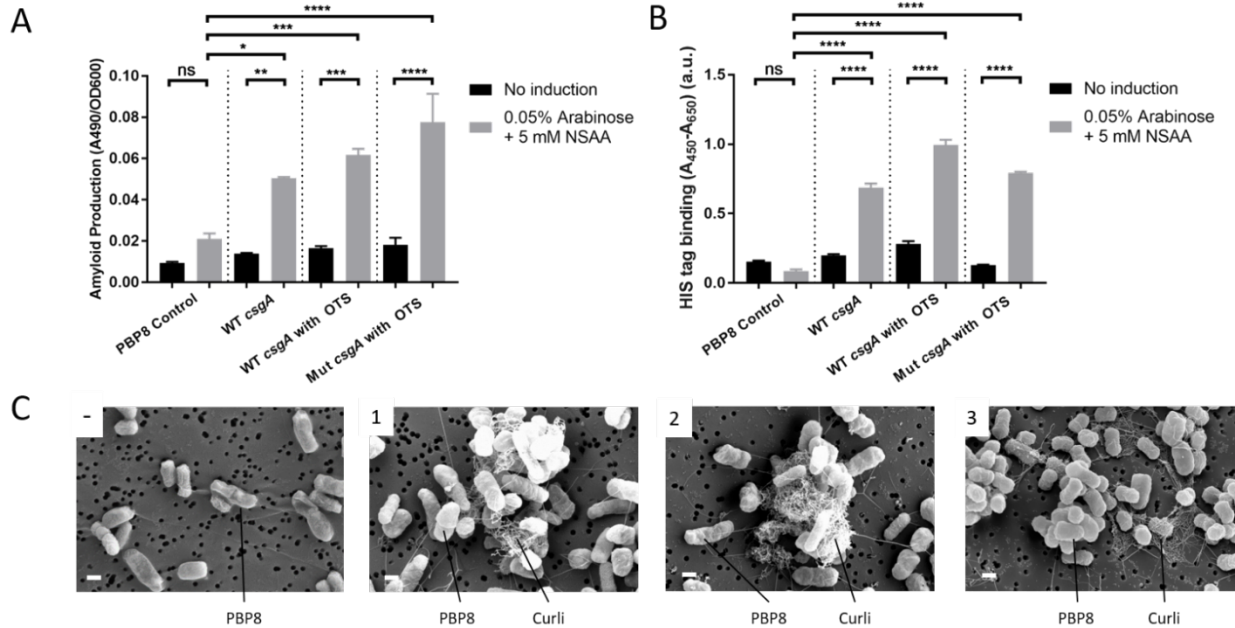


Figure 5.5 Engineered bacteria can produce mutant curli fiber. (A) Amyloid production assay for various strains, based on Congo Red binding, with and without induction. (B) Whole-cell filtration ELISA assays with anti-HIS antibody detection confirms the presence of extracellular HIS-tagged curli fibers under appropriate conditions. Ordinary one way ANOVA with Tukey's multiple comparison test $n=3$, $*P<0.05$, $**P<0.01$, $***P<0.001$, $****P<0.0001$ (C) Scanning electron microscopy of PBP8 transformed with various plasmid combinations: (-) no plasmid (1) pBb8k-wt (containing wild-type *csgA*) (2) pBb8k-wt and pEVOL-pAzF (containing OTS) (3) pBb8k-mut (containing mutant *csgA*) and pEVOL-pAzF. All samples with curli genes successfully express curli fibers including the mutant curli fibers (scale bar = 1 μm)

Overproduction of recombinant proteins can be metabolically taxing, hindering the ability of engineered bacteria to compete in the stringent environment of the gut^{34,35}. We used growth curves of engineered EcN strains to evaluate fitness. We observed little variation in doubling times between the parent strain and those harboring either plasmid with and without induction (Figure 5.7), suggesting that neither OTS nor curli expression negatively affects growth.

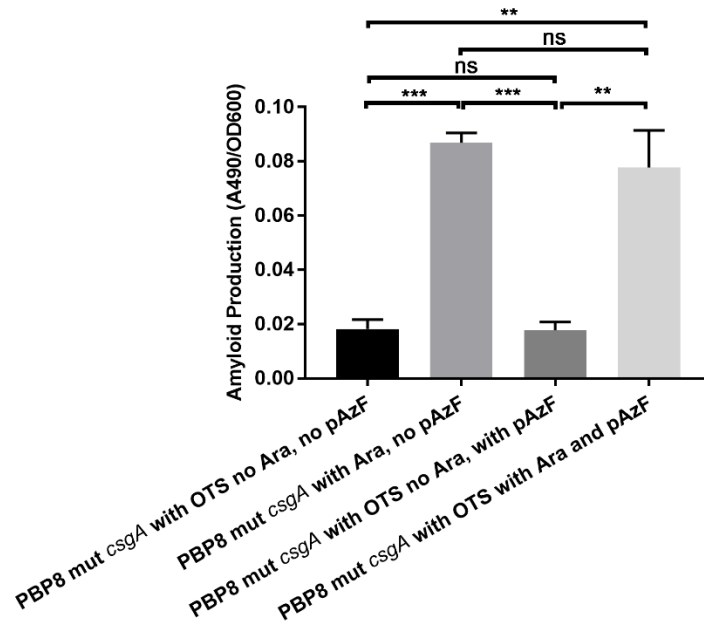


Figure 5.6 Amyloid production assay for PBP8 mut *csgA* strain with various induction conditions (Ara = L-arabinose, pAzF = *p*-azido-L-phenylalanine)

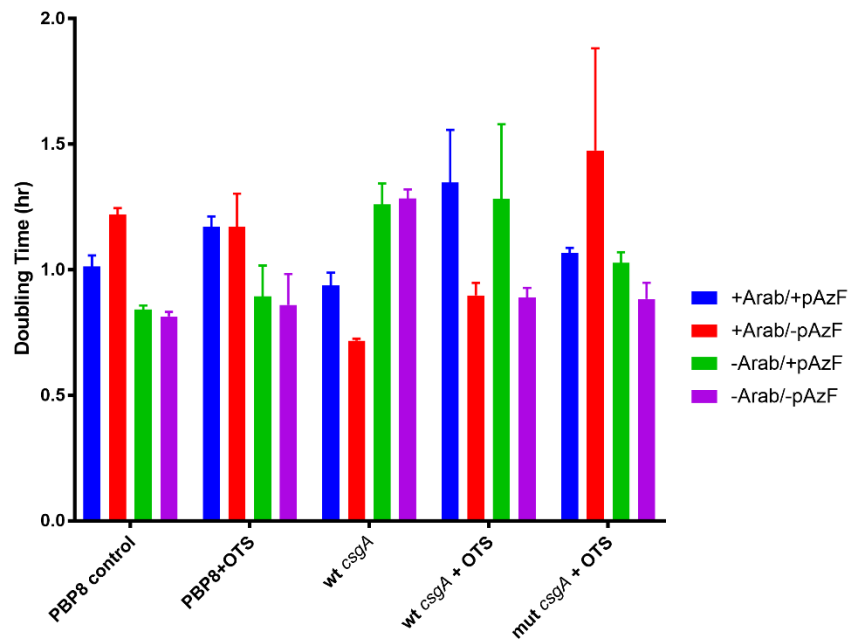


Figure 5.7 Doubling time comparison of PBP8 variants across different types of induction conditions.

5.3.2 Engineered curli fibers containing non-standard amino acids can perform click chemistry *in vitro*

To determine the ability of the mutant curli fibers to perform click chemistry labeling, we exposed induced broth cultures to a Cy5-dibenzocyclooctyl (DBCO) conjugate, a probe designed to react with pAzF. In this case, the cycloalkyne group of DBCO is able to undergo copper-free click chemistry with the azide moiety of pAzF³⁶. After exposure to the probe conjugate, the bacterial cells were pelleted and washed by resuspending several times in PBS, then aliquots were spotted onto a nitrocellulose membrane and imaged. As expected, PBP8 cultures induced to express mutant curli gave the highest fluorescence signal. However, induced cultures producing wild-type curli exhibited increased signal over the background, suggesting that non-specific adsorption of the Cy5 dye to curli fibers could be a factor in determining labeling efficiency (Figure 5.8A). The click reaction yield was not affected significantly by Cy5-DBCO concentrations above 20 μ M and labeling times above 1 hour, underscoring the robustness of the azide-DBCO reaction for rapid labeling under a range of conditions (Figure 5.9).

To test the labeling efficiency of the mutant curli fibers while removing the effects of non-specific binding to the bacterial cells themselves, we performed labeling reactions on crudely purified curli fibers. We employed a previously established isolation protocol to obtain curli fiber mats in the absence of cells³⁷. The filter membrane-supported curli mats were incubated with Cy5-DBCO, washed, and imaged (Figure 5.8B). The fluorescence results indicate that the dye bound specifically to the curli fiber mats only when the mutant fibers, OTS, and pAzF were present.

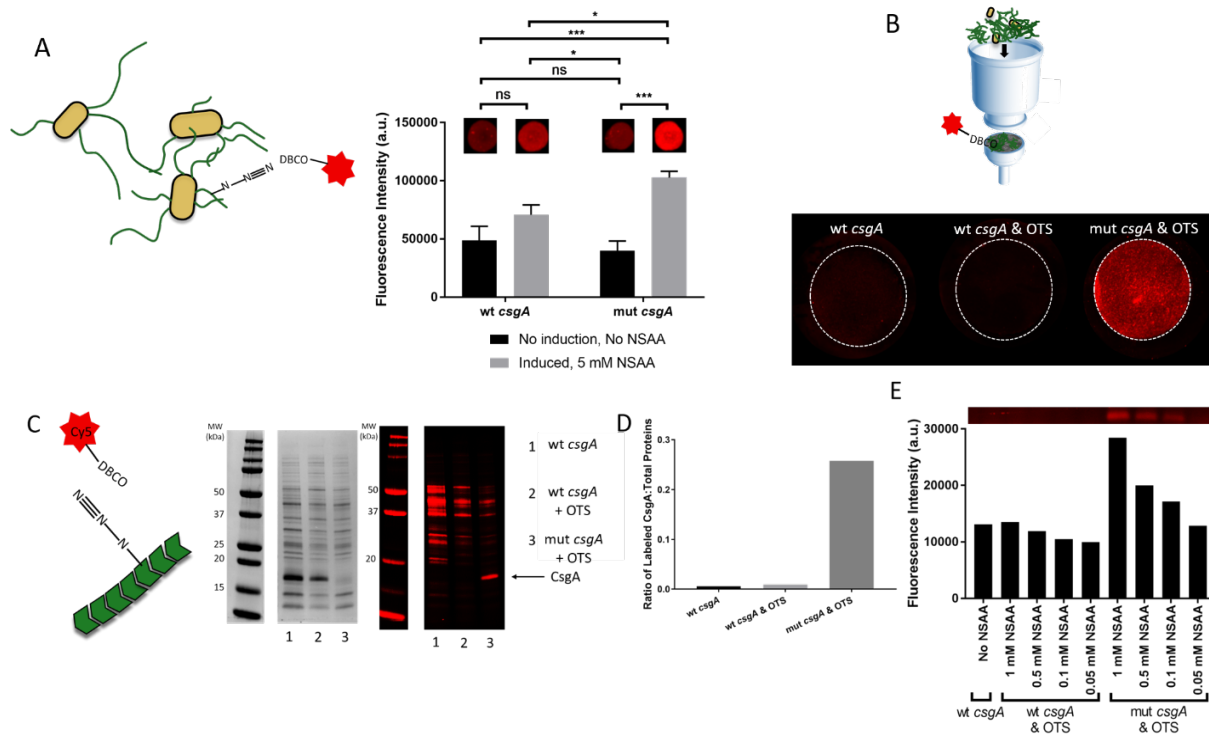


Figure 5.8 *In vitro* click chemistry-dependent labeling of engineered curli fibers, (A) Fluorescence signal from cell cultures spotted onto nitrocellulose membranes and labeled with Cy5-DBCO. Ordinary one way ANOVA with Tukey's multiple comparison test $n=3$, * $P<0.05$, ** $P<0.01$, *** $P<0.001$, **** $P<0.0001$ (B) Fluorescence signal after labeling of curli amyloid mats after cell removal. (C) SDS-PAGE analysis of cells after induction and semi-purification of curli fibers. Coomassie blue stained gel (left) and fluorescence signal from unstained gel (right). (D) Ratio of labeled CsgA to total labeled proteins from various experiment conditions (E) Fluorescence intensity of CsgA variants as a function of pAzF concentration.

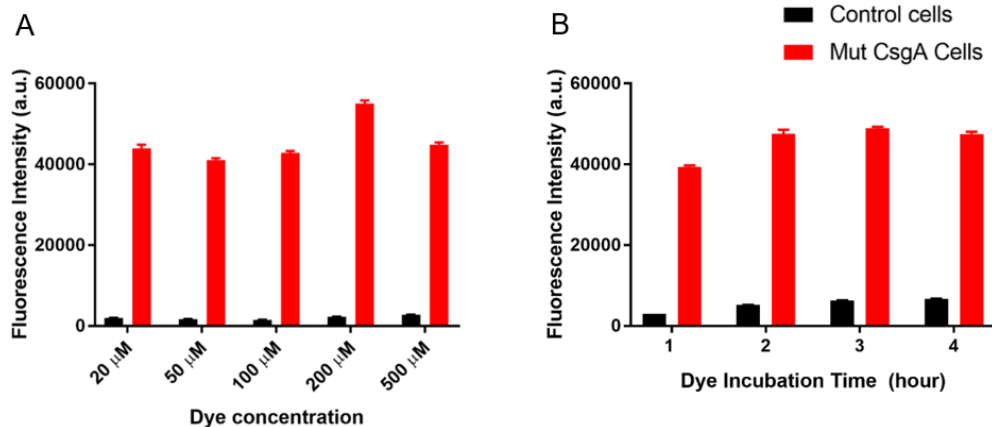


Figure 5.9 Fluorescence intensity as functions of dye concentration and incubation time, (A) Fluorescence intensity after labeling of PBP8 cells (grey) and mut CsgA cells (red) as a function of Cy5-DBCO concentration (B) Fluorescence intensity after labeling of PBP8 cells (grey) and mut CsgA cells (red) as a function of incubation time with Cy5-DBCO.

5.3.3 Click labeling is specific to mutant curli fibers

We selected the OTS designed for pAzF incorporation at UAG sites (pEVOL) for several reasons. First, pAzF and the pEVOL system are well-characterized and have been shown to have high incorporation efficiency into mutant proteins^{24,35}. Second, UAG is the rarest codon in the *E. coli* genome, with only 366 instances in EcN. Notably, efforts have been made to increase the specificity and efficiency of NSAA incorporation by replacing all native instances of UAG with a synonymous stop codon across the *E. coli* genome, permitting the deletion of RF-1, which terminates translation at UAG codons³⁸. Since we did not use a recoded strain for this work, there remained the possibility of pAzF incorporation at other genes terminated by UAG in the presence of the OTS. Although it was unclear how much this would affect the success of the *in vivo* labeling scheme, we wanted to characterize the level of pAzF incorporation in proteins other than CsgA and demonstrate the preferential binding of the dye to the mutant CsgA. We performed SDS-PAGE analysis on semi-purified labeled lysed cells to determine the distribution of dye across the PBP8 proteome (Figure 5.8C). In the Coomassie-stained gel, the semi-purified proteins from cultures expressing wild-type curli with and without the OTS showed stronger CsgA bands near 17 kDa, compared to those expressing mutant CsgA (Figure 5.8C). This is perhaps the result of inefficient translation of full-length CsgA, since pAzF incorporation must compete with premature termination from the cell's native release factor-1 (RF-1). The fluorescence-imaged gel showed that cells expressing mut *csgA* and the OTS exhibited higher intensity for the CsgA band compared to other background proteins in the lysate, whereas those expressing wild-type fibers showed higher non-specific labeling of other proteins. Expressed as a ratio of fluorescence intensities between (CsgA):(all other proteins), the labeling specificity for CsgA was 45x higher when the

mut *csgA* gene was present compared to the wt *csgA* gene, in the presence of the OTS (Figure 5.8D). Even with the lower absolute amount of mutant CsgA, we observed much higher dye labeling efficiency for the mutant CsgA compared to wild-type CsgA. Furthermore, the fluorescence intensity of the CsgA band in the gel increases in a dose-dependent manner with pAzF concentration, with labeling being indistinguishable from background signal at a concentration of 0.05 mM (Figure 5.8E).

5.3.4 Labeling efficiency of engineered bacteria

We assessed the labeling efficiency on a per cell basis by subjecting bacterial cultures that had been induced to produce curli fibers and exposed to Cy5-DBCO to flow cytometry analysis. This confirmed that there was some dye association with cells producing wild-type CsgA both without (17.9% labeling) and with (26.2% labeling) the OTS present. However, more than 63.8% of PBP8 cells producing mutant CsgA in the presence of the OTS and the NSAA were labeled (Figure 5.10A, Figure 5.11). The non-specific labeling appeared to be dependent on curli production, since it was present at a lower level in the case of untransformed or non-induced PBP8 cells, corroborating the results shown in Figure 5.8B. Confocal microscopy qualitatively supported the flow cytometry data, with more than half of the cells exhibiting a signal for the Cy5 dye (Figure 5.10B).

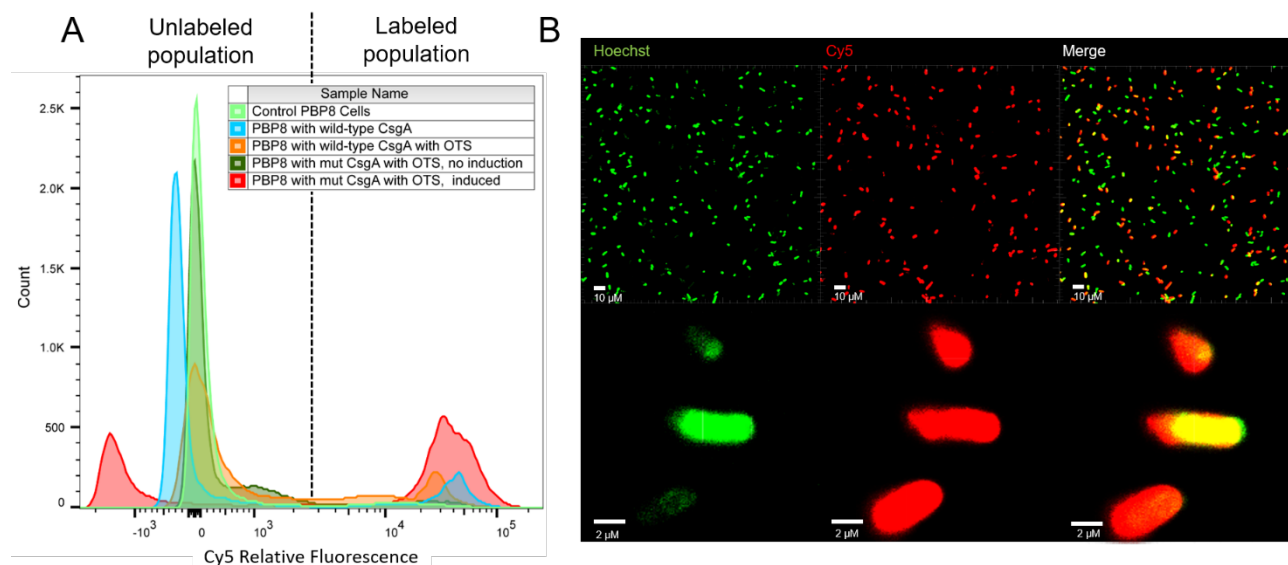


Figure 5.10 Labeling efficiency of engineered bacteria, (A) Flow cytometry histogram of cell cultures under various conditions after exposure to Cy5-DBCO. (B) Confocal fluorescent micrographs of PBP8 harboring pBb8k-mut and pEVOL-pAzF after induction and labeling.

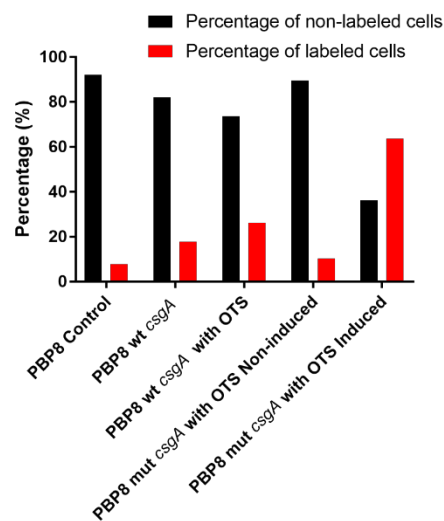


Figure 5.11 Percentage of non-labeled and labeled PBP8 cells as interpreted by flow cytometry data.

5.3.5 Engineered probiotic bacteria with mutant curli fibers are able to perform click chemistry *in vivo* in murine model

In order to demonstrate the feasibility of performing the labeling reaction *in vivo*, we administered the engineered EcN to mice via oral gavage and induced the expression of mutant curli using arabinose and pAzF in their drinking water. Cy-5-DBCO was administered orally 42

hours after administering the bacteria, and Cy5 fluorescence signals from the abdominal area were detected using an *in vivo* imaging system (IVIS) over the course of 48 hours (Figure 5.12A). Fluorescence intensity remained high in mice that had been administered the engineered PBP8 up to 24 hours after dye administration. Control experiments with no bacterial administration showed signal decay after 6 hours. However, subsequent experiments with non-induced bacteria made it difficult to distinguish click chemistry-based labeling from non-specific dye binding and tissue autofluorescence (Figure 5.13). We, therefore, sought to demonstrate the specificity of the labeling reaction using *ex vivo* methods and additional experimental conditions (i.e. with and without bacteria administration, dye administration, and pAzF administration). Based on the previous experiments, we selected 36 hours post-dye administration as an experimental endpoint that would ensure that even non-specifically bound dye would have been cleared from the GI tract. The *in vivo* experimental scheme is depicted in Figure 5.14. After harvesting of the GI tracts, Cy5 signal was measured using the IVIS. Significant tissue/food autofluorescence was observed from the stomach, so analysis was confined to the cecum and lower intestine. Qualitative and quantitative analysis showed that the experimental group containing all the necessary components (bacteria, mutant CsgA, pAzF, and inducer) showed a distinct increase in fluorescence intensity measured at 675 nm in the cecum, which is the primary location of *E. coli* in the mice³⁹, compared to any of the other experimental conditions (Figure 5.12B,C). Low intensities were observed in the cecum of mice that had been administered bacteria producing wild-type curli fibers, which correlated to the non-specific dye adsorption observed *in vitro* (Figure 5.12B, panels 3 and 4). Conditions in which pAzF was administered without the necessary machinery for incorporation exhibited cecal fluorescence intensities that were not significantly higher than that observed for dye administration alone, suggesting that non-specific incorporation of pAzF by host cells or other microbes using

native machinery did not contribute significantly to the signal observed for the desired click labeling. Finally, we performed SDS-PAGE analysis of homogenized cecum tissue in order to determine if the fluorescence signals that we observed from the lower GI tract were actually from the click-labeled CsgA protein (Figure 5.12D). Coomassie staining revealed protein bands at the expected size for mutant CsgA (14.7 kDa) in group 3 (induced PBP8, wild-type curli) and group 6 (induced PBP8, mutant curli). Fluorescence analysis of the gels before Coomassie staining revealed that the observed signal could be attributed to these same bands, with higher intensities for the mutant curli. No other labeled proteins were observed, confirming the reaction specificity for the incorporated pAzF probe and engineered bacteria.

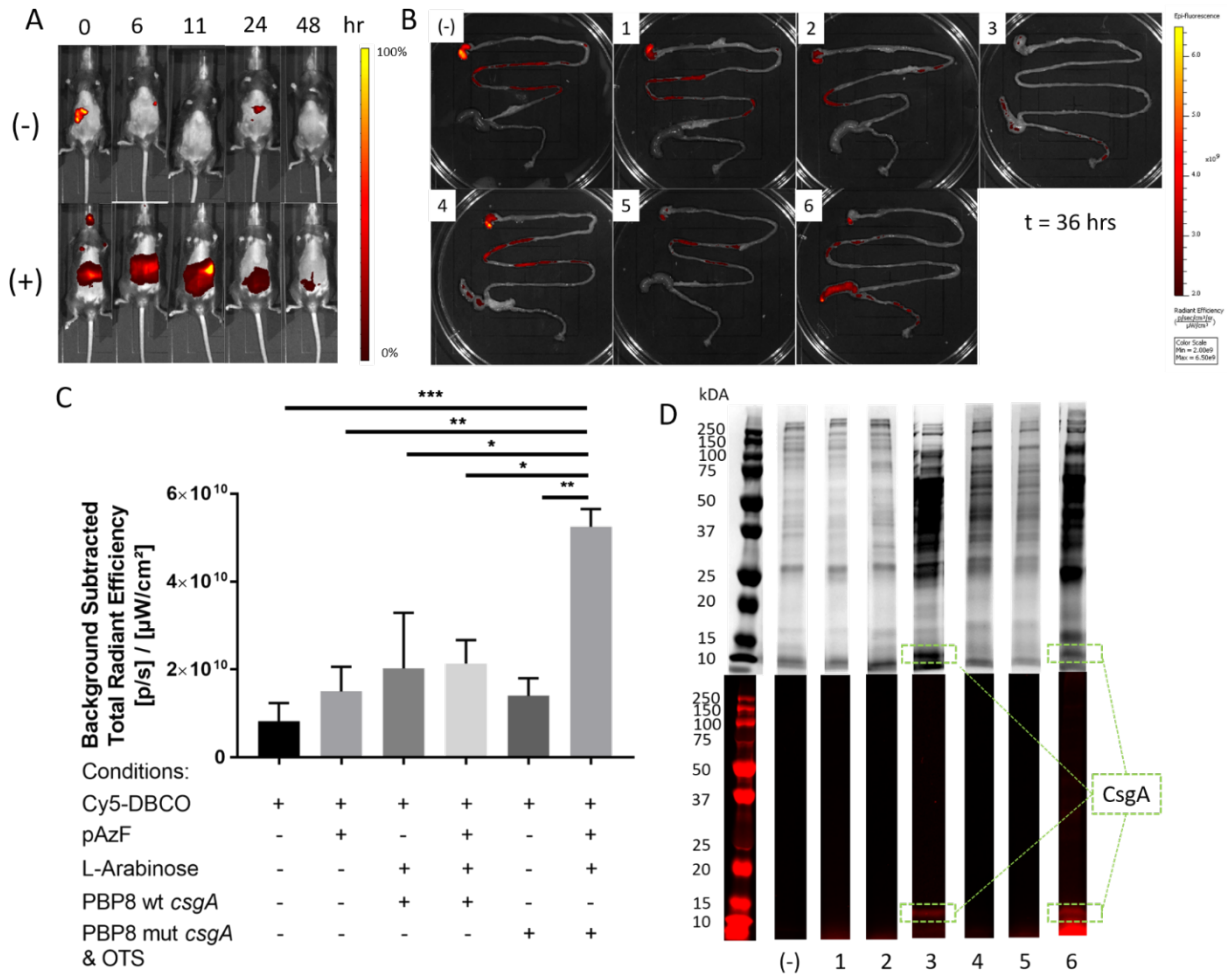


Figure 5.12 Engineered bacteria are labeled via click chemistry *in vivo*, (A) Fluorescence imaging of live mice fed with either PBS only (-), or PBP8 harboring pBbk8-mut and pEVOL-pAzF (+). The mice were given arabinose and pAzF to induce mutant curli expression 2 days prior to the start of the experiment. Images were taken at a different time points after Cy5-DBCO administration at time = 0 hours. (B) Representative fluorescence images of harvested mouse GI tracts, collected 36 hours after Cy5-DBCO administration under various conditions: (-) negative control with no bacteria or dye administration, (1) no bacteria, (2) no bacteria, but with pAzF in drinking water, (3) PBP8 expressing wt-*csgA*, (4) PBP8 expressing wt-*csgA* with pAzF in water, (5) non-induced PBP8 expressing mut-*csgA* with OTS (6) PBP8 expressing mut-*csgA* with OTS. (C) Quantification of Cy5 fluorescence signals from the lower GI tracts. Ordinary one way ANOVA with Tukey's multiple comparison test n=3, *P<0.05, **P<0.01, ***P<0.001, ****P<0.0001 (D) SDS-PAGE analysis of homogenized cecal contents stained with Coomassie blue (*top*) and unstained fluorescent imaging (*bottom*). Lane markers correspond to numbering in part B.

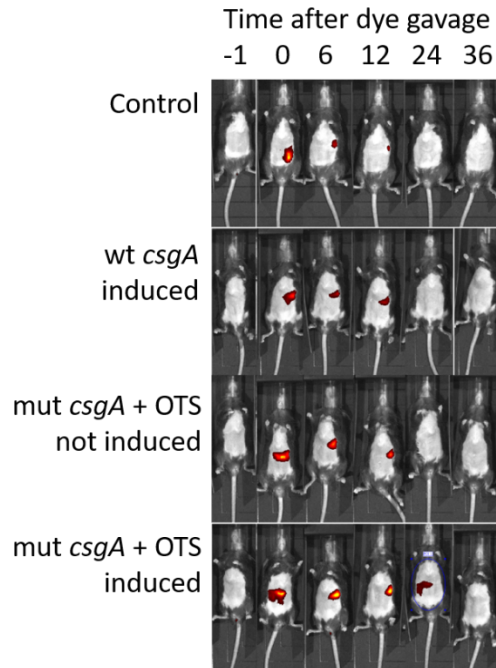


Figure 5.13 Auto-fluorescence of the *in vivo* mouse imaging.

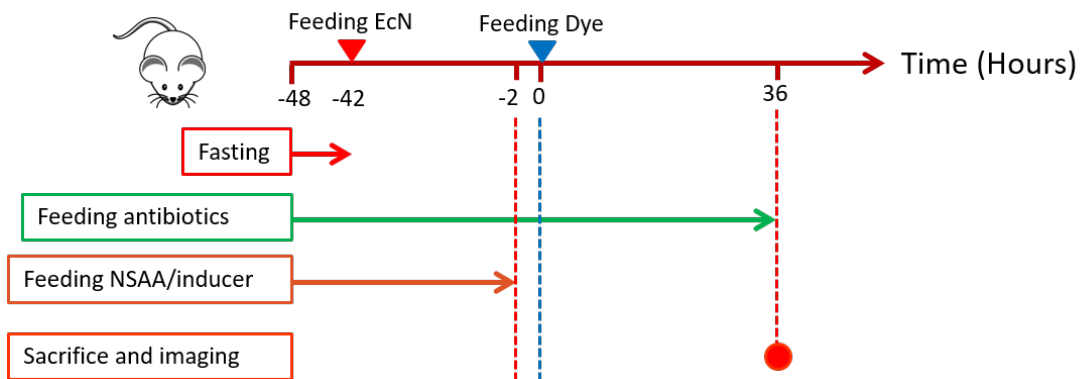


Figure 5.14 Mouse experiment timing illustration.

5.4 Conclusions

Most existing methods for studying the spatiotemporal dynamics within the gut microbiome rely on analytical techniques that are either indirect (e.g. fecal bioinformatics), or highly invasive (e.g. histology). Less invasive methods to track microbes in live animals would benefit fundamental microbiome research as well as the development of living microbial therapeutics and diagnostics. Here we describe a new method to label engineered bacteria *in vivo* using bio-

orthogonal click chemistry. This technique enables monitoring of microbial localization several days after ingestion and should be compatible with any “click-able” imaging probe.

This work shows a basic proof-of-concept that such a labeling strategy can be successfully performed. However, there are several ways in which the technique could be improved upon. The *in vitro* results suggest that inefficient translation of the mutant CsgA, even in the presence of the OTS, could limit the amount of CsgA that was produced. Although we did not find this to prevent the proof-of-concept demonstration, a recoded *E. coli* strain might significantly improve the NSAA incorporation efficiency by removing the possibility for premature termination via RF-1. The labeling efficiency on a per microbe basis *in vitro* was also only ~60%, which we speculated was related to the well-documented nature of arabinose-inducible promoter systems⁴⁰. This suggests that further optimization of promoter systems could also contribute to higher signals *in vivo*. Detachment of curli fibers from bacteria in the gut could also complicate interpretation of the imaging results, so other proteins bound directly to the cell surface could be worth exploring as alternative labeling targets. Other cell-surface proteins as labeling targets could also ameliorate the non-specific dye labeling observed for assembled CgsA. Autofluorescence of the upper GI tract and long clearance times for the Cy5-DBCO dye also hindered effective *in vivo* imaging of the engineered bacteria. Other imaging probes with further red-shifted emissions or probes that incorporate a “turn-on” function upon undergoing the click reaction could improve signal-to-noise ratios. With regard to the potential toxicity of pAzF as *in vivo*, there is limited data. It is worth noting that copper-free chemistry using Cy5-DBCO has been performed in live mice and rat with no apparent toxicity⁴¹⁻⁴⁴. We did not observe any apparent toxicity in our short term study, though

a more thorough toxicity study may have to be performed in the future to assess the safety of pAzF in mouse models.

The approach we demonstrate here could enable the development of analytical techniques with new capabilities. For example, the in-frame UAG mutation could be used to report specifically on the production of other extracellularly displayed proteins. Furthermore, the proliferation of OTS systems compatible with different NSAAs and organisms could enable a multiplexed approach to tracking multiple microbes simultaneously. By changing the nature of the probe, one could envision longitudinal, non-invasive imaging of microbial populations in humans or large animals using clinical imaging modalities, like MRI or PET, which enhance tissue penetration in the way that fluorescence or luminescence signals cannot. Excitement for such prospects must be tempered with the requirement that the cellular population to be tracked using this technique must be genetically engineered to enable NSAA incorporation. However, with the meteoric rise of CRISPR/Cas9-based techniques to rapidly modify genomes and the continuing development of new OTS, this could become increasingly accessible in the near future.

Ongoing studies in our lab are focused on the development of a second generation system that, in addition to addressing the issues raised above, would rely on incorporation of the OTS and mutant genes in to the bacterial chromosome so that antibiotic selection would not be required during *in vivo* deployment. Overall, our approach enables a wider selection of imaging probes compared to conventional microbe tracking methods, such as fluorescent labelling or luminescent proteins expression. Non-protein dyes or inorganic probes can be utilized because they are provided externally and do not have to rely on oxygen-dependent maturation chemistry, like some fluorescent proteins. Alternatively, the incorporation and display of the azide bearing amino acid

could be tied to other environmental sensing mechanisms relevant to the gut^{11,45}, leading to diagnostics that would report on disease states with spatial resolution within the GI tract. Furthermore, the approach may be useful for tracking the progression of infections in model systems.

5.5 Materials and Methods

5.5.1 Cell strains and plasmids

The divergent curli operon regions consisting of *csgBAC* and *csgEFG* were PCR isolated from *E. coli* K12 substr. W3110 and cloned by overlap extension into the pBbB8k plasmid, to create a single operon, *csgBACEFG*, under the control of the araBAD promoter. The cloning of the curli operon was performed in an analogous manner to our previously published work³⁷. A six-histidine tag (HisTag) was added to the C-terminus of CsgA to allow for immunodetection (pBbB8k-WT) (See plasmid map in Figure 5.15). A control plasmid was constructed by cloning the *malE* gene encoding for the maltose binding protein (MBP) from the W3110 genome into the pBbB8k plasmid under the control of the araBp promoter (pBbB8k-MBP).

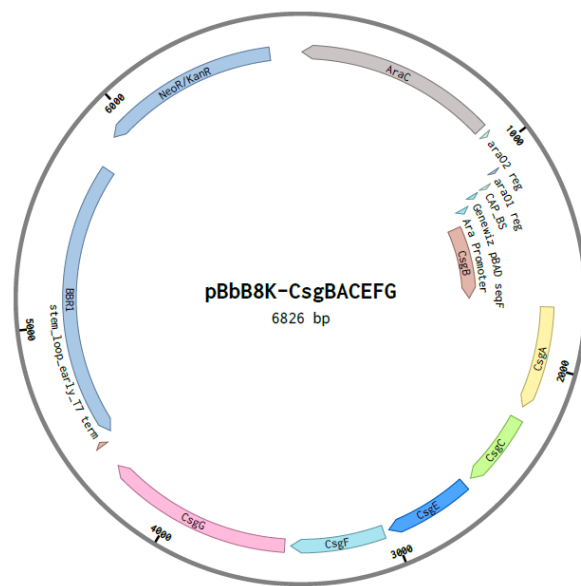


Figure 5.15 pBbB8k-wt csgA plasmid map.

To allow for the incorporation of the NSAA, a mutation encoding for the amber stop codon (UAG) was inserted within the open-reading frame of CsgA (pBbB8k-Mut csgA). Using site-directed mutagenesis, we directed the amber mutation in place of a UCA codon, which normally encodes for serine at amino acid position 89 of CsgA (See DNA sequences in supporting information 1 and 2).

The orthogonal translation system (OTS) plasmid pEVOL-pAzF²⁴ was obtained from the Church Lab with slight modification where the chloramphenicol resistance was swapped to spectinomycin resistance and the sequences were codon optimized.

Protein expression was performed in a curli operon deletion mutant, PBP8, an *E. coli* strain derived from *Nissle 1917* (ECN). PBP8 strain was constructed using lambda red recombineering method described previously by Datsenko and Wanner⁴⁶. In brief, the chloramphenicol acetyltransferase (CAT) cassette was constructed with 500 bp homology arms upstream and downstream of the curli operon using SOEing PCR. The CAT cassette was transformed into

electrocompetent EcN with pre-induced lambda red genes from the pKD46 plasmid using 0.5% arabinose (Sigma) during the growth step of electrocompetent cell preparation. The transformant was expanded using SOC media at 30°C shaking incubator for 3 hours to promote the genomic replacement of the curli operon with CAT cassette. The transformant was then plated onto Luria Broth (LB) agar plates (Sigma) containing 25 µg/mL chloramphenicol (RPI) and incubated overnight at 37°C. Colonies that are resistant to chloramphenicol were selected and verify the curli operon knockout by colony PCR and genomic DNA sequencing comparing to wild-type EcN.

5.5.2 Mice

Female 6- to 8-week-old C57BL/6 mice were purchased from Charles River Laboratories. Mice were housed in SPF conditions with sterile food and water *ad libitum*. The animal chow included LabDiets 5K67 and the non-fluorescent food LabDiets 5V5R. Mice were maintained in sterile vinyl isolators equipped with food, water and bedding in the Harvard Medical School animal facility. Before any experiment, mice had at least one week to acclimatize to the facility environment. All experiments were conducted in accordance with US National Institutes of Health guidelines and approved by the Harvard Medical Area Standing Committee on Animals.

5.5.3 *In vitro* expression of curli fibers

PBP8 cells transformed with a pBbB8k plasmid were streaked onto LB agar plates containing 50 µg/mL kanamycin (Teknova). PBP8 cells transformed both with a pBbB8k plasmid and with the OTS plasmid were streaked onto LB agar plates containing both 50 µg/mL kanamycin and 50 µg/mL spectinomycin (RPI). Colonies were picked from the plates and 5 mL cultures were inoculated (in LB containing the appropriate antibiotics). Cultures were grown overnight at 37°C.

The overnight cultures were diluted 100-fold in fresh LB medium containing the appropriate antibiotics, and cultured at 37°C until they reached an optical density (OD) at 600nm of 0.6 to 0.8. Arabinose was added to the bacterial cultures at a final concentration of 0.05 % to induce protein expression. If NSAA incorporation was desired, the NSAA *p*-azido-L-phenylalanine (pAzF) (Toronto Research Chemicals) was also added to the cultures to a final concentration ranging between 1 mM and 5mM. Higher concentrations affected cell growth. Protein expression was allowed to occur at 37°C overnight.

5.5.4 Quantitative Congo Red binding assay

The quantitative CR binding assay was adapted from a previously published protocol³². In brief, one mL of testing bacteria culture was centrifuged at 8,000 rpm for 10 minutes. The pellet was resuspended gently in 0.025 mM CR in phosphate buffered saline (PBS), incubated at 25 °C for 10 minutes and centrifuged at 15,000 rpm for 10 minutes. 150 µL of the supernatant was transferred to a 96-well plate with clear bottom (Corning) and the absorbance at 490 nm was read using a BioTek H1 microplate reader. The amount of CR binding was calculated by subtracting the measured absorbance from the 0.025 mM CR in PBS control absorbance and normalized by the OD₆₀₀ of the culture.

5.5.5 Whole-cell filtration ELISA

The whole-cell filtration ELISA assay was adapted from a previously published protocol^{47,48}. In brief, the testing bacteria cultures were chilled on ice for at least 20 minutes and diluted to OD₆₀₀ of 0.3 using tris-buffered saline (TBS) (Thermo Fisher Scientific). 200 µL of the diluted samples were added to a Multiscreen-GV 96-well filter plate (0.22 µm pore size; EMD Millipore) and

filtered. The sample wells were washed three times with a wash buffer (TBS, 0.1% Tween-20 (Sigma)) and blocked by incubating with 1% bovine serum albumin (BSA) (Sigma) and 0.01% H₂O₂ (Sigma) in wash buffer for 1.5 hours at 37 °C. The 3-time wash step was repeated. The wells were incubated with 50 µL of anti-HIS antibody-horseradish peroxidase (HRP) conjugated (1:200 dilution) (Thermo Fisher Scientific) for 2 hours at 25 °C and washed 3 times. 100 µL of Ultra-TMB (3,3',5,5'-tetramethylbenzidine) ELISA substrate (Thermo Fisher Scientific) was added to each well and incubated for 20 minutes at 25 °C. Then, 50 µL of 2 M H₂SO₄ (Alfa Aesar) was added to the wells to stop the reaction. 100 µL of this reaction was transferred to a 96-well plate where the absorbance at 450 nm and 650 nm was measure. The relative amount of displayed HIS tag was obtained by subtracting absorbance at 450 nm with absorbance at 650 nm.

5.5.6 Electron microscopy

Cells expressing curli fibers (with and without pAzF) were imaged by scanning electron microscopy (SEM) to assess the formation of fibers. 100 µl of cell cultures were filtered onto Nucleopore filter membranes (0.22 µm pore size, GE Healthcare Bio-Sciences) under vacuum. The samples were fixed with 2 % (m/v) glutaraldehyde and 2 % (m/v) paraformaldehyde in 0.1 M sodium cacodylate buffer for 2 hours at room temperature. The membranes were then gently washed with water, and the solvent was gradually exchanged to ethanol with an increasing ethanol 15-minute incubation step gradient (25 %, 50 %, 75 % and 100 % (v/v) ethanol). The samples were dried in a critical point dryer, placed onto SEM sample holders using silver adhesive (Electron Microscopy Sciences), and sputtered until they were coated in a 5 nm layer of Pt/Pd. Imaging was performed using a Zeiss Ultra 55 Field Emission SEM.

5.5.7 Growth curves and doubling times

The cells were grown in LB broth containing appropriate antibiotics overnight, diluted 1:100 in fresh LB Broth with antibiotics, and grown in a 1mL 96 well plate at 37°C and shaken at 900 rpm. Once the cells reached an OD₆₀₀ of 0.6, they were again diluted 1:100 in fresh LB Broth in a 250mL 96 well plate. Half the cells were induced with 0.05% Arabinose and incubated with 5 mM pAzF. The other half of the cells were used as negative controls and were not induced with Arabinose and weren't exposed to pAzF. Cells expressing the curli operon, or, as controls, PBP8 cells, were used. After this preparation, the 96 well plate was placed in a Biotek Kinetics Machine, which measured OD₆₀₀ every 5 minutes and shook the plate on medium speed for 24 hours. The data were then plotted and the linear slope during exponential growth was used to calculate doubling times. Because curli-expression cells derivatives had more irregular exponential growths than control cells, we used the first exponential growth “hump” of curli variants to determine doubling times.

5.5.8 *In vitro* labeling of click microbes

Cells expressing curli fibers were pelleted at 4000xg for 10 min. The cells were resuspended in phosphate buffer saline (PBS) containing 1 % (m/v) bovine serum albumin (BSA). The centrifugation and resuspension process was repeated 3 times to clean the cells from any excess free NSAA present in the culture medium. The appropriate volume for the experiments was taken (200 µl of OD 5 per sample), pelleted and incubated at OD₆₀₀ of 10 in 100 µL Cy5-DBCO (5 µM) in PBS + 1% BSA for 2 hours at 37°C with agitation. The labeled cells were pelleted again and resuspended in PBS containing 3% (m/v) BSA. This washing step was repeated 3 times to remove unbound dye.

Labeling was assessed by spotting 10 µl of labeled cells on a nitrocellulose membrane and detecting the fluorescence of Cy5 using a FluorChem™ M system (Protein Simple).

5.5.9 Labeling of simulated curli fiber mats

Curli fiber mats from bacteria in different conditions were created by following published protocol³⁷. In brief, we used *E. coli* PQN4 lab strain, which has been previously characterized to produce a high amount of curli materials³⁷. Following curli expression protocol, we induced PQN4 wild type curli, wild type curli with OTS and mutant curli with OTS by adding 0.05% arabinose and 0.1 mM pAzF in the culture media. After the induction period, guanidinium chloride (GdmCl) (Sigma) was added to the cultures to 0.8 M final concentration and incubated for 1-2 hours at 4 °C prior to filtration. 30 to 50 mL of the GdmCl treated cultures were vacuum-filtered onto polycarbonate filter membranes (47 mm diameter, 10 µm pore size, EMD Millipore). The filter membranes were incubated with 5 mL of 8 M GdmCl for 5 minutes and vacuum filtered to eliminate the cell debris, and rinsed with 5 mL of deionized water 3 times. Then, the membranes were incubated with 5 mL of nuclease solution (1.5 U/ml of Benzonase, EMD Millipore, with 2 mM MgCl₂ (Sigma)) for 10 minutes and vacuum filtered to remove remaining nucleic acids, and rinsed with 5 mL of deionized water 3 times. Then, the semipurified curli fiber mats on the filters were incubated with 2 mL 5 µM Cy5-DBCO for 1 hour and rinsed with 5 mL of deionized water 3 times to remove unbound dyes, before imaging with a FluorChem™ M system (Protein Simple).

5.5.10 Purification and identification of proteins labeled *in vitro*

500mL of pre-labeled cells at OD₆₀₀ 1 were pelleted at 4000xg for 20 min and resuspended in 30mL of lysis buffer (50 mM phosphate buffer, 300 mM NaCl, 7M guanidinium hydrochloride).

A protease inhibitor cocktail was added, and the suspension was stored at $-20\text{ }^{\circ}\text{C}$ overnight. The suspension was thawed on ice and sonicated to fully lyse the cells (40 % amplitude, 3x25s ON, 35s OFF, QSONICA Q700 Sonicator). After centrifugation at 10,000xg for 30 min, the supernatant was applied to a NiNTA beads and incubated 2 h with agitation at room temperature in the presence of 10 mM imidazole. The beads were then transferred into the plastic columns. His-tag purification was performed by washing the column 3 times with 40 mM imidazole, and eluting his-tagged CsgA proteins with 500 mM imidazole (both in 50 mM phosphate buffer with 100 mM NaCl).

The eluate was concentrated using 3kDa Amicon ultracentrifugal filters (EMD Millipore) and ran on a 4-20% SDS-PAGE gel. Prior to staining with Coomassie blue, the Cy5 fluorescence within the gel was detected.

5.5.11 Flow cytometry and confocal microscopy

Flow cytometry was used to determine the fraction of cells that were labeled. The cells were further diluted to an OD_{600} of 0.01 per mL in PBS and analyzed with a BD LSRFortessa Flow Cytometer System (BD Biosciences) using the APC channel for Cy5 fluorescence detection. For confocal microscopy the cells were also stained with 5 μM Hoechst 33342 (Thermo Fischer Scientific) in 1x PBS for 1 h and washed 3 times with 1 mL of PBS. Subsequently, the cells were fixed in 2% paraformaldehyde for 10 min at $25\text{ }^{\circ}\text{C}$ and washed 3 times with 1 mL of PBS. 10 μl of cells were deposited on a glass slide for imaging with a Leica SP5 X MP Inverted Confocal Microscope (Leica Microsystems).

5.5.12 *In vivo* tracking of click microbes

Prior to the experiment, mice were given a non-fluorescent food (alfalfa-free) for at least 5 days to minimize background autofluorescence. At 12 hours prior to oral gavage of bacteria, mice were fasted and given special water containing antibiotics (1 g/L kanamycin, 1 g/L spectinomycin), inducer (10 g/L L-(+)-arabinose) and pAzF (5 mM) based on their assigned experimental conditions. The inducer concentration was chosen based on comparison to previously published examples of engineered bacteria in mice^{16,49}. Then, the starting culture of PBP8 transformed with pBbB8k-WT was expanded 1:100 dilution in LB containing 50 µg/mL kanamycin, while that of PBP8 transformed with pBbB8k-Mut and pEVOL-pAzF was expanded 1:100 dilution in LB containing 50 µg/mL kanamycin and spectinomycin to OD₆₀₀ of 0.5. The log-phase cultures were centrifuged at 4000 g for 15 minutes at 4°C and resuspended in 20% sucrose (OmniPur) in PBS to OD₆₀₀ of 10. Once the mice have been fasted for 12 hours, 100 µL of the prepared log-phase bacteria were administered to the mice via oral gavage.

The alfalfa-free food was returned to the mice as well as the special water to allow proliferation and protein induction of engineered bacteria inside the mouse gut. Meanwhile, the mouse's abdominal hair was removed to allow the upcoming IVIS imaging. 30 hours after the bacteria gavage, mice were fasted for another 12 hours to remove the food from the GI tract. 10 hours after that, the NSAA and arabinose containing water was switched into antibiotic-only water to prepare the mice for dye administration.

Two hours after the water has been switched and the food has been withheld, 100 µL of 100 µM of Cy5-DBCO in 20% sucrose in PBS are administered to the mice by oral gavage. The alfalfa-free food and antibiotic water were returned to the mice. Then, mice were imaged under anesthesia

using IVIS Lumina II (PerkinElmer) at $t = 0$ (before the gavage), 6, 11, 24, and 48 hours. The IVIS instrument is equipped with 10 narrow-band excitation filters (30 nm bandwidth) and 4 broadband emission filters (60- and 75-nm bandwidth). At time point, the mice were imaged using excitation filter at 675 nm, and 500 nm for background subtraction, and emission filter at 695-770 nm, with field of view (FOV) = D (12.5 cm), fstop = 2 and medium binning. Living Image software version 4.3.1/4.4 was used for image analysis.

5.5.13 Whole GI tract *ex vivo* fluorescence imaging

The mouse experiment was performed in the same manner as the *in vivo* tracking experiment up to the dye administration. 36 hours following the dye administration, the mice were euthanized to harvest the whole GI tract for *ex vivo* fluorescence imaging. The GI tract was placed on the lid of 150x25 mm polystyrene tissue culture plate (Falcon) and imaged using IVIS Lumina II with the same setting as the *in vivo* imaging. After imaging, the GI tract was kept at -20°C for protein extraction. The images were then analyzed using ImageJ software for the fluorescence signal from the lower GI tract.

5.5.14 Whole cecum fluorescence and protein analysis

The GI tract specimens used in the *ex vivo* fluorescence imaging were further analyzed for curli and Cy5-DBCO interaction. The mouse GI tracts were removed from -20°C . The cecum from each sample was excised, transferred to a 15-ml falcon tube, and crushed to homogenize. 3 mL of PBS was added to each sample, supplemented with 4 μL of benzonase nuclease (Novagen) and 8 μL of 1 M magnesium sulfate (MgSO_4) (Sigma). The samples were incubated at 37°C overnight.

Each sample was transferred to 2-ml microtube and centrifuged at 14,000 rpm for 10 minutes to extract the supernatant. The supernatant samples were transferred to another set of tubes, and concentrated using 10-kDa Amicon Ultra 0.5 mL centrifugal filters (Millipore) at 10,000 rpm centrifugation for 15 minutes twice. The pellet samples were resuspended in 200 μ L of PBS. Both supernatant and pellet samples were diluted five times, mixed with 2X dyeless Laemli buffer in 1:1 ratio, incubated at 95°C for 5 minutes and run on 12% SDS-PAGE gel (Bio-Rad) at 200 Volts for 30 minutes.

After the gel electrophoresis, the gels were rinsed with water and imaged to detect the fluorescence of Cy5 using a FluorChem™ M system (Protein Simple). Then, the gels were stained with Coomassie Brilliant Blue to detect the presence of proteins and compared the size against standard protein ladder (Bio-Rad).

5.6 Acknowledgments

This work was done in collaboration with Dr.Noémie-Manuelle Dorval Courchesne, Ilona den Hartog, Chaochen Lu, Jessica J. Kim, and Dr. Peter Q. Nguyen. This work made use of the Harvard Center for Nanoscale Systems (CNS) and Harvard Medical School ICCB-Longwood Screening Facility, and the Wyss Institute for Biologically Inspired Engineering. We would like to thank Alexis Rovner, Amanda Graveline, Andyna Vernet, Frank Urena, Thomas Ferrante, Garry Cuneo and Franziska Bahl for their help. Dr. Noémie-Manuelle Dorval Courchesne gratefully acknowledged a Postdoctoral research fellowship from the Fonds de Recherche Nature et Technologies du Québec (FRQNT). Jessica J. Kim thankfully acknowledged the Harvard College Program for Research in Science and Engineering (PRISE) and the Harvard College Research

Program (HCRP) fellowships. This work was supported by National Institutes of Health (1R01DK110770-01A1) and the Wyss Institute for Biologically Inspired Engineering. Adapted with permission from Pichet Praveschotinunt, Noémie-Manuelle Dorval Courchesne, Ilona Den Hartog, Chaochen Lu, Jessica J Kim, Peter Q Nguyen, Neel S Joshi “Tracking of Engineered Bacteria In Vivo Using Nonstandard Amino Acid Incorporation”, *ACS synthetic biology* **7** (6), 1640-1650, 2018. Copyright© 2018 American Chemical Society."

5.7 References

1. Clemente, J. C., Ursell, L. K., Parfrey, L. W. & Knight, R. The Impact of the Gut Microbiota on Human Health: An Integrative View. *Cell*. **148**, 1258-1270 (2012).
2. Lynch, S. V. & Pedersen, O. The Human Intestinal Microbiome in Health and Disease. *New England Journal of Medicine*. **375**, 2369-2379 (2016).
3. Tamboli, C. P., Neut, C., Desreumaux, P. & Colombel, J. F. Dysbiosis in inflammatory bowel disease. *Gut*. **53**, 1-4 (2004).
4. Goodrich, J. K. *et al.* Conducting a Microbiome Study. *Cell*. **158**, 250-262 (2014).
5. Thomas, V., Clark, J. & Doré, J. Fecal microbiota analysis: an overview of sample collection methods and sequencing strategies. *Future Microbiology*. **10**, 1485-1504 (2015).
6. Jeffery, I. B. *et al.* An irritable bowel syndrome subtype defined by species-specific alterations in faecal microbiota. *Gut*. **61**, 997 (2012).
7. Aziz, Q., Doré, J., Emmanuel, A., Guarner, F. & Quigley, E. M. M. Gut microbiota and gastrointestinal health: current concepts and future directions. *Neurogastroenterology & Motility*. **25**, 4-15 (2013).
8. Ashton, J. J. *et al.* 16S sequencing and functional analysis of the fecal microbiome during treatment of newly diagnosed pediatric inflammatory bowel disease. *Medicine*. **96**, e7347 (2017).
9. Earle, Kristen A. *et al.* Quantitative Imaging of Gut Microbiota Spatial Organization. *Cell Host & Microbe*. **18**, 478-488 (2015).
10. Tropini, C., Earle, K. A., Huang, K. C. & Sonnenburg, J. L. The Gut Microbiome: Connecting Spatial Organization to Function. *Cell Host & Microbe*. **21**, 433-442 (2017).
11. Riglar, D. T. *et al.* Engineered bacteria can function in the mammalian gut long-term as live diagnostics of inflammation. *Nature Biotechnology*. **35**, 653 (2017).
12. Yaung, S. J. *et al.* Improving microbial fitness in the mammalian gut by in vivo temporal functional metagenomics. *Molecular Systems Biology*. **11**, 788 (2015).
13. Hwang, I. Y. *et al.* Engineered probiotic *Escherichia coli* can eliminate and prevent *Pseudomonas aeruginosa* gut infection in animal models. *Nature Communications*. **8**, 15028 (2017).
14. Vandenbroucke, K. *et al.* Orally administered *L. lactis* secreting an anti-TNF Nanobody demonstrate efficacy in chronic colitis. *Mucosal Immunology*. **3**, 49 (2009).

15. Duan, F. F., Liu, J. H. & March, J. C. Engineered Commensal Bacteria Reprogram Intestinal Cells Into Glucose-Responsive Insulin-Secreting Cells for the Treatment of Diabetes. *Diabetes*. **64**, 1794-1803 (2015).
16. Danino, T. *et al.* Programmable probiotics for detection of cancer in urine. *Science Translational Medicine*. **7**, 289ra284 (2015).
17. Campbell-Valois, F. X. & Sansonetti, P. J. Tracking bacterial pathogens with genetically-encoded reporters. *FEBS Letters*. **588**, 2428-2436 (2014).
18. Karimi, S. *et al.* In Vivo and In Vitro Detection of Luminescent and Fluorescent *Lactobacillus reuteri* and Application of Red Fluorescent mCherry for Assessing Plasmid Persistence. *PLOS ONE*. **11**, e0151969 (2016).
19. Rhee, K.-J. *et al.* Determination of spatial and temporal colonization of enteropathogenic *E. coli* and enterohemorrhagic *E. coli* in mice using bioluminescent in vivo imaging. *Gut Microbes*. **2**, 34-41 (2011).
20. Belas, R. *et al.* Bacterial Bioluminescence: Isolation and Expression of the Luciferase Genes from *Vibrio harveyi*. *Science*. **218**, 791-793 (1982).
21. Geva-Zatorsky, N. *et al.* In vivo imaging and tracking of host-microbiota interactions via metabolic labeling of gut anaerobic bacteria. *Nat Med*. **21**, 1091-1100 (2015).
22. Wang, W., Zhu, Y. & Chen, X. Selective Imaging of Gram-Negative and Gram-Positive Microbiotas in the Mouse Gut. *Biochemistry*. **56**, 3889-3893 (2017).
23. Hudak, J. E., Alvarez, D., Skelly, A., von Andrian, U. H. & Kasper, D. L. Illuminating vital surface molecules of symbionts in health and disease. *Nature Microbiology*. **2**, 17099 (2017).
24. Young, T. S., Ahmad, I., Yin, J. A. & Schultz, P. G. An Enhanced System for Unnatural Amino Acid Mutagenesis in *E. coli*. *Journal of Molecular Biology*. **395**, 361-374 (2010).
25. Barnhart, M. M. & Chapman, M. R. Curli Biogenesis and Function. *Annual review of microbiology*. **60**, 131-147 (2006).
26. Blanco, L. P., Evans, M. L., Smith, D. R., Badtke, M. P. & Chapman, M. R. Diversity, biogenesis and function of microbial amyloids. *Trends Microbiol*. **20**, 66-73 (2012).
27. Collinson, S. K., Parker, J. M. R., Hodges, R. S. & Kay, W. W. Structural predictions of AgfA, the insoluble fimbrial subunit of *Salmonella* thin aggregative fimbriae11Edited by W. Baumeister. *Journal of Molecular Biology*. **290**, 741-756 (1999).
28. Tian, P. *et al.* Structure of a Functional Amyloid Protein Subunit Computed Using Sequence Variation. *Journal of the American Chemical Society*. **137**, 22-25 (2015).

29. DeBenedictis, E. P., Ma, D. & Keten, S. Structural predictions for curli amyloid fibril subunits CsgA and CsgB. *RSC Advances*. **7**, 48102-48112 (2017).
30. Marcus, A., Sadimin, E., Richardson, M., Goodell, L. & Fyfe, B. Fluorescence Microscopy Is Superior to Polarized Microscopy for Detecting Amyloid Deposits in Congo Red–Stained Trephine Bone Marrow Biopsy Specimens. *American Journal of Clinical Pathology*. **138**, 590-593 (2012).
31. Chapman, M. R. *et al.* Role of Escherichia coli Curli Operons in Directing Amyloid Fiber Formation. *Science*. **295**, 851 (2002).
32. Botyanszki, Z., Tay, P. K. R., Nguyen, P. Q., Nussbaumer, M. G. & Joshi, N. S. Engineered catalytic biofilms: Site-specific enzyme immobilization onto E. coli curli nanofibers. *Biotechnology and Bioengineering*. **112**, 2016-2024 (2015).
33. Monteiro, C. *et al.* Characterization of cellulose production in Escherichia coli Nissle 1917 and its biological consequences. *Environmental Microbiology*. **11**, 1105-1116 (2009).
34. Rosano, G. L. & Ceccarelli, E. A. Recombinant protein expression in Escherichia coli: advances and challenges. *Frontiers in Microbiology*. **5**, 172 (2014).
35. Amiram, M. *et al.* Evolution of translation machinery in recoded bacteria enables multi-site incorporation of nonstandard amino acids. *Nature biotechnology*. **33**, 1272-1279 (2015).
36. Chang, P. V. *et al.* Copper-free click chemistry in living animals. *Proceedings of the National Academy of Sciences*. **107**, 1821-1826 (2010).
37. Dorval Courchesne, N.-M., Duraj-Thatte, A., Tay, P. K. R., Nguyen, P. Q. & Joshi, N. S. Scalable Production of Genetically Engineered Nanofibrous Macroscopic Materials via Filtration. *ACS Biomaterials Science & Engineering*. **3**, 733-741 (2017).
38. Lajoie, M. J. *et al.* Genomically Recoded Organisms Expand Biological Functions. *Science*. **342**, 357 (2013).
39. Gu, S. *et al.* Bacterial Community Mapping of the Mouse Gastrointestinal Tract. *PLOS ONE*. **8**, e74957 (2013).
40. Khlebnikov, A., Risa, Ø., Skaug, T., Carrier, T. A. & Keasling, J. D. Regulatable Arabinose-Inducible Gene Expression System with Consistent Control in All Cells of a Culture. *Journal of Bacteriology*. **182**, 7029-7034 (2000).
41. Kang, S.-W. *et al.* Cell Labeling and Tracking Method without Distorted Signals by Phagocytosis of Macrophages. *Theranostics*. **4**, 420-431 (2014).

42. Xie, R. *et al.* In vivo metabolic labeling of sialoglycans in the mouse brain by using a liposome-assisted bioorthogonal reporter strategy. *Proceedings of the National Academy of Sciences of the United States of America*. **113**, 5173-5178 (2016).
43. Rong, J. *et al.* Glycan Imaging in Intact Rat Hearts and Glycoproteomic Analysis Reveal the Upregulation of Sialylation during Cardiac Hypertrophy. *Journal of the American Chemical Society*. **136**, 17468-17476 (2014).
44. Xie, R. *et al.* Targeted Imaging and Proteomic Analysis of Tumor-Associated Glycans in Living Animals. *Angewandte Chemie International Edition*. **53**, 14082-14086 (2014).
45. Kotula, J. W. *et al.* Programmable bacteria detect and record an environmental signal in the mammalian gut. *Proceedings of the National Academy of Sciences*. **111**, 4838-4843 (2014).
46. Datsenko, K. A. & Wanner, B. L. One-step inactivation of chromosomal genes in *Escherichia coli* K-12 using PCR products. *Proceedings of the National Academy of Sciences of the United States of America*. **97**, 6640-6645 (2000).
47. Nguyen, P. Q., Botyanszki, Z., Tay, P. K. R. & Joshi, N. S. Programmable biofilm-based materials from engineered curli nanofibres. *Nature Communications*. **5**, 4945 (2014).
48. Duraj-Thatte, A. M., Praveschotinunt, P., Nash, T. R., Ward, F. R. & Joshi, N. S. Modulating bacterial and gut mucosal interactions with engineered biofilm matrix proteins. *Scientific Reports*. **8**, 3475 (2018).
49. Grespi, F., Ottina, E., Yannoutsos, N., Geley, S. & Villunger, A. Generation and Evaluation of an IPTG-Regulated Version of Vav-Gene Promoter for Mouse Transgenesis. *PLoS ONE*. **6**, e18051 (2011).

Page intentionally left blank

Chapter 6 Conclusions, Limitations and Future Directions

6.1 Summary

Overall, the dissertation presents a novel platform where probiotic bacteria produce modified extracellular matrix proteins for therapeutic and diagnostic purposes. The genetic engineering capability of curli fibers gives rise to a vast variety of functionality within the platform while preserving the beneficial effects of the probiotic bacteria as an organism chassis. As a result, this work significantly expands both the toolbox from which scientists can pull to create novel engineered probiotic bacteria with programmable features and properties, and the number of possible therapeutic and diagnostic applications of the probiotic bacteria. The last part of the dissertation focuses on utilizing bioorthogonal click reactions on engineered curli fibers for non-invasive tracking of engineered bacteria. This further expands the possible modifications to this platform making it extremely versatile for future therapeutic and diagnostic uses.

In chapter 2 of the dissertation, we have expanded the capability of the BIND platform by fusing the trefoil factor family (TFF) domain, an anti-inflammatory peptide, to the curli fiber subunit, CsgA. We demonstrated that a commensal strain of *E. coli* (PHL628 Δ csgA) successfully expressed curli fused TFF1-3, which are larger than 50 amino acids and contain secondary structures, albeit with slight growth defects. This added to the existing knowledge in terms of the possible domain sizes and structures that could be fused to CsgA and expanded the versatility of the BIND platform. We then showed for the first time that engineered curli fibers displaying biologically active peptides could influence the interaction of engineered bacteria with biological surfaces, as the bacteria with curli fused TFFs bound preferentially to soluble mucin type-2 (Muc-2), caco-2 human intestinal cell line and goat intestinal explant. Curli fused TFFs also have different rheological properties compared to wild-type curli. This showed that the TFFs displayed

on curli fibers were still bioactive. We also demonstrated that curli fused TFF3 could enhance Caco-2 cell migration in a simulated wound model, which makes them potentially valuable for treating inflammation in the gut. Overall, we have not only shown a new method for altering host-microbe interactions through a rational engineering platform, but also a potential therapeutic platform for treating inflammatory bowel diseases (IBD).

In chapter 3, the Probiotic Associated Therapeutic Curli Hybrid (PATCH) platform was created as we programmed probiotic *E. coli* Nissle 1917 (EcN) to produce curli fused TFFs both *in vitro* under simulated physiological conditions and *in situ* within the gastrointestinal (GI) tract. The modified curli fibers did not appear to alter EcN's intrinsic non-pathogenicity against the Caco-2 model. Engineered EcN and curli fibers could be detected from fecal samples and from histology samples using various immunostaining techniques. Administration of the engineered EcN expressing curli fused TFF3 before and during colitis induction with dextran sodium sulfate (DSS) in mice led to amelioration of inflammation in the colon. The prophylactic effect of the engineered EcN correlated with enhanced barrier functions, reduction of Th17 responses, and reduction of pro-inflammatory cytokines and enzymes in the colonic tissues. The results shown in this chapter demonstrate the feasibility of the PATCH platform in a pre-clinical model of IBD, and suggest downstream applications in many other GI-related diseases.

In chapter 4, we created living hydrogels consisting of engineered curli nanofibers with a viable commensal strain of *E. coli*. Using a filtration protocol invented in our group, we successfully concentrated curli fibers embedded with live bacterial cells on filter membranes. Upon exposure of the filtered biomass to a surfactant like sodium dodecyl sulfate (SDS), the nanofibers became dispersed and hydrated into hydrogel-like materials. The rheological properties

of these gels were different based on the domain that was displayed on the curli fibers and the cellular components present in the hydrogels. The curli fused TFF2 gels showed improved binding to the mucosa, while the curli fused fibronectin gels adhered better to the serosa of goat intestinal explants. Importantly, the biomass of the hydrogels expanded more than four-fold when the gels were incubated in growth-promoting conditions for 24 hours. Oral administration of living hydrogels to mice led to an extended residence time of the bacteria. Novel curli materials continued to be produced within the gut even after the original materials had been cleared out, indicating that the live gels were able to grow and self-renew *in vivo* as well. The ability of the hydrogels to self-renew, undergo genetic modifications, and withstand harsh conditions throughout the GI transit sets this material apart from other composite living materials, implying their future utility for therapeutic applications in the gut, especially in cases where the viscosity of the gels and the benefits of living microbes are desired.

In chapter 5, we demonstrated a preliminary novel technique for studying the spatiotemporal dynamics of engineered gut microbes via non-invasive labeling and tracking using bioorthogonal click chemistry. First, we incorporated an in-frame amber stop codon into the *csgA* gene in the curli operon. We then transformed plasmids containing an orthogonal translation system (OTS) and the amber-containing curli operon into engineered EcN and induced expression with arabinose and *p*-azido-L-phenylalanine (pAzF), which is a non-standard amino acid (NSAA) capable of undergoing the click reaction. We observed successful expression of mutant curli fibers with minimal growth defects in the bacteria, indicating that the amber codon suppression system was well tolerated. We demonstrated *in vitro* labeling of EcN with mutant curli fibers using dibenzocyclooctyne (DBCO) conjugated to Cy5 dye with minimal non-specific labeling of wild-

type curli fibers. Through the use of flow cytometry, we found that about 60% of the engineered bacterial population was labeled by DBCO-Cy5 likely due to variation in pBAD expression. We then performed the labeling in mice and found that the labeled bacteria could be detected up to several days longer after dye administration compared to the dye-only group. Moreover, the fluorescence signal from the gut explant of the engineered bacteria group was significantly higher than all the other control groups, in which certain components of the click reaction were omitted. We were able to retrieve the covalently labeled CsgA from the cecal tissue homogenate as well, indicating successful *in vivo* labeling of the mutant bacteria. This proof-of-concept study opens up the possibility of non-invasive tracking of engineered microbes using imaging probes that are suitable for studying large animals or humans, such as MRI and PET/CT probes, which could be useful for tracking pharmacokinetics, whole body distribution, and even pathogenicity of the bacteria.

6.2 Limitations

Throughout the work in this dissertation, we discovered a number of limitations to our experiments that are worth discussing for future improvements to the platform. In chapter 2, we followed the original BIND platform procedures, meaning we performed all experiments using the PHL628 $\Delta csgA$ strain and complemented it with an exogenous plasmid containing various *csgA* constructs. We relied on the native curli operon in the *E. coli* genome to provide adequate amounts of CsgB-CsgG proteins for CsgA to be properly secreted and assembled. However, endogenous expression of CsgB-CsgG was not always sufficient to process the overexpressed CsgA, leading to cell stress and cytotoxicity. Hence, in order to optimize the expression, we had to lower the

amount of IPTG, the inducer of plasmid expression, or to omit it completely and relied solely on the leaky expression of the CsgA promoter instead.

To address the expression issues from chapter 2, we created an improved expression system for EcN in chapter 3. Instead of relying on the native *csg* operon, we decided to knock out the entire *csg* operon from the genome of EcN (creating the PBP8 strain) and complemented it with an engineered plasmid that contained modified CsgA, CsgB-C, and CsgE-G under the pBAD promoter. In this case, we were able to control the expression of the whole operon in an inducible manner, which significantly reduced the toxicity due to CsgA overexpression. However, this system still requires further optimization owing to multiple limitations. First, an inducible system with small molecule inducers such as arabinose is a good starting place for proof-of-concept study, but it is not suitable for *in vivo* usage because of the difficulties in determining the appropriate inducer concentration to use and in ensuring a homogeneous expression level among the population. In addition, the recombinant plasmid system requires antibiotic selection for plasmid retention. Though antibiotic administration favors a long residence time for our engineered EcN, it interferes with the normal gut microbiome and the extent of DSS-induced inflammation, confounding the effects of the engineered bacteria. The ways to improve upon these plasmid limitations are discussed later in the future direction section.

In addition, it is worth mentioning that in the anti-CsgA whole cell ELISA experiment, there were lower signals from the TFF2 and TFF3 constructs, which could reflect the hindered accessibility of anti-CsgA antibodies to CsgA proteins due to steric effects from TFF2 and TFF3. In the *in vitro* binding experiments with mucins, Caco-2 cells, and gut explants, even though we showed that the CsgA-TFFs had preferential binding to those surfaces, we could not definitively

say that this would translate directly to the *in vivo* environment since there was no other type of bacteria to interfere with the binding and the amount of the bacteria incubated was likely higher than the typical amount of *E. coli* in the gut. The main takeaway from these experiments is that the TFFs tethered to curli fibers remain bioactive and exhibit biological properties distinct from wild-type curli fibers. A similar analysis extends to the cell migration experiment. Even though we demonstrated that purified curli fused TFF3 could enhance *in vitro* wound healing compared to wild-type, the same may not hold true in an *in vivo* model because of two reasons. First, the purified curli concentration may not reflect the *in vivo* concentration, and second, live bacterial cells were excluded from the *in vitro* experiments because they could negatively impact the health of Caco-2 cells, whereas live bacteria would be present *in vivo*.

While it was promising that engineered curli did not confer pathogenicity to EcN in various *in vitro* polarized Caco-2 assays, more experiments should be done to assess the anti-inflammatory properties of PBP8 CsgA-TFF3. However, such an experiment would require extensive methodology development, such as the induction of inflammation in the polarized Caco-2 system and the co-culture of Caco-2 with live bacterial cells. In the *in vivo* DSS colitis experiment, we observed appreciable differences in weight change and the disease activity index when comparing the colitic and PBP8 CsgA-TFF3 groups. However, we did not observe big differences between PBP8 wt-CsgA and CsgA-TFF3 in many of the data sets, suggesting that the anti-inflammatory effects could have partly arisen from the curli fibers. More studies will have to be done to tease apart the contribution from wild-type curli alone and curli fused TFFs. Experiments using *in vitro* polarized Caco-2 or toll-like receptor 1 or 2 knockout mice, which are unable to recognize curli

fibers, could be done to answer some of these questions, which are crucial for further platform development.

The process of generating living hydrogels in chapter 4 was novel yet required further optimization. First, we were still uncertain about the effects of SDS on live bacterial cells. Even though we could recover live cells that were capable of regeneration, SDS might have affected their health and genomic information. Second, we observed changes in rheological properties of various hydrogels that contain different components such as cells, DNA, and secondary structures of TFF2, but the mechanisms and the implications of those changes were still unclear. In addition, when we successfully showed the renewal of the curli fibers in a mouse model using Cy5-Ni-NTA nanoparticle labeling, but we could not say conclusively whether the new fibers exhibited gel-like properties. This would be difficult to study as there is no obvious way to observe and measure gel properties within the mouse GI tract.

In chapter 5, we demonstrated the proof-of-concept study for non-invasive labeling of engineered bacteria *in vivo* with preliminary techniques that could be improved upon. Although the expression system, which contains both an OTS plasmid and a synthetic operon plasmid with mutant CsgA, worked relatively well for this study, it was not the optimal system because the PBP8 cells still contained native amber stop codons and release factor-1, which could lead to non-specific incorporation of pAzF into amber stop codons and premature termination of mutant CsgA, respectively. A recoded *E. coli* strain, which has no native amber stop codons and no release factor-1, might be an appropriate model to follow up on as we engineer a future iteration of EcN because it should help improve NSAA incorporation specificity and obviate premature termination. In addition, the curli fibers might not be the best option to use for tracking cells because the fibers

could detach from the cells, leading to false-positive signals. We could consider other cell surface displayed proteins that are attached directly to the cells as alternative targets. Moreover, the labeling efficiency for the microbes was only 60%, which might be related to the efficiency of arabinose inducible promoters. Another point to consider is that the autofluorescence of the GI tract could interfere with the signal of the Cy5 dye. In the future, we could consider click dyes with near-IR emissions to avoid the autofluorescence. Moreover, a “turn-on” probe that lights up upon the click chemistry reaction, which can help reduce the signal from the non-specific binding with the cells and wild-type curli, should be considered for future use as well.

6.3 Future Directions

6.3.1 Potential of the PATCH platform

In this work, we demonstrated the potential use of the PATCH platform to ameliorate inflammation in mouse models of colitis through peptides that enhance wound healing and strengthen barrier functions. This opens up new possibilities for other classes of therapeutic and diagnostic peptides to be applied to the platform. For example, we can try to fuse tumor homing peptides onto curli fibers and determine whether we can alter the localization of the bacteria to the tumors^{1,2}. If that is the case, we can further utilize the bacteria as a biosensor to diagnose the tumors based on bioluminescence of the bacteria or based on a chemical labeling technique like in chapter 5. Furthermore, we could engineer the bacteria to produce anti-tumor molecules for therapeutic purposes. For applications that require the release of the fused peptide into the surroundings, we can engineer a protease cleavable linker between CsgA and the therapeutic peptide. Such a linker can be cleaved upon contact with proteases such as matrix metalloprotease (MMP), Cathepsin, or

other disease related proteases to release the displayed peptides. The peptides could then exert therapeutic effects by being internalized into the cell or by directly interacting with symptomatic areas³⁻⁶.

The PATCH platform could be useful as a combination therapy with traditional drugs. In future experiments, we study whether the anti-inflammatory PATCH bacteria can act synergistically with local or systemic anti-inflammatory drugs such as 5-ASA, corticosteroids, or anti-TNF α . The combinations that are effective should be studied further.

6.3.2 Improvement of engineered plasmids for the PATCH platform

As mentioned earlier, the current PATCH system requires small molecules to induce gene expression and antibiotics to retain the plasmids in the bacterial cells. These external factors could interfere with the experiment by, for example, changing the microbiome in the host. Therefore, the second generation of the PATCH system should include promoters that can sense and respond to the environment. For example, hypoxia-induced promoters would be appropriate for expression inside the GI tract where oxygen levels are low⁷. For IBD, tetrathionate and thiosulfate inducible promoters could be utilized to sense the extent of inflammation in the GI tract, which could lead to specific expression of therapeutic molecules at the site of inflammation^{8,9}. Overall, we can utilize promoters that are appropriate for the given application to achieve the best therapeutic and diagnostic outcomes.

As for plasmid retention, there have been multiple examples in the literature from which we could draw inspirations to develop a second-generation system. A toxin-antitoxin system relies on having a plasmid expressing a long-lived protein toxin and a short-lived RNA antitoxin, forcing

the cells to keep the plasmids for their survival^{10,11}. Danino et al. have utilized the hok-sok toxin-antitoxin system along with the alp system to facilitate efficient plasmid segregation in engineered EcN for liver metastasis detection. These cells could retain the plasmids at a rate of more than 96% after 72 hours *in vivo*¹². An auxotrophic system can also be used for plasmid retention by removing one of the essential amino acid synthesis pathways or enzymes from the genomic DNA of the organism chassis and putting it in the plasmid instead. Such a complementation system would force the cells to keep the plasmid for essential amino acid production without the need for antibiotics^{13,14}. Young et al. have demonstrated the use of an auxotrophic system for engineered EcN used to eliminate *Pseudomonas aeruginosa* in animal models without the need for antibiotic resistance genes¹⁵. Another promising strategy specific to EcN is the engineering of EcN's cryptic plasmids. EcN carry two small cryptic plasmids, pMUT1 and pMUT2, which propagate with EcN autonomously. They are unique to EcN and can be used as a marker for this strain of *E. coli*¹⁶. Though the mechanisms of retention of these plasmids remain to be discovered, these plasmids could potentially serve as platforms for protein expression in EcN without antibiotic selection. By comparing these strategies in terms of their retention and expression efficacies, we could use them to further optimize the PATCH system toward a future therapeutic platform.

6.3.3 Non-invasive tracking of engineered bacteria with probes that are suitable for human medical imaging

We demonstrated the proof-of-concept study for the non-invasive tracking of engineered bacteria using click chemistry with fluorescence dyes. While this illustrates a novel strategy for *in vivo* labeling, it may have little utility in humans due to the limited tissue penetration of fluorescence and the hurdles of a multi-step labeling process compared to constitutive expression

of bioluminescent proteins in bacteria. What makes this system stand out is that we can utilize a wider range of imaging probes compared to conventional fluorescent protein-based labeling methods. Non-protein dyes or inorganic probes can be used as they can be chemically conjugated to a click chemistry handle and do not rely on oxygen-dependent maturation like traditional fluorescent proteins. This becomes particularly useful for human and large animal imaging. Carbon-11 or Fluorine-18 labeled amino acids that emit positrons for PET/CT imaging could be incorporated, which would be revolutionary for the *in vivo* imaging of engineered microbes in humans¹⁷⁻¹⁹. Furthermore, the OTS system for NSAA incorporation still needs antibiotic selection. One can improve upon the system by applying plasmid retention systems mentioned previously or by integrating the OTS system into the genome of the engineered bacteria because the OTS system does not need to be expressed in large quantities.

6.4 Concluding remarks

Throughout this dissertation, we demonstrated the great versatility of engineered curli-expressing probiotic bacteria, making them valuable as a therapeutic and diagnostic platform. The system provides a vast variety of possible therapeutic domains to be displayed on the curli fibers of engineered bacteria. Molecules with unique properties like non-standard amino acids can also be incorporated into the fibers, adding another layer of functionality to the system. On the other hand, a lot is yet to be learned about the system's interaction with the host's body and how the system can be optimized and programmed for protein expression under desired physiological conditions. It is crucial to continue gathering knowledge and understanding of the system itself, along with the effects it has on the host and the target disease. The more we understand the system,

the better we can anticipate the effects of the rationally designed probiotic bacteria on human health and on diseases.

We have placed our focus on studying the biological effects of the displayed peptides or click moieties. Our studies demonstrated that the displayed domains or click moieties are able to carry out biological functions, undergo chemical reactions, and modulate interaction with the host environments. Nevertheless, the displayed moieties are not the only components to study and optimize when designing the system. Other critical aspects include organism chassis, protein scaffolds (in this case curli fibers), plasmid retention, promoters, expression systems, locations of the target disease, etc. The next generation platform can be achieved through optimization of these parameters collectively.

In conclusion, this dissertation has contributed to the development of novel therapeutic and diagnostic platforms using rationally designed, bottom-up approaches to engineer biofilm-derived matrix protein materials in living and programmable probiotic bacteria. The novel therapeutic protein display and delivery strategies developed here could be applied to multiple species of beneficial microbes suitable for a wide range of niches and diseases in the host. Positive impacts were made in the fields of microbiome on health and disease, engineered living therapeutics, living materials, and the biology of the curli operon and probiotic *E. coli* Nissle 1917. In the future, the engineered probiotic bacterial technology may be developed further until it can be employed in patients. The engineered bioactive curli fiber scaffolds with live probiotic bacteria demonstrates one of the possible approaches toward engineered beneficial microbes for therapeutics and diagnostics.

6.5 References

1. King, A. et al. Tumor-homing peptides as tools for targeted delivery of payloads to the placenta. *Science advances*. 2, e1600349-e1600349 (2016).
2. Gautam, A. et al. Tumor Homing Peptides as Molecular Probes for Cancer Therapeutics, Diagnostics and Theranostics. *Current Medicinal Chemistry*. 21, 2367-2391 (2014).
3. Weidle, U., Tiefenthaler, G. & Georges, G. Proteases as Activators for Cytotoxic Prodrugs in Antitumor Therapy. *Cancer Genomics & Proteomics*. 11, 67-80 (2014).
4. Zhang, X. et al. Matrix metalloproteinases-2/9-sensitive peptide-conjugated polymer micelles for site-specific release of drugs and enhancing tumor accumulation: preparation and in vitro and in vivo evaluation. *International journal of nanomedicine*. 11, 1643-1661 (2016).
5. Vartak, D. G. & Gemeinhart, R. A. Matrix metalloproteases: underutilized targets for drug delivery. *Journal of drug targeting*. 15, 1-20 (2007).
6. Dal Corso, A., Cazzamalli, S., Gébleux, R., Mattarella, M. & Neri, D. Protease-Cleavable Linkers Modulate the Anticancer Activity of Noninternalizing Antibody–Drug Conjugates. *Bioconjugate Chemistry*. 28, 1826-1833 (2017).
7. Yu, B. et al. Explicit hypoxia targeting with tumor suppression by creating an “obligate” anaerobic *Salmonella Typhimurium* strain. *Scientific Reports*. 2, 436 (2012).
8. Daeffler, K. N. M. et al. Engineering bacterial thiosulfate and tetrathionate sensors for detecting gut inflammation. *Molecular Systems Biology*. 13, 923 (2017).
9. Riglar, D. T. et al. Engineered bacteria can function in the mammalian gut long-term as live diagnostics of inflammation. *Nature Biotechnology*. 35, 653 (2017).
10. Unterholzner, S. J., Poppenberger, B. & Rozhon, W. Toxin-antitoxin systems: Biology, identification, and application. *Mobile genetic elements*. 3, e26219-e26219 (2013).
11. Yamaguchi, Y., Park, J. H. & Inouye, M. Toxin-antitoxin systems in bacteria and archaea. *Annu Rev Genet*. 45, 61-79 (2011).
12. Danino, T. et al. Programmable probiotics for detection of cancer in urine. *Science Translational Medicine*. 7, 289ra284 (2015).
13. Vidal, L., Pinsach, J., Striedner, G., Caminal, G. & Ferrer, P. Development of an antibiotic-free plasmid selection system based on glycine auxotrophy for recombinant protein overproduction in *Escherichia coli*. *Journal of Biotechnology*. 134, 127-136 (2008).

14. Dong, W.-R., Xiang, L.-X. & Shao, J.-Z. Novel Antibiotic-Free Plasmid Selection System Based on Complementation of Host Auxotrophy in the NAD &De Novo Synthesis Pathway. *Applied and Environmental Microbiology*. 76, 2295 (2010).
15. Hwang, I. Y. et al. Engineered probiotic *Escherichia coli* can eliminate and prevent *Pseudomonas aeruginosa* gut infection in animal models. *Nature Communications*. 8, 15028 (2017).
16. Blum-Oehler, G. et al. Development of strain-specific PCR reactions for the detection of the probiotic *Escherichia coli* strain Nissle 1917 in fecal samples. *Research in Microbiology*. 154, 59-66 (2003).
17. Jia, L., Li, X., Cheng, D. & Zhang, L. Fluorine-18 click radiosynthesis and microPET/CT evaluation of a small peptide-a potential PET probe for carbonic anhydrase IX. *Bioorganic & Medicinal Chemistry*. 27, 785-789 (2019).
18. Sun, A., Liu, X. & Tang, G. Carbon-11 and Fluorine-18 Labeled Amino Acid Tracers for Positron Emission Tomography Imaging of Tumors. *Frontiers in Chemistry*. 5, 124 (2018).
19. Qi, Y., Liu, X., Li, J., Yao, H. & Yuan, S. Fluorine-18 labeled amino acids for tumor PET/CT imaging. *Oncotarget*. 8, 60581-60588 (2017).

Page intentionally left blank